

# Revista Română de Inginerie Civilă

Indexată în bazele de date internaționale (BDI)

ProQuest, IET INSPEC, EBSCO, GOOGLE SCHOLAR, CROSSREF,  
TDNET, DIMENSIONS, DRJI, J-GATE, INDEX COPERNICUS,  
ULRICH'S, JOURNALSEEK, RESEARCH GATE,  
SEMANTIC SCHOLAR, ERIHPLUS, WORLDCAT

Volumul 16 (2025), Numărul 4

A novel H <sub>2</sub> O/LiBr absorption heat pump with heat recovery for combined heating and cooling production using renewable energy	
O pompă de căldură cu absorbție H <sub>2</sub> O/LiBr de tip nou, cu recuperare de căldură, pentru producerea combinată de încălzire și răcire utilizând energie regenerabilă	353-362
<i>Alina GIRIP, Răzvan CALOTĂ, Mădălina NICHITA, Anica ILIE, Constantin LAZĂR, Andreea IFTENE</i>	
<hr/>	
Analysis of Thermal Comfort in Public Buildings: A Case Study	
Analiza confortului termic în clădirile publice. Studiu de caz.	363-376
<i>Natalia BEGLET, Elena NICOLAEV</i>	
<hr/>	
Strategies for reducing energy consumption in existing buildings through ecological renovation	
Strategii de reducere a consumului de energie în clădirile existente prin renovare ecologică	377-391
<i>Horia- Alexandru VARSA, Catalin LUNGU, Tiberiu CATALINA</i>	
<hr/>	
Comparative simulation of a fire in a paint storage warehouse: with and without an ESFR sprinkler system	
Simularea comparativă a unui incendiu într-o hală de depozitare cu vopseluri: cu și fără sistem de stingere ESFR	392-406
<i>Emanuil-Petru OVADIUC, Răzvan CALOTĂ, Ilinca NĂSTASE, Manuel SERBAN</i>	
<hr/>	
Analysis of the Global Impact of Light Pollution. Ecological Environment Perspectives	
Analiza impactului global al poluării luminoase. Perspectivă ecologică și de mediu	407-419
<i>Anca MANOLESCU, Ionuț STĂNESCU</i>	
<hr/>	
Integrated Modeling and Simulation of Smart Building Energy Systems	
Modelarea și simularea integrată a sistemelor de energie pentru clădiri inteligente	420-435
<i>Petre- Marian PIRVULESCU, Catalin LUNGU, Tiberiu CATALINA, Ahmed HAMZE</i>	

On increasing the energy sustainability of localities in the security zone of the Republic of Moldova	
Cu privire la sporirea sustenabilității energetice a localităților din zona de securitate a Republicii Moldova	436-449
<i>Valentin TONU, Vadim CEBAN</i>	
<hr/>	
Improving the Energy Efficiency of Electric Domestic Water Heaters through Alternative Heating and Thermal Energy Storage Solutions	
Îmbunătățirea eficienței energetice a boilerelor electrice pentru apă caldă menajeră prin soluții alternative de încălzire și stocare a energiei termice	450-460
<i>Tudor T. NASCA, Raul R. IUGA, Octavian-Gabriel O. POP</i>	
<hr/>	
Development of a Digital Twin for a thermal manikin used in the evaluation of indoor environmental quality	
Dezvoltarea unui geamăn digital pentru un manechin termic utilizat în evaluarea calității mediului interior	461-473
<i>Diana LEMIAN, Ilinca NASTASE</i>	
<hr/>	
Efficiency Enhancement of Photovoltaic Panels through Passive Heat Pipe Technology	
Creșterea eficienței panourilor fotovoltaice prin utilizarea tehnologiei pasive cu țevi termice	474-486
<i>Sebastian BREZAN, Suraj-Laurențiu-Gabriel DIACONU</i>	
<hr/>	
Mioritic Loop: A Smart and Sustainable Closed-Loop Farm Based on Renewable Resources	
Mioritic Loop: O fermă inteligentă și durabilă, cu circuit închis, bazată pe resurse regenerabile	487-494
<i>Diana Patricia ȚUCU</i>	
<hr/>	
Testul de răspuns termic pentru utilizarea eficientă a aplicațiilor geotermale în România	
Thermal Response Test for the Efficient Use of Geothermal Applications in Romania	495-507
<i>Virgil FLORESCU, Bahadır KIVANC, Tiberiu CATALINA</i>	

**MATRIX ROM**  
**3 Politehnicii Street, Bucharest, Romania**  
**Tel. +4021.4113617, +40733882137**  
**e-mail: [office@matrixrom.ro](mailto:office@matrixrom.ro)**  
**[www.matrixrom.ro](http://www.matrixrom.ro)**

**Editorii acestui număr:**      **Conf. Univ. Dr. Ing. Cătălin LUNGU**  
   **Conf. Univ. Dr. Ing. Răzvan CALOTĂ**

## **EDITORIAL BOARD**

Ph.D. Harish Chandra ARORA, *CSIR-Central Building Research Institute, Roorkee, India*  
Ph.D. Assoc. Prof. Arch. Eur. Ing. Lino BIANCO, *University of Malta, Malta*  
Ph.D.Prof.Eng. Ioan BOIAN, *Transilvania University of Brasov, Romania*  
Ph.D.Assoc.Prof.Eng. Vasilica CIOCAN, *Gh. Asachi Technical University of Iasi, Romania*  
Ph.D.Prof. Stefano CORGNATI, *Politecnico di Torino, Italy*  
Ph.D.Assoc.Prof.Eng. Andrei DAMIAN, *Technical University of Constructions Bucharest, Romania*  
Ph.D.Prof. Yves FAUTRELLE, *Grenoble Institute of Technology, France*  
Ph.D.Prof.Eng. Carlos Infante FERREIRA, *Delft University of Technology, The Netherlands*  
Ph.D.Prof. Manuel GAMEIRO da SILVA, *University of Coimbra, Portugal*  
Ph.D.Prof.Eng. Dragos HERA, *Technical University of Constructions Bucharest, Romania, honorary member*  
Ph.D. Jaap HOGELING, *Dutch Building Services Knowledge Centre, The Netherlands*  
Ph.D.Lawyer Cristina Vasilica ICOCIU, *Polytechnic University of Bucharest, Romania*  
Ph.D.Prof.Eng. Anica ILIE, *Technical University of Constructions Bucharest, Romania*  
Ph.D.Prof.Eng. Gheorghe Constantin IONESCU, *Oradea University, Romania*  
Ph.D.Prof.Eng. Florin IORDACHE, *Technical University of Constructions Bucharest, Romania - director editorial*  
Ph.D.Prof.Eng. Vlad IORDACHE, *Technical University of Constructions Bucharest, Romania*  
Ph.D.Prof.Eng. Karel KABELE, *Czech Technical University, Prague, Czech Republic*  
Ph.D.Prof. Birol KILKIS, *Baskent University, Ankara, Turkey*  
Ph.D.Assoc.Prof.Eng. Catalin LUNGU, *Technical University of Constructions Bucharest, Romania*  
Ph.D.habil. Assoc.Prof. Zoltan MAGYAR, *Budapest University of Technology and Economics, Hungary*  
Ph.D.Assoc.Prof.Eng. Carmen MARZA, *Technical University of Cluj Napoca, Romania*  
Ph.D.Prof.Eng. Ioan MOGA, *Technical University of Cluj Napoca, Romania*  
Ph.D.Assoc.Prof.Eng. Gilles NOTTON, *Pascal Paoli University of Corsica, France*  
Ph.D.Prof.Eng. Daniela PREDA, *Technical University of Constructions Bucharest, Romania*  
Ph.D.Prof.Eng. Adrian RETEZAN, *Polytechnic University of Timisoara, Romania*  
Ph.D.Prof. Emeritus Aleksandar SEDMAK, *University of Belgrad, Serbia*  
Ph.D. Boukarta SOUFIANE, *Institute of Architecture and Urban Planning, BLIDAI, Algeria*  
Ph.D.Assoc.Prof.Eng. Daniel STOICA, *Technical University of Constructions Bucharest, Romania*  
Ph.D.Prof. Branislav TODOROVIC, *Belgrad University, Serbia*  
Ph.D.Prof. Marija S. TODOROVIC, *Academy of Engineering Sciences of Serbia*  
Ph.D.Eng. Ionut-Ovidiu TOMA, *Gh. Asachi Technical University of Iasi, Romania*  
Ph.D.Prof.Eng. Ioan TUNS, *Transilvania University of Brasov, Romania*  
Ph.D.Assoc.Prof.Eng. Constantin TULEANU, *Technical University of Moldova Chisinau, Republic of Moldova*  
Ph.D.Prof.Eng. Ioannis VAYAS, *National Technical University of Athens, Greece*  
Ph.D.Assoc.Prof.Eng. Eugen VITAN, *Technical University of Cluj Napoca, Romania*

**Romanian Journal of Civil Engineering is founded, published and funded by**  
**publishing house MATRIX ROM**  
**Executive Director: mat. Iancu ILIE**

**Online edition ISSN 2559-7485**

**Print edition ISSN 2068-3987; ISSN-L 2068-3987**





## A novel H<sub>2</sub>O/LiBr absorption heat pump with heat recovery for combined heating and cooling production using renewable energy

O pompă de căldură cu absorbție H<sub>2</sub>O/LiBr de tip nou, cu recuperare de căldură, pentru producerea combinată de încălzire și răcire utilizând energie regenerabilă

Alina GIRIP, Răzvan CALOTĂ, Mădălina NICHITA, Anica ILIE,  
Constantin LAZĂR, Andreea IFTENE

Technical University of Civil Engineering of Bucharest  
122-124 Bvd Lacul Tei, Bucharest, Sector 2, Romania

E-mail: [alina.girip@utcb.ro](mailto:alina.girip@utcb.ro), [razvan.calota@utcb.ro](mailto:razvan.calota@utcb.ro), [madalina.nichita@utcb.ro](mailto:madalina.nichita@utcb.ro), [ilie.anica@utcb.ro](mailto:ilie.anica@utcb.ro),  
[constantin.lazar@phd.utcb.ro](mailto:constantin.lazar@phd.utcb.ro), [andreea.iftene@utcb.ro](mailto:andreea.iftene@utcb.ro)

DOI: 10.37789/rjce.2025.16.4.1

### Abstract

Absorption refrigeration technology was developed as a response to major challenges, including the energy crisis, rising fuel costs, and the environmental drawbacks of conventional vapor-compression refrigeration systems. Extensive research has focused on developing strategies to enhance the COP of absorption systems, with the aim of making absorption refrigeration technology more competitive compared to conventional compression systems. This study investigates a hybrid absorption heat pump integrated with heat recovery combined heating and cooling production to improve the COP of absorption refrigeration systems. The system is based on low- and high-pressure absorber/evaporator pairs, operating with H<sub>2</sub>O/LiBr as the working fluid, and driven by a low-temperature heat source. In order to drive the heat pump's heat generator, natural gas (prepared in a boiler) or/and solar energy (prepared in solar panels) was used. The experimental research were conducted on an experimental stand located in the Department of Heat Engineering and Thermal Equipment Laboratory from the Technical University of Civil Engineering, Bucharest. It can simultaneously supply both cooling and heating for preparation of domestic hot water. A performance analysis is carried out through experimental measuring data to calculate the total COP vs. COP for conventional single-effect absorption chiller under the same conditions. In recovery mode, the maximum total COP increases to **5.446** because of heat recovery from condenser and absorber. Nevertheless, the system achieves a temperature of hot water between 33.58–43.92 °C. Notably, the recovery heat mode performance is strongly influenced by the solar radiation during the month, which therefore represents a key design parameter for the proposed system.

**Key-words:** heat pump, heat recovery, H<sub>2</sub>O absorption

## 1. Introduction

Considering the global long-term low greenhouse gas Emission Development Strategies based on the Paris Agreement adopted in 2015 [1], measures to reduce carbon emissions by expanding the use of high-energy-efficiency products and promoting renewable energy usage are being proposed. The use of renewable energy sources in buildings is essential. However, renewable energy has two major drawbacks: a low heat-source temperature and an imbalance between the energy supply and demand [2,3]. Therefore, the aforementioned problems must be overcome to increase the utilization of renewable energy for building cooling and heating.

In Europe, the building stock alone is responsible for 40% of total energy consumption and 36% of greenhouse gas (GHG) emissions in the European Union (EU) [4,5].

Decarbonizing the heating and cooling sector is essential to achieving the EU's climate neutrality target by 2050 and the interim objective of reducing net GHG emissions by at least 55% by 2030 [6].

The deployment of heat pumps offers a practical pathway for both buildings and industry to reduce dependence on fossil fuels while accelerating the decarbonization of heating and cooling applications across the EU. The absorption cycle has the advantage of obtaining cooling and heating effects with a low-temperature heat source at 100°C [7].

Heat pumping technologies are commonly designed to provide either heating or cooling, functioning as heaters, refrigerators, or chillers. With an appropriate choice of working fluid (refrigerant) and careful system design, heat pumps can be configured to deliver heating and cooling simultaneously. As examples, there are *hotels* (space cooling and domestic hot water production) [8], *office buildings* (server room cooling and space heating), *sports complexes* (swimming pool heating and ice rink cooling) [9]. Also, industries as *food processing* simultaneous refrigeration, process heating and cooling, and hot water generation [10–12] and other applications like *seawater desalination* combined with space cooling in coastal regions [13].

The earliest AHP cycle configuration proposed for the combined heating and cooling production dates back to the 1980s, using an H<sub>2</sub>O/LiBr working pair by Eisa et al. [14]. The thermodynamic design data for the potential combinations of operating temperatures of the absorber (30–50°C), condenser (50–100°C), evaporator (2–15°C), and generator (70–170°C) of the single-effect H<sub>2</sub>O/LiBr AHP cycle were obtained using simulation and reported taking into consideration of the LiBr crystallization limit in the absorber and generator. Further, Kumar et al. [15] carried out an experimental study on the single-effect H<sub>2</sub>O/LiBr AHP for combined heating and cooling production taking advantage of the heat released during the absorption and condensation processes.

Prieto et al. [16] carried out a theoretical study on the single-effect H<sub>2</sub>O/LiBr AHP for combining heating and cooling production to analyze the feasibility of the single-effect H<sub>2</sub>O/LiBr absorption heat pump. The cycle is theoretically studied for five

different types of applications that require simultaneous heating and cooling: building air conditioning, a 4th generation district heating and cooling network, a sports center with an indoor swimming pool, a hybrid air conditioning system with an absorption heat pump and a desiccant evaporative cooling system, and simultaneous cooling and water purification application for coastal areas.

According to Zhaia et al. [17], the vast majority of the chillers used for air conditioning applications operate with lithium bromide - water solution and use steam or hot water as the heat source. It has been testified that single-effect LiBr-H<sub>2</sub>O absorption units using fossil fuels are not competitive from the energy, economic and environmental points of view. They become competitive when using waste or renewable energy.

Although both solar electric and solar thermal systems can be used to produce refrigeration, solar thermal absorption systems are more efficient, specifies Siddiqui et. Al [18]. Such systems can be used in areas where conventional sources of energy are not available or expensive, and also in order to limit the release of the greenhouse gas emissions caused by the usage of the fossil fuels.

Numerous experimental models describing the functioning of a single effect, LiBr-H<sub>2</sub>O absorption heat pump at steady conditions were presented in the last years, [19-20]. As a general conclusion, the result shows that experimental and simulated systems which are based on combinations of different types of solar thermal collectors and absorption chillers, have a COP value for the absorption chillers between 0.6 and 0.8 for simulated, and between 0.40 and 0.85 for experimental systems, for generator inlet temperature between 70 and 100 °C, [21].

The authors have an experience in the study of absorption heat pumps powered by solar energy, [22-23] and in this paper have analysed the operation conditions for cold season, and also the opportunity of using the heat recovered in the condenser and absorber to heat the air in a heating coil, part of an air handling unit.

The experimental results were obtained using an experimental stand located in the Department of Heat Engineering and Thermal Equipment Laboratory from the Technical University of Civil Engineering, Bucharest. The flat plate solar panels, in great measure, cover the heat demand of the heat generator in the hot season. The nominal capacity of the absorption chiller is 17 kW.

## 2. System description

The proposed absorption heat pump for combined cooling and heating is built on a single-effect H<sub>2</sub>O/LiBr chiller whose cycle is modified to recover the heat of condensation and absorption at a useful temperature level. By reclaiming this heat, the system reaches higher energy-use efficiency and delivers multiple outputs at the same time, including domestic hot water. The integration shows that the unit can supply cooling and heating simultaneously while improving overall efficiency and sustainability.

Beyond the change in high pressure, the cycle runs at four temperature levels instead of three as in a conventional single-effect H<sub>2</sub>O/LiBr chiller. The evaporator provides the

cooling effect at 6.8 to 12.5°C. The absorber releases heat at 26.3 to 43.8°C, a range that in standard systems is usually rejected to the environment. The condenser also releases heat, between 26.3 and 42.3°C, which becomes available for heating use. The generator receives the driving heat input at 79 to 98.6°C.

In this application the heat from both the condenser and the absorber is fully recovered because the laboratory users require 26/44°C at inlet and outlet, which matches the available temperature levels. Cooling towers are not needed, which simplifies operation and lowers water and energy use. The hybrid system has the thermal power provided by 30 solar collectors with a total area of 66 m<sup>2</sup> and an auxiliary heat source, respectively a 40 kW natural gas boiler as can be depicted from Figure 1.

The water and 30% wt. ethylene glycol solution from the solar collectors fed a heat exchanger with 3 circuits:

- the first circuit where the water-ethylene glycol solution transfers the heat from solar panels.
- the second circuit (for the cold season) where the temperature of chilled water from absorption heat pump is increased by the simulated load.
- in the third circuit (for the hot season) is prepared the hot water which will action the absorption plant's heat generator.

The parameters were measured using the following sensors (table 1):

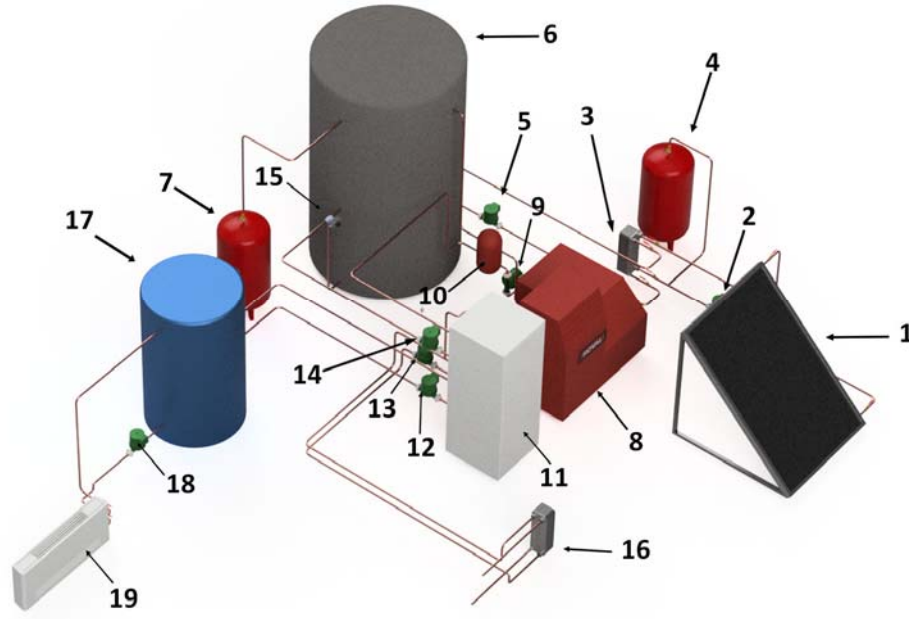
Table 1.

**Measured parameters and their uncertainties**

Instrument	Measured parameter	Range	Uncertainty (%)
<b>Thermocouples (°C)</b>	ARS inlet temperature	0–100 (°C)	± 0.25 K
	ARS outlet temperature	0–100 (°C)	± 0.25 K
<b>Insulated thermocouple type K NiCr-Ni (Immersion length = 50 mm)</b>	ARS circuits	–20–200 (°C)	± 0.1 K
<b>Flow meter (l/min)</b>	ARS circuit fluid flow rate	4–160 (l/min)	± 0.5...2%

The working principle of the heat pump is as follows: in the solar circuit, the solar collectors deliver the thermal power to a solution consisting of water and 30% wt. ethylene glycol. In the heat exchanger, the water-ethylene glycol solution transfers the heat to a hot water circuit used for driving the generator of the absorption refrigerating machine in the hot season.

The heat absorbed by the water from the condenser-absorber group is recovery using a plate heat exchanger by transferring it to the domestic hot circuit from laboratory. When working as refrigeration plant, the installation prepares cold water in the evaporator, which is used to cool down the air in the fan coil unit.



1 – Solar thermal panel, 2 – Hydraulic kit for solar circuit, 3 – PHE, 4 – Expansion vessel (solar circuit), 5 – Pump, 6 – Domestic hot water storage tank, 7 – Expansion vessel (domestic hot water circuit), 8 – Boiler, 9 – Boiler circulation pump, 10 – Hydraulic separator, 11 – Absorption heat pump, 12 – Chilled water pump, 13 – Cooling water pump, 14 – Hot water pump, 15 – Storage tank recirculation pump, 16 – PHE for recovery system, 17 – Chilled water tank, 18 – Chilled water circulation pump, 19 – Fan coil unit

Figure 1. Experimental stand

### 3. Methodology

The AHP cycle is modelled using the energy and mass balances on each cycle component. The temperatures and mass flow rate of the external circuits are from experimental data based recorded between May and August 2025.

The experimental performances of the proposed H<sub>2</sub>O/LiBr AHP stand are obtained in terms of cooling coefficient of performance ( $COP_C$ ), heating coefficient of performance ( $COP_H$ ) and total coefficient of performance ( $COP_{TOTAL}$ ). The  $COP_C$  is defined as the ratio of the cooling output produced by the evaporator ( $Q_E$ ) and driving heat input in the generator ( $Q_G$ ):

$$COP_C = \frac{Q_E}{Q_G} \quad [-] \quad (1)$$

where the cooling output produced by the evaporator ( $Q_E$ ) and the driving heat input in the generator are calculated from their respective energy balance equations:

$$Q_E = \dot{m}_w \cdot c_{pw} \cdot (t_{in \text{ chilled water}} - t_{out \text{ chilled water}}) \quad [\text{kW}] \quad (2)$$

$$Q_G = \dot{m}_{hot \text{ water}} \cdot c_{p \text{ hot water}} \cdot (t_{in \text{ hot water}} - t_{out \text{ hot water}}) \quad [\text{kW}] \quad (3)$$

The  $COP_H$  is defined as the ratio of the heating provided by the condenser ( $Q_C$ ) and the absorber ( $Q_A$ ) to the driving heat input in the generator ( $Q_G$ ) for the applications where the absorber heat is dissipated to the ambient:

$$COP_H = \frac{Q_C + Q_A}{Q_G} \quad [-] \quad (4)$$

where the heating provided by the condenser ( $Q_C$ ) and the absorber ( $Q_A$ ) are calculated from their respective energy balance equations:

$$Q_C = \dot{m}_w \cdot c_{pw} \cdot (t_{out \text{ cooling water condenser}} - t_{in \text{ cooling water condenser}}) \text{ [kW]} \quad (5)$$

$$Q_A = \dot{m}_w \cdot c_{pw} \cdot (t_{out \text{ cooling water absorber}} - t_{in \text{ cooling water absorber}}) \text{ [kW]} \quad (6)$$

Where

$\dot{m}_w$  – mass flow rate of water (kg/s)

$c_{pw}$  – specific heat of water (kJ/kg·K)

Finally, the combined COP ( $COP_{TOTAL}$ ) is calculated by considering both the heating and the cooling outputs of the AHP cycle, which is defined as:

$$COP_{TOTAL} = COP_C + COP_H \quad [-] \quad (7)$$

In these calculations, the pumps (chilled water pump at evaporator P<sub>1</sub>, cooling water pump at condenser and absorber P<sub>2</sub>, hot feed water pump at generator P<sub>3</sub> and H<sub>2</sub>O/LiBr solution pump) and fans (at cooling tower) consumption is included in equation 5.

In the conventional installation at cooling towers, the heat removed from condenser and absorber, as latent heat, will be discharged into the environment in the form of water vapour carried by the outgoing current of air, whose humidity will thus be higher than that of the intake air, normally to the point of saturation. The proposed solution from this study is based to recovery heat from condenser and absorber using for domestic hot water in laboratory from Faculty of Building Services Engineering.

#### 4. Result and discussion

In this research project, the feasibility of a new experimental test bench configuration for an H<sub>2</sub>O/LiBr absorption heat pump (AHP) is investigated for the combined production of cooling and heating under different operating conditions. Thus, the new system can be integrated into several types of end-use applications. A numerical model of the thermodynamic cycle for the AHP was developed, and the operational limits of the cycle in terms of temperature were identified; therefore, the results can be used to determine suitable potential applications for the proposed configuration. Based on the available literature, there is a lack of information regarding heat recovery from the condenser and absorber of an absorption refrigeration system entirely powered by flat-plate solar collectors or by a bivalent system (flat-plate solar collectors + gas-fired boiler).

A novel  $\text{H}_2\text{O}/\text{LiBr}$  absorption heat pump with heat recovery for combined heating and cooling production using renewable energy

The experimental dataset includes nine channels. *Channel 0* records the chilled water supply temperature at the evaporator, and *Channel 1* records the chilled water return temperature at the evaporator. *Channel 2* measures the hot water supply temperature at the generator, while *Channel 3* measures the hot water return temperature at the generator. *Channel 4* tracks the cooling water supply temperature to the condenser and absorber. *Channel 5* tracks the cooling water return temperature from the condenser, and *Channel 6* tracks the cooling water return temperature from the absorber. *Channel 7* logs the absorber cooling water flow rate, and *Channel 8* logs the condenser cooling water flow rate.

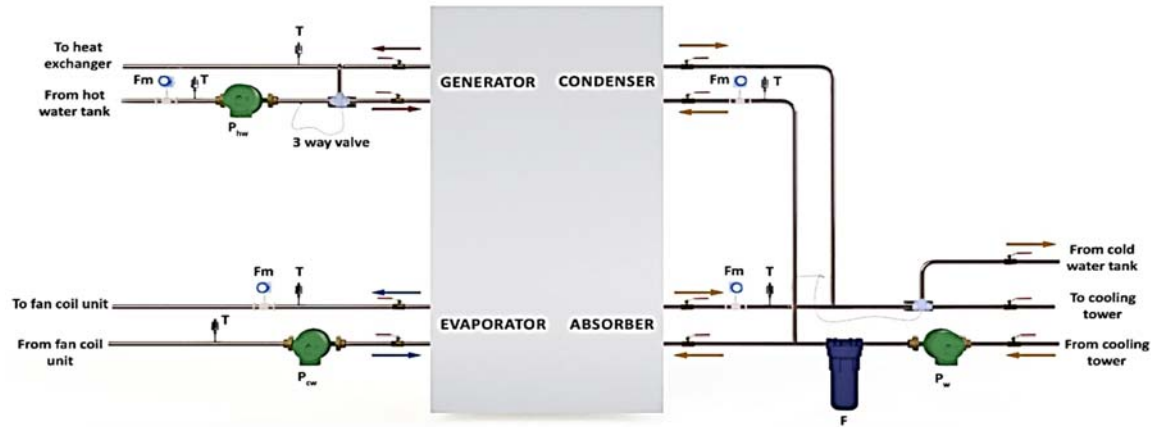


**Figure 2.** Measurement points schematic of the  $\text{H}_2\text{O}/\text{LiBr}$  absorption system

The flow rates were measured with an ultrasonic flowmeter. Chilled water flow rate at evaporator. Each experimental measurement set is recorded every 2 hours from the start-up of the experimental test bench, in order to avoid fluctuations of thermodynamic parameters during long-term operation. For each set, all parameters are measured and logged in real time at 5-minute intervals.

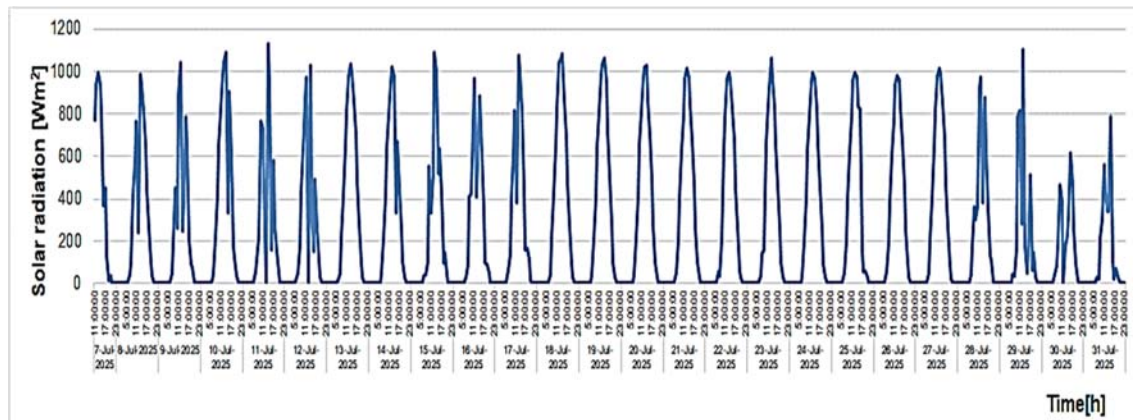


**Figure 3.** Solar radiation recording for July 2025.

The inefficiency of the flat-plate solar collector before 8:00 a.m. and after 5:00 p.m. makes solar radiation negligible outside this time interval as it can be noticed from Figures 3 and 4. Practically, the solar system does not contribute to heating or generating the thermal load outside these hours, as the flat-plate collector cannot capture enough thermal solar energy to drive the absorption refrigeration system. Initially, the solar system does not contribute to meeting the generator's thermal load (**FNP – Fraction of Net Production = 0**).

As the day progresses, the solar panels continue to operate, and during the period roughly between 12:00 and 15:00, the generator covers **80–95% of the required thermal load**. Experimental recordings on the solar system allowed the determination of precise **FNP values for flat-plate solar collectors (FPST)** depending on the climate in Romania, taking into account: geographical location, climatic data, solar panel model, and operating conditions.

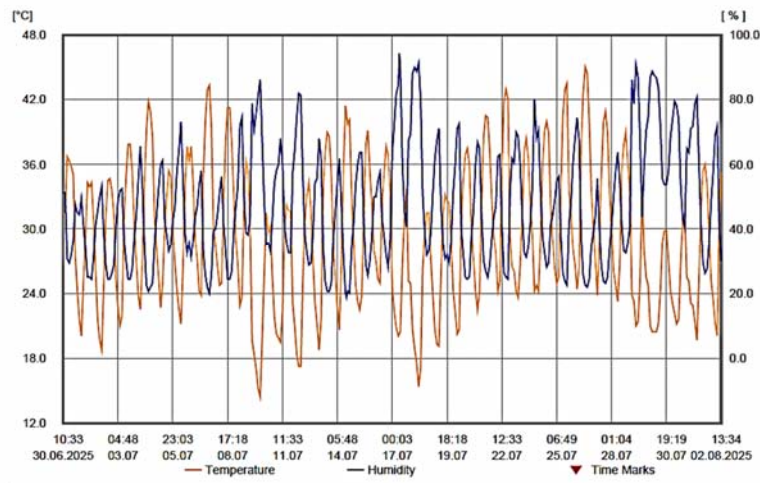


**Figure 4.** Ambient temperature and relative humidity for July 2025

The absorption heat pump delivers chilled water at 6–7 °C to the air-conditioning system with fan coil units, and hot water up to about 44 °C to the recovery circuit from the condenser and absorber, as reported in Table 2. The measured return temperatures are 6.84–7.04 °C for the chilled water circuit and 33.58–43.92 °C for the hot water circuit.

The heat released in the condenser and absorber during the absorption process is not suitable for space heating, since the supply level, around 35 °C, is below the typical heating requirement of about 50 °C. This residual heat is therefore directed to domestic hot water preparation through a water-to-water heat exchanger, which matches the temperature needs while keeping the cycle stable. This configuration improves performance compared with conventional air-conditioning systems. It recovers heat that would otherwise be rejected, removes the need for a cooling tower, and fits low-temperature hydronic networks such as radiant heating circuits.



Table 2.

Characteristic values of the absorption refrigeration system

Condenser/Absorber cooling inlet water temperature [°C]	Calculated Values					
	Cooling capacity [kW]	Generator capacity [kW]	Condenser capacity [kW]	Absorber capacity [kW]	Relative deviation [-]	COP <sub>TOTAL</sub> [-]
26.72	17.3	30.36	18.6	28.72	1.04	4.228
32.34	16.1	30.84	18.64	28.50	0.5	5.092
36.70	15.32	28.41	18.45	27.76	3.65	5.262
36.96	12.86	26.43	15.2	22.56	3.9	5.446

## 5. Conclusions

This paper proposed a novel absorption heat pump (AHP) based on a single-effect H<sub>2</sub>O/LiBr absorption chiller, modified to enable the combined production of cooling and heating for domestic hot water. Unlike a conventional single-effect absorption chiller, where condensation and absorption heat is rejected to the ambient, the proposed system recovers condensation and absorption heat at a useful temperature level. The research focused on introducing advanced heat recovery strategies aimed at improving system-wide heat recovery.

Environmental test of the prototype was performed, and several main conclusions was drawn as follows.

- The experimental stand ran stably to provide 12-17 kW cooling and heating in a wide temperature range from 79 to 98.6°C, with solar thermal ratio of 80-95% in different weather conditions during the period roughly between 12:00 and 15:00
- The COP for cooling (COP<sub>C</sub>) full boiler source reached 0.462 to 0.545 for inlet chilled water temperature range 6.8 to 12.5°C and the COP of cooling (COP<sub>C</sub>) bivalent source reached 1.992 to 2.285 for inlet cooling water temperature range 26.72 to 36.96°C.
- The total COP (cooling COP<sub>C</sub> and heating COP<sub>H</sub>) for bivalent source reached 4.228-5.446 with cooling water temperatures reduced from 43.8 to 26.3°C. Advanced systems have been proposed to improve the system performance with heat recovery provide enhanced of COP over the classic AHP cycle when considering cooling or heating propose.
- results demonstrated that the proposed AHP with recovery system mode has significant energy and carbon reduction potential and is an excellent solution for combined cooling and heating in distributed areas.

The future studies involves validation of the AHP in the lab to confirm simulations and tune the design; size new heat-recovery units for the highest achievable temperatures and nominal flows; if reusing an existing unit, verify temperature, flow, and capacity compatibility, since the AHP must not be bound by a legacy system.

## ACKNOWLEDGEMENT

This research was supported by *GNaC<sup>ARUST</sup><sub>2024</sub>* – *UTCB 20* project from Technical University of Civil Engineering, Bucharest, project number 1404/06.02.2025

## References

- [1] Paris Agreement - <https://www.un.org/en/climatechange/paris-agreement>. (Accessed 29 august 2025)
- [2] G. Wang, E. Sbai, Le Wen, M. S. Sheng - The impact of renewable energy on extreme volatility in wholesale electricity prices: Evidence from organization for economic co-operation and development countries, *Journal of Cleaner Production* 484 (2024) 144343, <https://doi.org/10.1016/j.jclepro.2024.144343>
- [3] Ember - Global electricity review 2023, <https://ember-climate.org/insights/research/global-electricity-review-2023/>. (Accessed 22 august 2025)
- [4] Eurostat - [https://ec.europa.eu/eurostat/statistics-explained/index.php?title=Glossary:Renewable\\_energy\\_sources](https://ec.europa.eu/eurostat/statistics-explained/index.php?title=Glossary:Renewable_energy_sources) (Accessed 29 august 2025)
- [5] European Comision - [https://commission.europa.eu/news-and-media/news/focus-energy-efficiency-buildings-2020-02-17\\_en](https://commission.europa.eu/news-and-media/news/focus-energy-efficiency-buildings-2020-02-17_en). (Accessed 20 July 2025)
- [6] C.Maduta, D. D'Agostino, S. Tsemekidi-Tzeiranaki, L. Castellazzi, G. Melica, P. Bertoldi - Towards climate neutrality within the European Union: Assessment of the Energy Performance of Buildings Directive implementation in Member States, *Energy and Buildings*, Volume 301, 15 December 2023, 113716, <https://doi.org/10.1016/j.enbuild.2023.113716>
- [7] R. Nikbakhti, X. Wang, A. K. Hussein, A. Iranmanesh - Absorption cooling systems – Review of various techniques for energy performance enhancement, *Alexandria Engineering Journal*, Volume 59, Issue 2, April 2020, Pages 707-738, <https://doi.org/10.1016/j.aej.2020.01.036>
- [8] Ghoubali, R.; Byrne, P.; Miriel, J.; Bazantay, F. Simulation study of a heat pump for simultaneous heating and cooling coupled to buildings. *Energy Build* **2014**, 72, 141–149. <https://doi.org/10.1016/j.enbuild.2013.12.047>Get rights and content
- [9] Buonomano, A., *et al.*, Dynamic Simulation and Thermo-Economic Analysis of a Photo Voltaic/Thermal Collector Heating System for an Indoor–Outdoor Swimming Pool, *Energy Conversion and Management*, 99 (2015), July, pp. 176-192
- [10] Ramírez, C.A.; Patel, M.; Blok, K. From fluid milk to milk powder: Energy use and energy efficiency in the European dairy industry. *Energy* **2006**, 31, 1984–2004. <https://doi.org/10.1016/j.energy.2005.10.014>
- [11] Liu, Y.; Groll, E.A.; Yazawa, K.; Kurtulus, O. Theoretical analysis of energy-saving performance and economics of CO<sub>2</sub> and NH<sub>3</sub> heat pumps with simultaneous cooling and heating applications in food processing. *Int. J. Refrig.* **2016**, 65, 129–141. <https://doi.org/10.1016/j.ijrefrig.2016.01.020>
- [12] Liu, Y.; Groll, E.A.; Yazawa, K.; Kurtulus, O. Energy-saving performance and economics of CO<sub>2</sub> and NH<sub>3</sub> heat pumps with simultaneous cooling and heating applications in food processing: Case studies. *Int. J. Refrig.* **2017**, 73, 111–124. <https://doi.org/10.1016/j.ijrefrig.2016.09.014>
- [13] Byrne, P.; Fournaison, L.; Delahaye, A.; Oumeziane, Y.A.; Serres, L.; Loulergue, P.; Szymczyk, A.; Mugnier, D.; Malaval, J.L.; Bourdais, R.; et al. A review on the coupling of cooling, desalination and solar photovoltaic systems. *Renew. Sustain. Energy Rev.* **2015**, 47, 703–717. <https://doi.org/10.1016/j.rser.2015.03.083>
- [14] Eisa, M.A.R.; Devotta, S.; Holland, F.A. Thermodynamic design data for absorption heat pump systems operating on water-lithium bromide: Part III-Simultaneous cooling and heating. *Appl. Energy* **1986**, 25, 83–96. [https://doi.org/10.1016/0306-2619\(86\)90068-1](https://doi.org/10.1016/0306-2619(86)90068-1)
- [15] Kumar, P.; Sane, M.G.; Devotta, S.; Holland, F.A. Experimental studies with an absorption system for simultaneous cooling and heating. *Chem. Eng. Res. Des.* **1985**, 63, 133–136. ISSN 0263-8762
- [16] Juan Prieto, Dereje S. Ayoub, Alberto Coronas - A Novel H<sub>2</sub>O/LiBr Absorption Heat Pump with Condensation Heat Recovery for Combined Heating and Cooling Production: Energy Analysis for Different Applications, *Clean Technol.*

# Analysis of Thermal Comfort in Public Buildings: A Case Study

Analiza confortului termic în clădirile publice. Studiu de caz.

**Natalia BEGLET<sup>1</sup>, Elena NICOLAEV<sup>2</sup>**

<sup>1</sup> Universitatea Tehnică a Moldovei  
168 Ștefan cel Mare și Sfânt, Chișinău, Republica Moldova  
E-mail: [natalia.beglet@acagpm.utm.md](mailto:natalia.beglet@acagpm.utm.md)

<sup>2</sup> Centrul de Excelență în Construcții  
71 Gh. Asachi, Chișinău, Republica Moldova  
E-mail: [elenanycolaev@gmail.com](mailto:elenanycolaev@gmail.com)

DOI: 10.37789/rjce.2025.16.4.2

**Abstract.** *This paper presents study of thermal comfort calculations in public buildings, using Fanger's method and ASHRAE standards. The influence of six main parameters – air temperature, radiant temperature, air velocity, relative humidity, metabolic rate, and clothing insulation – on human comfort sensation is analyzed. Results show that Fanger's method provides a more accurate evaluation of parameter interaction, while ASHRAE offers simplified comfort ranges for practical design. The comfort zone for the analyzed cases ranges between 18–24 °C, depending on specific indoor conditions.*

**Key words:** *thermal comfort, public buildings, Fanger's method, ASHRAE, microclimate, clothing insulation.*

**Rezumat.** *Lucrarea prezintă studiul condițiilor de confort termic în spații publice, utilizând metoda Fanger și datele standardului ASHRAE. Se analizează influența principalilor parametri microclimatici – temperatura aerului, temperatura radiantă, viteza aerului, umiditatea relativă, nivelul de activitate și rezistența termică a îmbrăcămintei – asupra senzației de confort. Rezultatele arată că metoda Fanger permite o evaluare mai exactă a interacțiunii factorilor, în timp ce standardul ASHRAE oferă valori orientative rapide. Intervalul de confort termic pentru spațiile analizate este cuprins între 18–24 °C, în funcție de condițiile specifice.*

**Cuvinte cheie:** *confort termic, clădiri publice, metoda Fanger, ASHRAE, microclimat, îmbrăcămintă.*

## 1. Introducere

Problematica asigurării confortului termic în clădirile publice este esențială pentru proiectarea și exploatarea sistemelor de climatizare, întrucât condițiile interioare adecvate contribuie direct la bunăstarea utilizatorilor, la performanța activităților desfășurate și la reducerea consumului de energie. Confortul termic reprezintă starea de satisfacție a ocupanților față de mediul ambiant și depinde de interacțiunea complexă dintre parametri fizici ai aerului interior și caracteristicile fiziologice ale persoanelor.

Factorii microclimatici – temperatura aerului, temperatura medie radiantă, umiditatea relativă, viteza aerului, activitatea metabolică și rezistența termică a îmbrăcămintei – influențează atât percepția subiectivă a confortului, cât și procesele biologice ale organismului. Abaterile de la intervalele optime pot provoca disconfort, scăderea capacității de concentrare, oboseală, dar și probleme de sănătate, cum ar fi afecțiuni respiratorii sau cardiovasculare. În același timp, menținerea parametrilor microclimatici în limitele recomandate permite o exploatare mai eficientă a instalațiilor de încălzire, ventilație și aer condiționat, reducând pierderile de energie și costurile operaționale.

Metodele consacrate de evaluare a confortului termic includ metoda **Fanger**, care se bazează pe calculul indicelui PMV (Predicted Mean Vote) și PPD (Predicted Percentage of Dissatisfied). Această metodă analizează simultan cei șase parametri relevanți – temperatura aerului, temperatura medie radiantă, umiditatea relativă, viteza aerului, activitatea metabolică și rezistența termică a îmbrăcămintei – pentru a estima nivelul de satisfacție termică a ocupanților. Pe de altă parte, standardele **ASHRAE** (American Society of Heating, Refrigerating and Air-Conditioning Engineers) stabilesc zonele de confort acceptabile, oferind valori orientative și intervale de referință pentru diferite condiții de utilizare, tipuri de activități și perioade ale anului.

În practica proiectării și exploatarei clădirilor publice, aplicarea acestor metode permite nu doar asigurarea unui climat interior sănătos și plăcut, ci și fundamentarea unor strategii eficiente de management energetic. Integrarea evaluării confortului termic cu tehnologii moderne de monitorizare și control – cum ar fi senzori inteligenți, sisteme BMS (Building Management System) și soluții de automatizare – facilitează reglarea dinamică a parametrilor microclimatici, contribuind la creșterea sustenabilității clădirilor și la respectarea normelor de eficiență energetică impuse de legislația națională și europeană.

## 2. Metodologie

Analiza celor trei studii de caz, corespunzătoare unor încăperi administrative și spații de proiectare, a urmărit evaluarea detaliată a condițiilor microclimatice și a impactului acestora asupra confortului termic al ocupanților. Alegerea acestor tipuri de spații nu este întâmplătoare, deoarece ele se caracterizează prin perioade lungi de utilizare, densitate variabilă a ocupanților și activități preponderent sedentare, ceea ce le face deosebit de sensibile la fluctuațiile parametrilor de mediu.

Parametrii considerați în evaluare – **temperatura aerului ( $t_a$ )**, **temperatura medie radiantă ( $t_r$ )**, **viteza aerului ( $u$ )**, **umiditatea relativă**, **nivelul activității metabolice ( $M$ )** și **rezistența termică a îmbrăcăminte ( $clo$ )** – reprezintă factorii cheie ai echilibrului termic dintre corpul uman și mediul ambiant. Temperatura aerului și temperatura medie radiantă determină schimbul de căldură prin convecție și radiație, viteza aerului influențează procesele de evaporare și senzația de prospețime, iar umiditatea relativă afectează atât evaporarea transpirației, cât și percepția generală a confortului. Activitatea metabolică ( $M$ ), exprimată în met (unitate metabolică), reflectă cantitatea de căldură generată de organism în funcție de tipul de activitate (în cazul analizat, activități sedentare de birou, cu valori cuprinse de obicei între 1,0 și 1,2 met), iar rezistența termică a îmbrăcăminte ( $clo$ ) depinde de tipul vestimentației și de stratificarea acesteia, fiind un factor crucial pentru menținerea echilibrului termic individual.

Pentru a determina gradul de confort, a fost aplicată **metoda Fanger**, recunoscută la nivel internațional pentru acuratețea sa în evaluarea percepției termice. Această metodă se bazează pe ecuațiile de bilanț energetic ale corpului uman, calculând **indicele PMV (Predicted Mean Vote)** – care indică votul termic mediu al unui grup de persoane pe o scară de la -3 (foarte rece) la +3 (foarte cald) – și **indicele PPD (Predicted Percentage of Dissatisfied)** – care estimează procentul de ocupanți ce ar putea fi nemulțumiți de condițiile existente, chiar și atunci când PMV se află în zona neutră. Valori ale PMV cuprinse între -0,5 și +0,5, corespunzătoare unui PPD mai mic de 10%, sunt considerate optime pentru confortul termic, conform standardelor internaționale.

Rezultatele obținute prin metoda Fanger au fost comparate cu **standardele ASHRAE 55**, care stabilesc limitele parametrilor de microclimat pentru zonele de confort acceptabile, ținând cont de activități specifice, tipul îmbrăcăminte și condițiile climatice sezoniere. Această comparație a permis verificarea gradului de conformitate al fiecărei încăperi cu valorile recomandate, evidențiind eventualele abateri și indicând măsuri corective. De exemplu, în situațiile în care viteza aerului s-a dovedit prea scăzută, se poate recomanda îmbunătățirea ventilației pentru a evita senzația de aer stagnant, iar în cazurile cu umiditate relativă scăzută, se pot propune soluții de umidificare controlată pentru prevenirea disconfortului respirator și a uscării mucoaselor.

În plus, analiza a relevat că, pentru spațiile administrative și de proiectare, unde activitatea metabolică este redusă și ocupanții petrec multe ore consecutiv, chiar mici deviații ale temperaturii sau umidității pot conduce la scăderea productivității, apariția oboselii și diminuarea capacității de concentrare. Astfel, asigurarea unui microclimat stabil și plăcut nu reprezintă doar o condiție de confort, ci și o necesitate pentru menținerea sănătății și eficienței angajaților.

Integrarea acestor rezultate în strategiile de management al clădirilor permite adoptarea unor soluții inteligente, cum ar fi implementarea sistemelor **BMS (Building Management System)**, care monitorizează și reglează automat parametrii de climatizare în timp real. Corelarea dintre datele obținute prin metoda Fanger și recomandările ASHRAE oferă o bază solidă pentru optimizarea reglajelor instalațiilor

de încălzire, ventilație și aer condiționat (HVAC), contribuind astfel la reducerea consumului de energie, la creșterea duratei de viață a echipamentelor și la îndeplinirea cerințelor actuale de eficiență energetică și sustenabilitate impuse de legislația națională și europeană.

În concluzie, aplicarea unei evaluări complexe a confortului termic, combinând metoda Fanger și standardele ASHRAE, reprezintă un instrument indispensabil pentru proiectarea și exploatarea responsabilă a clădirilor publice, asigurând atât bunăstarea ocupanților, cât și performanța energetică a spațiilor analizate.

### 3. Studiu de caz

Analiza celor trei exemple evidențiază modul în care combinația dintre parametrii microclimatici, tipul activității și caracteristicile vestimentare influențează percepția de confort termic și recomandările pentru climatizarea spațiilor interioare.

#### 3.1. Bibliotecă

Biblioteca reprezintă un spațiu administrativ în care activitatea metabolică a ocupanților este foarte redusă (citit, lucrul la calculator, aranjarea documentelor), ceea ce determină o sensibilitate sporită la variațiile parametrilor microclimatici. Persoanele prezente petrec perioade îndelungate în același loc, iar confortul termic devine esențial atât pentru menținerea stării de bine, cât și pentru productivitatea activităților. În astfel de încăperi, echilibrul dintre temperatura aerului, umiditatea relativă și viteza de circulație a aerului are o importanță critică, mai ales în condițiile unei îmbrăcăminti ușoare.

#### Parametri măsurați și implicații:

- **Îmbrăcăminte: 0,6 clo** – Valoarea indică o vestimentație ușoară, tipică sezonului cald sau unui interior bine încălzit (de exemplu, cămașă subțire, pantaloni ușori). Rezistența termică redusă a îmbrăcăminteii limitează capacitatea corpului de a reține căldura, ceea ce înseamnă că orice scădere a temperaturii aerului sub intervalul optim poate fi percepută rapid ca senzație de frig.
- **Viteză aer: 0,1 m/s** – Este o valoare foarte scăzută, caracteristică unui spațiu static, cu ventilație slabă sau difuză. Deși lipsa curenților de aer reduce riscul de disconfort datorat „zugrăvirii” (curenți reci percepuți ca neplăcuți), ea limitează și posibilitatea organismului de a-și regla temperatura prin convecție. Astfel, ocupanții pot simți aerul mai „greu” și pot resimți mai puternic eventualele diferențe dintre temperatura aerului și cea a suprafețelor radiante (pereți, ferestre, mobilier).
- **Umiditate relativă: 60%** – Se află în zona optimă pentru confort, contribuind la menținerea unei senzații plăcute și prevenind uscarea mucoaselor respiratorii.

Totuși, dacă temperatura aerului scade, umiditatea poate accentua percepția de răcoare prin diminuarea pierderilor de căldură prin evaporare.

### Rezultate și comparație cu standarde:

- **Metoda Fanger:** Calculul indicilor PMV și PPD a condus la **valori nerealiste pentru temperatura aerului**, un fenomen explicabil prin combinația de activitate metabolică foarte redusă și îmbrăcăminte subțire. În aceste condiții, ecuațiile de echilibru termic pot genera abateri, deoarece organismul uman reacționează mai sensibil la variațiile de temperatură radiantă decât la cele ale aerului propriu-zis.
- **Standard ASHRAE:** Zona de confort termic recomandată este cuprinsă între **23 și 24 °C**, fiind ideală pentru activități sedentare desfășurate cu o vestimentație ușoară. Menținerea temperaturii în acest interval permite ca valoarea PMV să se apropie de zero (neutralitate termică), iar PPD să rămână sub pragul de 10%, corespunzător unui procent mic de persoane nemulțumite.

### Interpretare și implicații practice:

- La o **viteză de aer atât de scăzută**, corpul pierde căldură aproape exclusiv prin radiație și conducție, ceea ce face ca diferențele dintre temperatura aerului și temperatura suprafețelor interioare să aibă un efect direct asupra senzației de confort. De exemplu, dacă pereții sau ferestrele au o temperatură mai scăzută decât aerul interior, ocupanții pot percepe o senzație de frig chiar dacă termometrul indică valori în intervalul optim.
- **Stabilitatea climatică** devine crucială, deoarece variațiile bruște de temperatură sau umiditate pot fi percepute imediat și pot provoca disconfort. Sistemele de climatizare trebuie să mențină parametrii constanți, evitând oscilațiile frecvente.
- Întrucât activitatea metabolică este foarte redusă, **posibilitățile de autoreglare termică ale organismului sunt limitate**, ceea ce face ca și abateri minore (0,5–1 °C) să fie resimțite.

### Recomandări pentru exploatare:

1. **Monitorizarea temperaturii radiante** – Utilizarea senzorilor pentru măsurarea temperaturii pereților și a suprafețelor vitrate, pentru a preveni disconfortul cauzat de radiații reci sau calde.
2. **Control precis al temperaturii aerului** – Menținerea valorilor între 23 și 24 °C, cu o toleranță maximă de  $\pm 0,5$  °C, mai ales în sezonul rece.
3. **Ventilație discretă dar constantă** – Chiar dacă viteza aerului trebuie să rămână mică pentru a evita curenții, este necesară o ventilație minimă pentru asigurarea calității aerului și prevenirea stăgării.

4. **Echipamente de reglaj automat** – Implementarea unui sistem de management al clădirii (BMS) care să ajusteze în timp real parametrii microclimatici, în funcție de variațiile de ocupare și de condițiile exterioare.

Biblioteca, ca spațiu administrativ cu activitate redusă și îmbrăcăminte ușoară, impune o **mare precizie în reglarea climatului interior**. Intervalul de confort de 23–24 °C conform ASHRAE este adecvat, dar trebuie dublat de un control atent al temperaturii radiante și al umidității, pentru a evita disconfortul care poate apărea chiar și la abateri minime.

### 3.2. Birou

Biroul este un spațiu tipic pentru activități de tip sedentar (scriere, lucru la calculator, convorbiri telefonice), caracterizate printr-un nivel metabolic redus (aprox. 1,2 met). Spre deosebire de bibliotecă, unde vestimentația era ușoară, aici este analizată situația sezonului rece, cu **îmbrăcăminte groasă de 1,5 clo**, ceea ce influențează considerabil percepția de confort.

#### Parametri măsurați și implicații:

- **Îmbrăcăminte: 1,5 clo (iarna)** – Acest nivel corespunde unei vestimentații groase (sacou, pulover, cămașă, pantaloni groși, încălțăminte de iarnă). Rezistența termică ridicată a îmbrăcăminte reduce pierderile de căldură prin convecție și radiație, ceea ce permite ca ocupanții să se simtă confortabil și la temperaturi mai scăzute ale aerului ( $\approx 18,5$  °C). Totuși, același factor poate genera **supraîncălzire** dacă temperatura aerului urcă peste 23,5 °C.
- **Viteză aer: 0,2 m/s** – O valoare corespunzătoare pentru spații de birouri. Este suficientă pentru a asigura un schimb minim de aer, prevenind senzația de aer stagnant, dar nu atât de mare încât să creeze curenți neplăcuți. Contribuie, astfel, la reglarea subtilă a pierderilor de căldură prin convecție.
- **Umiditate relativă: 50%** – În intervalul optim recomandat de ASHRAE (30–60%). Menține o bună calitate a aerului, prevenind uscarea mucoaselor și favorizând o senzație termică neutră.

#### Rezultate și comparație cu standarde:

- **Zona de confort ASHRAE (pentru 1,5 clo):** între 18,5–23,5 °C, cu limită superioară admisă de 25,5 °C.
- **Zona de confort pentru 1 clo:** se restrânge la 20,5–23,5 °C, ceea ce reflectă necesitatea ajustării temperaturii odată cu reducerea stratului de îmbrăcăminte.

Această variație evidențiază faptul că **îmbrăcăminte este un factor decisiv** pentru reglarea confortului în spațiile administrative. O temperatură care iarna poate fi



percepută ca neutră (ex. 19 °C cu îmbrăcăminte groasă) ar fi resimțită ca rece vara, când ocupanții poartă haine mai subțiri.

### Interpretare și implicații practice:

- **Iarna:** Îmbrăcămintea groasă permite reducerea temperaturii de încălzire până la ~18,5 °C, ceea ce poate conduce la **economii de energie** semnificative în clădirile de birouri. Totuși, depășirea limitei superioare de 23,5 °C, mai ales în încăperi cu suprafețe vitrate mari și expunere la soare, poate provoca senzația de supraîncălzire.
- **Primăvara/vara:** Odată cu reducerea stratului de îmbrăcăminte (1 clo sau mai puțin), temperatura aerului trebuie ajustată în sus (20,5–23,5 °C), pentru a menține confortul și a preveni senzația de frig.
- **Rolul vitezei aerului:** Valoarea de 0,2 m/s este optimă pentru a evita stagnarea aerului și pentru a sprijini mecanismele naturale de termoreglare ale organismului, fără a provoca curenți percepuți ca neplăcuți.

### Recomandări pentru exploatare:

1. **Reglarea temperaturii în funcție de sezon și vestimentație:**
  - Iarna: menținerea temperaturii în intervalul **19–22 °C**.
  - Vara/primăvara: ajustarea la **21–23 °C**, corelat cu vestimentația mai ușoară.
2. **Monitorizarea temperaturii radiante:** În spațiile cu suprafețe vitrate mari, diferențele dintre temperatura aerului și cea a pereților/ferestrelor pot genera disconfort.
3. **Control individual (unde este posibil):** Birourile dotate cu termostate locale sau sisteme de ventilație reglabile permit adaptarea mai precisă la preferințele ocupanților.
4. **Optimizarea consumului energetic:** Ajustarea setărilor HVAC în funcție de sezon și îmbrăcămintea estimată a ocupanților poate reduce semnificativ costurile energetice, fără a compromite confortul.

Biroul, ca spațiu administrativ utilizat pe termen lung, necesită un **management flexibil al microclimatului**. Îmbrăcămintea groasă (1,5 clo) permite reducerea temperaturii până la 18,5 °C, dar riscul de supraîncălzire crește rapid peste 23,5 °C. În perioadele calde, zona de confort se deplasează la 20,5–23,5 °C, subliniind necesitatea adaptării continue a parametrilor în funcție de sezon și vestimentație. Astfel, confortul termic poate fi menținut la nivel optim, în paralel cu reducerea consumului de energie.

### 3.3. Spațiu de proiectare

Spațiul de proiectare este destinat activităților intelectuale cu un nivel metabolic ușor superior celui de birou clasic ( $\approx 116 \text{ W/m}^2$ ), datorită mobilității mai mari și manipulării frecvente a documentelor sau echipamentelor. Condițiile analizate corespund unui sezon cald, când vestimentația este redusă la **0,5 clo**, ceea ce influențează semnificativ percepția de confort.

#### Parametri măsurați și implicații:

- **Îmbrăcăminte: 0,5 clo (vară)** – Corespunde unei vestimentații foarte ușoare (tricou subțire, pantaloni lejeri, încălțăminte ușoară). Rezistența termică redusă favorizează pierderea rapidă de căldură, dar face ocupanții mult mai sensibili la temperaturi scăzute și la curenții de aer. Zona de confort se restrânge în jurul temperaturii de **21,5 °C**, cu un interval acceptabil relativ îngust.
- **Viteză aer: 0,5 m/s** – Valoare peste media pentru spațiile administrative. Asigură un schimb bun de aer și o senzație de prospețime, însă la temperaturi mai joase poate genera **senzația de disconfort prin curenți**. În condițiile analizate, viteza ridicată contribuie la intensificarea pierderilor de căldură prin convecție.
- **Umiditate relativă: 80%** – Semnificativ peste intervalul optim recomandat (30–60%). La acest nivel, organismul întâmpină dificultăți în procesul de evaporare a transpirației, ceea ce reduce eficiența mecanismului natural de termoreglare. Senzația termică resimțită este mai grea și mai puțin plăcută, chiar dacă temperatura aerului se menține în zona neutră.

#### Rezultate și comparație cu standarde:

- **Zona de confort estimată (pentru 0,5 clo, 0,5 m/s și umiditate 80%):  $\approx 21\text{--}22 \text{ °C}$ .**
- **Efectul radiației solare:** expunerea la câștiguri solare suplimentare permite reducerea temperaturii aerului cu **0,5–1 °C**, menținând senzația neutră de confort.
- **Raport cu ASHRAE:** standardele indică zone mai largi de confort pentru valori normale ale umidității (până la 60%), însă aici umiditatea ridicată și viteza aerului restrâng considerabil intervalul acceptabil.

#### Interpretare și implicații practice:

- **Influența vitezei aerului:** La 0,5 m/s, ocupanții percep o intensificare a senzației de răcoare. În condiții de vară, acest efect este pozitiv, dar necesită atenție pentru a evita disconfortul atunci când temperatura scade sub **21 °C**.
- **Impactul umidității ridicate:** Menținerea RH la 80% creează un microclimat greu de tolerat pe termen lung. Evaporarea transpirației este diminuată, iar

ocupanții pot resimți oboseală sau disconfort termic chiar și la temperaturi moderate.

- **Rolul radiației solare și al echipamentelor tehnice:** Prezența calculatoarelor, iluminării intense și a altor surse de căldură crește sarcina termică internă, ceea ce justifică scăderea temperaturii optime de aer sub nivelul utilizat în spațiile administrative.

#### Recomandări pentru exploatare:

##### 1. Reglarea temperaturii:

- Interval optim: **21–22 °C**, cu posibilitatea reducerii la **20,5–21 °C** în prezența radiației solare sau a sarcinii interne crescute.

2. **Controlul vitezei aerului:** Menținerea la max. 0,5 m/s; la temperaturi mai scăzute, reducerea vitezei pentru a preveni senzația de curent rece.

3. **Umiditatea relativă:** Scăderea valorii spre 60% este esențială pentru creșterea confortului și prevenirea problemelor de sănătate (mucegai, aer greu respirabil).

4. **Managementul sarcinii interne:** Utilizarea corpurilor de iluminat eficiente și a echipamentelor cu consum redus de energie pentru a limita aporturile termice nedorite.

Spațiul de proiectare, caracterizat prin vestimentație foarte ușoară (0,5 clo), viteză a aerului relativ ridicată (0,5 m/s) și umiditate mare (80%), are o zonă de confort restrânsă, centrată pe 21–22 °C. Radiația solară și echipamentele tehnice pot justifica reducerea suplimentară a temperaturii aerului pentru a evita supraîncălzirea percepută. Gestionarea atentă a umidității și a vitezei aerului este decisivă pentru menținerea unui microclimat adecvat și pentru prevenirea disconfortului.

#### 4. Analiză comparativă a spațiilor administrative și de proiectare

##### 4.1. Parametrii de intrare

Tabelul 1

Analiza comparativă a parametrilor de confort termic în diferite spații interioare

Parametru	Exemplul 1 – Bibliotecă	Exemplul 2 – Birou	Exemplul 3 – Spațiu de proiectare
Îmbrăcăminte (clo)	0,6 clo (ușoară)	1,5 clo (grea, iarna)	0,5 clo (foarte ușoară, vară)
Viteză aer (m/s)	0,1 (foarte scăzută)	0,2 (optimă, discretă)	0,5 (ridicăta)
Umiditate relativă (%)	60% (optimă)	50% (optimă)	80% (excesivă)
Activitate	Foarte redusă (citit,	Redusă (≈1,2 met)	Ușor mai intensă (≈116

Parametru	Exemplul 1 – Bibliotecă	Exemplul 2 – Birou	Exemplul 3 – Spațiu de proiectare
metabolică	lucrat la PC)		W/m <sup>2</sup> )
Interval confortabil (°C)	23–24 °C	18,5–23,5 °C (1,5 clo) / 20,5–23,5 °C (1 clo)	21–22 °C (restrâns)

#### 4.2. Influența factorilor principali

- **Îmbrăcămintea:**

- Bibliotecă: îmbrăcămintea subțire (0,6 clo) → sensibilitate mare la scăderea temperaturii.
- Birou: îmbrăcămintea groasă (1,5 clo) → permite temperaturi mai joase (18,5 °C), dar crește riscul de supraîncălzire >23,5 °C.
- Spațiu de proiectare: vestimentație foarte ușoară (0,5 clo) → zona de confort foarte restrânsă, ocupanții devin vulnerabili la curenți și scăderi de temperatură.

- **Viteza aerului:**

- Bibliotecă: foarte scăzută (0,1 m/s) → confort stabil, dar aer stagnant.
- Birou: moderată (0,2 m/s) → echilibru între ventilație și evitarea curenților.
- Spațiu de proiectare: ridicată (0,5 m/s) → senzație de răcoare binevenită vara, dar poate genera disconfort sub 21 °C.

- **Umiditatea relativă:**

- Bibliotecă & Birou: optimă (50–60 %), condiții confortabile.
- Proiectare: excesivă (80 %) → transpirația nu se evaporă eficient, senzație de aer greu și disconfort.

#### 4.3. Comparație cu standardele (ASHRAE & Fanger)

- **Bibliotecă:** Standardul ASHRAE confirmă zona îngustă de confort (23–24 °C). Fanger poate da abateri la valori scăzute din cauza metabolismului minim și îmbrăcămintei subțiri.
- **Birou:** Standardul ASHRAE evidențiază rolul vestimentației – zona se lărgeste/îngustează în funcție de clo. Posibilitatea de economii energetice prin setarea temperaturii mai jos iarna.

- **Proiectare:** Condițiile reale (RH=80 %) nu respectă recomandările ASHRAE. Zona de confort este mai restrânsă decât cea teoretică, iar viteza mare a aerului accentuează pierderile de căldură.

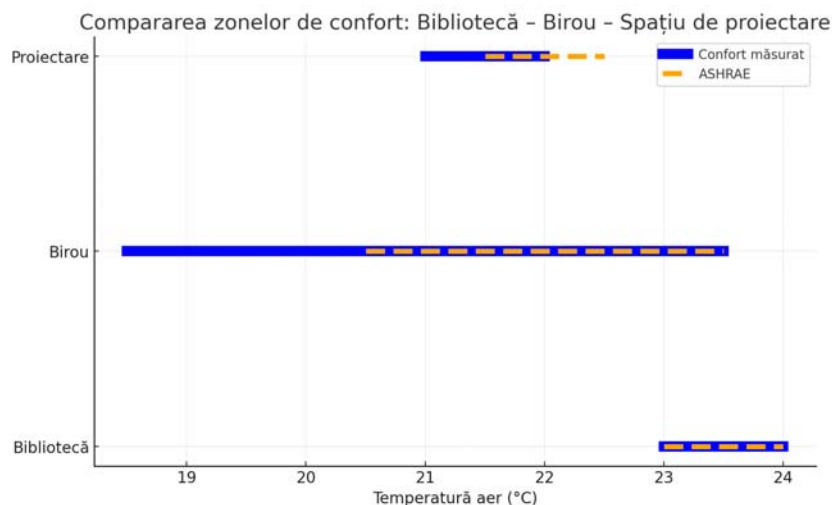


Fig. 1. Graficul comparativ al zonelor de confort

Din graficul comparativ al zonelor de confort pentru cele trei spații se observă cu **albastru** → intervalul de confort măsurat în fiecare spațiu, cu **portocaliu** → intervalul recomandat de ASHRAE pentru condiții standard.

Din grafic se observă că în bibliotecă: zona măsurată se aliniază bine cu ASHRAE, fiind foarte îngustă (23–24 °C), pentru birou: zona măsurată iarna (18,5–23,5 °C) este mai largă decât zona ASHRAE pentru 1 clo (20,5–23,5 °C), evidențiind flexibilitatea permisă de îmbrăcămintea groasă, pentru spațiu de proiectare: zona măsurată (21–22 °C) este restrânsă, apropiată de limitele ASHRAE, cu umiditate ridicată și viteză a aerului ce pot reduce confortul perceput. Graficul permite vizualizarea rapidă a diferențelor și evidențiază importanța **vestimentației, vitezei aerului și umidității** în reglarea confortului termic.

#### 4.4. Implicații practice pentru exploatare

În bibliotecă, microclimatul este extrem de sensibil și trebuie menținut într-un interval foarte îngust, de aproximativ **23–24 °C**. Stabilitatea este esențială nu doar pentru confortul utilizatorilor, ci și pentru protejarea fondului de carte, care poate fi afectat de variații chiar și mici de temperatură și umiditate. Variațiile de temperatură sunt resimțite imediat de către vizitatori, dar în același timp pot accelera procesele de degradare a hârtiei și cernelurilor. Prin urmare, este necesar un **control strict al temperaturii radiante** (pereți, ferestre, tavane), precum și evitarea zonelor reci sau supraîncălzite care ar putea genera curenți de aer sau condens. O soluție eficientă o reprezintă utilizarea sistemelor de **climatizare radiantă** sau a suprafețelor termoactive, împreună cu un sistem precis de monitorizare și reglare automată.

În spațiile de birouri, intervalul de confort este mai larg, situat între **18,5–23,5 °C**, ceea ce oferă o anumită flexibilitate în exploatare. Factorul principal care permite această variație îl constituie **adaptabilitatea vestimentației** (îmbrăcăminte mai groasă iarna și mai lejeră vara). Totuși, aceste spații sunt expuse riscului de **supraîncălzire**, în special datorită radiației solare directe și a sarcinilor interne provenite de la echipamentele IT și iluminat. Managementul temperaturii trebuie să fie **sezonier și adaptiv**, prin implementarea unor strategii precum:

- reducerea temperaturii setate iarna pentru economisirea energiei,
- controlul radiației solare prin **jaluzele exterioare, geamuri cu protecție solară sau pergole**,
- ventilare naturală controlată în perioadele intermediare.

Aceste măsuri permit menținerea confortului termic și, în același timp, reducerea costurilor de exploatare.

Zonele destinate activităților de proiectare sunt cele mai problematice din punct de vedere al confortului și sănătății ocupanților, deoarece necesită un interval foarte restrâns de **21–22 °C**. Confortul termic este puternic influențat de **umiditatea relativă ridicată** și de **viteza aerului**, care pot genera disconfort prin senzația de curenți reci sau de aer uscat. Din acest motiv, aceste spații impun un **control riguros al umidității**, menținându-se valorile în jur de 60% și evitând depășirea acestui prag. Totodată, este necesară **reglarea vitezei aerului** la nivelul zonelor ocupate pentru a preveni disconfortul local.

Un alt factor esențial îl constituie **sarcina internă de căldură** provenită de la echipamentele utilizate (stații grafice, monitoare mari, servere locale). Pentru a limita creșterea temperaturii și a reduce consumul de energie al sistemelor de climatizare, este recomandată utilizarea de **echipamente și surse de iluminat cu randament ridicat și emisii reduse de căldură** (LED, aparatură cu consum redus). În plus, proiectarea acestor spații ar trebui să ia în calcul **sisteme avansate de ventilare cu recuperarea căldurii**, care asigură atât calitatea aerului, cât și un microclimat stabil.

Tabelul 2

**Sinteza parametrilor de confort și a soluțiilor de optimizare pentru diferite tipuri de spații**

Spațiu	Interval de temperatură (°C)	Sensibilitate la variații	Factori critici	Soluții recomandate
<b>Biblioteca</b>	23–24	Foarte mare	Stabilitate termică, radianță	Climatizare radiantă, control automatizat
<b>Birou</b>	18,5–23,5	Medie	Radiație solară, sarcini interne	Jaluzele exterioare, ventilație naturală, management sezonier
<b>Spațiu de proiectare</b>	21–22	Mare	Umiditate, curenți de aer, sarcini interne	Control umiditate, echipamente eficiente, ventilare cu recuperare

## 5. Concluzii și recomandări finale

Analiza condițiilor de microclimat pentru diferite tipuri de spații (bibliotecă, birou, spațiu de proiectare) a evidențiat importanța diferențierii strategiilor de control climatic în funcție de destinația încăperilor.

Astfel, bibliotecile necesită un microclimat extrem de stabil, cu interval foarte restrâns al temperaturii (23–24 °C), pentru protecția fondului de carte și confortul utilizatorilor. Birourile dispun de o zonă de confort mai largă (18,5–23,5 °C), ceea ce permite flexibilitate și posibilități de economisire a energiei, dar cu riscul supraîncălzirii. În schimb, spațiile de proiectare sunt cele mai problematice, datorită sensibilității la umiditate și curenți de aer, necesitând un interval strict (21–22 °C) și un control atent al umidității și sarcinii interne.

Rezultatele confirmă faptul că **stabilitatea parametrilor de microclimat este esențială** pentru confortul termic, sănătatea ocupanților și eficiența energetică. Mai mult, se dovedește că **tehnologiile moderne și soluțiile pasive** pot contribui semnificativ la reducerea consumului de energie și la menținerea condițiilor optime.

În acest sens, se recomandă:

- implementarea unui **sistem integrat de monitorizare și control (BMS)** pentru reglarea în timp real a temperaturii, umidității și vitezei aerului;
- aplicarea unor **strategii diferențiate de climatizare** în funcție de tipul spațiului: climatizare radiantă în biblioteci, control flexibil și sezonă în birouri, control riguros al umidității și echipamente eficiente în spațiile de proiectare;
- utilizarea soluțiilor **pasive de reducere a sarcinii termice** (jaluzele exterioare, geamuri cu protecție solară, ventilație naturală controlată);
- optimizarea consumului energetic prin **adaptarea vestimentației utilizatorilor** și informarea acestora asupra rolului său în menținerea confortului;
- adoptarea **ventilației adaptive și a recuperării de energie** pentru reducerea pierderilor și menținerea calității aerului interior;
- corelarea permanentă a datelor obținute prin metode validate (ex. Fanger PMV/PPD) cu standardele internaționale (ASHRAE, EN, ISO), pentru fundamentarea deciziilor și asigurarea durabilității în exploatarea clădirilor.

În concluzie, **integrarea măsurilor de control climatic cu soluțiile de eficiență energetică și standardele internaționale reprezintă cheia realizării unui echilibru optim între confortul ocupanților, conservarea resurselor și performanța energetică a clădirilor publice.**

## Referințe

- [1] Fanger, P.O. Thermal Comfort: Analysis and Applications in Environmental Engineering. New York: McGraw-Hill, 1970.
- [2] ASHRAE Standard 55-2021. Thermal Environmental Conditions for Human Occupancy. Atlanta: American Society of Heating, Refrigerating and Air-Conditioning Engineers, 2021.
- [3] ISO 7730:2005. Ergonomics of the Thermal Environment – Analytical Determination and Interpretation of Thermal Comfort Using Calculation of the PMV and PPD Indices and Local Thermal Comfort Criteria. Geneva: International Organization for Standardization, 2005.

- [4] Begleț, Natalia; Colomieț, Tatiana. *Termotehnica construcțiilor: Îndrumar aplicativ pentru orele practice*. Chișinău: Tehnica-UTM, 2024. 78 p. ISBN 978-9975-64-382-5.
- [5] Begleț, N.; Nicolaev, E.; Haiducova, M.; Leanca, L., *Evoluția cerințelor de performanță energetică a clădirilor în Republica Moldova: analiză comparativă și aplicații practice*. În: Conferințele „Energie, Eficiență, Ecologie și Educație” (ediția a VIII-a) și „Instalații pentru construcții și economia de energie” (ediția a XXXV-a), 11–12 iulie 2025, Iași. ISSN 2069-1211.
- [6] Haiducova, M.; Șapovalov, N.; Begleț, N.; *Contribuția reabilitării termice la dezvoltarea durabilă a instituțiilor preșcolare*, În: Conferințele „Energie, Eficiență, Ecologie și Educație” (ediția a VIII-a) și „Instalații pentru construcții și economia de energie” (ediția a XXXV-a), 11–12 iulie 2025, Iași. ISSN 2069-1211.
- [7] Begleț, N.; Nicolaev, E.; M.; Leanca, L., *Evaluarea eficienței energetice în instituțiile de învățământ din Republica Moldova: Studiu de caz pe baza rapoartelor de audit energetic elaborate în cadrul proiectului GIZ*, În: Conferințele „Energie, Eficiență, Ecologie și Educație” (ediția a VIII-a) și „Instalații pentru construcții și economia de energie” (ediția a XXXV-a), 11–12 iulie 2025, Iași. ISSN 2069-1211.
- [8] Olesen, B.W. “International Standards for the Indoor Environment.” *Indoor Air*, vol. 12, no. 4, 2002, pp. 18–26.
- [9] Frontczak, M., Wargocki, P. “Literature Survey on How Different Factors Influence Human Comfort in Indoor Environments.” *Building and Environment*, vol. 46, no. 4, 2011, pp. 922–937.
- [10] Parsons, K. *Human Thermal Environments: The Effects of Hot, Moderate, and Cold Environments on Human Health, Comfort and Performance*. 3rd ed., London: CRC Press, 2014.
- [11] EN 16798-1:2019. *Energy Performance of Buildings – Ventilation for Buildings – Indoor Environmental Input Parameters for Design and Assessment of Energy Performance of Buildings*. Brussels: European Committee for Standardization (CEN), 2019.
- [12] Al horr, Y., Arif, M., Katafygiotou, M., Mazroei, A., Kaushik, A., Elsarrag, E. “Impact of Indoor Environmental Quality on Occupant Well-being and Comfort: A Review of the Literature.” *International Journal of Sustainable Built Environment*, vol. 5, no. 1, 2016, pp. 1–11.
- [13] Nikolopoulou, M., Steemers, K. “Thermal Comfort and Psychological Adaptation as a Design Strategy for Outdoor Spaces.” *Building and Environment*, vol. 38, no. 1, 2003, pp. 381–393.
- [14] Carlucci, S., Causone, F., De Rosa, F., Pagliano, L. “A Review of Indices for Assessing Visual, Thermal, Acoustic, and Indoor Air Quality Comfort in Built Environments.” *Building and Environment*, vol. 86, 2015, pp. 190–201.



# Strategies for reducing energy consumption in existing buildings through ecological renovation

Strategii de reducere a consumului de energie în clădirile existente prin renovare ecologică

Horia- Alexandru VARSA<sup>1</sup>, Catalin LUNGU<sup>1,\*</sup>, Tiberiu CATALINA<sup>1</sup>

<sup>1</sup>Technical University of Civil Engineering Bucharest  
124 Lacul Tei Blvd., Bucharest, Romania

E-mail: [tiberiu.catalina@utcb.ro](mailto:tiberiu.catalina@utcb.ro), [catalin.lungu@utcb.ro](mailto:catalin.lungu@utcb.ro), [horia.varsa@utcb.ro](mailto:horia.varsa@utcb.ro)

DOI: 10.37789/rjce.2025.16.4.3

**Abstract.** *This paper presents an original approach to energy-efficient renovation of existing buildings by evaluating thermal insulation materials and their impact on energy consumption and CO<sub>2</sub> emissions. Five insulation scenarios were analyzed using simulation software, focusing on both environmental and economic performance. The results highlight the effectiveness of innovative and sustainable solutions, providing guidelines for optimizing thermal insulation in line with the European Green Deal and EPBD 2024 requirements.*

**Key words:** *energy-efficient renovation, thermal insulation, CO<sub>2</sub> emissions, existing buildings, simulation, European Green Deal, EPBD 2024*

**Rezumat.** *Articolul prezintă o abordare originală a renovării eficiente energetic a clădirilor existente prin evaluarea materialelor termoizolante și a impactului acestora asupra consumului de energie și emisiilor de CO<sub>2</sub>. Au fost analizate cinci scenarii de izolație folosind software de simulare, concentrându-se pe performanța de mediu și economică. Rezultatele evidențiază eficiența soluțiilor inovative și durabile, oferind ghiduri pentru optimizarea izolației termice conform Green Deal-ului European și cerințelor EPBD 2024.*

**Cuvinte cheie:** *renovare eficientă energetic, izolație termică, emisii CO<sub>2</sub>, clădiri existente, simulare, Green Deal European, EPBD 2024*

## 1. Introduction

The present article addresses a critically important and timely topic in the context of global climate change and the urgent need to reduce CO<sub>2</sub> emissions:

---

The article was received on 20.10.2025, accepted on 27.10.2025 and published on 27.11.2025

strategies for enhancing energy efficiency in existing buildings through ecological renovation. By conducting a comparative analysis of both conventional and ecological thermal insulation materials, this study aims to provide practical, sustainable, and scalable solutions for improving the energy performance of the existing building stock.

The selection of this topic is motivated by the authors' professional expertise in building installations, combined with a strong commitment to environmental protection.

Buildings account for approximately 40% of global energy consumption and a similar share of greenhouse gas emissions 37% in 2021 [1], highlighting the pressing need for effective interventions. In this context, ecological renovation of office buildings represents one of the most impactful approaches to reduce carbon footprint and support the European Union's sustainability agenda.

In the current context of climate challenges and increasingly strict energy-efficiency regulations in the construction sector, the choice of thermal insulation materials has become crucial, not only in terms of performance but also from a long-term sustainability perspective. Life Cycle Assessment (LCA) is a key tool in this evaluation, quantifying environmental impacts from raw material extraction to end-of-life. Recent studies illustrate this multidimensional approach: Valentini et al. (2025) [18] show that combining high-performance insulation with recycling strategies can significantly reduce carbon footprints in Italy; Kilis, Ploskas, and Panaras (2025) [19] propose a framework integrating LCA, economic, and technical criteria to optimize insulation type and thickness, highlighting trade-offs between thermal efficiency, environmental impact, and cost; and Ramakrishnan and Jambunathan (2025) [20] demonstrate that EPS-enhanced concrete provides both improved thermal insulation and lower greenhouse gas emissions. Collectively, these works emphasize that insulation selection should balance thermal performance, sustainability, and lifecycle considerations

This research is driven by the aspiration to contribute to a healthier built environment for future generations through the implementation of ecological solutions capable of significantly reducing CO<sub>2</sub> emissions. Practical experience in the field has revealed the potential of sustainable insulation materials, as well as the necessity for rigorous scientific evaluation of their performance in comparison with traditional alternatives.

The novelty and relevance of this study are reinforced by the evolving European legislative and normative framework. The European Level framework, launched by the European Commission in 2017, provides a standardized methodology for assessing building sustainability throughout their life cycle, incorporating energy performance, environmental impact, occupant health and comfort, and climate resilience. [2]

International initiatives such as BREEAM, LEED, and the Passivhaus standard further emphasize the growing importance of ecological renovation. Moreover, the European Green Deal and the objective of climate neutrality by 2050 position energy-efficient renovation at the core of sustainable construction strategies. [3] [4]

The originality of this research lies in the comprehensive comparative evaluation of five insulation materials: expanded and extruded polystyrene

(conventional solutions) versus basalt wool, sheep wool, cellulose, wood fibers. Both energy performance and environmental impact are analyzed to achieve the following objectives:

- Perform a comparative assessment of the energy efficiency of conventional versus ecological insulation materials in the context of renovating an existing office building;
- Quantify the environmental impact of each insulation material, with a focus on CO<sub>2</sub> emissions throughout their life cycle;
- Demonstrate the viability of ecological materials as sustainable alternatives to conventional solutions;
- Provide practical recommendations for industry professionals to facilitate widespread adoption of ecological insulation;
- Contribute to the application of Level principles and other international sustainability standards in Romanian construction practice.

This study adopts a mixed-methods approach, integrating theoretical analysis with a practical case study. The methodology includes:

- Quantitative comparison of the thermophysical properties of the studied insulation materials;
- Energy modeling of a selected office building using specialized software (DesignBuilder v7.3.1.003);
- Life Cycle Assessment (LCA) to evaluate the environmental impact of each material using DesignBuilder v7.3.1.003 and One Click LCA;
- Integration of Level(s) principles in the overall assessment of renovation interventions.

Grounded in the principles of sustainable architecture, building physics, and European energy efficiency standards, this study applies its methodology to a real office building, yielding concrete and actionable results. Ultimately, this research aims to advance knowledge in ecological renovation and equip construction professionals with the tools required to implement sustainable solutions that align with environmental protection and CO<sub>2</sub> reduction objectives.

## **2. Building description and characteristics**

### **2.1 Building Description**

#### **2.1.1 Geometric characteristics**

The analyzed building is an office building with a P+1 height, a total usable area of 850 m<sup>2</sup>, and a usable volume of 2,978 m<sup>3</sup>. The building geometry has been optimized to ensure efficient use of interior space while complying with local urban regulations. Location: Bucharest, Romania, climate zone II, characterized by warm summers and moderate winters, which is crucial for the design of heating, cooling, and ventilation systems.

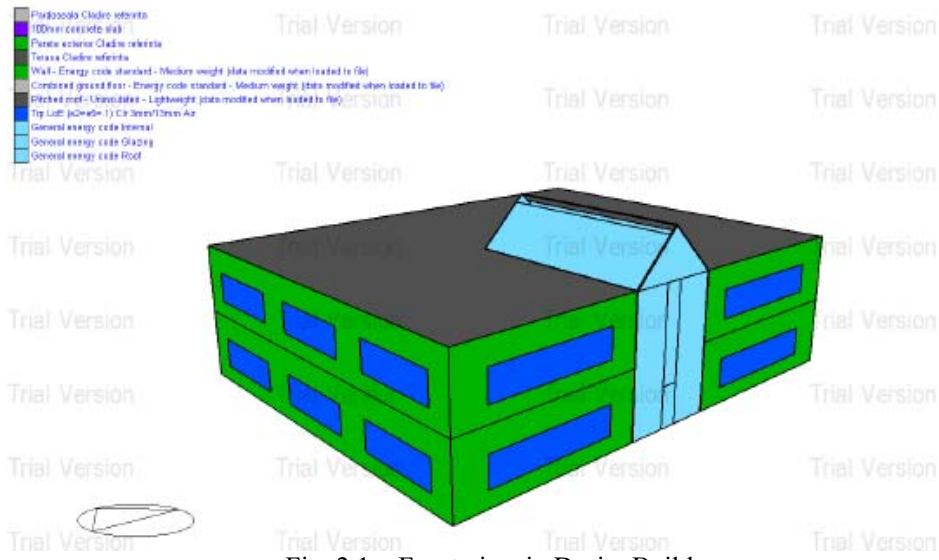


Fig. 2.1 – Front view in DesignBuilder

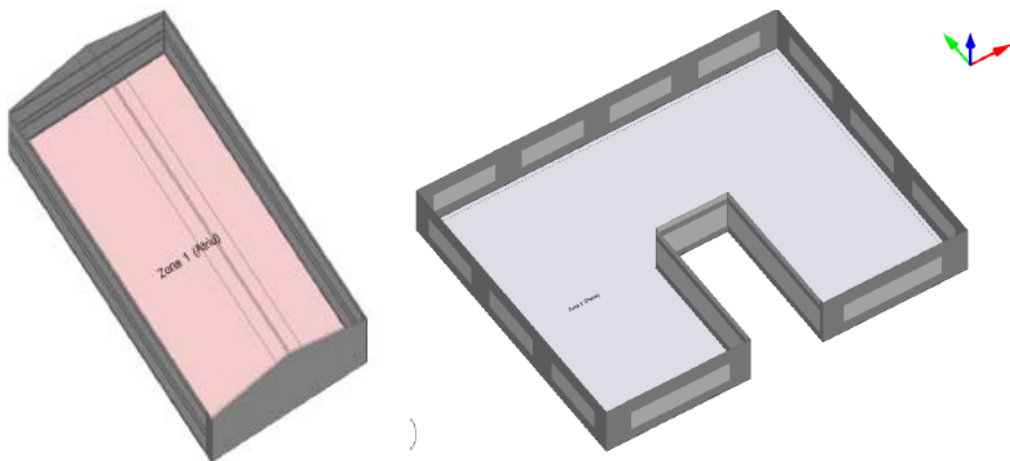


Fig. 2.2 – Top view of thermal zone 1 (Atrium) and thermal zone 2 (Ground Floor)

### 2.1.2 Occupancy and requirements

The building has an occupancy density of 12 m<sup>2</sup> per person, which results in a maximum of 70 people. The activity carried out by the occupants corresponds to sedentary office work. The working schedule follows a standard pattern, with 21 days of annual leave excluded from the operating period.

The daily domestic hot water demand is estimated at 5 liters per person, which corresponds to a total of 350 liters per day at a reference temperature of 60°C. The indoor temperature during the heating season is maintained at 20°C, with a setback temperature of 12°C outside working hours. In the cooling season, the setpoint is

25°C, with a setback temperature of 30°C. The acceptable relative humidity range is set between 35% and 70%, ensuring comfort and compliance with indoor air quality standards.

The minimum fresh air supply is 4,000 m<sup>3</sup>/h, designed in accordance with 15/2022 requirements for category IDA 2. The infiltration rate is assumed at 0.1 h<sup>-1</sup>, reflecting the air exchange due to building envelope permeability.

Artificial lighting is provided to achieve an average illuminance level of 300 lux in occupied spaces.

## **2.2 Building Envelope**

The vertical opaque elements consist of a multilayer wall with the following structure: 3 cm lime-cement plaster, 10 cm insulation (five variants considered: EPS, basalt wool, sheep wool, cellulose, or wood), 30 cm hollow brick, and 1.3 cm gypsum plaster. This configuration ensures thermal resistance while allowing comparison between conventional and bio-based insulating materials.

The horizontal opaque elements are represented by two cases. For the roof terrace, the buildup includes 3 cm gravel, 1.5 cm waterproofing, 3 cm cement screed, 20 cm insulation (XPS, basalt wool, sheep wool, cellulose, or wood), 0.8 cm vapor barrier, 5 cm lightweight concrete screed, 10 cm reinforced concrete, and 1.5 cm lime plaster. For the ground floor slab, the composition includes 3 cm lime-cement plaster, 15 cm insulation (EPS, basalt wool, sheep wool, cellulose, or wood), 10 cm reinforced concrete, 5 cm leveling screed, and 2 cm wooden parquet.

The transparent elements are defined by exterior joinery with triple glazing of the type Clr 3 mm / 13 mm air gap. This solution ensures a low thermal transmittance, contributing to reduced heat losses in winter and minimized heat gains in summer.

All materials sourced from DesignBuilder v7.3.1.003 library, except manually input thermal insulation properties

## **2.3 Building Systems**

### **2.3.1 Heating System**

The heating system is based on an air-to-water heat pump with a nominal capacity of 72.70 kW and a coefficient of performance (COP) of 4.33. This indicates that for every unit of electricity consumed, the system can provide more than four units of thermal energy, ensuring both high efficiency and reduced operating costs.

Heat distribution is primarily achieved through underfloor heating, which ensures uniform temperature levels, improved thermal comfort, and low supply water temperatures that are well-suited to heat pump operation. To cover peak load conditions or sudden variations in demand, the system is supplemented with fan coil units. The integration of underfloor heating and fan coil units allows the heat pump to operate closer to its optimal efficiency range, avoiding oversizing and ensuring adaptability to varying thermal loads.

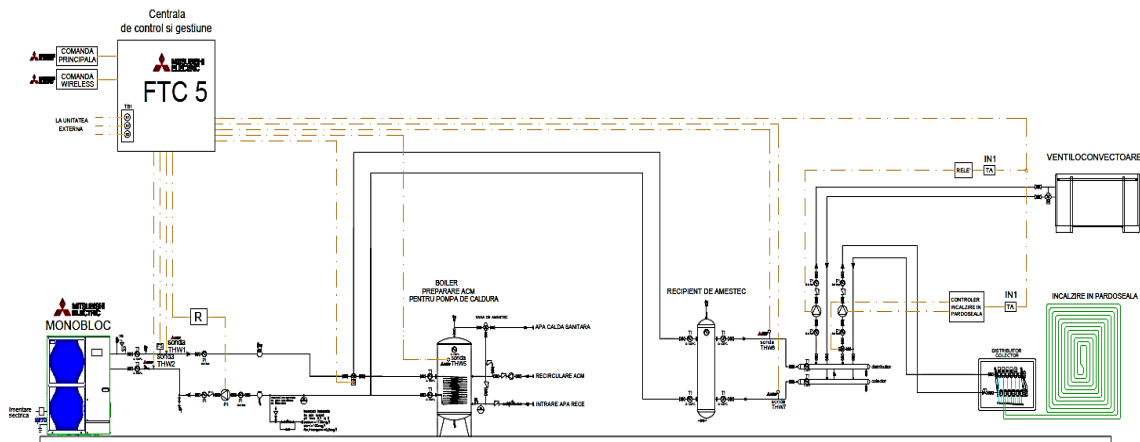


Fig. 2.3 – Heating system schematic [5]

### 2.3.2 Ventilation and Air Conditioning System

The cooling and ventilation system relies on a reversible air-to-water heat pump with a nominal cooling capacity of 61.50 kW and an energy efficiency ratio (EER) of 3.12. This performance ensures efficient operation during the cooling season, with the ability to switch to heating mode when required.

Fresh air supply is provided through an Air Handling Unit (AHU) with a capacity of 4,000 m<sup>3</sup>/h. The AHU is equipped with a heat recovery system, capable of recovering between 50% and 85% of the exhaust air energy, thereby reducing the overall cooling and heating demand and improving indoor air quality.

Thermal energy is distributed via fan coil units, each equipped with individual control for every office. This setup allows occupants to adjust temperature according to their comfort needs while enabling zone-level energy management.

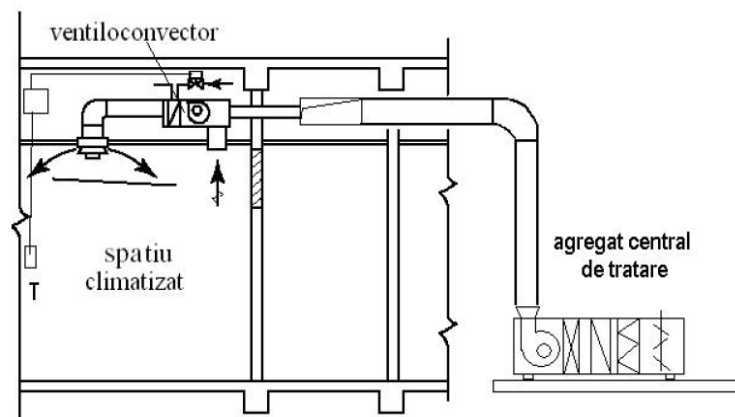


Fig. 2.4 – Centralized fresh air system to fan coils [6]

### 2.3.3 Domestic Hot Water System

A 500 L storage boiler, connected to the heat pump via an extended coil, maintains water at 60°C and ensures continuous domestic hot water availability during the working day.

## 3. Energy and Environmental Analysis Methodology

### 3.1 Software Tools

DesignBuilder is used for dynamic energy simulation, comfort evaluation, lighting performance, energy use, and operational emissions assessment. [7]. One Click LCA supports whole-life environmental impact analysis from “Cradle-to-Grave,” with BIM integration and access to a verified database. [8].

### 3.2 Simulation Parameters

The simulation uses a meteorological file for Bucharest, containing hourly data for a typical year. This ensures that both heating and cooling loads are accurately calculated under local climatic conditions.

The occupancy profile is defined at 12 m<sup>2</sup> per person, consistent with a standard office schedule. This setting reflects typical workplace density and usage patterns.

Internal gains are considered as 120 W per person from occupants, 15 W/m<sup>2</sup> from equipment, and 10 W/m<sup>2</sup> from lighting. These inputs capture the main sources of internal heat load in office environments.

The Life Cycle Assessment (LCA) is based on a building lifespan of 50 years. Replacement cycles are included: HVAC systems every 25 years, exterior joinery every 30 years, and the structure and envelope every 50 years. This approach allows for a comprehensive evaluation of environmental impacts across the full life cycle of the building.

### 3.3 Life Cycle Assessment and CO<sub>2</sub> Emissions

The evaluation covers the full life cycle of the building according to EN 15804, including:

- **A1–A3 (Product stage):** raw material extraction, transport, manufacturing
- **A4 (Construction stage):** transport to site, construction processes
- **B4–B5 (Use stage – replacements and renovations):** HVAC systems (25 years), joinery (30 years), generating additional emissions
- **C1–C4 (End-of-life stage):** demolition, waste transport, recycling/recovery, final disposal

DesignBuilder calculates operational emissions and allows manual input for construction and demolition stages. One Click LCA provides full life-cycle CO<sub>2</sub>-equivalent emissions per m<sup>2</sup> of usable floor area, using verified datasets and including CO<sub>2</sub>, CH<sub>4</sub>, and N<sub>2</sub>O equivalences based on IPCC AR5/AR6 methodology.

### 3.4 Analysis Scenarios

The comparative study evaluates **5 insulation materials** applied to the building envelope, assessing their thermal performance, energy consumption, and life cycle CO<sub>2</sub> emissions. *The analysis combines results from DesignBuilder simulations, and One Click LCA for a comprehensive "Cradle-to-Grave" assessment (A1–C4).*

#### 3.4.1. Scenario 1 - Expanded and Extruded Polystyrene (EPS & XPS)

Scenario 1 evaluates a combined thermal insulation system using EPS ( $\lambda = 0.04$  W/mK, 16 kg/m<sup>3</sup> [9], embodied carbon 4.205 kgCO<sub>2</sub>e/kg) and XPS ( $\lambda = 0.037$  W/mK, 32 kg/m<sup>3</sup> [10], embodied carbon 5.84 kgCO<sub>2</sub>e/kg) in an 850 m<sup>2</sup> office building. [11] The difference in embodied carbon reflects the more complex manufacturing process and use of blowing agents for XPS. The thermal resistance achieved is  $R = 2.67$  m<sup>2</sup>K/W for walls and  $R = 3.74$  m<sup>2</sup>K/W for the floor. The building's heating demand is 62.66 kW and cooling demand is 57.02 kW (DesignBuilder).

Annual final energy consumption: 68.388 MWh/year, with specific final energy 80.46 kWh/m<sup>2</sup>·year and specific primary energy 201.14 kWh/m<sup>2</sup>·year.

Energy breakdown:

- Heating: 29.051 MWh
- Cooling: 24.531 MWh
- Domestic hot water: 1.305 MWh
- Ventilation: 5.628 MWh
- Lighting: 7.872 MWh

Auxiliary pumps: Heating 1.072 kWh, Cooling 715 kWh

Operational CO<sub>2</sub> emissions were calculated using  $fCO_2 = 0.107$  kgCO<sub>2</sub>/kWh (electricity from SEN). Annual CO<sub>2</sub>: 21.52 kgCO<sub>2</sub>/m<sup>2</sup>·year and thus 50-year operational CO<sub>2</sub>: 914.70 tCO<sub>2</sub>e. Distribution by system: Heating 388.56 tCO<sub>2</sub>e, Cooling 328.11 tCO<sub>2</sub>e, Auxiliary systems 198.03 tCO<sub>2</sub>e

Life Cycle Assessment (LCA) calculated with the software One Click LCA 53.4 tCO<sub>2</sub>e

- Building LCA (phases A1–A4, B4–B5, C1–C4): 2,169.772 tCO<sub>2</sub>e
- Total LCA including operational use: 3,084.47 tCO<sub>2</sub>e
- Specific LCA emissions: 3.63 tCO<sub>2</sub>e/m<sup>2</sup>



## Strategies for reducing energy consumption in existing buildings through ecological renovation













▼ Most contributing materials (Global warming)					Compare data (1)
No.	Resource	Cradle to gate impacts (A1-A3)	Of cradle to gate (A1-A3)	Sustainable alternatives	
1.	Wood plastic composite products, 23.24 kg/m <sup>2</sup> , 1180 kg/m <sup>3</sup>  ?	26 tonnes CO <sub>2</sub> e	13.7 %	Show sustainable alternatives	Add to compare
2.	Bricks, 226x104x60, 226x85x60 mm  ?	24 tonnes CO <sub>2</sub> e	12.5 %	Show sustainable alternatives	Add to compare
3.	EPS insulation, L=0.038 W/mK, R=4.59 m <sup>2</sup> K/W, 120 mm, 5.44 kg/m <sup>2</sup> , 45.33 kg/m <sup>3</sup> , Lambda=0.038 W/(m.K)  ?	22 tonnes CO <sub>2</sub> e	11.2 %	Show sustainable alternatives	Add to compare
4.	Levelling screed for floor heating, 1.7 kg/m <sup>2</sup> /mm, 1700 kg/m <sup>3</sup>  ?	17 tonnes CO <sub>2</sub> e	8.6 %	Show sustainable alternatives	Add to compare
5.	Ready-mix concrete, 50 MPa, 2301 kg/m <sup>3</sup>  ?	16 tonnes CO <sub>2</sub> e	8.1 %	Show sustainable alternatives	Add to compare
6.	Ready-mix concrete for foundations and infrastructure for aggressive soils, C45 XF1 CEM III/A, [A4 = 0 km] ?	15 tonnes CO <sub>2</sub> e	8.0 %	Show sustainable alternatives	Add to compare
7.	XPS Insulation board, L=0.035 W/mK, R=1 m <sup>2</sup> K/W, 150 mm, 600 mm x 1200-2400 mm, 5.4 kg/m <sup>2</sup> , 36 kg/m <sup>3</sup>  ?	13 tonnes CO <sub>2</sub> e	6.5 %	Show sustainable alternatives	Add to compare
8.	Ready-mix concrete, 25 Mpa, 2400 kg/m <sup>3</sup>  ?	9.9 tonnes CO <sub>2</sub> e	5.1 %	Show sustainable alternatives	Add to compare
9.	Aluminium frame window triple glazed, non-operable, 50% recycled aluminium, 1.48 m x 2.18 m, 30.7 kg/m <sup>2</sup>  ?	9.9 tonnes CO <sub>2</sub> e	5.1 %	Show sustainable alternatives	Add to compare
10.	Argon gas filled insulating glass unit (IGU) with clear float glass panes, triple glazed, 4-14-4-14-4, 30 kg/m <sup>2</sup>  ?	9 tonnes CO <sub>2</sub> e	4.7 %	Show sustainable alternatives	Add to compare
11.	Autoclaved concrete block, 425 kg/m <sup>3</sup>  ?	8.7 tonnes CO <sub>2</sub> e	4.5 %	Show sustainable alternatives	Add to compare
12.	Heat pump, 14 kW, 226 kg/unit  ?	8.7 tonnes CO <sub>2</sub> e	4.5 %	Show sustainable alternatives	Add to compare
13.	Reinforcement steel, French average, ?	8.1 tonnes CO <sub>2</sub> e	4.2 %	Show sustainable alternatives	Add to compare
14.	Solidwood flooring, multiple species, thickness range: 8 - 22mm, 4.38kg/m <sup>2</sup> , 548 kg/m <sup>3</sup> oven-dry, moisture content < 13%  ?	1.8 tonnes CO <sub>2</sub> e	0.9 %	Show sustainable alternatives	Add to compare

Figure 3.1: One Click LCA overview of embodied carbon. - (EPS & XPS)

### 3.4.2. Scenario 2 - Basalt Wool

Scenario 2 evaluates the use of basalt wool as thermal insulation, a mineral product with  $\lambda = 0.035$  W/mK, density 40 kg/m<sup>3</sup> [12], and embodied carbon 1.12 kgCO<sub>2</sub>e/kg [13]. The lower embodied carbon compared to plastics reflects the manufacturing process based on melting volcanic rocks. Thermal resistance achieved: R = 2.98 m<sup>2</sup>K/W for Walls, 4.91 m<sup>2</sup>K/W for roof and 4.22 m<sup>2</sup>K/W for the floor Heating demand: 61.68 kW; Cooling demand: 56.12 kW (DesignBuilder).

Annual final energy consumption: 62.969 MWh/year, with specific final energy 74.08 kWh/m<sup>2</sup>·year and specific primary energy 185.21 kWh/m<sup>2</sup>·year. Energy breakdown:

- Heating: 25.847 MWh
- Cooling: 22.317 MWh
- Domestic hot water: 1.306 MWh
- Ventilation: 5.628 MWh
- Lighting: 7.872 MWh

Auxiliary pumps: Heating 1.072 kWh, Cooling 715 kWh

Operational CO<sub>2</sub> emissions were calculated using fCO<sub>2</sub> = 0.107 kgCO<sub>2</sub>/kWh (electricity from SEN). Annual CO<sub>2</sub>: 19.82 kgCO<sub>2</sub>/m<sup>2</sup>·year and 50-year operational CO<sub>2</sub>: 842,22 tCO<sub>2</sub>e. Distribution by system: Heating 345.7 tCO<sub>2</sub>e, Cooling 298,49 tCO<sub>2</sub>e, Auxiliary systems 198.03 tCO<sub>2</sub>e

Life Cycle Assessment (LCA) calculated with the software One Click LCA was 8,44 tCO<sub>2</sub>e

- Building LCA (A1–A4, B4–B5, C1–C4): 2,124.815 tCO<sub>2</sub>e
- Total LCA (including operational use): 2,967.04 tCO<sub>2</sub>e
- Specific LCA emissions: 3.49 tCO<sub>2</sub>e/m<sup>2</sup>

### 3.4.3. Scenario 3 - Sheep Wool insulation

Scenario 3 evaluates sheep wool as a natural insulation material with  $\lambda = 0.038$  W/mK, density 18 kg/m<sup>3</sup> [14], and embodied carbon of only 0.14 kgCO<sub>2</sub>e/kg [13], the lowest value among all previously analyzed materials. This performance results from its natural origin and minimal processing, wool being a by-product of the textile and food industries. Thermal resistance achieved:  $R = 2.79$  m<sup>2</sup>K/W for Walls, 4.55 m<sup>2</sup>K/W for roof and 3.92 m<sup>2</sup>K/W for the floor Heating demand: 62.4 kW; Cooling demand: 56.92 kW (DesignBuilder). Sheep wool also provides additional benefits such as natural humidity regulation and the ability to absorb and neutralize air pollutants Annual final energy consumption: 67.257 MWh/year, with specific final energy 79.13 kWh/m<sup>2</sup>·year and specific primary energy 197.82 kWh/m<sup>2</sup>·year.

Energy breakdown:

- Heating: 28.400 MWh
- Cooling: 24.051 MWh
- Domestic hot water: 1.306MWh
- Ventilation: 5.628 MWh
- Lighting: 7.872 MWh

Auxiliary pumps: Heating 1.072 kWh, Cooling 715 kWh

Operational CO<sub>2</sub> emissions were calculated using  $f\text{CO}_2 = 0.107$  kgCO<sub>2</sub>/kWh (electricity from SEN). Annual CO<sub>2</sub>: 19.82 kgCO<sub>2</sub>/m<sup>2</sup>·year and 50-year operational CO<sub>2</sub>: 842,22 tCO<sub>2</sub>e

Distribution by system: Heating 345.7 tCO<sub>2</sub>e, Cooling 298,49 tCO<sub>2</sub>e, Auxiliary systems 198.03 tCO<sub>2</sub>e

Life Cycle Assessment (LCA) calculated with the software One Click LCA was 6.28 tCO<sub>2</sub>e (One Click LCA)

- Building LCA (A1–A4, B4–B5, C1–C4): 2,122.655 tCO<sub>2</sub>e
- Total LCA (including operational use): 3,022.22 tCO<sub>2</sub>e
- Specific LCA emissions: 3.56 tCO<sub>2</sub>e/m<sup>2</sup>

### 3.4.4. Scenario 4 - Cellulose Insulation

Scenario 4 considers cellulose as the insulation material, with a thermal conductivity of  $\lambda = 0.039$  W/mK and a density of 40 kg/m<sup>3</sup> [15]. The embodied carbon is negative, at -0.39 kgCO<sub>2</sub>e/kg [15], reflecting its origin from recycled paper and recovered wood fibers. Thermal resistance achieved:  $R = 2.73$  m<sup>2</sup>K/W for Walls, 4.45 m<sup>2</sup>K/W for roof and 3.83 m<sup>2</sup>K/W for the floor

Heating demand: 62.73 kW; Cooling demand: 57.27 kW (DesignBuilder).

Annual final energy consumption: 68.298 MWh/year, with specific final energy 80.35 kWh/m<sup>2</sup>·year and specific primary energy 200.88 kWh/m<sup>2</sup>·year.

Energy breakdown:

- Heating: 29.0 MWh
- Cooling: 24.491 MWh
- Domestic hot water: 1.306 MWh
- Ventilation: 5.628 MWh
- Lighting: 7.872 MWh

Auxiliary pumps: Heating 1.072 kWh, Cooling 715 kWh

- Operational CO<sub>2</sub> Emissions

Operational CO<sub>2</sub> emissions were calculated using  $fCO_2 = 0.107 \text{ kgCO}_2/\text{kWh}$  (Mc 001-2022) [21] (electricity from SEN).

- Annual CO<sub>2</sub>: 21.49 kgCO<sub>2</sub>/m<sup>2</sup>·year
- 50-year operational CO<sub>2</sub>: 913.49 tCO<sub>2e</sub>

Distribution by system: Heating 387.89 tCO<sub>2e</sub>, Cooling 327.57 tCO<sub>2e</sub>, Auxiliary systems 198.03 tCO<sub>2e</sub>

Life Cycle Assessment (LCA) calculated with the software One Click LCA was 2.80 tCO<sub>2e</sub> (One Click LCA)

- Building LCA (A1–A4, B4–B5, C1–C4): 2,119.17 tCO<sub>2e</sub>
- Total LCA (including operational use): 3,032.66tCO<sub>2e</sub>
- Specific LCA emissions: 3.57 tCO<sub>2e</sub>/m<sup>2</sup>

### 3.4.5. Scenario 5 -Wood Fibers Insulation

- Insulation System Characteristics

Scenario 6 evaluates wood fibers as an insulation material, with a thermal conductivity of  $\lambda = 0.038 \text{ W/mK}$  and a high density of 110 kg/m<sup>3</sup> [16]. The embodied carbon is negative, at -1.05 kgCO<sub>2e</sub>/kg [17], reflecting the long-term carbon storage capability of wood.

- Thermal Performance

Thermal resistance achieved:  $R = 2.73 \text{ m}^2\text{K/W}$  for Walls, 4.55 m<sup>2</sup>K/W for roof and 3.92 m<sup>2</sup>K/W for the floor

Heating demand: 62.4 kW; Cooling demand: 56.92 kW (DesignBuilder).

Annual final energy consumption: 67.257 MWh/year, with specific final energy 79.13 kWh/m<sup>2</sup>·year and specific primary energy 197.82 kWh/m<sup>2</sup>·year.

Energy breakdown:

- Heating: 28.4 MWh
- Cooling: 24.051 MWh
- Domestic hot water: 1.305 MWh
- Ventilation: 5.627 MWh
- Lighting: 7.872 MWh

Auxiliary pumps: Heating 1.072 kWh, Cooling 715 kWh

Operational CO<sub>2</sub> emissions were calculated using  $f\text{CO}_2 = 0.107 \text{ kgCO}_2/\text{kWh}$  (Mc 001-2022 [44]). Annual CO<sub>2</sub>: 21.17 kgCO<sub>2</sub>/m<sup>2</sup>·year and 50-year operational CO<sub>2</sub>: 899.57 tCO<sub>2</sub>e. Distribution by system: Heating 379.85 tCO<sub>2</sub>e, Cooling 321.69 tCO<sub>2</sub>e, Auxiliary systems 198.03 tCO<sub>2</sub>e

Life Cycle Assessment (LCA) calculated with the software One Click LCA was 5.32 tCO<sub>2</sub>e (One Click LCA)

- Building LCA (A1–A4, B4–B5, C1–C4): 2,121.696 tCO<sub>2</sub>e
- Total LCA (including operational use): 3,021.26 tCO<sub>2</sub>e
- Specific LCA emissions: 3.57 tCO<sub>2</sub>e/m<sup>2</sup>

#### 4. Results summary

From Table 1 we can see that EPS & XPS record the highest embodied emissions with 2,169.77 tCO<sub>2</sub>e, while basalt wool and natural materials remain slightly lower, around 2,120 tCO<sub>2</sub>e. When operational use is included, total life-cycle emissions reach 3,084.47 tCO<sub>2</sub>e for EPS/XPS and only 2,967.04 tCO<sub>2</sub>e for basalt wool, the lowest among all cases. Natural materials fall in between, with values around 3,021–3,033 tCO<sub>2</sub>e. Specific emissions per square meter confirm this trend: EPS/XPS has the highest value at 3.63 tCO<sub>2</sub>e/m<sup>2</sup>, while basalt wool achieves the best performance at 3.49 tCO<sub>2</sub>e/m<sup>2</sup>. Natural options remain slightly higher, 3.56–3.57 tCO<sub>2</sub>e/m<sup>2</sup>, but still perform better than EPS/XPS. Overall, basalt wool offers the most favorable balance between energy efficiency and environmental impact, while natural materials provide ecological benefits yet show slightly higher operational contributions. EPS/XPS, although cheaper, ranks lowest in sustainability.

Table 1

LCA indicators					
	EPS & XPS	Basalt Wool	Sheep Wool	Cellulose	Wood Fibers
Building LCA (phases A1–A4, B4–B5, C1–C4) tCO <sub>2</sub> e	2169,772	2124,815	2122,655	2119,17	2121,69
Total LCA including operational use: tCO <sub>2</sub> e	3084,47	2967,04	3022,22	3032,66	3021,26
Specific LCA emissions: tCO <sub>2</sub> e/m <sup>2</sup>	3,63	3,49	3,56	3,57	3,57

The comparative graphs show that basalt wool consistently performs best, with the lowest specific primary energy (185.21 kWh/m<sup>2</sup>·year), the lowest total LCA emissions (2,967.04 tCO<sub>2</sub>e), and the lowest specific LCA emissions (3.49 tCO<sub>2</sub>e/m<sup>2</sup>). Natural materials such as sheep wool, cellulose, and wood fibers provide intermediate results, slightly higher in total and specific emissions but still significantly better than EPS/XPS. EPS/XPS achieves the lowest cost but performs worst environmentally, with the highest specific final energy (80.46 kWh/m<sup>2</sup>·year), highest total LCA

emissions (3,084.47 tCO<sub>2</sub>e), and highest specific LCA emissions (3.63 tCO<sub>2</sub>e/m<sup>2</sup>). Overall, basalt wool offers the most balanced and sustainable solution, while natural materials represent viable ecological alternatives, and EPS/XPS remains the least sustainable despite its cost advantage.

Comparative Analysis of Insulation Scenarios

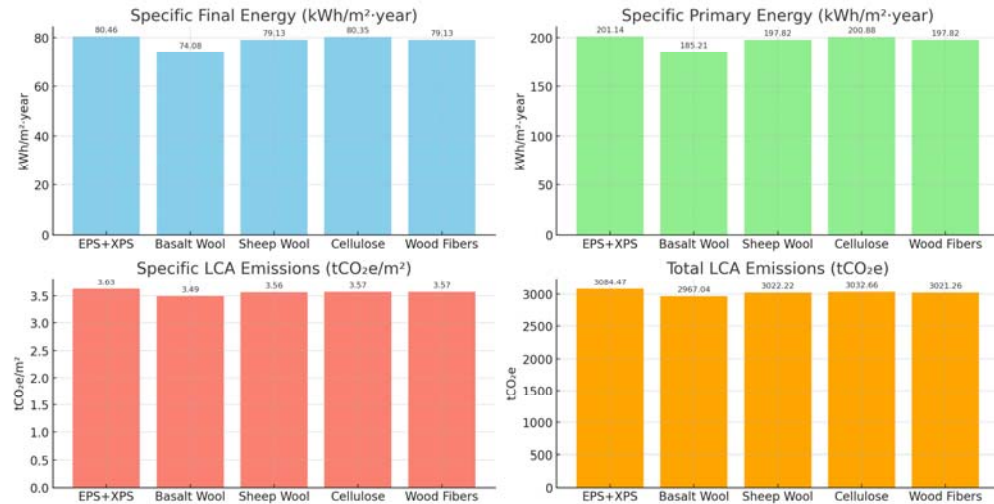


Figure 3.2: Comparison between the different insulation materials

## 5. Conclusions

This study comparatively evaluated five thermal insulation solutions for an office building, integrating energy, environmental, and economic perspectives. Results indicate that no single material is universally optimal; rather, choices depend on specific priorities and constraints.

Basalt wool delivers the best overall performance, with the lowest primary energy demand (185.21 kWh/m<sup>2</sup>·year) and life-cycle CO<sub>2</sub> emissions (2,967 tCO<sub>2</sub>e). It reduces energy use by 7.9% compared to EPS/XPS and ensures stable thermal comfort.

Natural insulation materials (cellulose, hemp, wood fibers, sheep wool) achieve intermediate energy performance (197.82–200.88 kWh/m<sup>2</sup>·year). Their major advantage is negative embodied carbon, acting as carbon sinks and offsetting operational emissions.

From a cost perspective, EPS/XPS has the lowest investment (29.33 kRON) but the highest environmental burden. Cellulose provides the best balance at 71.20 kRON, while sheep wool and wood fibers exceed 200 kRON, positioning them as premium solutions.

Overall, basalt wool ranks highest in energy and environmental performance, natural materials add value through sustainability and comfort, while EPS/XPS ranks lowest despite its low cost.

Energy performance converges across materials, with differences below 8%, highlighting that careful design and material thickness can be as influential as material selection itself. In contrast, environmental impact varies significantly, with natural materials offering carbon storage that transforms buildings into temporary CO<sub>2</sub> sinks. Economic analysis reveals a wide range of initial costs, reflecting market maturity and adoption challenges for emerging materials. Hybrid strategies that combine different insulation types emerge as the most promising approach, optimizing thermal efficiency, cost, and sustainability simultaneously. Overall, the research demonstrates the value of a holistic methodology that integrates life-cycle assessment, dynamic energy simulations, and real-market economic data, pointing toward innovative, resilient, and sustainable solutions for the building sector.

## 6. Acknowledgments

This work was supported by a grant of the Ministry of Research, Innovation and Digitization, CNCS/CCCDI - UEFISCDI, project number ERANET-PRE-ActiVer, within PNCDI IV.

## 7. References

- [1] *EU adopts law requiring all new buildings to be zero emissions by 2030*, *ESG Today*, April 12, 2024, available online: <https://www.esgtoday.com/eu-adopts-law-requiring-all-new-buildings-to-be-zero-emissions-by-2030/>.
- [2] European Commission, *Level(s)*, available online: [https://green-forum.ec.europa.eu/levels/quick-introduction-levels\\_en](https://green-forum.ec.europa.eu/levels/quick-introduction-levels_en)
- [3] BREEAM (Building Research Establishment Environmental Assessment Method), available online: <https://breeam.com/>
- [4] LEED (Leadership in Energy and Environmental Design), available online: <https://www.usgbc.org/leed>
- [5] Mitsubishi, *Functional schemes of heat pumps*, available online: <https://aerconditionatmitsubishi.ro/pompe-de-caldura-aer-apa>
- [6] A. Damian, *Climatizarea clădirilor multizonale*, note de curs, 2024
- [7] *DesignBuilder, Software v7.3.1.003*. Available online: <https://designbuilder.co.uk/download/release-software>.
- [8] *One Click LCA, Software*. Available online: <https://oneclicklca.com/>
- [9] Baudeman, *Fișă tehnică Polistiren expandat EPS 50*. Available online: [https://cdn.dedeman.ro/media/catalog/product/fise-tehnice/fisa\\_tehnica\\_polistiren\\_expandat\\_baudeman\\_eps\\_50.pdf](https://cdn.dedeman.ro/media/catalog/product/fise-tehnice/fisa_tehnica_polistiren_expandat_baudeman_eps_50.pdf).
- [10] Zentyss, *Fișă tehnică Panouri din polistiren extrudat XPan*. Available online: <https://media.hornbach.ro/hb/technicaldatasheet/as.56183883.pdf>.
- [11] A. Violano, M. Cannaviello, "The Carbon Footprint of Thermal Insulation: The Added Value of Circular Models Using Recycled Textile Waste," *Energies*, 16(19), p. 6768, 2023. doi:10.3390/en16196768.
- [12] Rockwool, *Fișă tehnică vată bazaltică Rockwool Acoustic*. Available online: <https://nzebshop.ro/content/fisa-tehnica/fisa-tehnica-rockwool-acoustic.pdf>



- [13] CIDB Malaysia, *Embodied carbon inventory data for construction materials*. Available online: [https://www.cidb.gov.my/wp-content/uploads/2022/11/V4\\_EMBODIED-CARBON-INVENTORY-TEMPLATE-final-1.pdf](https://www.cidb.gov.my/wp-content/uploads/2022/11/V4_EMBODIED-CARBON-INVENTORY-TEMPLATE-final-1.pdf)
- [14] ISOLENA, *Fișă tehnică lână de oaie ISOLENA OPTIMAL 0.038 W/mK pentru utilizări multiple*. Available online: <https://nzebshop.ro/content/fisa-tehnica/IW-Optimal-EN.pdf>
- [15] ISOBOARD, *Fișă tehnică ISOBOARD 100 – plăci de termoizolație semirigidă din fibre de celuloză*. Available online: <https://nzebshop.ro/content/fisa-tehnica/Placi-izolatie-celuloza-ISOBOARD.pdf>
- [16] GUTEX, *Fișă tehnică THERMOSAFE HOMOGEN – izolație fibrolemnoasă cu multiple utilizări*. Available online: [https://nzebshop.ro/content/fisa-tehnica/GUTEX\\_Thermosafe-homogen.pdf](https://nzebshop.ro/content/fisa-tehnica/GUTEX_Thermosafe-homogen.pdf)
- [17] F. Asdrubali, L. Evangelisti, C. Guattari, M. Roncone, D. Milone, “Experimental Analysis of the Thermal Performance of Wood Fiber Insulating Panels,” *Sustainability*, **15**, p. 1963, 2023.
- [18] F. Valentini, G. Maracchini, R. Di Filippo, A. Dorigato, M. Manzini, “A prospective life cycle assessment of insulation and window systems under evolving electricity and recycling scenarios for building energy retrofit in Italy,” *Energy and Buildings*, 2025. Available online: <https://www.sciencedirect.com/science/article/pii/S0378778825009752>
- [19] V. Kilis, N. Ploskas, G. Panaras, “Investigation of multi-objective decision making approaches for the optimization in building envelope thermal design,” *Energy Technologies and Assessments*, 2025. Available online: <https://www.sciencedirect.com/science/article/pii/S2213138825003376>
- [20] R. Ramakrishnan, L. Jambunathan, “EPS concrete: structural performance and environmental impact for sustainable insulation,” *Environmental Science and Pollution Research*, 2025. Available online: <https://link.springer.com/article/10.1007/s11356-025-36785-7>
- [21] *Metodologie de calcul al performanței energetice a clădirilor*, indicativ Mc 001-2022

## Comparative simulation of a fire in a paint storage warehouse: with and without an ESFR sprinkler system

Simularea comparativă a unui incendiu într-o hală de depozitare cu vopseluri: cu și fără sistem de stingere ESFR

Emanuil-Petru OVADIUC<sup>1</sup>, Răzvan CALOTĂ<sup>2</sup>, Ilinca NĂSTASE<sup>2</sup>,  
Manuel SERBAN<sup>1</sup>

<sup>1</sup> Fire Officers Faculty, Police Academy "Alexandru Ioan Cuza", Romania  
Aleea Privighetorilor nr. 1A, Bucharest

<sup>2</sup> Technical University of Civil Engineering of Bucharest, Romania  
122-124 Bvd Lacul Tei, Bucharest, Sector 2, Romania

E-mail: [emanuil-petru.ovadiuc@phd.utcb.ro](mailto:emanuil-petru.ovadiuc@phd.utcb.ro), [razvan.calota@utcb.ro](mailto:razvan.calota@utcb.ro), [ilinca.nastase@utcb.ro](mailto:ilinca.nastase@utcb.ro),  
[manuel.serban@gmail.com](mailto:manuel.serban@gmail.com)

DOI: 10.37789/rjce.2025.16.4.4

**Abstract.** *The paper presents a comparative analysis of two fire scenarios simulated using PyroSim, within a 7050 m<sup>2</sup> warehouse designated for paint storage. The first scenario excludes the activation of the ESFR sprinkler system, while the second evaluates its efficiency. Parameters such as heat release rate and temperature distribution are monitored. The results show a significant reduction in peak temperature (from 970 °C to 135 °C) and fire intensity, highlighting the essential role of sprinkler systems in limiting fire spread, protecting assets, and ensuring personnel safety.*

**Key words:** *PyroSim, Fire Dynamics Simulator, ESFR sprinklers, fire, warehouse*

**Rezumat.** *Lucrarea analizează comparativ două scenarii de incendiu simulate cu PyroSim, într-o hală de 7050 m<sup>2</sup> destinată depozitării vopselurilor. Primul scenariu nu include activarea sistemului de sprinklere ESFR, iar al doilea evaluează eficiența acestuia. Sunt urmăriți parametri precum rata de eliberare a căldurii și distribuția temperaturii. Rezultatele evidențiază o reducere considerabilă a temperaturii maxime (de la 970 °C la 135 °C) și a intensității incendiului, subliniind rolul esențial al sistemelor cu sprinklere în limitarea propagării, protejarea bunurilor și siguranța personalului.*

**Cuvinte cheie:** *PyroSim, Fire Dynamics Simulator, sprinklere ESFR, incendiu, deposit*

### 1. Introducere

PyroSim is an advanced software for fire simulation and is designed as a complementary tool to Fire Dynamics Simulator (FDS), a software created by the

The article was received on 24.10.2025, accepted on 27.10.2025 and published on 27.11.2025



National Institute of Standardization and Technology. SDS models were created to reproduce phenomena such as smoke propagation, temperature variations, carbon monoxide concentrations, and other products resulting from fires [1]

Two fire scenarios will be developed that will include the start of a fire following the ignition of paint cans, placed on racks, in a storage hall, which has an area of 7050 m<sup>2</sup>.

Determining the heat load is a mandatory step in the analysis of fire scenarios. In the present case, an average calorific value of the paints of 33 MJ/kg was considered, which leads to a total heat load of 22,102,542 MJ and a specific heat load of 3,135 MJ/m<sup>2</sup> for the surface of the analyzed hall, according to Table 1.

Table 1

Features of stored materials					
Material	Mass - Mi [kg]	Calorific value - Qi [MJ/kg]	Heat Load - SQ [MJ]	Area [sqm]	Thermal load - qs [MJ/sqm]
Paint	669774,00	33,00	22102542,00	7050,00	3135,11

Fire simulation involves the use of predefined parameters that describe the conditions inside the space affected by the fire. In this regard, the following characteristics have been established:

- Environment temperature: 20 degrees Celsius;
- Atmospheric pressure: 101325 Pa;
- Mass fraction of oxygen in ambient air: 0.2323 g/kg;
- Relative humidity: 40%;
- Gravitational constant: 9.81 m/s<sup>2</sup>.

First scenario: the storage hall is monitored with a detection, signaling and warning system, but the ESFR sprinkler extinguishing system is not put into operation;

Second scenario: the storage hall is monitored with a detection, signaling and warning system and the ESFR sprinkler extinguishing installation will be activated.

Following the interpretation of the results obtained from the two fire scenarios, the efficiency of the ESFR sprinkler extinguishing installation in extinguishing fires produced at a paint storage hall will be evaluated, as well as the ability to intervene on the outbreak, both on the part of the specialized personnel and the first intervention teams.

## 2. Content of the paper

### 2.1 Description of scenario I

Scenario I aims to analyze and interpret the data resulting from the simulation that will render the development of the fire within **600 seconds**.

The event occurred on a working day, around 14:30, during normal working hours. There were 12 workers in the hall, and the main activity was the handling of

paint containers, the stored substances being flammable. An employee used a makeshift extension cord to power a power tool. Due to an overload, an electric arc occurred, which ignited the accumulated vapors in the poorly ventilated work area. The flames spread quickly and ignited nearby materials. Shortly after the fire broke out, two workers tried to use portable fire extinguishers, but the flames were already too great, and the high temperature and dense smoke prevented them from approaching the outbreak. The automatic sprinkler extinguishing system did not work, due to a fault in the main valve, which was not reported and unchecked in recent months. Due to the stored substances, the fire generated large amounts of toxic smoke.

The 600-second interval was chosen considering the estimated time for equipping, moving and taking action of the intervention forces at the scene of the event. During this period, the phenomena produced by the fire are taken into account, as well as the analysis of the risks to which firefighters may be subjected during intervention operations to locate and extinguish fires.



Fig. 1. Location of the fire outbreak

## 2.2 Description of scenario II

Scenario II aims to analyze and interpret the data resulting from the simulation that will render the development of the fire within **600 seconds**.

The event occurred under the same conditions: an employee used an improvised extension cord to power a power tool, and due to an overload, an electric arc occurred, which ignited the solvent vapor accumulated in a poorly ventilated area. Shortly after the fire broke out, the automatic sprinkler extinguishing system was activated, as a

result of the high temperature detected in the affected area. The early activation of the sprinklers significantly reduced the intensity of the fire, limiting its spread to other areas of the hall.

Within this scenario, the evolution of temperature, smoke releases, flue gas movement and visibility are analyzed, in order to assess the impact of the parameters following the fire on the space in case of operation of the ESFR sprinkler extinguishing system.

Figure 2 shows the location of the sprinkler heads, which comply with the norms.

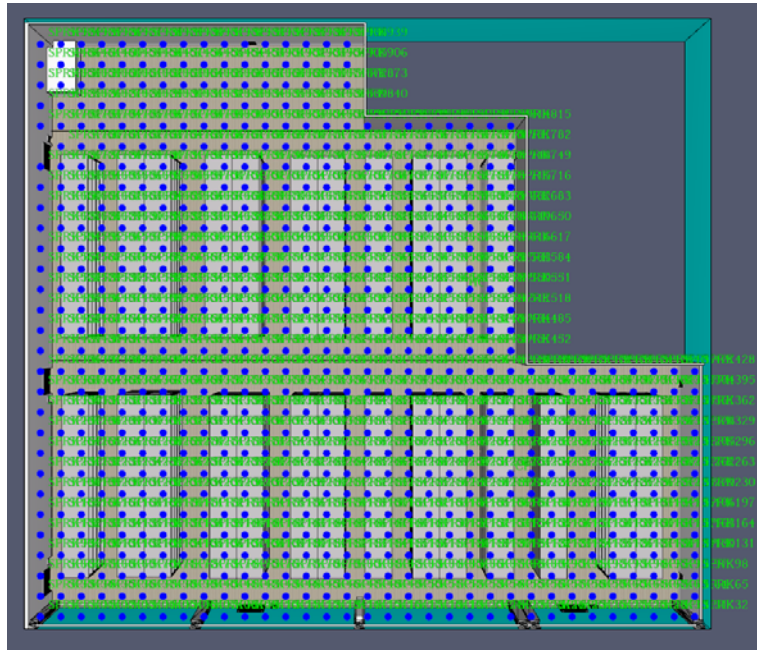


Fig.2. Location of sprinklers in the Pyrosim software

The characteristics of the sprinkler extinguishing system are multiple, but we extract the following characteristics:

- The technical solution for the installation: ESFR sprinkler extinguishing system;
- Maximum area covered by a sprinkler:  $A_p = 9 \text{ m}^2$ ;
- Calculation density:  $q_{ts} = 7,65 \frac{\text{l}}{\text{s}}$ ;
- Simultaneous Trigger Range:  $108 \text{ m}^2$ ;
- Pressure: 3.6 bar;
- Volume of water reserve:  $500 \text{ m}^3$ ;
- Sprinkler trigger temperature:  $74^\circ\text{C}$ ;
- Installation height: 1.8 m

### 3. Results

#### 3.1 Scenario I

##### 1. Location of the firebox

The main objects subject to combustion in the storage hall are considered to be the solvent-based paint boxes and the racks on which they are placed (see Fig. 3.), having a weight of 932.4 kg/pallet generating a quantity of 3135.11 MJ/sqm.

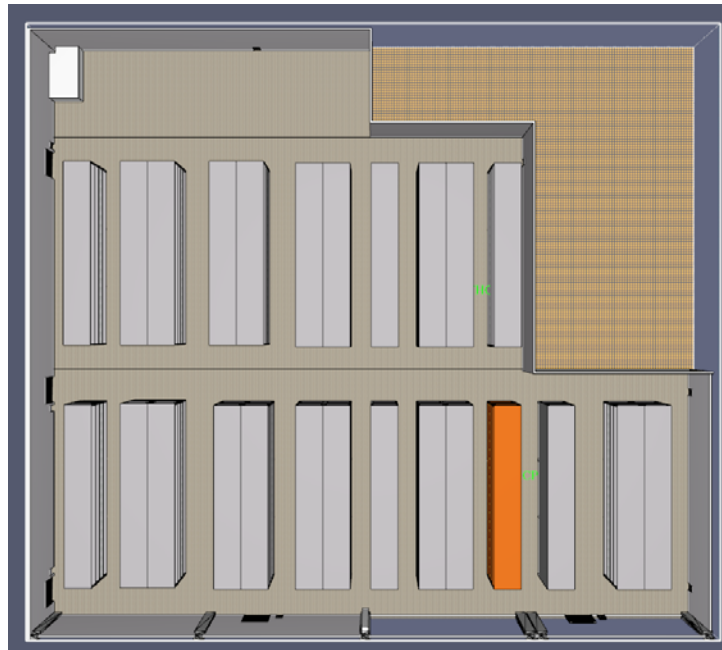


Fig. 3. Location of the fire outbreak

##### 2. Temperature

In the simulation carried out with the PyroSim software, the temperature is one of the fundamental parameters for assessing the development of the fire and the thermal impact on the analyzed space. This is measured by means of thermocouple devices, located at various points in the space. The values obtained allow the observation of the thermal distribution and variation over time and highlight the rapid temperature increases in the vicinity of the focus and the propagation of heat.

The constant evolution of the firebox determines the appearance of thermal fluxes that are transmitted to the materials in the hall through the 3 types of heat transfer: radiation, conduction and convection.

Heat transfer is highlighted in Figure 4. by means of a horizontal plane placed at a height of 1.8 m from the floor. This value was chosen because the overall average height of adult males is 171 centimeters. Thus, the positioning of the analysis plane at this height allows the evaluation of the impact of thermal parameters on the airways, eyes and skull. Exposure to high temperatures can cause shortness of breath or dizziness.

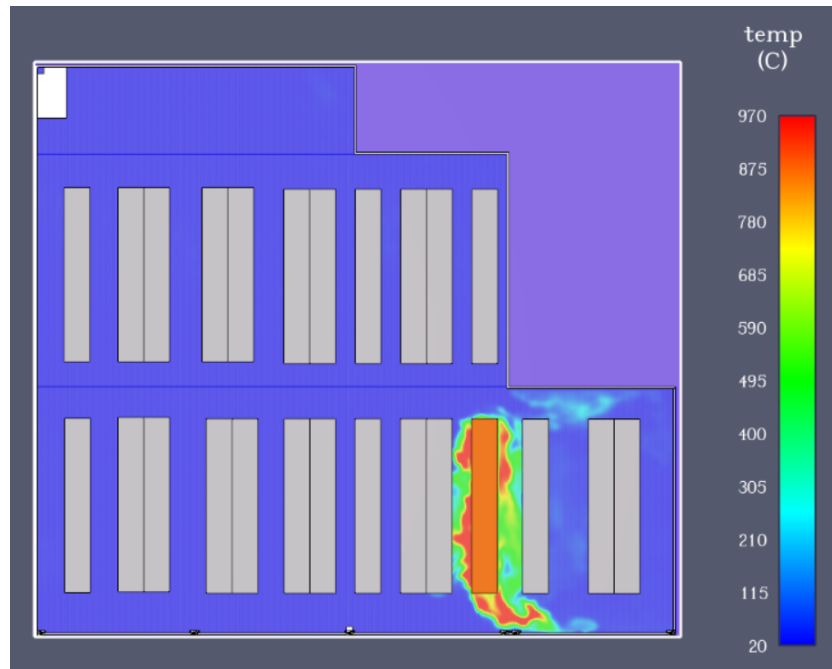


Fig. 4. Temperature variation in the hall for 600 seconds at a height of 1.8 m from the floor

It is observed that temperatures in the area of the outbreak start from 400°C and reach up to 970°C in the immediate vicinity.

In Fig. 5. The evolution of the temperature measured by the thermocouple located in the area of the firebox, 3 m from the floor, is presented. Following the analysis of the graph, an increase in temperature is observed in the range of 150-200 seconds, specific to the development phase of the fire. After reaching a value of about 1000°C, the temperature begins to oscillate slightly, as a result of the combustion of the combustible materials available in the combustion zone, and the heat energy input decreases.

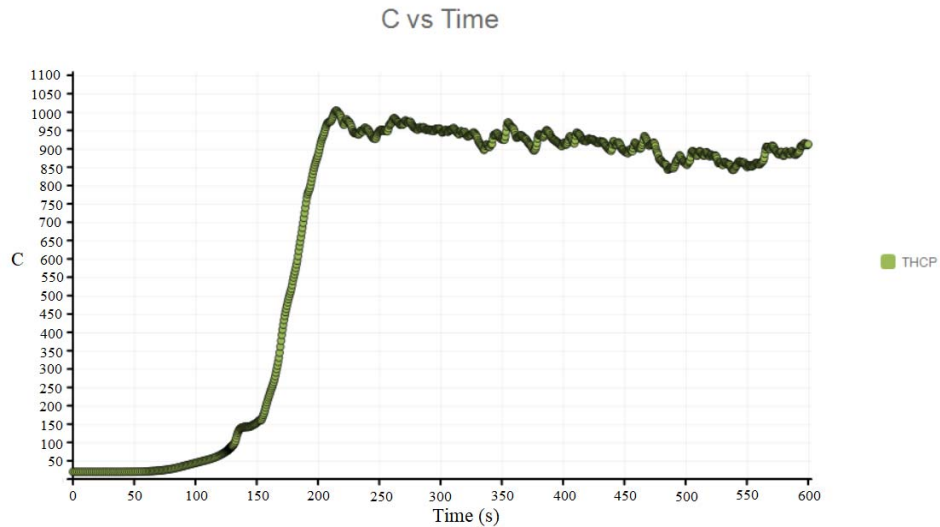


Fig. 5. The temperature measured by the thermocouple located in the area of the firebox

According to Figure 6, at the end of the 600 seconds, the temperature at the top of the hall in the outbreak area is around 970°C.

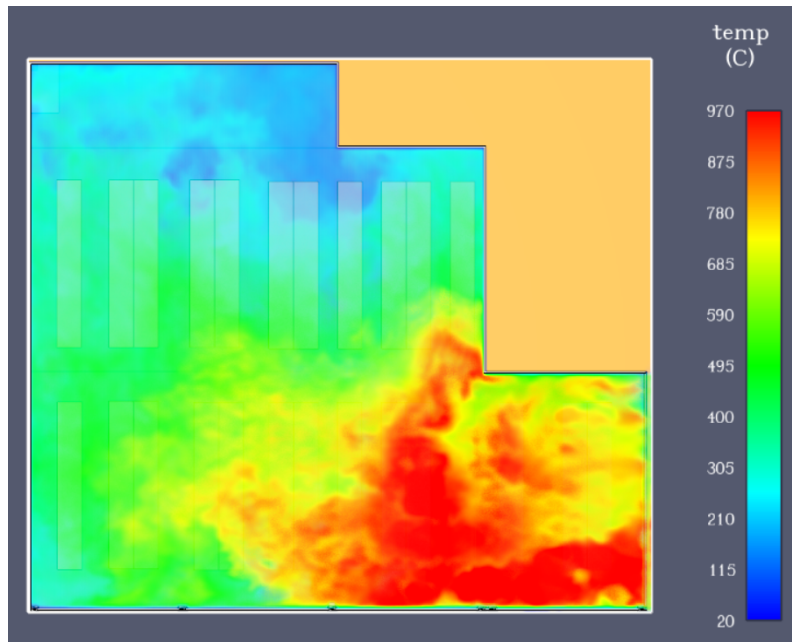


Fig. 6. Temperature at the top of the hall after 600 seconds

### 3. Flue gas movement

The combustion process, whether complete or incomplete, generates gases that influence the dynamics of the fire. The gases released from the combustion process have a lower density than the density of air and a higher temperature. These hot gases tend to rise rapidly vertically, moving towards the top of the room, after which they continue their movement horizontally, parallel to the ceiling. This phenomenon is essential in fire dynamics and has direct implications on visibility, exhaust conditions and heat transmission.

Figure 8 shows the movement and velocity of the flue gases in the storage hall. It is observed that in the area of the focus (shown in Figure 7) the speed of movement of the flue gases reaches values of up to 15 m/s, represented by the color red. The green color represents the areas where the speed of smoke movement has values of approximately 7.5 m/s. The blue color represents the areas where the speed has values of about 1.5 m/s or even lower, which happens in the corners of the hall, especially in those opposite the firebox.



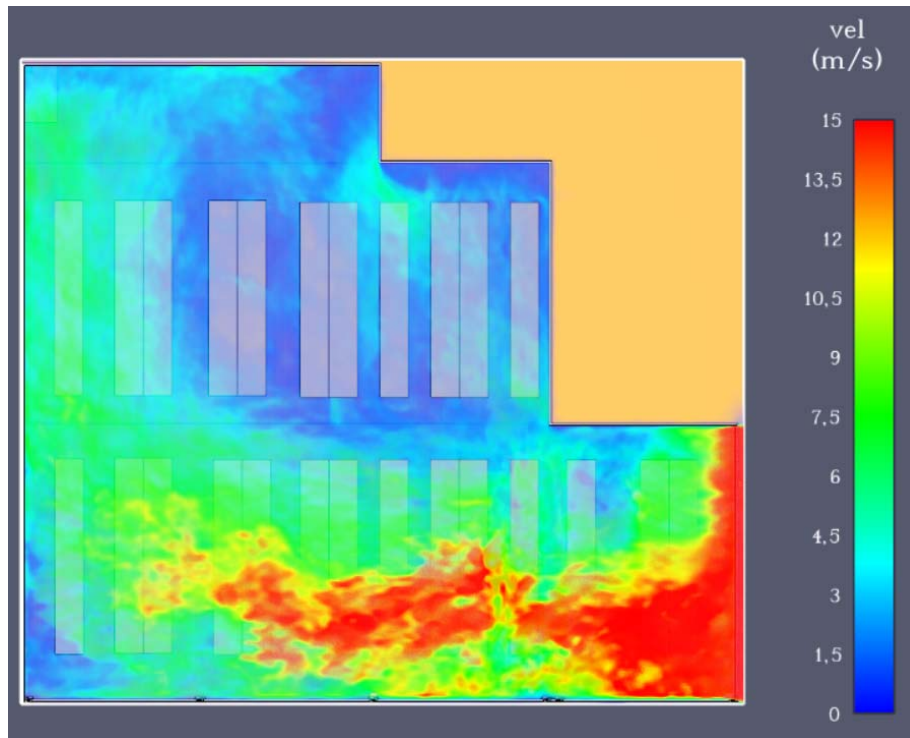


Fig. 7. Gas movement speed after 600 seconds at the top

#### 4. Visibility within the hall

Visibility is a critical factor for assessing the evacuation and intervention conditions in the event of a fire in a storage hall. As the combustion of combustible materials generates dense smoke, the field of vision is significantly reduced, especially in the upper areas of the room. Low visibility affects the orientation of people inside, delays the evacuation process and can lead to panic. Also, low visibility negatively influences the efficiency of the intervention teams, which encounter problems in locating the outbreak or the victims.

Visibility of less than 10 metres is considered to significantly diminish the safe escape capacity [3].

Figure 8 shows the degree of visibility inside the hall at a height of 1.8 m from the floor. It is observed that, in the area of the outbreak, the visibility for the intervention personnel is non-existent, but they benefit from a degree of visibility on the left side of the space. Carrying out reconnaissance and locating the outbreak in the burned space are difficult, but not impossible. However, the high temperatures in the area of the burned space make the entry of the intervention crews dangerous.

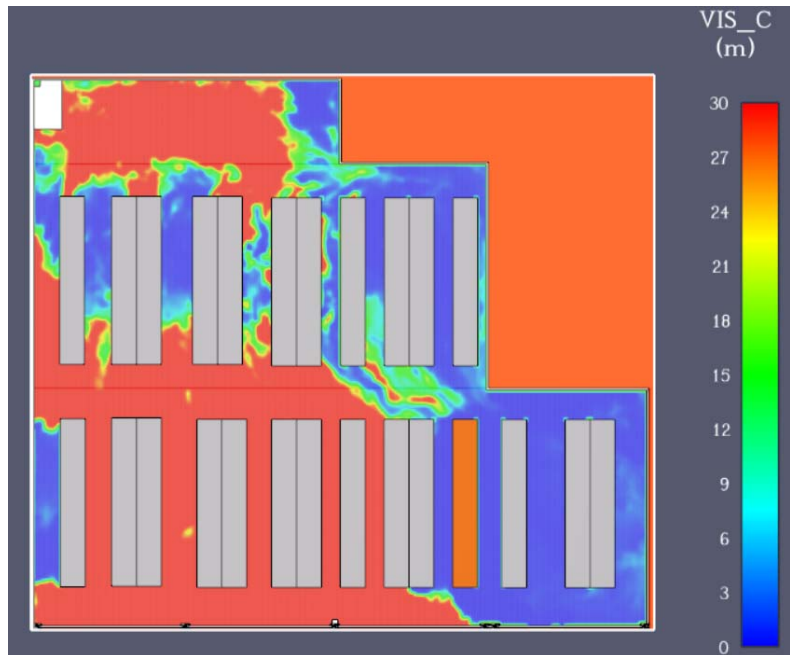


Fig. 8. Hall visibility after 600 seconds at a height of 1.8 m

Figure 9 shows the smoke stratification in the storage hall from different angles. Considering that the height of the hall is 12 m, it is observed that the smoke does not flood the entire hall vertically.



Fig. 9. Vertical smoke stratification after 600 seconds

### 3. Scenario II

#### 1. Temperature

Figure 10 shows the temperature variation in the focus area, over a duration of 600 seconds, with the help of a thermocouple (THCP). The temperature in the area of the outbreak begins to rise rapidly and reaches a maximum value of about 1100°C. Subsequently, the temperature decreases, as a result of the entry into operation of the sprinkler system. However, the moment of commissioning of the installation does not correspond to reaching the maximum temperature, but only when the trigger temperature in the area of the sprinkler head is reached. Thus, the temperature reduction becomes visible only after a few seconds after the trigger, and the decrease is constant until the end of the analyzed interval.



Comparative simulation of a fire in a paint storage warehouse: with and without an ESFR sprinkler system

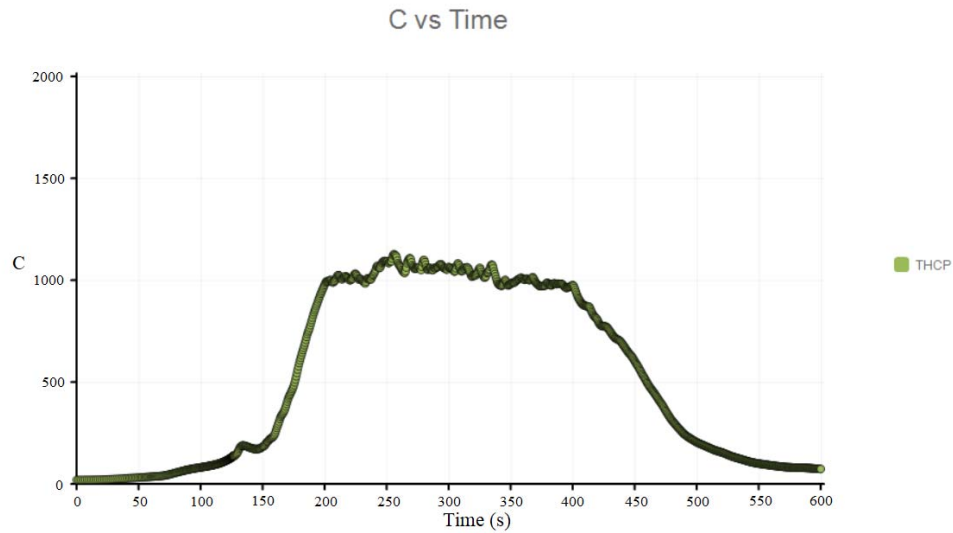


Fig. 10. The temperature measured by the thermocouple located in the area of the outbreak

The graph confirms the contribution of the sprinkler extinguishing installation in limiting the spread of the fire, even if the activation is not instantaneous. This underlines the importance of proper placement of the sprinkler heads, for maximum efficiency in the early phase of the fire.

Figure 11, taken at the end of the 600 seconds, confirms the efficiency of the sprinkler installation in limiting the spread of the fire, the outbreak being efficiently controlled and completely extinguished.

These images confirm the role that sprinkler extinguishing systems play in limiting the spread of fire and reducing temperature.

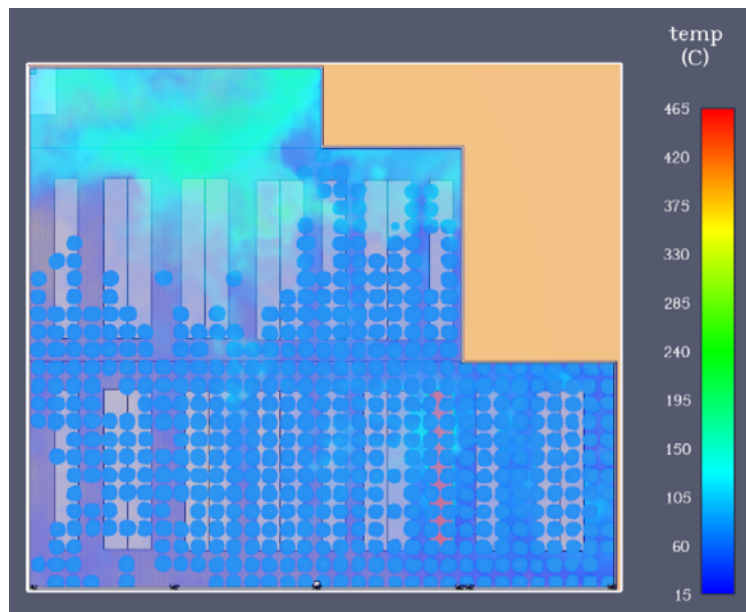


Fig. 11. Temperature in the ceiling area at the end of the 600 seconds

## 2. Flue gas movement

Figure 12 captures the moment a few seconds after the sprinkler installation is triggered, with the combustion process still active in the focus area. High flue gas velocities are observed, with values of 6.8 – 8.5 m/s, in shades of orange and red. These values signal the existence of strong currents that drive heat and smoke particles towards the ceiling, this stage being critical, because the gases contribute to the formation of the upper layer of smoke.

Figura 13 este realizată la finalul simulării, moment până în care acțiunea instalației de sprinklere și-a manifestat eficiența. Nuanțele albastre și verzi indică o scădere semnificativă a vitezi gazelor de ardere la nivelul plafonului, majoritatea valorilor fiind sub 2-3 m/s. Această reducere semnificativă evidențiază disiparea energiei acumulate și limitarea propagării incendiului.

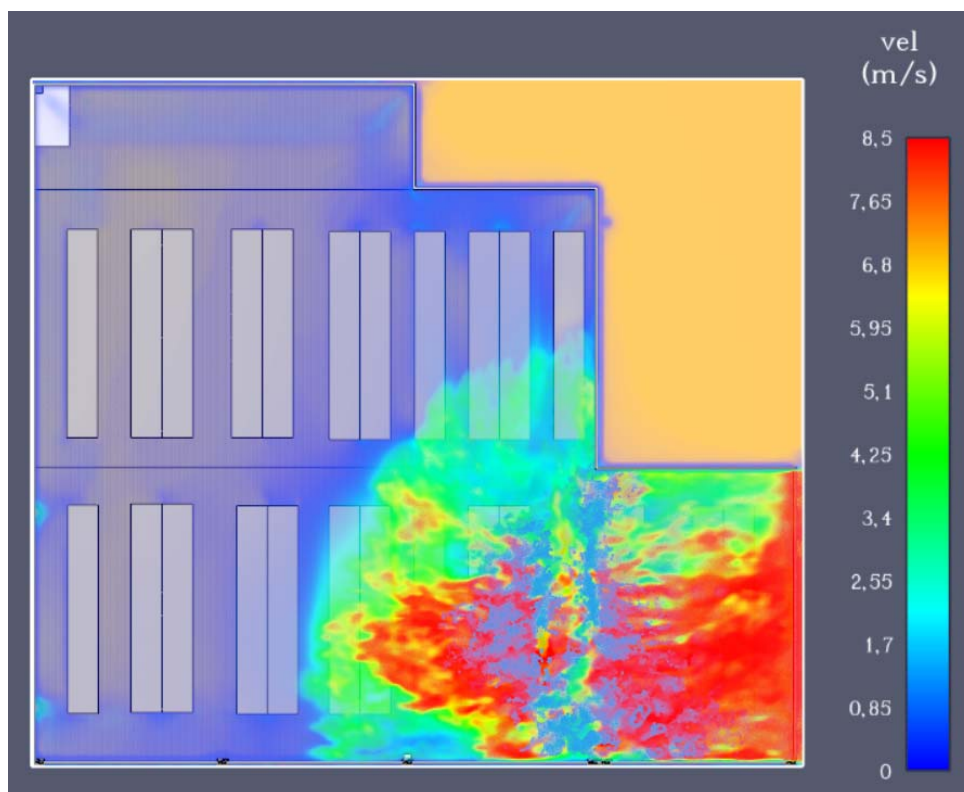


Fig. 12. Flue gas movement after sprinklers are triggered

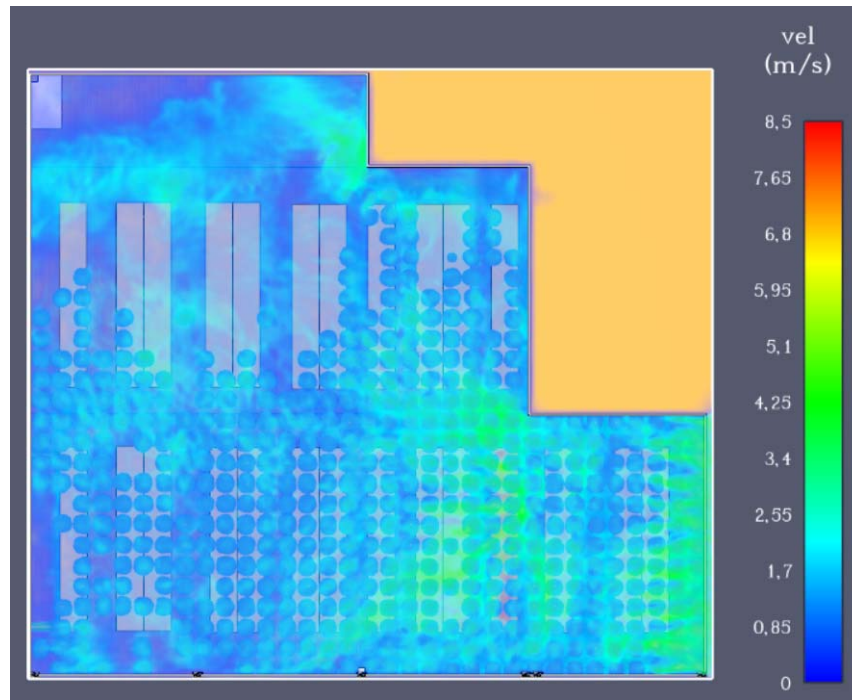


Fig. 13. Flue gas movement at the end of 600 seconds

### 3. Visibility within space

The images below show the visibility inside the hall at a height of 1.8 m from the floor, corresponding to the average level of the field of vision for an adult male.

Figure 14 shows a significant decrease in visibility in the area of the outbreak, caused by the accumulation of flue gases and dense smoke. Areas highlighted with shades of blue indicate visibility below 3 m, critical values that can affect people's orientation.

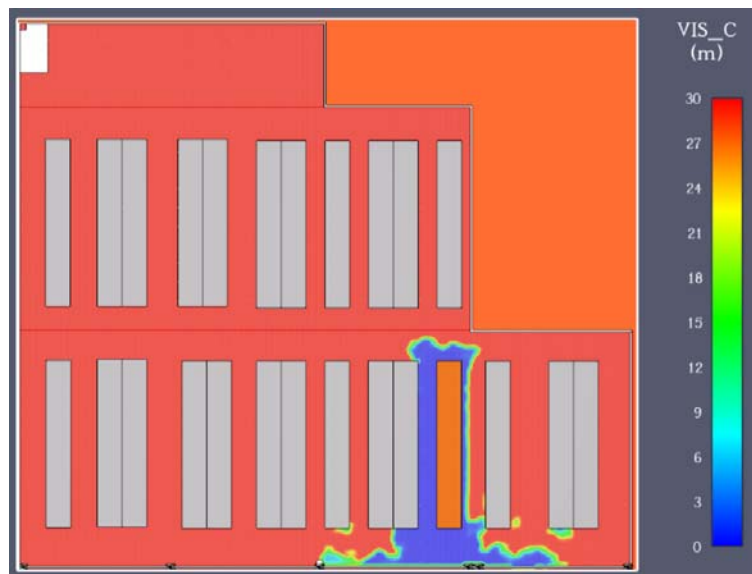


Fig. 14. Visibility inside the hall at a height of 1.8 m before the sprinklers are triggered

Figure 15 shows the situation at the end of the 600 seconds, after the sprinkler system has come into operation. In the area of the outbreak, visibility is almost non-existent, which is highlighted by the blue color. The central area allows good visibility, up to approx. 30 m.

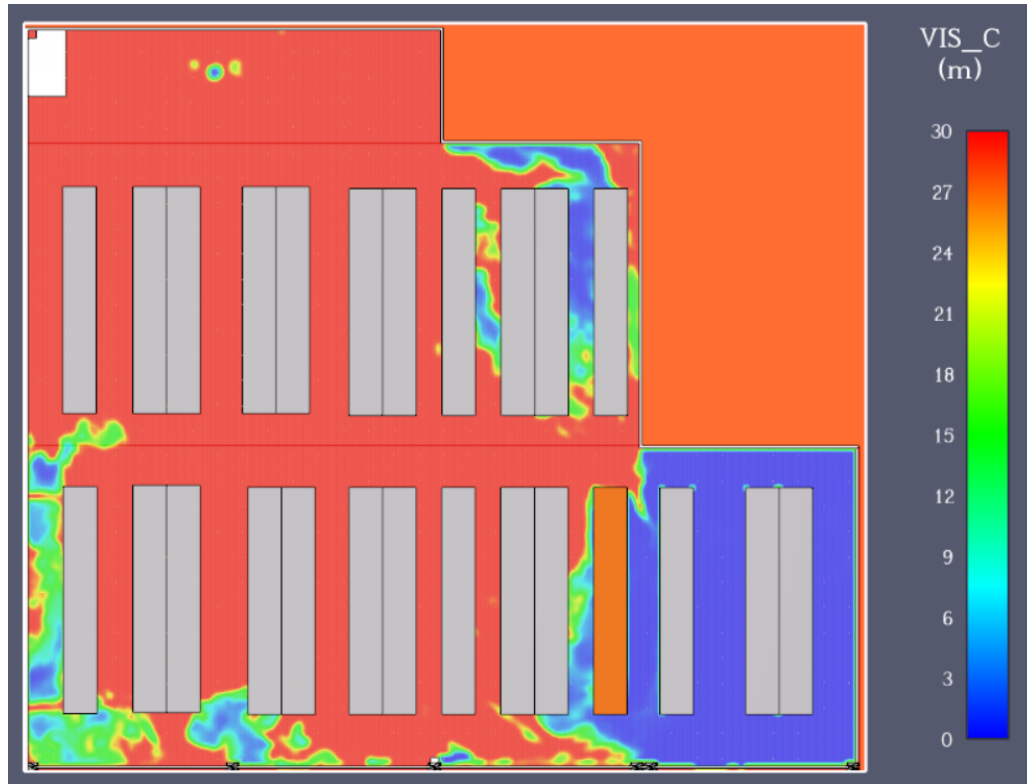


Fig. 15. Visibility inside the hall at a height of 1.8 m at the end of the 600 seconds

#### 4. Discussions

The analysis of the characteristic parameters of the fire in the two scenarios is shown in Table 2.

Table 2

Comparing the results of the two simulations

Studied parameter	Simulation 600 seconds without the use of ESFR sprinkler extinguishing system	600-second simulation with the use of ESFR sprinkler extinguishing system
Temperature variation in the ceiling area	210°C – 970°C	60°C – 135°C
Temperature variation at a height of 1.8 m from the floor	400°C – 970°C	60°C – 105°C

Studied parameter	Simulation 600 seconds without the use of ESFR sprinkler extinguishing system	600-second simulation with the use of ESFR sprinkler extinguishing system
Flue gas velocity	1.5 m/s – 15 m/s	0.85 m/s – 3.4 m/s
Visibility at a height of 1.8 m from the floor	0 m in the area of the firebox and the right side of the hall Up to 30 m on the left and central side of the hall	0 m – 15 m in the firebox area and the right side of the hall 15 m – 30 m in the central and left part of the hall
Smoke stratification	Complete flooding at ceiling level Partial flooding in the vertical plane	Complete flooding at ceiling level Partial flooding in the vertical plane

The analysis of the two scenarios, with and without the use of the ESFR sprinkler extinguishing system, highlights the efficiency of this system in the context of the active protection of a paint storage hall.

The commissioning of the installation causes a significant decrease in the maximum temperature recorded, both in the ceiling area and at a height of 1.8 m from the floor, which contributes to limiting the spread of fire and reducing the associated risks.

All these aspects underline the idea that the integration of an ESFR sprinkler installation not only limits the spread of fire, but also obviously contributes to the protection of property. This is an effective technical solution for industrial premises exposed to a high risk of fire.

## 5. Conclusions

Following the simulations carried out using PyroSim software, which analyzed fire behavior in two scenarios – one without the operation of the ESFR sprinkler system and one with its activation – the effectiveness of the automatic suppression system in limiting the effects of a fire in a paint storage hall was clearly demonstrated [4].

The scenario without sprinklers led to the development of a high-intensity fire, with extremely high temperatures (up to 970 °C at ceiling level). These conditions made human intervention impossible in the early phases and posed a significant risk to both personnel safety and the structural integrity of the building [5].

In contrast, the scenario in which the ESFR sprinkler system functioned correctly showed a substantial reduction in recorded temperatures, underlining the crucial role of this technology in rapid fire control. The activation of the system limited fire spread and reduced the thermal impact on both the structure and the occupants [6].

In conclusion, the implementation of ESFR sprinkler systems proves to be an essential solution for active fire protection in storage facilities with a high fire risk [7].

## Referințe

- [1] “Fire Dynamics Simulator (FDS) Graphical Interface (GUI) for 3D Fire and Smoke Modeling: PyroSim.” Accessed: July 19, 2025. [Online]. Available: <https://www.thunderheadeng.com/pyrosim/>
- [2] M. Roser, C. Appel, and H. Ritchie, “Human Height,” *Our World in Data*, May 2021, Accessed: July 19, 2025. [Online]. Available: <https://ourworldindata.org/human-height>
- [3] Purser, D. A. Toxicity Assessment of Combustion Products. In: SFPE Handbook of Fire Protection Engineering, 5th Edition
- [4] K. B. McGrattan, “Fire dynamics simulator (version 4): technical reference guide,” *NIST Special Publication*.
- [5] “NFPA | The National Fire Protection Association.” Accessed: July 19, 2025. [Online]. Available: <https://www.nfpa.org/en>
- [6] R. Peacock, “A Review of Building Evacuation Models: 2nd Edition”.
- [7] “(PDF) Numerical Simulation of Sprinkler Suppression of Rack Storage Fires,” *ResearchGate*, doi: 10.3801/IAFSS.FSS.11-1170.

# Analysis of the Global Impact of Light Pollution. Ecological Environment Perspectives

Analiza impactului global al poluării luminoase. Perspectivă ecologică și de mediu

Anca MANOLESCU<sup>1</sup>, Ionuț STĂNESCU<sup>1</sup>

<sup>1</sup> Technical University of Civil Engineering of Bucharest  
122-124 Bvd Lacul Tei, Bucharest, Sector 2, Romania

E-mail: [anca.manolescu@utcb.ro](mailto:anca.manolescu@utcb.ro), [ionut-mihail.stanescu@phd.utcb.ro](mailto:ionut-mihail.stanescu@phd.utcb.ro)

DOI: 10.37789/rjce.2025.16.4.5

**Abstract.** Light pollution is intensifying globally, affecting around 80% of the world's population, a figure that rises to 99% in Europe and North America. The use of artificial light at night increases annually by at least 10% due to urbanization, industrialization, and population growth. Efforts to enhance energy efficiency and reduce energy costs are leading to technological advancements and changes in consumer behavior that help mitigate light pollution. Annually, about \$50 billion is spent on energy for lighting that ultimately leaks into space, impacting nocturnal environments and various species. This pollution disrupts human sleep, circadian rhythms, and melatonin production, and alters the natural behaviors of wildlife, trees, and insects. Despite its extensive impact on health, biodiversity, and ecosystems, a unified legal framework to regulate light pollution is lacking in the EU. Effective strategies to minimize ecological impacts while maintaining city illumination are crucial.

**Key words:** light pollution, energy efficiency, human health

**Rezumat.** Poluarea luminoasă este în creștere la scară globală, expunând circa 80% din populația lumii - și până la 99% în Europa și America de Nord - unor niveluri excesive de lumină artificială nocturnă. Suprafața și intensitatea iluminatului pe timp de noapte cresc cu cel puțin 10% anual, impulsionate de urbanizare, industrializare și dinamica demografică. Inițiativele orientate spre eficiență energetică și reducerea costurilor stimulează inovația tehnologică și schimbă comportamentele de consum, contribuind la limitarea emisiilor luminoase inutile. Se estimează că, anual, aproximativ 50 de miliarde USD sunt irosite pe energie pentru iluminat care se disipă în atmosferă, degradând peisajele nocturne și afectând o gamă largă de specii. Consecințele includ perturbarea somnului, dereglarea ritmurilor circadiene și a secreției de melatonină la oameni, precum și alterarea comportamentelor naturale ale faunei sălbatice, arborilor și insectelor. În pofida amprentei semnificative asupra sănătății, biodiversității și funcționării ecosistemelor, Uniunea Europeană nu dispune încă de un cadru normativ coerent și unitar pentru gestionarea poluării luminoase. Sunt necesare strategii integrate

*care să reducă impactul ecologic al iluminatului menținând, în același timp, siguranța și funcționalitatea spațiului urban.*

**Cuvinte cheie:** *poluare luminoasă; eficiență energetică; sănătate umană; biodiversitate; politici publice*

## 1. Introducere

The majority of the global and particularly the U.S. and European populations live under light-polluted skies, obscuring views of the night sky and affecting natural light levels. Over 80% of the world experiences light-polluted nights, which not only diminishes human experience with the night sky but also has broader ecological impacts.

Economic and energy concerns are highlighted by the significant energy consumption of artificial lighting, which contributes to carbon emissions and financial costs. The adoption of energy-efficient lighting technologies offers a dual benefit of reducing expenses and minimizing environmental impact. Also, light pollution disrupts ecosystems by altering animal behaviors and affecting plant phenology. It also impacts human health by disrupting circadian rhythms and sleep patterns, with potential long-term health consequences.

Astronomical effects of increased skyglow from artificial lighting significantly hinder astronomical observations and diminish the visibility of celestial phenomena, which have historically played crucial roles in navigation and scientific discovery. Fig.1 illustrates a series of impacts caused by light pollution.



Fig. 1. Light pollution impact



## 2. Content of the paper

### 2.1 Overview of lighting pollution problem

Statistics on global exposure to artificial light reveal significant global and regional impacts, affecting the visibility of the Milky Way and extending geographically across vast areas. Over 80% of the world's population lives under light-polluted skies, where the natural darkness of the night is significantly altered by artificial lighting. This percentage rises to more than 99% for the U.S. and European populations, illustrating a profound loss of natural night environments in these regions. [1]

Light pollution obscures the visibility of the Milky Way for over one-third of humanity, including 60% of Europeans and nearly 80% of North Americans, representing a substantial cultural and natural loss as many are deprived of viewing this essential astronomical feature from their locations. Approximately 23% of the world's land areas between latitudes 75°N and 60°S suffer from light-polluted nights. This includes 88% of Europe and nearly half of the United States, demonstrating extensive environmental impact across large and diverse geographic areas.[1] These statistics underscore the extensive reach and growing problem of light pollution globally, affecting not just human health and energy consumption but also the ecological and atmospheric quality of our environment.

Light emitted from the Earth's surface into space is quantified as radiance, which is a measure of the intensity of brightness observed from a specific angle per unit area ( $\text{nW}/\text{cm}^2 \cdot \text{sr}$ ). Such measurements are used in remote sensing and astronomical observations to assess the brightness and light pollution of areas on Earth. This can include monitoring city lights, tracking changes in light emission over time, and studying ecological impacts of artificial light. Instruments like the Visible Infrared Imaging Radiometer Suite (VIIRS) on the Suomi National Polar-orbiting Partnership (NPP) satellite are commonly used to gather this type of data, allowing researchers to map and analyze how human activities light up the night on a global scale. The images below illustrate the changes in radiance around the world from 2014 to 2023 [2].

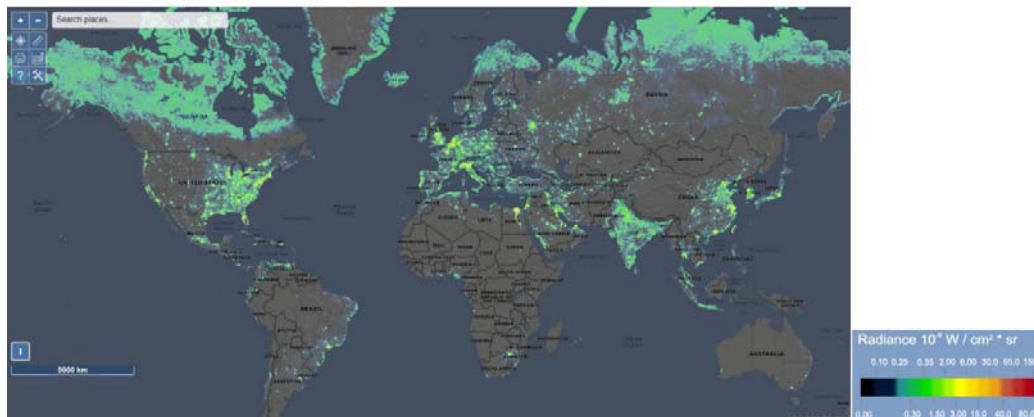


Fig. 2. World map light pollution 2014 [2]

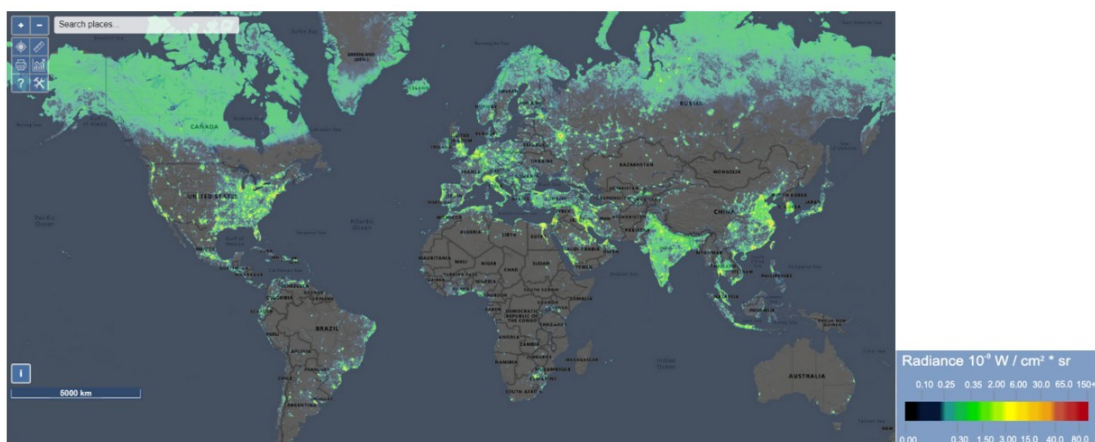


Fig. 3. World map light pollution 2023 [2]

In the following pictures we can see the numbers of observatories and sky dark cameras in 2023.

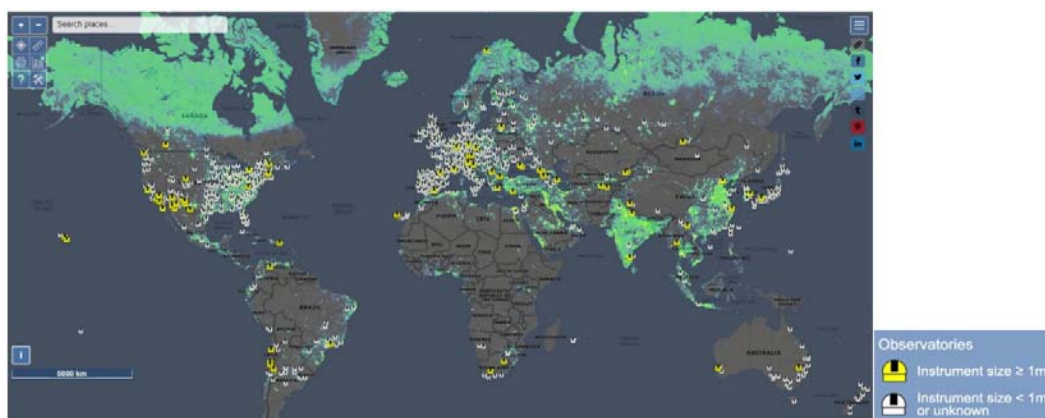


Fig. 4. World map observatories 2023 [2]

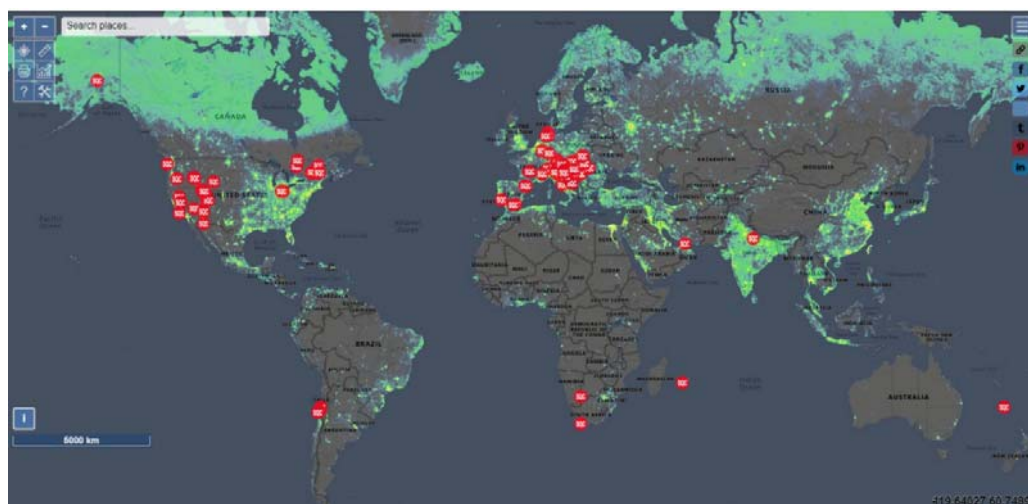


Fig. 5. World map sky quality cameras 2023 [2]

The images below illustrate the changes in radiance in Europe from 2014 to 2023.

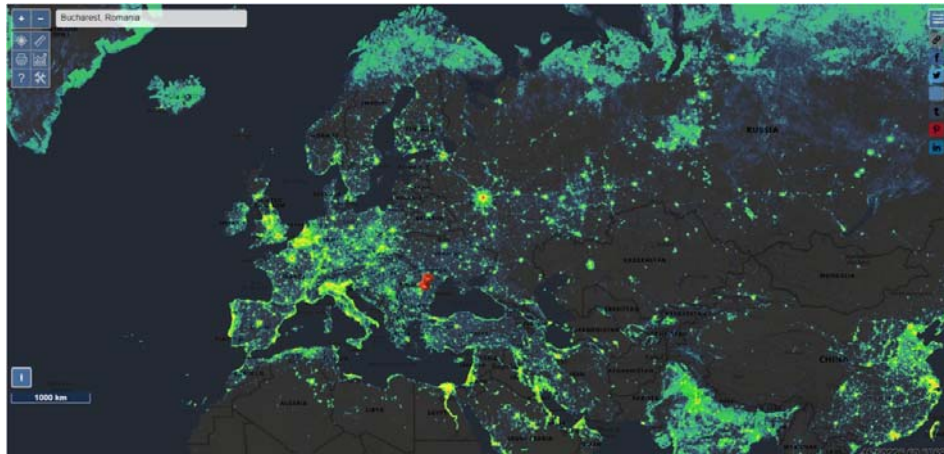


Fig. 6. Europe map light pollution 2014 [2]

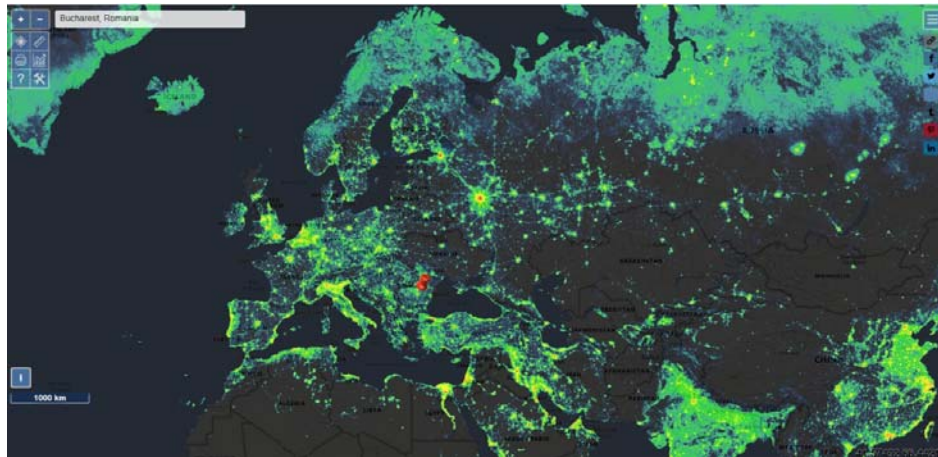


Fig. 7. Europe map light pollution 2023 [2]

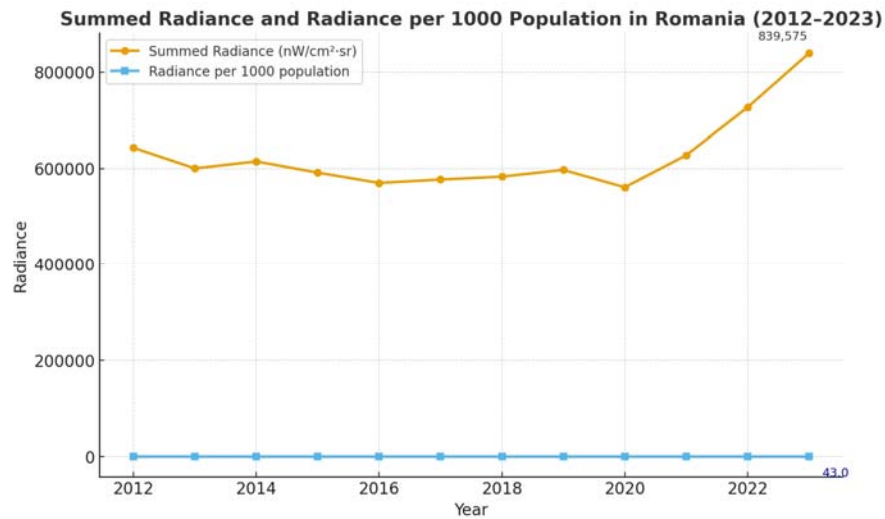


Fig. 8. Summed radiance for Romania 2012 – 2023 [2]

**Summed radiance for Tomania 2012 – 2023 [2]**

Year	Pixel count	Sum	Rad. / 1000 pop.	Mean
2012	1,591,881	643,413	33.0	0.5801
2013	1,591,881	600,621	30.8	0.5416
2014	1,591,881	615,013	31.5	0.5545
2015	1,591,881	591,867	30.3	0.5337
2016	1,591,881	570,367	29.2	0.5143
2017	1,591,881	577,425	29.6	0.5206
2018	1,591,881	583,535	29.9	0.5261
2019	1,591,881	597,434	30.6	0.5387
2020	1,591,881	561,326	28.8	0.5061
2021	1,591,881	627,882	32.2	0.5661
2022	1,591,881	726,855	37.2	0.6554
2023	1,591,881	839,575	43.0	0.7570

This study examined the evolution of artificial light at night (ALAN) in Romania using VIIRS satellite radiance data between 2012–2023. Our analysis confirmed the research hypothesis: radiance values show a measurable and consistent increase over the past decade, both in absolute terms and relative to population. These findings reflect the combined effects of urbanization, industrialization, and gaps in regulatory enforcement.

To ensure comparability across years, we relied on the VIIRS Annual V2 dataset, which has recently been validated and extended through global simulations by Tang et al. [5] and Chen et al. [6].

By integrating satellite-derived datasets with demographic normalization, the methodology provided both quantitative and comparative insights into light pollution trends. The results highlight that energy-efficient technologies alone do not necessarily reduce light pollution when urban expansion and increased consumption offset efficiency gains.

From a policy perspective, the evidence underscores the urgent need for harmonized European legislation, as well as local interventions such as stricter lighting codes, curfews for non-essential lighting, and adaptive smart lighting systems. Future research should expand this framework by incorporating cross-country comparisons, ecological impact assessments, and scenario-based modeling of mitigation strategies.

Overall, the findings strengthen the argument that light pollution must be treated not only as an energy or aesthetic issue, but as a measurable environmental pressure with direct consequences for biodiversity, human health, and cultural heritage.



## 2.2. Light pollution drivers

The main drivers of light pollution are industrialization and urbanization, complemented by population growth which escalates the use of artificial lighting. Meanwhile, the shift toward energy-efficient technologies seeks to lower energy expenses and mitigate climate change impacts. Industrialization and urbanization are significant drivers of increasing light pollution. As cities expand and industrial activities intensify, there is a corresponding rise in the use of artificial lighting. This increased lighting is not only a product of growth but also a facilitator for extended commercial hours and enhanced public safety. However, the side effects include disrupted ecosystems and altered human and wildlife circadian rhythms.

Urbanization leads to denser living spaces and more illuminated public areas, contributing significantly to "skyglow," which obscures the visibility of stars. The materials point out that as urban areas grow, there is a need for policies that address the balance between necessary illumination for safety and the prevention of excessive light that can be harmful to both environmental and human health. The challenge lies in implementing lighting that is effective yet minimizes the negative impacts of light pollution, urging a shift towards more strategic and lower impact lighting solutions in urban planning.

Population growth is a significant driver of increased artificial light use, leading to more widespread light pollution. As urban populations expand, there is a corresponding rise in the demand for lighting to support extended hours of activity and improved safety. This increase often leads to excessive night lighting in urban centers, which not only affects energy consumption but also disrupts ecosystems and human health. The challenge lies in balancing the benefits of artificial lighting for urban development and security with the need to minimize its ecological and health impacts. The documents suggest strategies like using energy-efficient lighting technologies and implementing better lighting designs that focus on limiting unnecessary light exposure to the environment.

The transition towards energy-efficient technologies, aimed at reducing energy costs and addressing climate change, is a critical response to the escalating impacts of light pollution. This shift is evident in the adoption of LED lighting and the implementation of energy-efficient fixtures that not only reduce power consumption but also minimize environmental impacts. For instance, the integration of LED technology is noted for its superior energy efficiency compared to traditional lighting solutions, reducing both energy costs and carbon emissions. This move towards LEDs and other energy-efficient lighting systems reflects a broader commitment to sustainability, particularly in urban settings where light pollution is most concentrated.

Light pollution extends beyond visual disturbance, influencing ecological and social well-being, as recent studies demonstrate [7].

Moreover, strategic approaches like the use of shielded fixtures to direct light precisely where it is needed and the implementation of smart lighting systems that adjust brightness based on real-time needs are being emphasized. These measures not only conserve energy but also help in preserving the natural night environment, reducing the adverse effects on both human health and wildlife. These transitions are supported by policies and guidelines encouraging the adoption of green technologies and practices

that align with broader environmental goals, demonstrating a concerted effort to tackle the dual challenges of energy efficiency and environmental sustainability.

### 2.3. Economic and environmental costs

Annual global expenditure on energy for lighting not only impacts financial resources but also contributes to light pollution, which significantly degrades the quality of nocturnal skies and atmospheric conditions and have several effects on health and biodiversity.

Global spending on energy for artificial lighting is estimated at \$50–70 billion annually, with street lighting alone accounting for approximately 19% of global electricity use [1]. This expenditure is particularly stark considering that much of this light is wasted, shining upwards or outwards rather than illuminating the intended areas, thereby adding unnecessary costs and environmental impacts. These wasteful practices not only result in financial loss but also exacerbate ecological disruptions by affecting nocturnal wildlife and contributing to energy inefficiency. It is important to adopt more efficient lighting practices, including the use of technologies that reduce light scatter and improve the directionality of lighting to minimize sky glow and light trespass. This shift towards more sustainable lighting practices is highlighted as a crucial step in reducing both the economic and environmental costs associated with light pollution.

Light pollution significantly degrades the quality of nocturnal skies and impacts atmospheric conditions. This form of pollution caused by the overuse and poor design of artificial lighting results in several environmental disturbances:

- Glare - bright, direct light that impairs human vision, making it difficult to see in the surrounding darkness. This can pose safety risks, particularly for drivers and pedestrians at night.
- Sky Glow - the excessive brightness that illuminates the sky overpopulated areas, obscuring the view of stars and planets. This glow extends far beyond the light sources, affecting even remote areas.
- Light trespass - light that spills into areas where it is not needed or wanted, such as residential windows, causing disruptions and reducing the quality of sleep for inhabitants.

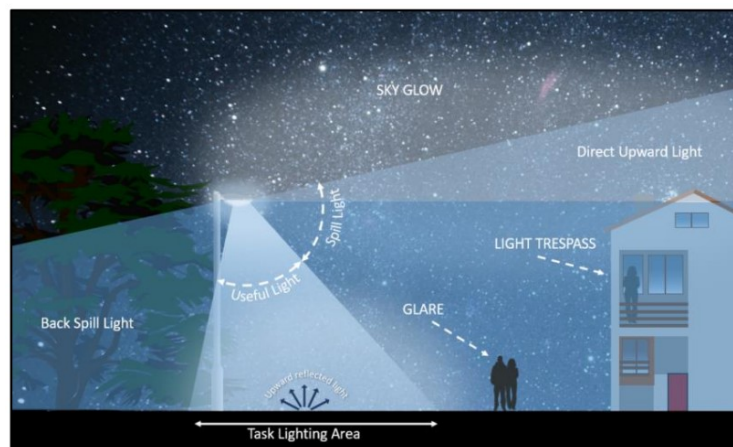


Fig. 9. Reduced sources of Light Pollution. The residual impacts of the lighting [3]

The impact of these aspects of light pollution is profound, affecting human health by disrupting circadian rhythms and suppressing melatonin production, which can lead to sleep disorders and other health issues.

At the global level, citizen science projects reveal a ~10% annual increase in sky brightness, underscoring that the problem is accelerating faster than satellite data alone suggests. [8]

In terms of biodiversity, light pollution has significant negative impacts on various species across different ecosystems. Nocturnal animals, which rely on the darkness for their natural behaviors such as feeding and reproduction, are especially affected. The altered light conditions can confuse animal navigation, alter predator-prey relationships, and disrupt the reproductive patterns of many species. This ecological imbalance extends to affecting plants and insects, fundamentally altering habitats and food chains.

Efforts to manage and mitigate these impacts are crucial, and they include designing lighting that minimizes sky glow, glare, and light trespass. Such designs involve using fully shielded fixtures, implementing lower light levels, and using lights only when necessary. These strategies not only improve the quality of the night environment but also save energy and reduce associated costs.

## **2.4. Light pollution in legal and policy frameworks**

Despite various national and local initiatives to mitigate light pollution effects, there is no comprehensive EU-wide regulation to consistently address this issue. The lack of a cohesive legal structure leads to varied approaches and standards among EU countries, which can hinder effective regional strategies for reducing light pollution.

For instance, France has implemented detailed national laws that regulate lighting intensities, schedules, and specific requirements for various areas, with penalties for non-compliance (for example, from July 1, 2018, illuminated advertisements must be turned off between 1:00 AM and 6:00 AM). Italy and Spain have more regional approaches, with some areas lacking comprehensive legislation. Liechtenstein is an example of a country that has already defined artificial light as source of potentially harmful radiation in the Environment Protection Act, which is a national binding document. Meanwhile, in Belgium, private light sources are regulated, but public lighting remains uncontrolled. Around the world, the Australian government was one of the first officially recognizing artificial light as a source of pollution in the Environment Protection Act in 1997 and therefore defining it as a threat to the human and environmental health.

The metropolitan government of Seoul adopted a national law called the ordinance on the prevention and management of light pollution in 2010. Over the last few decades Chile has established its status as astronomical capital of the world due to strong political efforts protecting the night sky. As early as the 1990s, the astronomical community was critical of the increasing light pollution. In Supreme Decree No. 686 by the Ministry of Economy in 1998 are included regulations on the features of

outdoor lights mitigating upward light emissions and additionally the Office of Sky Quality in North Chile (OPCC) was founded.

Hong Kong is considered the most polluted city in the world due to its high population density, thriving economy, and more than 1000 skyscrapers. A study states that a night here is a thousand times brighter than the normal limit.

While LEDs are widely promoted, their effectiveness depends on implementation. In France, the introduction of curfews and shielded LED fixtures reduced skyglow by ~7% between 2012–2019 [4]. In contrast, regions of Spain where lighting policy is fragmented have shown little improvement. Chile provides a strong example outside Europe: strict astronomical protection laws since the 1990s have successfully reduced upward light emissions around observatories [2]. These examples suggest that technology alone is insufficient - effectiveness depends on strong regulatory frameworks and enforcement.

In the next table (1) ✓ means that there is a designated legislative act (on local/regional/national level) addressing light pollution; (✓) means that there is no designated legislative act addressing light pollution, but provisions from other legislative acts can be used; X means that there is no legislation addressing light pollution; (2) ✓ means that a guidebook/manual for correct lighting has been issued in the country; (✓) means that a guidebook/manual is underway; X means that a manual/guidebook is existing or in preparation; (3) Others means the country e.g. Dark Sky Area, specific projects, dedicated to light pollution [4].

The European Ecodesign Directive and the Energy Labelling and Repealing Directive focus on energy-efficient installations but do not directly address the adverse impacts of light pollution. Additionally, light pollution is recognized under the EU Green Public Procurement (GPP), which recommends reducing light pollution levels, but adherence remains voluntary.

Table 2

**Overview of the European actions to reduce light pollution [4]**

Country	Legislation <sup>1</sup>	Standard	Manual <sup>2</sup>	Other <sup>3</sup>
Austria	X	✓	✓	✓
Belgium	X	✓	✓	✓
Bulgaria	X	✓	X	X
Croatia	✓	X	X	✓
Cyprus	X	X	X	✓
Czech Republic	(✓)	(✓)	✓	✓
Denmark	(✓)	X	✓	✓
Estonia	X	X	X	✓
Finland	(✓)	X	(✓)	X
France	✓	X	X	✓
Germany	✓	X	✓	✓
Greece	✓	X	X	✓



#### Analysis of the global impact of light pollution. Ecological environment perspectives

Hungary	(✓)	X	✓	✓
Iceland	X	X	X	✓
Ireland	X	X	✓	✓
Italy	✓	✓	X	X
Latvia	(✓)	X	X	✓
Liechtenstein	X	X	X	✓
Lithuania	X	X	X	X
Luxembourg	X	X	✓	✓
Malta	✓	✓	(✓)	✓
Netherlands	(✓)	X	✓	✓
Norway	X	X	✓	X
Poland	X	X	X	✓
Portugal	X	X	✓	✓
Romania	X	X	X	✓
Slovakia	(✓)	X	X	✓
Slovenia	(✓)	X	✓	✓
Spain	✓	X	✓	✓
Sweden	✓	(✓)	✓	X
Switzerland	(✓)	✓	✓	✓
United Kingdom	✓	X	✓	✓

Establishing more standardized regulations could better address the ecological impacts of artificial lighting and align with broader environmental goals. The need for an integrated policy approach is evident, aiming to harmonize light pollution measures across member states while considering local environmental conditions and urban development patterns, to better manage light pollution's ecological, health, and astronomical impacts.

## 2.5. Mitigation strategies

There are several strategies for mitigating light pollution while maintaining essential urban illumination:

- ✓ Implementing energy-efficient lights such as LEDs, which can be dimmed and directed more precisely, reduces overall light pollution without compromising safety or aesthetic lighting needs.
- ✓ Encouraging the installation of fully shielded fixtures ensures that light is directed downwards where it is needed, preventing unnecessary sky glow and light trespassing into natural areas or neighboring properties.
- ✓ Integrating advanced technologies, including motion sensors and adaptive lighting systems, can dynamically adjust lighting levels based on actual conditions, such as pedestrian or vehicular presence. This approach minimizes light waste during time of low activity.
- ✓ Developing policies that require or incentivize the adoption of low-impact lighting technologies can help scale these practices. Urban planning that

integrates light pollution reduction into broader environmental and public health strategies is also crucial.

- ✓ Educating and involving community members and stakeholders in light pollution reduction efforts can enhance the acceptance and effectiveness of these strategies. Collaborative approaches can lead to more sustainable practices that are supported by both public and private sectors.

These mitigation strategies, coupled with an understanding of the benefits of reducing light pollution - such as energy savings, improved public health, and better environmental outcomes - underscore the importance of concerted efforts at various levels of governance and society.

### 3. Conclusions

This study analyzed the evolution of artificial light at night (ALAN) using VIIRS satellite data from 2012 to 2023, with a specific focus on Romania. The findings support the initial hypothesis: radiance values have increased steadily over the last decade, both in absolute terms and normalized per population, reflecting the combined influence of urbanization, industrialization, and insufficient policy enforcement.

Beyond confirming these trends, the results highlight the limitations of technology-only approaches. While LEDs and smart lighting systems reduce energy consumption, they do not automatically mitigate light pollution without complementary policies. Comparative evidence from countries such as France, Germany, and Chile suggests that legally enforced curfews and shielding requirements are more effective than technology alone.

Future research should expand this framework in three directions:

1. Cross-country analysis - extending the comparative dataset beyond Romania, France, and Germany to other EU countries with different governance approaches.
2. Ecological monitoring - linking satellite-derived radiance trends with biodiversity indicators (e.g., insect decline, bird migration, plant phenology).
3. Policy evaluation - scenario-based modeling to test the impact of specific regulatory measures (curfews, zoning rules, adaptive lighting systems) on radiance trends.

Concrete collaboration between remote sensing experts, ecologists, and policymakers will be essential to translate radiance data into actionable strategies. Ultimately, addressing light pollution requires treating it as an environmental pressure comparable to air and noise pollution - with robust monitoring, enforcement, and community engagement.

### ACKNOWLEDGEMENT

This research was supported by **GNAC<sup>ARUST</sup><sub>2024</sub> – UTCB 25** project from Technical University of Civil Engineering, Bucharest, project number 1401/07.02.2025

## References

- [1] F. Falchi, P. Cinzano, D. Duriscoe, C. C. M. Kyba, C. D. Elvidge, K. Baugh, B. A. Portnov, N. A. Rybnikova, R. Furgoni, The new world atlas of artificial night sky brightness. *Sci. Adv.* 2, e1600377 (2016).
- [2] darksky.org, <https://www.lightpollutionmap.info>
- [3] Darkscape Consulting. Dedham Vale National Landscape & Coast & Heaths National Landscape 2023. LIGHTING DESIGN GUIDE. Guidance to reduce light pollution and protect our dark skies. <https://dedhamvale-nl.org.uk/>
- [4] Widmer, K., Beloconi, A., Marnane, I., Vounatsou, P., (2022). Review and Assessment of Available Information on Light Pollution in Europe (Eionet Report – ETC HE 2022/8), ISBN 978-82-93970-08-8, ETC HE c/o NILU, Kjeller, Norway.  
Science for Environment Policy (2023) *Light Pollution: Mitigation measures for environmental protection*. Future Brief 28. Brief produced for the European Commission DG Environment by the Science Communication Unit, UWE Bristol. Available at: <https://ec.europa.eu/science-environment-policy>.  
Welch, D., Dick, R., Trevino, K., Longcore, T., Rich, C., Hearnshaw, J., Ruggles, C., Dalton, A., Barentine, J. & Gyarmathy, I. (2024). *The world at night: Preserving natural darkness for heritage conservation and night sky appreciation*. IUCN WCPA Good Practice Guidelines Series No. 33, Gland, Switzerland: IUCN.
- [5] H. Tang, J. Liu, Z. Zhang, et al., “Global annual simulated VIIRS nighttime light dataset from 1992 to 2023,” *Scientific Data*, vol. 12, no. 143, pp. 1–15, 2025. doi: 10.1038/s41597-025-05246-8.
- [6] X. Chen, S. Xu, Q. Zhang, et al., “Global annual simulated VIIRS nighttime light dataset (SVNL) from 1992 to 2023,” *Scientific Data*, vol. 11, no. 567, pp. 1–14, 2024. doi: 10.1038/s41597-024-04228-6.
- [7] T. Balafoutis, “Light Pollution Beyond the Visible: Insights from People’s Perceptions,” *Urban Science*, vol. 9, no. 7, pp. 251, 2025. doi: 10.3390/urbansci9070251.
- [8] C. C. M. Kyba, F. Falchi, et al., “Rapid Brightening of Night Skies Globally: Recent Results from Citizen Science,” *Astronomy & Astrophysics Review*, vol. 31, pp. 1–25, 2023. doi: 10.1007/s00159-023-00139-0.

# Integrated Modeling and Simulation of Smart Building Energy Systems

Modelarea și simularea integrată a sistemelor de energie pentru clădiri inteligente

Petre- Marian PIRVULESCU<sup>1,\*</sup>, Catalin LUNGU<sup>1,\*</sup>, Tiberiu CATALINA<sup>1,\*</sup>, Ahmed HAMZE<sup>1</sup>

<sup>1</sup>Technical University of Civil Engineering Bucharest  
124 Lacul Tei Blvd., Bucharest, Romania

e-mail: [tiberiu.catalina@utcb.ro](mailto:tiberiu.catalina@utcb.ro), [catalin.lungu@utcb.ro](mailto:catalin.lungu@utcb.ro), [petre-marian.pirvulescu@student.utcb.ro](mailto:petre-marian.pirvulescu@student.utcb.ro), [ahmed.hamze@student.utcb.ro](mailto:ahmed.hamze@student.utcb.ro).

DOI: 10.37789/rjce.2025.16.4.6

**Abstract.** *This paper, entitled “Integrated Modeling and Simulation of Energy Systems for Smart Buildings”, aims to obtain relevant results regarding energy consumption in a smart building and compare them with those of a less intelligent building with the same functional regime. A comparative analysis of different building models highlights the impact of each smart transformation measure. Using DesignBuilder simulations, the study confirms the efficiency of intelligent control solutions for building energy systems. The results provide practical value for optimizing energy consumption, reducing costs, and supporting sustainable design decisions.*

**Key words:** *smart buildings, energy systems, simulation, DesignBuilder, energy efficiency*

**Rezumat.** *articolul, intitulat „Modelarea și simularea integrată a sistemelor de energie pentru clădiri inteligente”, urmărește obținerea de rezultate relevante privind consumurile de energie într-o clădire inteligentă și compararea acestora cu cele ale unei clădiri mai puțin inteligente, dar cu același regim funcțional. Analiza comparativă a diferitelor modele evidențiază impactul fiecărei măsuri de transformare inteligentă. Prin simulări în DesignBuilder, studiul reconfirmă eficiența soluțiilor inteligente de control pentru sistemele energetice din clădiri. Rezultatele oferă valoare practică în optimizarea consumurilor, reducerea costurilor și sprijinirea deciziilor de proiectare sustenabilă.*

**Cuvinte cheie:** *cuvinte reprezentative pentru articol*

## 1. Introduction

In the current context of climate change, resource constraints, and increasing demands for energy efficiency, smart buildings emerge as a cornerstone of the transition towards a sustainable built environment. The concept of the smart building integrates advanced technologies for automation, control, and data analytics in order to optimize energy consumption, occupant comfort, and system maintenance.

European regulations, such as the “Fit for 55” package and the Energy Performance of Buildings Directive (EPBD), have reinforced the need for digitalization and automation in the building sector. These frameworks establish more stringent requirements for both existing and new buildings, with a clear objective of achieving nearly zero-energy buildings (nZEB) in the short term and zero-emission buildings in the future.

Smart buildings are defined by the integration of interconnected systems that enable the automated control of HVAC equipment, lighting, ventilation, and other subsystems, based on parameters such as occupancy patterns, indoor CO<sub>2</sub> concentration, daylight availability, or weather forecasts. The goal is to enhance operational efficiency and reduce the energy footprint without compromising indoor environmental quality.

This study aims to analyze the impact of implementing selected *smart building* measures on the energy consumption of a virtually modelled office building. Given the wide range of possible interventions, the research focuses on those measures that have the greatest potential to reduce energy use and can be effectively quantified and simulated using the DesignBuilder software [14].

To achieve this goal, the following objectives were pursued:

- To model an office building within a dynamic simulation environment (DesignBuilder), including a complete definition of the envelope, climate conditions, occupancy schedules, and usage profiles.
- To configure a baseline HVAC scheme with standard operation, serving as the reference for initial energy performance.
- To gradually implement smart building strategies aimed at optimizing consumption (e.g., intelligent lighting control, demand-controlled ventilation based on CO<sub>2</sub> levels, etc.).
- To compare the resulting energy consumption across scenarios in order to assess the individual and cumulative impact of each applied measure.
- To formulate conclusions regarding the effectiveness of these measures within the broader framework of modern building design, targeting reduced energy demand and alignment with nZEB requirements.

## 2. Methodology and Standards

The evaluation of building energy performance is a crucial step in designing and optimizing smart and low-energy buildings. Traditional static calculation methods cannot capture the dynamic interactions between building elements and external

variables such as climate conditions or occupancy patterns. Therefore, dynamic energy simulations are essential tools, allowing detailed modeling of building systems over time, including weather effects, occupancy, operational schedules, and technical equipment characteristics.

In this study, simulations were performed using EnergyPlus via the DesignBuilder interface, providing an intuitive 3D modeling environment and efficient post-processing of results. The methodology ensures a rigorous, data-driven approach to assess the impact of smart building technologies on energy consumption and indoor comfort. Energy performance was evaluated in accordance with European standards, primarily EN ISO 52120-1:2022, which classifies automation systems into four performance levels (A–D) and defines correction factors for energy consumption. Additionally, the Smart Readiness Indicator (SRI) framework was considered to contextualize the building's adaptive capabilities. While these standards provide theoretical benchmarks, the study relied on detailed dynamic simulations to accurately quantify the effect of each smart measure, integrating automated lighting, demand-controlled ventilation, and optimized HVAC scheduling directly within the model. This approach ensures realistic assessment of energy savings without relying solely on generalized correction factors.

### **3. Case Study and Virtual Building Model**

#### **3.1. General Description of the Modelled Building**

The modelled building is primarily an office building with a height of basement + ground floor + 3 floors (B+G+3). The total usable area is 4,800 m<sup>2</sup>, which will serve as the reference area for annual energy consumption calculations.

The building includes a catering area for food services and commercial and service spaces. Floors 1 through 3 primarily consist of open-plan office spaces, meeting rooms, individual offices, sanitary cores, and two server rooms located in the building core. The technical area for building systems is mainly on the rooftop terrace, with successive layers and bituminous exterior finish. Some technical equipment is installed outdoors in designated areas. The building entrance features a reception area spanning two levels (ground floor and first floor) with a free height of 4.59 m on the ground floor. The envelope is mostly glazed with some opaque sections. Upper floors have a height of 3.55 m, with a façade composed of The façade consists of an opaque parapet measuring 0.64 m, a glazed panel of 2.34 m, and an upper opaque element of 0.51 m that serves as a cover for the technical space and provides support for the glazed panel.

The building is located in an urban area. For energy simulations, the climate file for Bucharest from the ASHRAE IWEC2 database was used, providing Typical Meteorological Year (TMY) data for international energy calculations. [1]. This includes:

- Dry and wet air temperature;
- Wind speed and direction;
- Solar radiation (modeled based on ASHRAE methods).



Fig. 3.1. Virtual Building Model used

### 3.2. Input Data and Operational Profiles

The building is divided into 27 unheated basement zones with negligible impact on energy use, while upper floors are zoned according to function, occupancy, and interaction with smart systems. The envelope (walls, roof, windows, doors) complies with MC-001/2022 and SR EN 12831-1, meeting NZEB recommendations. Glazed facades feature a solar factor  $g = 0.49$  and visible transmittance  $VT = 0.65$ . Occupancy profiles, based on the UK NCM database, vary by time, day, and space type (offices, commercial, catering, server rooms) to support accurate energy estimations. Internal heat gains derive from people, lighting, and equipment. Indoor conditions follow SR EN 16798-1:2019 (IDA1) with 22 °C in winter and 24 °C in summer, circulation areas at 15 °C and sanitary areas at 18 °C in winter, and server rooms constant at 24 °C. HVAC operation is set at 6/12 °C for cooling and 60/40 °C for heating, with airtightness of  $n_{50} \leq 1$  ach. Fresh airflows comply with I5/2022 for IDA 1 (36 m<sup>3</sup>/h·person and 3.6 m<sup>3</sup>/h·m<sup>2</sup>), dynamically adjusted via CO<sub>2</sub>-controlled ventilation, representing a first smart readiness measure.

### 3.3. Initial HVAC Configuration (Conventional Building)

The cooling system uses a chiller and PICV valves for local control, with a VFD-equipped pump and bypass circuit to maintain minimum flow. The heating system is a boiler with a simplified hydraulic scheme. Ventilation is provided via AHU with heat recovery and heating/cooling coils. Fan coil units operate at 12 °C (cooling) and 35 °C (heating).

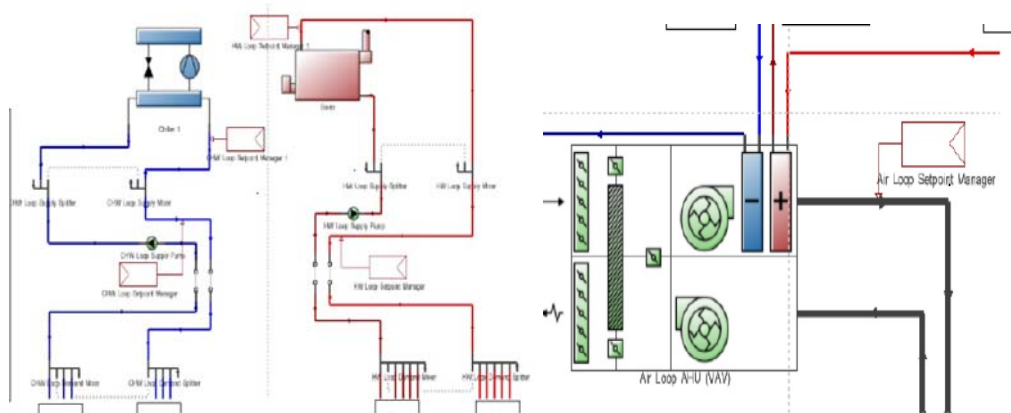


Fig. 3.2. Functional HVAC schemes

### 3.4 Simulation Scenarios and Implemented Smart Measures

To evaluate potential energy and operational optimization, several scenarios were simulated against the baseline configuration:

- **Automated lighting** , dynamic control based on natural light.
- **CO<sub>2</sub>-based ventilation (DCV)** , adjusting fresh air supply based on indoor air quality.
- **Automated exterior blinds** , dynamic shading to reduce solar gains.
- **EC fan coils** , replacing conventional fans with electronically commutated high-efficiency fans.

These scenarios allow analysis of the individual and cumulative impact of each measure on energy consumption and indoor comfort.

#### 4.1. Simulation of the System Integrating Smart Lighting – V1

Smart Lighting represents a modern and integrated approach to building lighting, which intelligently leverages natural daylight and energy-efficient artificial lighting. This concept promotes optimal use of natural and artificial light to create a comfortable, healthy, and energy-sustainable indoor environment.

Natural light is essential for the physical and emotional well-being of people. The HCL (Human Centric Light) concept highlights the benefits of natural light for occupant health and indicates the need for artificial lighting systems that closely reproduce the natural light cycle. Daylight helps regulate the circadian rhythm, positively influencing sleep, energy levels, and concentration. [5]

Another advantage of the smart lighting system is increased energy efficiency, resulting in significant reductions in electricity consumption for lighting, as well as for cooling, since heat gains are significantly reduced. Other categories of energy consumption are not significantly or directly affected, but rather indirectly through adaptations of the building's control system.

Example: Because there is no longer as much heat gain in the room, the heating system will operate for longer periods, with fewer start-stop cycles, which the software is capable of simulating.

A typical smart lighting system consists of the following essential elements, which ensure automated and efficient control of indoor lighting:

- **LED luminaire**, the source of artificial light, with low consumption and fine adjustment of intensity and color temperature to adapt lighting to natural conditions and user preferences.
- **Ambient light sensors**, devices that continuously measure the natural light level in the room and transmit this data to the control unit to adjust artificial lighting accordingly.
- **Occupancy sensors**, detect the presence of people in the space and allow lights to be switched on, off, or automatically adjusted to avoid unnecessary energy consumption.
- **Central control unit (server)**, the brain of the system, which processes information from the sensors and commands the luminaires through



standardized communication protocols, such as DALI (Digital Addressable Lighting Interface).

- **Control panels and user interface**, allow manual setting of lighting scenarios, monitoring of energy consumption, and adjustment of system parameters according to specific needs.

For the smart lighting simulation in DesignBuilder, natural lighting simulation must be activated in “detailed” mode. The software can also account for adjacent buildings, trees, reflections, or any other elements that may influence natural lighting in our building.

After this setting is activated, it is necessary to select automatic control, illuminance, and the electric power at which luminaires can operate in the “Lighting” tab, as well as the control type and the working plane height for which illuminance must reach the value set. The control type can be linear (via DALI dimmer), stepwise, or linear to off. The linear option is selected.

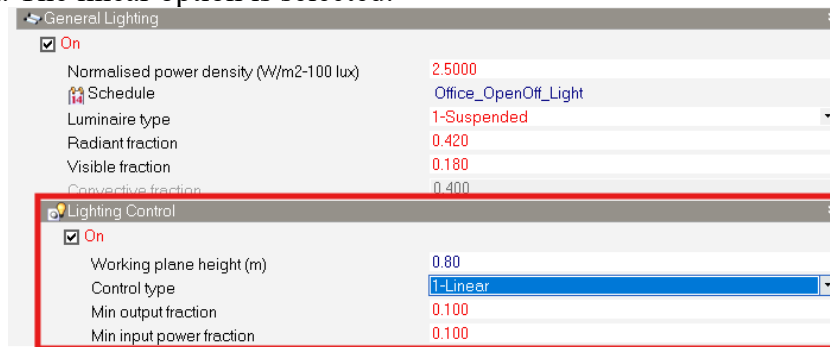


Figure 4.1. Presets for smart lighting control simulation in DesignBuilder

## 4.2. Simulation of the System with Demand-Controlled Ventilation – V2

Demand-Controlled Ventilation (DCV) is a modern energy-efficient strategy for buildings, adjusting fresh air supply according to actual occupancy. Unlike conventional systems operating at constant design airflow rates, DCV reduces airflow in partially occupied or unoccupied rooms while maintaining indoor air quality, particularly effective for offices, classrooms, and hotel rooms with variable occupancy [6].

### 4.2.1 Control Strategy

The system in DesignBuilder is modelled with the following elements:

- **Sensors:** CO<sub>2</sub> sensors measure indoor air concentration, while occupancy sensors detect presence.
- **Variable Air Volume (VAV) Dampers:** Modulate airflow to match real-time demand.
- **Fan Speed Control:** Variable Frequency Drives (VFD) adjust fan speed to maintain system pressure.
- **CO<sub>2</sub> Setpoint:** Indoor CO<sub>2</sub> is maintained 400 ppm above outdoor levels, based on NOAA measurements for Constanța.
- **Neutral AHU Role:** The Air Handling Unit (AHU) provides ventilation only, without heating or cooling the zones.

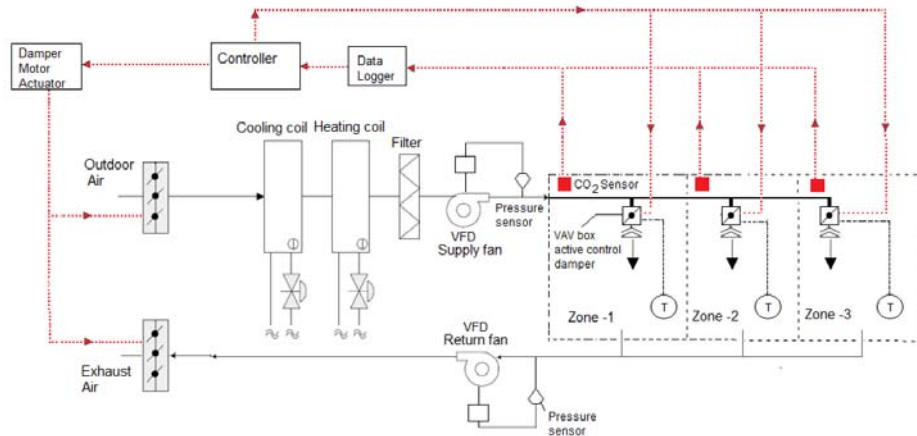


Figure 4.2. Functional scheme of the fresh air loop [7]

#### 4.2.2. Simulation Setup in DesignBuilder

The simulation includes three categories of settings:

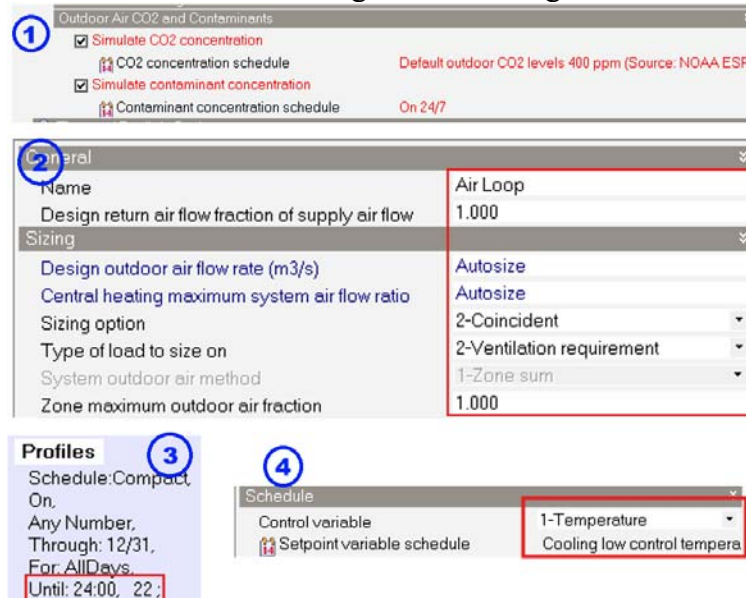


Figure 4.3. Site parameters setup in DesignBuilder

1. **Site Settings:** Outdoor CO<sub>2</sub> concentration, climate data, and location parameters. (constant outdoor CO<sub>2</sub> concentration of 400 ppm is assumed, based on NOAA measurements, considering this value appropriate for the purpose of the simulation). [8]
2. **Air Loop Settings:** Balanced supply and exhaust airflow, sizing according to zone demand, and neutral system load.
3. **Zone Groups Settings:** CO<sub>2</sub> setpoints, calculation of fresh air per zone, and system neutrality for heating/cooling.[3]
4. **Terminal Units (VAV Dampers):** Control airflow based on CO<sub>2</sub> and occupancy, adjusting schedules to each zone's demand.

#### 4.2.3 Benefits of DCV

- Avoids over-ventilation while maintaining high indoor air quality.
- Reduces energy consumption for heating, cooling, and dehumidification.
- Allows real-time monitoring of occupancy and ventilation rates.
- Enables zone-specific ventilation and flexible adaptation to changes in space use.
- Provides operational data for maintenance, energy management, and safety analysis

#### 4.3. Simulation of the System with Automated Solar Shading – V3

Solar radiation significantly affects both the energy performance and indoor comfort of office buildings. While natural light reduces artificial lighting demand and enhances occupant well-being, excessive solar gains may cause overheating, glare, and additional HVAC loads. [9]

##### 4.3.1. Classification of Shading Systems

- **External:** brise-soleil, canopies, light shelves, external blinds, solar films.
  - **Between-glass units:** louvers integrated in double glazing.
  - **Internal:** textile or metalized blinds, opaque or semi-transparent shades.
  - **Glazing-integrated:** reflective/absorptive glass, electrochromic glass.
- Control types:** manual, automated, or hybrid, depending on occupancy patterns and space function.

##### 4.3.2 Simulation Setup

For the energy simulation, **automated external blinds** were selected due to their efficiency in limiting unwanted solar gains:

- **Summer:** fixed angle optimized to reduce solar gains without compromising daylight.
- **Winter:** fully retractable to maximize passive solar heating.

This configuration balances summer solar protection with winter passive heating, enhancing overall building energy performance.

#### 4.4. Simulation of the System with EC Fan Coil Units – V4

Fan coil units (FCUs) equipped with Electronically Commutated (EC) brushless motors represent a significant upgrade in HVAC systems, offering improved energy efficiency, thermal comfort, and intelligent control compared to conventional AC motors. EC motors are DC motors with electronic commutation, eliminating carbon brushes and reducing friction, noise, and maintenance while increasing service life [10]

##### 4.4.1 Advantages of EC Fan Coil Units

1. **Energy Savings:** Continuous and precise fan speed control allows a 45–50% reduction in energy consumption compared to traditional AC units.

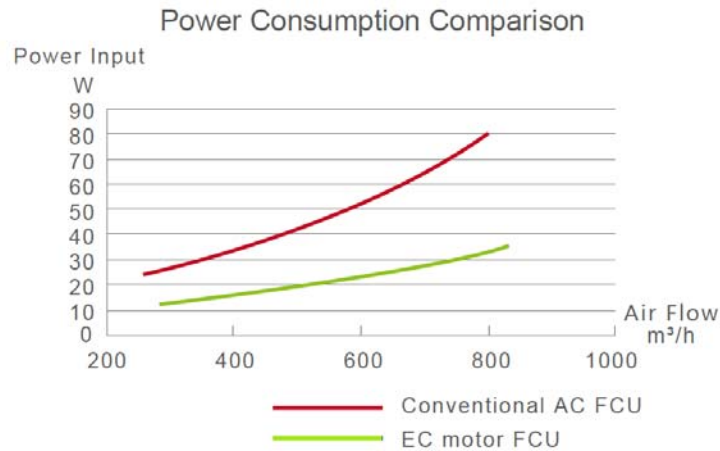


Fig. 4.4 – Electric power versus airflow for AC and EC motors. [10]

2. **Enhanced Thermal Comfort:** Proportional control via pulse-width modulation (PWM) ensures stable temperatures and humidity, minimizing thermal oscillations and discomfort.
3. **Quiet Operation:** Brushless operation, aerodynamic fan design, high-quality bearings, and acoustic insulation reduce noise, particularly at low to medium speeds.
4. **Flexible and Intelligent Control:** Compatible with both stand-alone and BMS-integrated systems, allowing individual unit control, zone-based operation, and real-time performance optimization [10]

#### 4.4.2. Simulation Setup

In DesignBuilder, EC FCUs were modeled with the “**variable fan**” option, enabling precise modulation of both airflow and thermal agent flow for each zone.

### 5. Analysis of Results and Energy Consumption Comparison

#### 5.1. Smart Lighting (V1)

The implementation of the smart lighting system had a significant impact on the building’s energy consumption, affecting lighting as well as cooling and heating loads. A comparison between the reference scenario (V0) and the optimized scenario (V1) shows a notable reduction in energy use for lighting and cooling, while heating experiences a slight increase due to reduced internal heat gains.

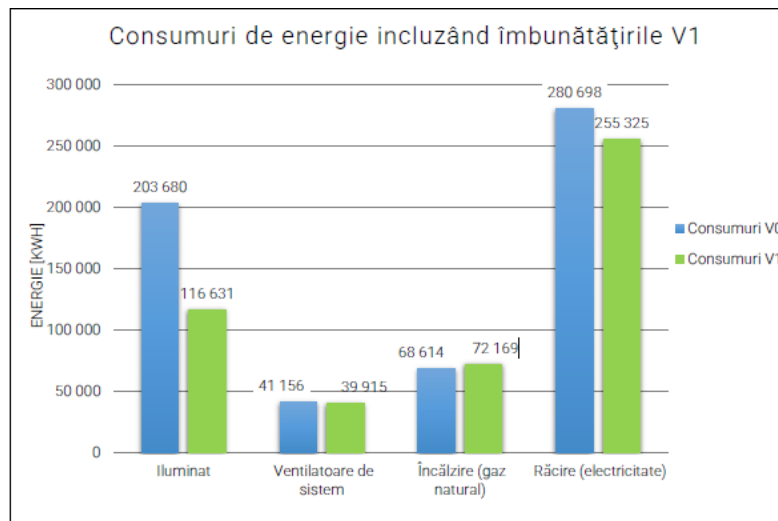


Figure 5.1 : Annual Energy Consumption for Lighting, Cooling, and Heating

Analyzing the share of each component in the cooling load indicates an indirect positive effect of the automated lighting system: lighting-related heat gains decrease significantly, while contributions from equipment, solar gains, and human presence remain relatively constant.

Overall, the smart lighting system achieves a net annual energy saving of approximately 12.7%, highlighting the efficiency of this simple and easily implementable measure in office buildings.

## 5.2. Demand-Controlled Ventilation (V2)

In this stage (V2), the system was enhanced by implementing Demand-Controlled Ventilation (DCV) over the previously optimized configuration with automated lighting (V1). The primary goal of DCV is to adjust the supply of fresh air based on occupancy levels and CO<sub>2</sub> concentration, reducing the energy consumption of fans and the heating load for outdoor air during the cold season.

The impact on cooling loads was minimal. Although a lower fresh air flow might be expected to reduce cooling demand, simulations show that the heat contribution from incoming air is mitigated by the heat recovery unit in the Air Handling Unit (AHU). Consequently, its share in the total cooling load remains negligible.

Similarly, latent loads at the fan coil units did not increase significantly. This indicates that the reduced fresh air in V2 did not adversely affect indoor humidity compared to V1, and thus did not increase the latent cooling requirement.

Overall, compared to V1, implementing DCV in V2 resulted in an additional **2.8% reduction in total energy consumption**, mainly due to decreased fan energy and lower heating demand for the fresh air supply. The effect on cooling requirements remains marginal, thanks to the efficiency of the heat recovery system and the limited contribution of fresh air to total cooling loads.

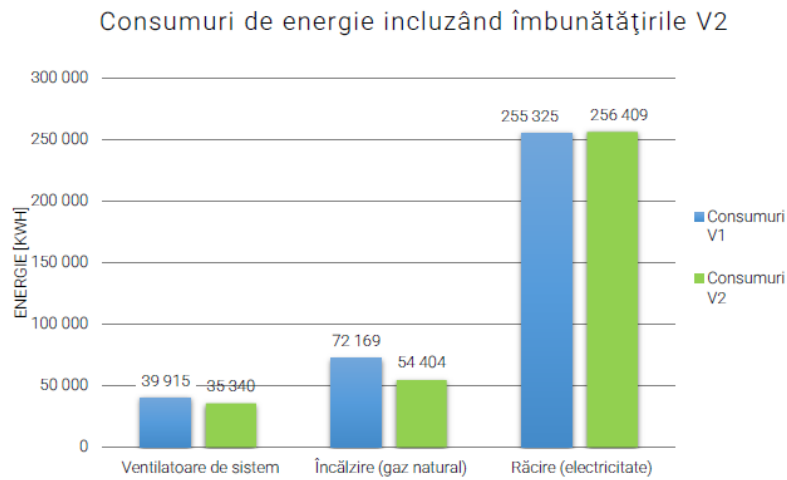


Figure 5.2. Energy consumption changes integrating demand-controlled ventilation

### 5.3. Automated Solar Shading (V3)

In this stage (V3), the system was enhanced through the integration of automated solar shading devices designed to reduce incident solar radiation on glazed surfaces. This optimization leads to a notable reduction in cooling energy demand, while slightly increasing artificial lighting consumption due to the lower availability of natural daylight indoors.[9]

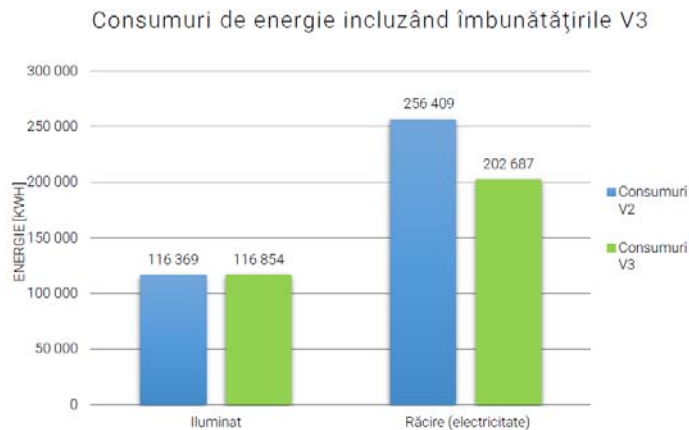


Figure 5.3. Energy consumption changes integrating Automated Solar shading

The energy performance of this configuration presents the consumption profiles obtained for scenarios V2 and V3.

A detailed breakdown of the cooling load is shown, where the share of solar gains through glazing decreases from 50% to 38% of the total cooling load. This confirms the effectiveness of automated shading in limiting solar heat input.

The overall annual energy balance indicates that the reduction in cooling demand compensates for the minor increase in lighting energy. The net effect of the measure is a total annual energy saving of approximately **8%**.

#### 5.4. EC Fan Motors for Fan Coil Units (V4)

The final optimization stage (V4) involved replacing conventional fan coil unit (FCU) fans with Electronically Commutated (EC) motors, enabling continuous modulation of airflow to match thermal loads. This measure reduces electricity consumption for fans while providing improved thermal comfort through more stable adherence to setpoint temperatures.

The results show a marked decrease in fan energy use, offset by slight increases in heating and cooling demand due to reduced heat recovery efficiency and finer control of indoor temperature. Thermal conditions in occupied zones became significantly more stable, with reduced deviations from the setpoint.

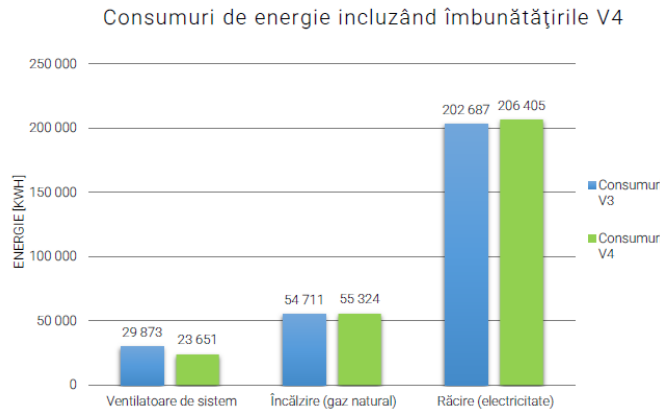


Figure 5.4. Energy consumption by end-use after integrating EC fan motors in FCUs

Daily operation analysis further highlights the enhanced precision of EC motors: during cooling, setpoint proximity was maintained with minor increases in energy demand, while in heating, energy use decreased locally at FCUs but required greater input from the central system to compensate for lower exhaust air temperature.

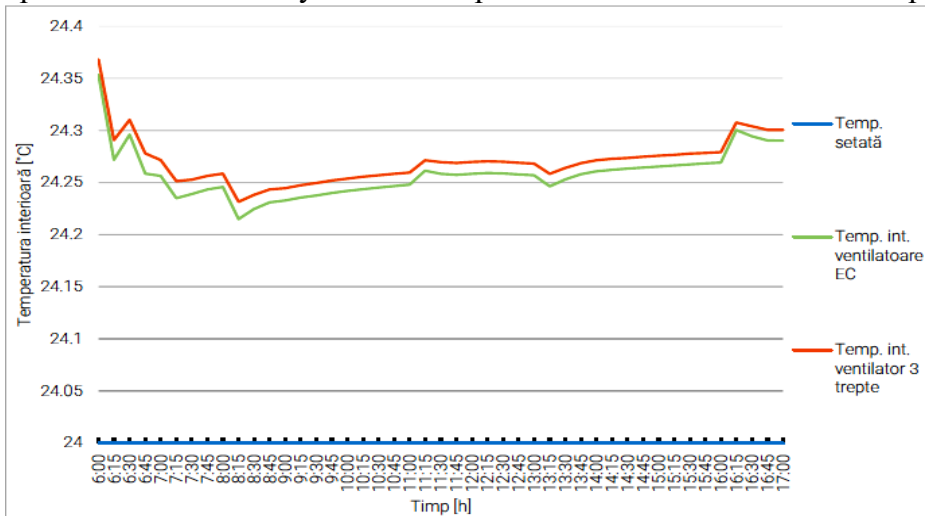


Figure 5.5. Indoor temperature variation during a summer day: comparison between conventional and EC fan motors



On an annual basis, the energy savings achieved were modest, 679,415 kWh/year compared to 677,523 kWh/year ( $\approx 0.22\%$ ). Nevertheless, EC motors provide qualitative advantages, including reduced noise, higher comfort stability, and seamless integration into smart building platforms. When aggregated with previous measures, the hierarchy of contributions to total savings becomes clear: intelligent lighting ( $\approx 12.7\%$ ), automated solar shading ( $\approx 6.7\%$ ), demand-controlled ventilation ( $\approx 2.5\%$ ), and EC fan motors ( $\approx 0.2\%$ ). The combined effect demonstrates the added value of layered optimization strategies in achieving superior energy efficiency

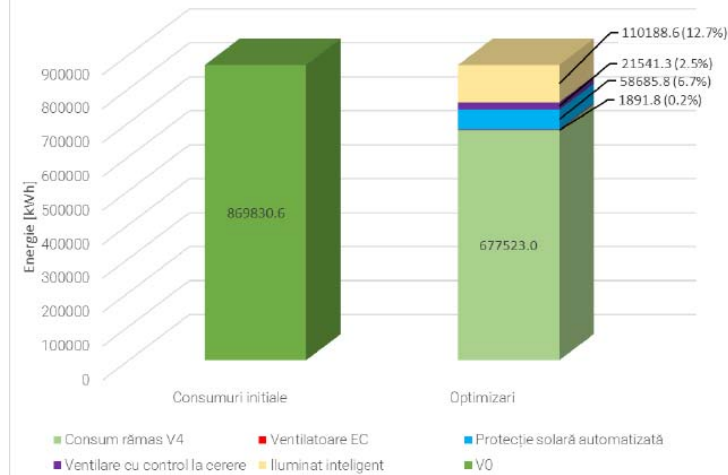


Figure 5.6. Cumulative impact of all optimization measures (V0–V4) on total building energy used

### 5.5. Payback Time Analysis for Smart Lighting [13]

The analysis is based on reference data from the Northwest Energy Efficiency Alliance (NEEA, 2020), with international costs converted from USD/ft<sup>2</sup> into RON/m<sup>2</sup>. The estimated cost of a conventional system is 55 RON/m<sup>2</sup>, while the smart lighting system reaches 82 RON/m<sup>2</sup>, representing a difference of about 49%, or an additional 27 RON/m<sup>2</sup>.

For the modeled building with a usable area of 4,800 m<sup>2</sup>, the total additional investment required for implementing smart lighting is approximately 131,100 RON. Considering an average electricity price of 1.19 RON/kWh, the annual operating cost of the conventional system is estimated at 242,379.6 RON, compared to 139,054.5 RON for the smart system. The resulting annual savings of around 103,325 RON lead to a payback period of only 1.27 years when considering the additional investment compared to a conventional solution, or 3.82 years when accounting for the total cost of the smart lighting system. These results confirm the strong economic feasibility of smart lighting and support its integration in both new projects and major renovations, particularly in the current context of energy efficiency requirements.



## 5.6. Smart Readiness Indicator (SRI) Evaluation

The Smart Readiness Indicator (SRI) [15] is a European assessment tool developed under the revised Energy Performance of Buildings Directive (EPBD) to quantify the level of building digitalization and automation. Its objective is to measure the building's ability to adapt operation for the benefit of occupants, energy efficiency, and interaction with surrounding energy networks. The evaluation in this dissertation was performed using the official European platform <https://srienact-tool.eu>

Two scenarios were analyzed: the baseline building (V0), equipped with conventional systems and no BMS, and the improved building (Vfinal), with all proposed smart solutions implemented. The results show a significant increase in SRI across most dimensions. Energy efficiency improved from 22.39% to 57%, comfort from 20.13% to 59.75%, health and accessibility from 22.22% to 61.11%, and predictive maintenance from 0% to 26.62%. Even communication with occupants rose from 3.19% to 19.31%, while flexibility and storage grew from 2.6% to 19.09%.

The only dimension with limited progress is the Grid component, increasing from 2.6% to 19%, reflecting the current lack of standardized methodologies and infrastructure for grid integration. Although these functionalities primarily aim at cost optimization (dynamic tariffs, demand response) rather than direct building energy efficiency.

Overall, the SRI evaluation demonstrates a major improvement in smart readiness after implementing the simulated measures. Despite the modest contribution of grid interaction, the indicator provides an essential complementary perspective to energy analysis, emphasizing adaptability, digital interaction, and systemic efficiency in smart buildings

## 5.7. Alternative Measures for Energy Optimization

An effective measure for reducing cooling loads is the integration of an adiabatic humidifier on the outdoor air stream before the heat recovery unit (CIBSE, 2016). For an AHU sized at 30,000 m<sup>3</sup>/h (outdoor air 35.3 °C, 35% RH; indoor air 24 °C, 50% RH), the cooling coil demand decreased from 142 kW (without humidification) to 83 kW (with adiabatic pre-cooling), representing a 41.5% reduction. Simultaneously, heat recovery increased from 89 kW to 139 kW. This demonstrates the significant potential of adiabatic pre-cooling in lowering cooling energy consumption. Water use can be optimized by reusing condensate collected from the building. [11]. In fan-coil based cooling systems, design temperatures (7/12 °C or 8/14 °C) are often oversized for transitional seasons. Raising the supply temperature (e.g., from 7 °C to 10 °C) increases return temperature proportionally (12 °C to 15 °C), reduces latent load, and improves the chiller's efficiency due to higher evaporator

operating temperatures. This strategy reduces electricity consumption and lowers dehumidification demand in fan-coils. TES systems decouple cooling production from demand by storing chilled water or ice during off-peak hours, when chillers operate at higher EER due to lower ambient temperatures (ASHRAE, 2020). During daytime, stored cooling is released, reducing peak electrical demand and enabling the use of smaller, more efficient chillers. Benefits include lower operating costs, deferred capital investment, and reduced stress on the electrical grid, making TES a sustainable and economically attractive solution. [12]

## 6. Conclusion

This study investigated the impact of implementing smart solutions in office buildings on overall energy performance. Using a detailed virtual model in DesignBuilder, simulated with EnergyPlus, four practical measures were evaluated for their demonstrated energy-saving potential: smart lighting, demand-controlled ventilation (DCV), automated shading, and EC fans in fan-coils.

The simulations revealed a total energy reduction of approximately **22%**, with the largest contributions from smart lighting (**12.7%**) and automated solar protection (**6.7%**). The cumulative effect of all applied measures decreased annual energy consumption from **869,830 kWh/year** to **677,523 kWh/year**, lowering the specific energy demand from **181 kWh/m<sup>2</sup>/year** to **141 kWh/m<sup>2</sup>/year**, approaching near-zero energy building (nZEB) standards.

Additional measures, such as indirect adiabatic cooling, chilled water reset, and thermal energy storage, were identified as further opportunities for optimization, either through advanced technologies or by enhancing the interaction of existing systems.

Beyond energy savings, the analyzed solutions enhance indoor comfort, reduce operational noise (notably from EC fans), and improve environmental controllability, which are critical aspects for modern buildings.

For the highest-impact measure—smart lighting—a payback analysis based on real cost data indicated a payback period of 1.27 years relative to additional investment over conventional systems, or 3.82 years relative to total system cost, demonstrating strong economic feasibility.

The Smart Readiness Indicator (SRI) assessment further highlighted the building's digital and automated capabilities. The overall SRI increased markedly from 9.3% (initial state) to 35.5% (optimized state), with the energy efficiency component improving from 22.39% to 57.11%. This confirms the ability of smart technologies to enhance not only automation but also operational efficiency and cost reduction.

In conclusion, dynamic simulations clearly demonstrate that smart building technologies can significantly reduce energy consumption, improve occupant comfort, and enhance sustainability. The results validate the technical and economic rationale for implementing these solutions, while the inclusion of SRI provides a comprehensive evaluation framework that captures both automation levels and the building's capacity to interact dynamically with external energy networks.

## 7. Acknowledgments

This work was supported by a grant of the Ministry of Research, Innovation and Digitization, CNCS/CCCDI - UEFISCDI, project number ERANET-PRE-ActiVer, within PNCDI IV.

## 8. References

- [1] *White Box Technologies / ASHRAE, FAQ page*. Available online: <http://ashrae.whiteboxtechnologies.com/faq> (Accessed: June 4, 2025)
- [2] *UK-NCM, Data source*. Available online: <https://www.uk-ncm.org.uk/download.jsp?id=35> (Accessed: May 15, 2025).
- [3] *ASRO, SR EN 16798-1:2019/NA:2019 – PEC: Ventilation of buildings. Part 1: Indoor environmental parameters for design and assessment of energy performance of buildings regarding indoor air quality, thermal comfort, lighting, and acoustics. Module M1-6. National annex*, Bucharest, 2019.
- [4] *ASRO, SR EN 12831-1:2017 – PEC: Method for calculating the design heat load. Part 1: Heating demand. Module M3-3*, Bucharest, 2017
- [5] *Ekinex, Smart Lighting*. Available online: <https://www.ekinex.com/media/doc/Smart-Lighting-EN.pdf> (Accessed: June 6, 2025).
- [6] A. Bhatia, *HVAC – Guide to Demand Control Ventilation*, Course No: M04-037, Continuing Education and Development, Inc.
- [7] A. Bhatia, *HVAC – Guide to Demand Control Ventilation*, Course No: M04-037, Continuing Education and Development, Inc., p. 29.
- [8] *NOAA – Global Monitoring Laboratory, CO<sub>2</sub> Monthly Surface Data*. Available online: [https://gml.noaa.gov/aftp/data/trace\\_gases/co2/flask/surface/txt/co2\\_bsc\\_surface-flask\\_1\\_ccgg\\_month.txt](https://gml.noaa.gov/aftp/data/trace_gases/co2/flask/surface/txt/co2_bsc_surface-flask_1_ccgg_month.txt) (Accessed: June 7, 2025).
- [9] *CIBSE, TM37: Design for Improved Solar Shading Control*, London: Chartered Institution of Building Services Engineers, 2006
- [10] *SharedDocs, HVAC Documentation*. Available online: [https://www.shreddocs.com/hvac/docs/1001/Public/00/CAT\\_42CND\\_E1506\\_03.pdf](https://www.shreddocs.com/hvac/docs/1001/Public/00/CAT_42CND_E1506_03.pdf) (Accessed: June 9, 2025).
- [11] *CIBSE (Chartered Institution of Building Services Engineers), Guide B3: Air Conditioning and Refrigeration*, London, 2016, ISBN 978-1-906846-78-7 (PDF).
- [12] *ASHRAE, ASHRAE Handbook—HVAC Systems and Equipment*, 2020 Edition, Atlanta, GA, ISBN 978-1-947192-53-9.
- [13] *NEEA, 2020 Luminaire Level Lighting Controls Incremental Cost Study*, 2021. Adapted.
- [14] *DesignBuilder, Help v7.0 – Window Blinds Slat Data*. Available online: [https://designbuilder.co.uk/helpv7.0/Content/Window\\_blinds\\_Slat\\_data.htm](https://designbuilder.co.uk/helpv7.0/Content/Window_blinds_Slat_data.htm) (Accessed: June 8, 2025).
- [15] *SRI ENACT Tool, Smart Readiness Indicator – Online Evaluation Platform*. Available online: <https://srienact-tool.eu/homepage> (Accessed: June 11, 2025).

## On increasing the energy sustainability of localities in the security zone of the Republic of Moldova

Cu privire la sporirea sustenabilității energetice a localităților din zona de securitate a Republicii Moldova

Valentin TONU<sup>1</sup>, Vadim CEBAN<sup>2</sup>

<sup>1</sup>SA "Moldovagaz", str. Pușchin 64, Chișinău, Republica Moldova,  
e-mail: [valentin.tonu@moldovagaz.md](mailto:valentin.tonu@moldovagaz.md)

<sup>2</sup>SA "Moldovagaz", str. Pușchin 64, Chișinău, Republica Moldova,  
e-mail: [vadim.ceban@moldovagaz.md](mailto:vadim.ceban@moldovagaz.md)

DOI: 10.37789/rjce.2025.16.4.7

**Abstract.** Natural gas supply to 11 786 customers with an consumption of 16 523,3 million m<sup>3</sup> per year from 12 localities of the Security Zone of the Republic of Moldova, connected to the transmission and distribution system of Transnistrian region, is subject to increased risk due to the lack of a clear policy of covering the costs by consumers in the region of the costs incurred by suppliers. It is worth noting that consumers in Transnistrian region pay for gas only about 11.4% of the real cost of the natural gas supplied. After the crisis of January 2025, the costs of gas supplied to the Transnistrian region are covered by a loan granted by the Russian Federation in tranches, every 10 days, the allocation of which is periodically withheld, which conditions the sectioning of the region's transmission system from the licensed operator's system. In addition, there is no clarity on the sustainability of this particular financing of the gas supplies in the future.

**Key words:** consumers, sustainability, security zone, Transnistrian region, risk.

**Rezumat.** Aprovizionarea cu gaze naturale a 11 786 clienți cu consumul anual 16 523,3 mil m<sup>3</sup> din 12 localități a Zonei de securitate a Republicii Moldova, racordate la sistemul de transport și distribuție din regiunea Transnistreană este supusă unui risc sporit datorită lipsei unei politici clare de acoperire de către consumatorii din regiune a costurilor suportate de furnizori. De menționat, că consumatorii din regiunea Transnistreană plătesc pentru gaze doar circa 11,4% din costul real al gazelor naturale furnizate. După criza din ianuarie 2025 costurile gazelor furnizate pentru regiunea transnistreană sunt suportate printr-un împrumut acordat de Federația Rusă în tranșe, la fiecare 10 zile, alocarea căruia periodic se reține, fapt care condiționează secționarea sistemului de transport din regiune de sistemul operatorului licențiat. În plus, nu există o claritate a durabilității acestei finanțări în perspectivă.

**Cuvinte cheie:** consumatori, sustenabilitate, zona de securitate, regiunea Transnistreană, risc.

## Introducere

Zona de securitate, creată în 1992 conform [1] și [2] în rezultatul încheierii conflictului armat de pe r. Nistru sau Zona conflictului militar, se consideră teritoriul situat pe malul drept al r. Nistru cu lățimea de 15 km, care mărginește la nord cu satele Vâșcăuți și Susleni, r-nul Orhei, la sud - cu orașul Căușeni, satele Talmaza și Răscăieți, r-nul Stefan Vodă. În zona nominalizată se includ și localitățile situate pe malul stâng al Nistrului: Cocieri, Corjova, Coșnița, Doroțcaia, Lunga, Molovata Nouă, Pârâta, Pohrebea, Roghi, r-nul Dubăsari și or. Dubăsari.

O parte din localitățile amplasate în Zona de securitate, cu parametrii prezentați în tabelul 1, sunt alimentate cu gaze naturale din rețelele regiunii Transnistrene care, în funcție de proprietatea rețelelor de distribuție, modul de racordare la sursa de gaze și de furnizare consumatorilor finali (fig.1), pot fi divizate în 3 grupuri:

Tabelul 1

**Informație privind consumul anual și numărul de consumatori racordați la rețelele de transport și distribuție ale „Tiraspoltransgaz” SRL la 31.12.2024**

Zonele de operare	Numărul de consumatori			consumul anual, mii m <sup>3</sup>
	Total	casnici	noncasnici	
<b>„Tiraspoltransgaz” SRL</b>	<b>3 256</b>	<b>3 207</b>	<b>49</b>	<b>6 672,131</b>
<b>SP Bender 2:</b> s. Varnița	1 354	1 328	26	2 661,000
<b>SP Dubăsari:</b> s. Molovata Nouă	632	625	7	1 356,586
s. Cocieri	1 257	1 243	14	2 533,704
s. Roghi	1	0	1	29,221
s. Vasilevca	11	11	0	66,920
s. Corjeva	1	-	1	24,700
<b>„Ialoveni-gaz” SRL</b>	<b>5 414</b>	<b>5 331</b>	<b>83</b>	<b>7 426,066</b>
<b>SP Coșnița:</b> s. Pohrebea	179	177	2	188,285
s. Coșnița	1 555	1 521	34	2 275,500
s. Pârâta	1 194	1 177	17	1 495,463
s. Doroțcaia	878	866	12	1 094,005
<b>PD Copanca 2:</b> s. Hârbovăț	1 608	1 590	18	2 372,813
<b>„Ștefan Vodă-gaz” SRL</b>	<b>3 116</b>	<b>3 096</b>	<b>20</b>	<b>2 425,099</b>
<b>PD Copanca 2:</b> s. Fârlădeni	1 017	1 009	8	800,968
s. Hagimus	902	896	6	676,197
s. Copanca	1 197	1 191	6	947,934
<b>TOTAL</b>	<b>11 786</b>	<b>11 634</b>	<b>152</b>	<b>16 523,296</b>

*Grupul 1:* Hârbovăț, r-nul Anenii Noi (zona de distribuție „Ialoveni-gaz” SRL), Copanca, Fârlădeni și Hagimus, r-nul Căușeni (zona de distribuție „Ștefan Vodă-gaz” SRL), amplasate pe malul drept al r. Nistru, dar racordate la rețelele de distribuție ale or. Bender, Transnistria, furnizorul fiind „Moldovagaz” SA;

*Grupul 2:* Coșnița, Pohrebea, Doroțcaia și Pârâta, r-nul Dubăsari, amplasate pe malul stâng a r. Nistru, racordate la SP Coșnița, deservită de operatorul licențiat de transport



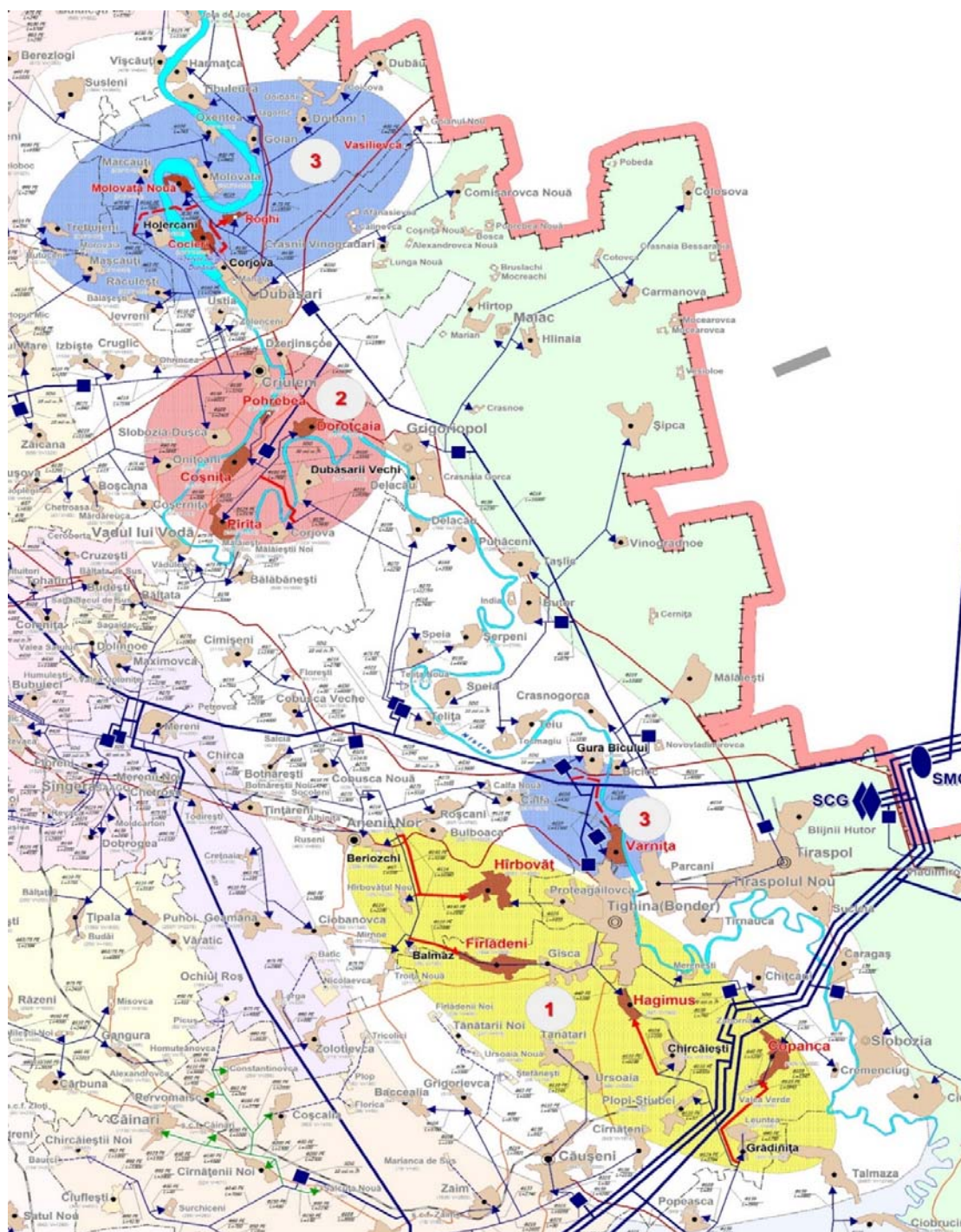


Fig.1. Amplasarea geografică a Grupurilor de localități nr.1, nr.2 și nr.3 din Zona de securitate a Republicii Moldova (marcată cu roz), racordate la sistemul de transport și distribuție a regiunii Transnistrene.

„Vestmoldtransgaz” SRL, dar racordată la rețelele de transport „Tiraspoltransgaz” SRL, distribuitorul fiind „Ialoveni-gaz” SRL, iar furnizorul de gaze - „Moldovagaz” SA;

*Grupul 3:* Varnița, r-nul Anenii Noi și Cocieri, Molovata Nouă, Rogi, Vasilevca, r-nul Dubăsari, consumatorii cărora sunt alimentați cu gaze naturale în baza contractului de furnizare cu întreprinderile de distribuție „Bender-gaz” și „Dubăsari – gaz” ale „Tiraspoltransgaz” SRL, cu funcții duble de distribuitori și furnizori, la prețurile aplicate pentru consumatorii din regiunea Transnistreană, deoarece rețelele de distribuție istoric aparțin cu drept de proprietate Administrației de la Tiraspol.

De menționat că în timpul crizei gazelor naturale din ianuarie 2009, cauzată de expirarea termenului Contractului de transportare a gazelor naturale rusești în regim de tranzit prin Ucraina spre țările din Europa de vest, regiunea Balcani și Turcia pentru peri-oada 1999-2008 și dezacordul „Naftogaz Ucraina” NAK cu condițiile impuse de „Gaz-prom” SAP în proiectul contractului pentru următoarea perioadă, tranzitul a fost întrerupt timp de 9 zile și în rezultat regiunea Transnistreană a rămas fără gaze naturale. De rând cu consumatorii regiunii Transnistrene a fost sistată furnizarea gazelor naturale și consu-matorilor din localitățile menționate supra din jurisdicția autorităților constituționale ale Republicii Moldova, racordați la tronsonul transbalcanic respectiv de conducte magistrale.

În continuare Autoritățile constituționale ale Republicii Moldova urmau să exami-neze posibilitatea și fezabilitatea reconectării consumatorilor din localitățile menționate la rețelele operatorilor de distribuție licențiați din partea dreaptă a r. Nistru în cazul riscului întreruperii livrărilor de gaze naturale în regiunea Transnistreană.

## **1. Cauzele și condițiile crizei energetice din Republica Moldova în 2021-2025**

În urma neînțelegerilor la nivel politic între Federația Rusă și Republica Moldova începând cu 1 octombrie 2022 „Gazprom” SAP a redus livrările de gaze naturale către Republica Moldova de la cele contractate (15 mil m<sup>3</sup>/zi - în sezonul de încălzire) până la 5,7 mil m<sup>3</sup>/zi – cantitatea minimă anuală zilnică stabilită pentru Republica Moldova în contractul de tranzit cu „Naftogaz Ucraina” NAK pentru perioada 2020-2024, pentru care nu era necesar a fi rezervate capacități de transport la licitații, motivând refuzul părții ucrainene să transporte gaze prin punctul de interconectare Sohranovca la hotarul Federația Rusă – Ucraina, intrarea în regiunea Donețk, Ucraina. Dat fiind că volumele reduse de import gaze naturale din Rusia nu puteau acoperi cererea consumatorilor de pe ambele maluri ale r. Nistru în sezonul rece, Guvernul Republicii Moldova a decis să cedeze începând cu 3 noiembrie 2022 volumele menționate pentru acoperirea cererii consumatorilor din regiunea Transnistreană și pentru producerea de energie electrică la Centrala electrică de la Cuciurgan (în continuare CEC) pentru consumatorii malului drept a r. Nistru. Consumatorii de pe malul drept al r. Nistru erau asigurați cu gaze naturale din achizițiile de pe piețele regionale din Europa.

De rând cu cele menționate merită de subliniat faptul că din momentul fondării „Moldovagaz” SA (1999) „Tiraspoltransgaz” SRL a achitat doar parțial costul gazelor primite de la Gazprom din contul costului serviciilor prestate pentru tranzitul de gaze

rusești către țările balcanice și Turcia, acumulând la finele anului 2024 o datorie de circa 11 268,8 mil dolari SUA față de importator. Consumatorii finali din regiunea Transnistreană plătesc pentru gazele naturale utilizate un preț convențional, în funcție de categoria de consum, de circa 10,0 - 24,2% din costul real al celor furnizate de "Moldovagaz" SA "Tiraspoltransgaz" SRL. Pentru asigurarea bilanțului "venituri și cheltuieli" gazele naturale importate erau și sunt ieftinite substanțial în cadrul "Tiraspoltransgaz" SRL, iar sumele colectate de la consumatorii finali sunt direcționate pentru acoperirea costurilor de transport și distribuție ale operatorilor de sistem de transport (OST) și de distribuție (OSD) în perimetrul regiunii Transnistrene și menținerea sistemului ei bugetar.

În ultima zi a anului 2024 expira termenul Contractului de transportare a gazelor naturale rusești în regim de tranzit prin Ucraina spre țările din Europa de vest, în baza căruia erau transportate gazele naturale și pentru Republica Moldova.

Conștientizând faptul că Gazprom va sista furnizarea gazelor naturale către Republica Moldova începând cu 1.01.2025 și ne-dorința autorităților de la Tiraspol de a colabora cu SA "Moldovagaz" în vederea furnizării de gaze naturale contra plată, achiziționate pe bursele regionale, având ca bază lipsa rezervărilor de capacitate la punctele de interconectare pentru luna ianuarie, documentele [3], [4], [5], [6] echipele "Moldova-gaz" SA, „Vestmoldtransgaz” SRL și „Tiraspoltransgaz” SRL au elaborat și semnat un *Plan comun de acțiuni* privind procedura de deconectare a consumatorilor de pe malul stâng a r. Nistru de la rețeaua de gaze naturale cu excepția celor din blocurile locative multietajate, a furnizorilor de produse alimentare, bunuri și servicii de primă necesitate, cât și a celor din localitățile Grupurilor 1 și 2, jurisdicția autorităților constituționale ale Republicii Moldova, alimentate fizic și tehnologic din rețeaua „Tiraspoltransgaz” SRL, care ar putea fi afectate din cauza sistării livrărilor de gaze naturale către malul stâng.

Totodată se remarcă faptul că localitățile: Varnița (r-nul Anenii Noi), Cocieri, Molovata Nouă, Vasilievca, Gimnaziile din cadru Ministerului Educației și Cercetării a Republicii Moldova din satele Roghi și Corjova, controlate de Administrația de la Tiraspol și Centru de plasament pentru persoane vârstnice și persoane cu dizabilități (în continuare - Centru de plasament) din comuna Cocieri, r-nul Dubăsari, consumatorii cărora sunt alimentați cu gaze naturale în baza contractelor de furnizare cu filialele "Bender-gaz" și "Dubăsari – gaz" ale „Tiraspoltransgaz” SRL la prețurile pentru consumatorii din regiunea Transnistreană nu au fost incluse în lista celor din Grupurile 1 și 2.

De rând cu aceasta a fost coordonat modul de secționare a segmentului transnistrean de conducte magistrale prin închiderea de către „Vestmoldtransgaz” SRL a robinetelor de secționare la ora 7.00 pe data de 1 ianuarie 2025 – ora de finisare a zilei gaziere de 31.12.2024.

În scopul creării rezervelor de gaze naturale în rețelele magistrale de pe teritoriul Transnistriei în data de 28.12.2024 „Tiraspoltransgaz” SRL a sistat alimentarea cu gaze naturale către consumatorii non-casnici (cu excepția consumatorilor protejați), pe



motivul sărbătorilor de iarnă, fără impact asupra economiei regiunii. Astfel, în conductele magistrale s-a înregistrat un stoc de gaze naturale de aproximativ 8 mil m<sup>3</sup>, format din cantitățile furnizate de la Gazprom, iar la data de 1.01.2025 „Tiraspoltransgaz” SRL a înregistrat o rezervă de gaze în conductele magistrale (volum acumulat + perna tehnologică accesibilă a rețelelor de transport) de aproximativ 9,8 mil m<sup>3</sup>, dintre care 8 mil m<sup>3</sup> erau destinate pentru acoperirea cererii de consum a regiunii Transnistrene din culoarul transbalcanic pentru o perioadă de 21,5 zile, și în partea de nord (Râbnîța) pentru o perioadă de 5 zile, iar 1,8 mil m<sup>3</sup> - pentru producerea energiei electrice la CEC pentru consumatorii din dreapta Nistrului. „Vestmoldtransgaz” SRL a depus eforturi considerabile în vederea stocării până la data de 01.01.2025 în conductele magistrale a rezervelor de gaze naturale înregistrate de „Tiraspoltransgaz” SRL. În acest sens „Tiraspoltransgaz” SRL a pus în funcțiune pe o perioadă rezonabilă Stația de compresoare Tiraspol-2 pentru a mări presiunea în vederea majorării volumelor în conductele magistrale, culoarul Transbalcanic: ATI, RI, ŞDKRI.

## **2. Criza gazelor naturale din regiunea Transnistreană în 2025**

„Gazprom” SAP a anunțat „Moldovagaz” SA prin [7] că începând cu 1 ianuarie 2025 unilateral sistează furnizarea gazelor naturale în Republica Moldova conform Contractului IGM -2007 – 2026 pe motiv că „Moldovagaz” SA nu-și onorează obligațiunile de plată.

Conform *Planui comun de acțiuni* în data de 01.01.2025, ora 07:00 „Vestmoldtrans-gaz” SRL și „Tiraspoltransgaz” SRL a secționat segmentul transnistrean de conducte magistrale prin închiderea robinetelor respective și au semnat un Proces verbal de constatare a volumului fizic de gaze din rețelele de transport din zonele cu bilanț comun, inclusiv volumele de gaze constatate la punctele de delimitare a proprietății ale ambilor OST.

În data de 01.01.2025 „Tiraspoltransgaz SRL a sistat alimentarea cu gaze naturale a consumatorilor din 154 de localități, inclusiv satele Varnița, Cocieri, Molovata Nouă, Vasilievca, Gimnaziile din satele Roghi și Corjova, în total au fost deconectați 79 688 consumatori casnici și 2030 – noncasnici (tabelul 2), și a transferat CEC la combustibil alternativ.

În luna ianuarie 2025 „Tiraspoltransgaz” SRL a furnizat gaze naturale din stocuri în volum de circa 252,9 - 283,9 mii m<sup>3</sup>/zi (în perioada similară a anului precedent - 3880,7 mii m<sup>3</sup>/zi) doar consumatorilor săi preocupați de aprovizionarea populației cu produse alimentare, bunuri și servicii de primă necesitate în număr de 261 unități și a celor din blocurile locative în număr de 120 158, deoarece în urma deconectărilor consumatorilor casnici în perioada crizei din 2009, livrarea gazelor naturale în blocurile locative a fost restabilită integral timp de 3 luni, pe motivul lipsei accesului la locurile de consum din cauza plecării locatarilor peste hotare la muncă.

Tabelul 2.

**Informația despre numărul de consumatori deconectați și ne deconectați de la sistemul de gaze naturale în perioada crizei naturale din ianuarie 2025**

<b>Nr. poziție</b>	<b>Consumatori</b>	<b>Total</b>	<b>Deconectați /limitați</b>	<b>Nedeconectați</b>
<b>1.</b>	<b><i>Consumatori casnici</i></b> , inclusiv	199 846	79 688	120 158
1.2	sectorul individual în zona urbană	37 730	22 004	15 726
1.3	apartamente la bloc în zona urbană	105 364	932	104 432
1.4	sectorul individual în zona rurală	56 732	56 732	
<b>2.</b>	<b><i>Consumatori noncasnici bujetari și alte categorii protejate</i></b>	2291	2 030	261
2.1	consumatori - surse de căldură	188	188	-
2.2	consumatori sociali și administrativi din sfera bugetară	387	370	17
2.3	consumatori din sfera de realizare a produselor alimentare	77	-	77
2.4	consumatori din sfera de alimentație publică	98	-	98
2.5	Alte categorii de consumatori protejați	1541	1472	69

„Vestmoldtransgaz” SRL și „Tiraspoltransgaz” SRL periodic efectuau manevrele necesare pentru transferul de gaze naturale ale „Moldovagaz” SA din conductele OST - ului din dreapta r. Nistru în conductele celui din partea stângă pentru asigurarea livrărilor de gaze naturale consumatorilor din localitățile aflate sub jurisdicția autorităților constituționale ale Republicii Moldova.

„Tiraspoltransgaz” SRL a asigurat alimentarea cu gaze naturale a localităților Pohrebea, Dorotcaia, Coșnița și Pârâta prin SP Coșnița în volum de circa 26,5 mii m<sup>3</sup>/zi, până la atingerea presiunii minime tehnologice în bransamentul Dubăsari (10 bar) al conductelor magistrale. Ulterior, la solicitarea „Moldovagaz” SA „Tiraspoltransgaz” SRL, în colaborare cu „Vestmoldtransgaz” SRL deschidea periodic robinetul de by-pass de pe conducta Odessa - Chișinău la hotarul de delimitare a proprietății celor doi OST în vederea asigurării în continuare cu gaze naturale a consumatorilor satelor Coșnița, Pohrebea, Dorotcaia și Pârâta (raionul Dubăsari, jurisdicția autorităților constituționale ale Republicii Moldova).

În paralel, „Tiraspoltransgaz” SRL a menținut alimentarea cu gaze naturale a consumatorilor satelor Hârbovăț, Copanca, Fârlădeni și Hagimus în volumul de circa 23 mii m<sup>3</sup>/zi, alimentate de la SP Bender-2, asigurând presiunea în conductele magistrale peste cea critică și neadmițând epuizarea pernei tehnologice din rețelele de distribuție ale orașului Bender.

Monitorizarea operativă la distanță a presiunilor și consumului de gaze naturale la intrarea în localitățile menționate se efectua de OSD ”Ialoveni-gaz” SRL și ”Stefan Vodă-gaz” SRL la fiecare 2 ore cu informarea Centrului Dispecerat „Vestmoldtransgaz” SRL și a ”Moldovagaz” SA.

Totodată, „Vestmoldtransgaz” SRL, la solicitarea „Moldovagaz” SA, a realizat transportarea și transferul gazelor către or. Râbnița prin deschiderea periodică a

robinetului de by-pass, aferent punctului de delimitare Rezina, de pe conducta Chișinău - Râbnița.

Urmare a sistării livrării gazelor naturale de către „Gazprom” SAP pentru consumatori din stânga r. Nistru, furnizarea gazelor naturale în regiunea transnistreană a fost reluată la 1 februarie de către Guvernul Republicii Moldova în baza Grantului acordat de Uniunea Europeană în sumă de 20 mil euro cu care s-au achiziționat gaze naturale în volum de 26,5 mil m<sup>3</sup> și cu care s-a asigurat regiunea timp de 10 zile.

În perioada menționată, în vederea asigurării în continuare a livrării gazelor naturale către regiunea transnistreană, „Moldovagaz” SA a elaborat și a semnat următoarele documente:

1. Cu furnizorii externi:

1.1 MET Gas and Energy Marketing AG (*în continuare MET GEM*) - Contractul- Cadru de vânzare și cumpărare a gazelor naturale din 28.01.2025 și Contractele Individuale nr. 1 din 29.01.2025; nr. 2 din 06.02.2025, nr. 3 din 10.02.2025; nr. 4 din 13.02.2025; nr. 5 din 20.02.2025; nr. 6 din 26.02.2025 la el;

1.2 MOL Commodity Trading - Contractul-Cadru privind vânzarea și cumpărarea de gaze naturale (EFET) din 03.02.2025.

2. Cu „Tiraspoltransgaz” SRL în temeiul [9]:

- Acordul de organizare a livrării gazelor naturale „Tiraspoltransgaz” SRL din 10.02.2025;

- Contractul de vânzare-cumpărare a gazelor naturale din 10.02.2025 și Suplimentele nr. 1- 6 la acesta;

- Contractul de echilibrare din 10.02.2025;

- Contractul privind prestarea serviciului de flexibilitate prin stocare în conductă din 10.02.2025.

În scopul restabilirii funcționalității sistemului de transport gaze naturale și asigurării funcționării stabile a sistemului electroenergetic al Republicii Moldova Moldovagaz a predat Tiraspoltransgaz pe 1 și 11 februarie gaze naturale în volum a câte 3 mil m<sup>3</sup> în baza contractelor de împrumut conform [8] și [9], care au fost restituite Moldovagaz în formă nemonetară până la 01.03.2025 și 31.03.2025, respectiv.

În baza Contractului Individual nr.2 din 06.02.2025 la Contractul-Cadru pe data de 08.02.2025 a fost organizată în formă de test livrarea gazelor naturale în Republica Moldova în cantitate de 72 MWh prin punctele de interconectare (PI) – PI Ungheni, PI Caușeni și PI Alexeevka, care s-a realizat cu succes.

La solicitarea și din mijloacele financiare ale „Tiraspoltransgaz” SRL, cu achitarea în avans, „Moldovagaz” SA a organizat pe data de 11 și 12 februarie 2025 procurarea gazelor naturale pe platforma „Bursa Română de Mărfuri (Romanian Commodities Exchange) Est” SRL, cu livrarea în ziua următoare celei de achiziție. Astfel, pe data de 12.02.2025 au fost livrate „Tiraspoltransgaz” SRL – 2,579 mil m<sup>3</sup>, iar pe 13.02.2025 – 2,691 mil m<sup>3</sup>. În mod similar, cu plata în avans, se organizează

achizițiile zilnice de capacități de transport pentru „Tiraspoltransgaz” SRL la licitațiile desfășurate pe platforma RBP a OST.

Începând cu data de 14 februarie 2025 „Moldovagaz” SA a lansat livrarea gazelor naturale importate de la MET GEM către „Tiraspoltransgaz” SRL, din mijloacele financiare ale acesteia. În perioada 14.02 - 28.02.2025 au fost livrate „Tiraspoltransgaz” SRL circa 50,6 mil. m<sup>3</sup> de gaze naturale din care în zilele de 26, 27 și 28 februarie 2025 „Tiraspoltransgaz” SRL a restituit „Moldovagaz” SA împrumutul în volum de 3 mil. m<sup>3</sup> (câte 1 mil m<sup>3</sup>/zi), acordat pe data de 01.02.2025, iar 2,4 mil m<sup>3</sup> primite supra consum de „Tiraspoltransgaz” SRL în aceleași zilele au fost depozitate în conductele „Vestmoldtransgaz” SRL. Pentru perioada 01 – 03 martie curent a fost organizată livrarea de la MET GEM a circa 6,8 mil m<sup>3</sup> de gaze naturale. Deficitul de 2,2 mil m<sup>3</sup> gaze naturale în ziua de 03.03.2025 a fost acoperit din rezervele „Tiraspoltransgaz” SRL stocate în conductele magistrale. Utilizând mecanismele descrise în perioada februarie – septembrie „Moldovagaz” SA a livrat „Tiraspoltransgaz” SRL gaze naturale în volum total de 442,31 mil m<sup>3</sup>, inclusiv: februarie – 50,54 mil m<sup>3</sup>, martie - 75,95 mil m<sup>3</sup>, aprilie - 57,34 mil m<sup>3</sup>, mai - 50,30 mil m<sup>3</sup>, iunie - 39,65 mil m<sup>3</sup>, iulie - 64,36 mil m<sup>3</sup>, august - 56,28 mil m<sup>3</sup>, septembrie – 47,89 mil m<sup>3</sup>.

### **3. Soluții de racordare a rețelelor de gaze din localitățile Grupurilor 1 și 2 din Zona de Securitate la rețelele operatorilor din cadrul grupului Moldovagaz**

În vederea executării prevederilor [10] referitor la reconectarea localităților Hagimus, Copanca, Fârlădeni din r-nul Căușeni, Hârbovăț din r-nul Anenii Noi și Pohrebea, Coșnița, Pârâta, Doroțcaia din r-nul Dubăsari OSD din cadrul grupului Moldovagaz au întreprins măsurile necesare: au elaborat avizele de racordare și obținut certificatele de urbanism, elaborat planurile de situații (schițe de proiect, coordonate cu APL), proiectele de execuție și devizele de cheltuieli, au obținut autorizațiile de construire și au efectuat lucrările de construcție – montaj a stațiilor de reglare - măsurare gaze, nodurilor de evidență gaze pe fiecare ramificație și a conductelor de presiune înaltă (10 bar), inclusiv pe direcțiile:

- Beriozchi – Hârbovăț - 8,1 km de rețea cu D=140 mm, cu recepția obiectului în exploatare și executarea lucrărilor de racordare pe data de 05.05.2025;

- Balmaz – Fârlădeni - 7,6 km de rețea cu D=110 mm, cu darea obiectului în exploatare pe 08.05.2025;

- Grădinița – Copanca - 6,9 km de rețea cu D=125 mm, cu punerea obiectului în funcțiune pe data de 12.05.2025.

- Chircăiești – Hagimus - 7,0 km de rețea cu *D=110 mm*, cu punerea obiectului în operare pe 14.05.2025.

La gazoductul Dubăsarii Vechi – Coșnița au fost montate 7,9 km cu D=160 mm, trei stații de reglare – măsurare gaze (s. Corjova, s. Telița și s. Dubăsarii Vechi) și nodul de evidență gaze, executate lucrările de traversare a r. Nistru prin forare dirijată

subacvatică cu lungimea de 0,4 km. Obiectul a fost recepționat în exploatare pe 30.09.2025, iar redirectionarea fluxurilor de gaze a fost efectuată pe 1 octombrie curent.

#### **4. Scenariile de aprovizionare cu gaze naturale a localităților Grupului 3 din Zona de securitate**

Întru executarea prevederilor [10] privind continuitatea și fiabilitatea alimentării cu energie electrică și gaze naturale a consumatorilor finali din localitățile Molovata Nouă, Cocieri, Vasilievca, Roghi, r-nul Dubăsari și Varnița, r-nul Anenii Noi, „Moldovagaz” SA a lansat procedura de proiectare a rețelelor de distribuție ale gazelor naturale pentru re-racordarea localităților respective, aflate în zona de operare a „Ialoveni-Gaz” SRL, dar racordate la rețelele „Tiraspoltransgaz” SRL. Planul de investiții reînnoit a Ialoveni-Gaz prevede construcția rețelelor de gaze naturale interrurale cu lungimea totală de 34,4 km, inclusiv: tronsonul Gura Bâcului – Varnița - lungimea 4,2 km, diametrul 160 mm; tronsonul Holercani – Molovata Nouă - lungimea 30,2 km, D=160 mm.

Rețelele planificate pentru construcție vor fi racordate la conductele existente de distribuție, proprietate a Administrației din Transnistria, care se află pe teritoriu controlat de autoritățile constituționale ale Republicii Moldova.

În vederea menținerii continuității furnizării gazelor naturale către consumatorii fi-nali din localitățile Molovata Nouă, Cocieri, Vasilievca, Roghi din r-nul Dubăsari și Varni-ța din r-nul Anenii Noi, în eventualitatea declarării unei situații excepționale sau a apariției unor disfuncționalități tehnice din partea „Tiraspoltransgaz” SRL, „Moldovagaz” SA a analizat trei opțiuni posibile de realizare:

1) Preluarea în locațiune de „Ialoveni-gaz” SRL de la „Tiraspoltransgaz” SRL a rețelelor de distribuție gaze naturale din localitățile menționate.

2) Transmiterea la deservire tehnică a rețelelor de distribuție gaze naturale din localitățile menționate de la „Tiraspoltransgaz” SRL către „Ialoveni-gaz” SRL conform [11];

3) Utilizarea serviciilor de distribuție prestate de „Tiraspoltransgaz” SRL „Moldovagaz” SA prin intermediul „Ialoveni-Gaz” SRL.

În vederea determinării opțiuni rezonabile de implementare, la data de 15.04.2025 „Moldovagaz” SA a organizat o ședință comună cu reprezentanții „Tiraspoltransgaz” SRL și ai Administrației din regiunea Transnistreană, în cadrul căreia s-a constatat, că în circumstanțele actuale, soluția oportună este utilizarea serviciilor de distribuție prestate de „Tiraspoltransgaz” SRL, deoarece rețelele de distribuție nu aparțin „Tiraspoltransgaz” SRL (proprietarul este Comitetul pentru gestionarea proprietății publice din regiunea Transnistreană) și nu pot fi transmise în locațiune sau deservire tehnică de către societatea menționată, iar Administrația de la Tiraspol are o atitudine neprietenoasă față de autoritățile constituționale ale Republicii

Moldova și agenții economici de pe malul drept al r.Nistru. În baza celor menționate, în cadrul ședinței opțiunea nr.3 a fost acceptată de către toate părțile participante [12], iar ca urmare, s-a convenit asupra necesității elaborării proiectului de contract privind prestarea serviciilor de distribuție a gazelor naturale de către sucursalele Bender-Gaz și Dubăsari-Gaz ale „Tiraspoltransgaz” SRL. În plus, s-a constatat că soluția de furnizare a gazelor de către „Moldovagaz” SA consumatorilor din localitățile menționate este favorabilă pentru „Tiraspoltransgaz” SRL, deoarece ultimul este scutit de cheltuielile pentru achiziția gazelor naturale și ieftinirea lor la nivelul prețurilor de furnizare consumatorilor finali din regiune, procurarea serviciilor de transport și distribuție, dat fiind că Tiraspolul este foarte restrâns în resurse financiare.

Pentru reconectarea localităților Roghi, Molovata Nouă, Corjova, Vasilievca, Cocieri, r-nul Dubăsari și Varnița, r-nul Anenii Noi, la rețelele Ialoveni-gaz s-au elaborat avizele de racordare, obținut certificatele de urbanism, elaborat planurile de situații și proiectele de execuție cu lungimea totală a rețelor de distribuție gaze de 34,4 km, inclusiv pe obiecte:

1. „Conducta interrurală Gura Bâcului – Varnița”, L=4,2 km, D=160 mm;
2. „Conducta interrurală Holercani - Molovata Nouă”, L=30,2 km, inclusiv:
  - a) traversarea râului Nistru prin forare dirijată subacvatică în două fire cu lungimea fiecărui L=1,1 km și D=140 mm, în tuburi de protecție oțel cu diametrul - 324 mm;
  - b) ramificația spre s. Molovata Nouă L=6,4 km, D=160 mm;
  - c) ramificațiile spre s. Corjova, s. Cocieri și Roghi L=3,5 km, D=140 mm;
  - d) ramificația spre s. Vasilievca L=18,1 km, D=90 mm.

La finele lunii aprilie „Ialoveni-gaz” SRL a publicat pe platforma electronică MTender anunțul de participare privind achiziționarea lucrărilor de construcție a obiectelor menționate. În perioada prescrisă în legislație (30 zile) pentru obiectul „Conducta inter-rurală Gura Bâcului - Varnița” au fost depuse 5 oferte.

În prima zi a lunii iunie 2025 a avut loc deschiderea ofertelor pentru obiectul „Conducta interrurală Holercani - Molovata Nouă”, 4 loturi, inclusiv:

Lot 1. Construcția ramificației interrurale de înaltă presiune, direcția Holercani – Molovata Nouă, r-nul Dubăsari – depuse 6 oferte.

Lot 2. Traversarea r. Nistru (Holercani – Molovata Nouă) în 2 fire paralele, prin metoda forării orizontale dirijate (HHD) - o ofertă, câștigător a fost desemnat „Turboener-gy Power” SRL în asociere cu „Centrul de foraje pentru infrastructură” SA din România.

Lot 3. Construcția ramificației interrurale de înaltă presiune, direcția Cocieri, Corjova, r-nul Dubăsari –4 oferte.

Lot 4. Construcția conductei de gaze naturale interrurale de înaltă presiune, direcția Vasilievca, r-nul Dubăsari – procedura de achiziție pentru lotul menționat a fost anulată în baza acceptării de către Ministerul Energiei a propunerilor SA „Moldovagaz” privind recunoașterea obiectului ca fiind nefezabil (18,1 km conductă, D=90 mm pentru

11 consumatori casnici) cu identificarea unor soluții alternative de aprovizionare cu resurse energetice a localității, precum și în baza deciziei ulterioare a ANRE [13], prin care a fost exclus obiectul corespunzător lotului examinat.

Pentru obiectele 1 și 2, divizat pe loturi (loturile 1 și 3), Beneficiarul a selectat câștigătorii, dar în termenii legali stabiliți au fost depuse contestații privind desemnarea lor. Pentru examinarea contestațiilor a fost organizate ședințe on-line cu toate părțile interesate. În rezultat, Agenția Națională pentru Soluționarea Contestațiilor (în continuare - ANSC) a emis Hotărârea corespunzătoare privind obligarea „Ialoveni-gaz” SRL de reevaluare în termen de 25 zile a rezultatelor concursurilor, luând în considerare argumentările prezentate în cadru ședințelor.

La deciziile ulterior adoptate de SRL „Ialoveni-gaz” pe obiectele 1 și 2 (loturile 1 și 3) au fost depuse contestații repetate, pe care ANSC pe 26 și 29 august curent le-a acceptat, fapt care prelungește procedura de selectare finală a câștigătorilor.

Totodată, prin [14] și [15] „Ialoveni-gaz” SRL a solicitat coordonarea „Tiraspoltransgaz” SRL a interconectării rețelelor de gaze proiectate cu rețelele de gaze exploatare de filialele Bender-gaz și Dubăsari-gaz, în baza Planurilor de situație și a schemelor de gazificare la obiectele „conducta interrurală Gura Bâcului - Varnița” și „Conducta inter-rurală Holercani - Molovata Nouă”, și respectiv a proiectului contractului de distribuție al gazelor naturale între „Ialoveni-gaz” SRL și „Tiraspoltransgaz” SRL pentru asigurarea continuității livrării gazelor naturale a consumatorilor din localitățile Molovata Nouă, Cocieri, Corjova, Roghi și Varnița. Prin [16] „Tiraspoltransgaz” SRL a enunțat problemele tehnice de conectare a conductelor proiectate la rețelele de distribuție ale localităților menționate, specificând că o parte dintre ele sunt situate în imediata vecinătate a aglomerațiilor urbane și, din punct de vedere funcțional sunt integrate de facto în infrastructura orașelor Dubăsari și Bender. Această circumstanță creează dificultăți tehnice și organizatorice suplimentare, în special în ceea ce privește secționarea tehnologică a acestor tronsoane de rețeaua de bază în caz de situații neprevăzute sau de criză, deconectarea operativă de la rețele este extrem de dificilă atât din punct de vedere tehnic, cât și logistic. În particular, conducta care alimentează s. Varnița reprezintă un tronson al rețelelor or. Bender interconectat în rețelele urbei - între rețelele de bază și ale cartierului nr.10 a orașului, situat în zona lui de nord. Aici sunt necesare lucrări de montare a robinetelor de secționare din ambele pâți a tronsonului, care traversează s. Varnița către cartierul nr.10, cu montarea nodului de racordare a conductei nou construite.

De asemenea, având în vedere că problemele de alimentare cu gaze și energie electrică ale localităților Varnița, Molovata Nouă, Roghi, Cocieri și Corjova au fost anterior examinate în cadrul consultărilor bilaterale ale autorităților de pe ambele maluri ale r. Nistru, „Tiraspoltransgaz” SRL a purtat discuții la acest subiect cu structurile de profil ale regiunii Transnistrene, în vederea formulării unei poziții unice. În urma consultărilor interdepartamentale s-a constatat că implementarea proiectului vizează o

serie de aspecte care necesită evaluare suplimentară. În special, este necesară respectarea principiului condițiilor egale pentru toți consumatorii din teritoriul respectiv, inclusiv în ceea ce privește reglementarea tarifară și distribuția echitabilă a resurselor, mai ales în eventualitatea unor situații de criză. Suplimentar, s-a menționat că desfășurarea unor lucrări de construcție - montaj extinse în Zona de Securitate va impune parcurgerea unor proceduri adiționale de coordonare. Astfel, „Tiraspoltransgaz” SRL consideră că problema alimentării cu gaze a localităților specificate și a posibilei reconectări al acestora presupune o analiză suplimentară în format de cooperare bilaterală între instituțiile organelor centrale de profil a Republicii Moldova și regiunii transnistrene, cu respectarea tuturor aspectelor juridice, tehnice, sociale și politice.

În baza [16] a fost pregătită și remisă adresarea [17] către ANRE, Ministerul Energiei și Biroul Politici de Reintegrare, privind desfășurarea unor consultări bilaterale pentru adoptarea unei decizii în scopul continuării executării măsurilor privind reconectarea localităților din zona de securitate.

## Concluzii

După criza din ianuarie 2025, generată de întreruperea livrărilor de gaze de la „Gazprom” SAP, începând cu 14 februarie costurile gazelor achiziționate de pe piață și furnizate consumatorilor din Transnistria sunt acoperite printr-un împrumut, acordat în tranșe de Federația Rusă, la fiecare 10 zile. De menționat că alocarea tranșelor de împrumut periodic se reține, fapt care condiționează secționarea sistemului de transport din regiune de sistemul operatorului licențiat. În plus, nu există o claritate a durabilității acestei finanțări a achizițiilor de gaze pentru regiunea Transnistreană în perspectiva.

În aceste circumstanțe, există riscul eminent de întrerupere a furnizării de gaze naturale în regiune, fapt care generează riscuri majore de sistare a livrărilor de gaze consumatorilor Zonei de securitate din localitățile racordate la sistemul de transport și distribuție din Transnistria.

În lipsa unei politici clare de formare a prețurilor reale la gazele naturale suportate de consumatorii finali din Transnistria, prin care să fie asigurate achiziții ferme pentru furnizarea lor ulterioară continuă în regiune, Parlamentul și Guvernul Republicii Moldova, Agenția Națională pentru Reglementare în Energetică au acordat suportul necesar, iar „Moldovagaz” SA a executat finanțarea, proiectarea și construcția conductelor de reconectare a consumatorilor din:

1. Grupul 1, în număr de 4724 cu consumul anual de 4,798 mil m<sup>3</sup>, la rețelele de distribuție ale OSD Ialoveni-gaz (s. Hârbovăț din r-nul Anenii Noi) și Ștefan Vodă-gaz (localitățile Hagimus, Copanca, Fârlădeni din r-nul Căușeni) în perioada februarie - mai 2025.

2. Grupul 2 (localitățile Pohrebea, Coșnița, Pârâta, Doroțcaia, r-nul Dubăsari), în număr de 3806 cu consumul anual de 5,053 mil m<sup>3</sup>, la rețelele de distribuție ale OSD Ialoveni-gaz în perioada februarie – septembrie 2025.



Lucrările de construcție - montaj pentru racordarea Grupului 3 de consumatori (localitățile Molovata Nouă, Cocieri, Roghi, r-nul Dubăsari și Varnița, r-nul Anenii Noi) în număr de 3 256 consumatori cu consumul anual de 6,672 mil m<sup>3</sup>, la rețelele de distribuție ale OSD Ialoveni-gaz vor demara după coordonarea bilaterală a tuturor aspectelor juridice, tehnice, sociale și politice între instituțiile organelor centrale de profil a Republicii Moldova și a regiunii transnistrene.

### Referințe

- [1] Convenția cu privire la principiile reglementării pașnice a conflictului armat din zona nistreană a Republicii Moldova, semnată între Republica Moldova și Federația Rusă la 21 iulie 1992.
- [2] Hotărârea Guvernului Republicii Moldova nr.662 din 12.10.92 "Cu privire la stabilirea perimetrului zonei conflictului armat și perioadei acțiunilor de luptă din zona nistreană a Republicii Moldova", Monitorul Oficial nr.10/308 din 30.10.1992.
- [3] Hotărârea Parlamentului Republicii Moldova nr. 286 din 12.12.2024 privind declararea stării de urgență.
- [4] Hotărârea Guvernului nr. 728 din 30.10.2024 cu privire la aprobarea Regulamentului privind situațiile excepționale în sectorul gazelor naturale și a Planului de acțiuni pentru situații excepționale în sectorul gazelor naturale.
- [5] Hotărârea Guvernului nr.677 din 02.10.2024 cu privire la aprobarea Planului de măsuri pentru pregătirea de sezonul de încălzire 2024-2025.
- [6] Procesul verbal al ședinței de lucru a Ministerului Energiei cu participarea autorităților și întreprinderilor energetice privind incertitudinile livrărilor de gaze naturale de către SAP „Gazprom” către Republica Moldova (malul stâng) începând cu 1 ianuarie 2025.
- [7] Adresarea "Gazprom" SAP nr. 03/12-6735 din 28.12.24.
- [8] Dispoziția Comisiei pentru Situații Excepționale nr. 5 din 27.01.2025.
- [9] Dispoziția Comisiei pentru Situații Excepționale nr. 8 din 10.02.2025.
- [10] Dispoziția Comisiei pentru Situații Excepționale nr. 3 din 06 ianuarie 2025.
- [11] Hotărârea Guvernului Republicii Moldova nr. 683 din 18.06.2004 "Cu privire la aprobarea Regulamentului referitor la ordinea de transmitere a rețelilor de gaze pentru deservire tehnică întreprinderilor de gaze afiliate SA "Moldovagaz"".
- [12] Procesul verbal al ședinței de lucru a reprezentanților "Moldovagaz" SA, „Tiraspoltransgaz” SRL și „Tiraspoltransgaz - Pridnestrovie” SRL nr. 02-12/59 din 15.04.2025.
- [13] Hotărârea ANRE nr. 303 din 10.06.2025 privind re-examinarea Programului investițional al „Ialoveni-gaz” SRL pentru anul 2025 (modificat).
- [14] Adresarea „Ialoveni-Gaz” SRL nr. 334 din 10.06.2025 privind coordonarea proiectelor conductelor de gaze naturale interurale de înaltă presiune către localitățile Varnița, Molovata Nouă și Cocieri.
- [15] Adresarea „Ialoveni-Gaz” SRL nr. 371 din 20.06.2025 privind coordonarea proiectului contractului de distribuție a gazelor naturale consumatorilor din satele Varnița, Molovata Nouă, Cocieri, Roghi și Corjova.
- [16] Răspunsul „Tiraspoltransgaz” SRL nr. 01-05/93 din 18.07.2025 privind alimentarea cu gaze naturale ale unor localități.
- [17] Adresarea „Moldovagaz” SA nr. 03/1-2088 din 21.07.2025, către ANRE, Ministerul Energiei și Biroul Politici de Reintegrare privind adoptarea unei decizii în scopul continuării executării măsurilor privind reconectarea localităților din zona de securitate.

# Improving the Energy Efficiency of Electric Domestic Water Heaters through Alternative Heating and Thermal Energy Storage Solutions

Îmbunătățirea eficienței energetice a boilerelor electrice pentru apă caldă menajeră prin soluții alternative de încălzire și stocare a energiei termice

Tudor T. NASCA<sup>1</sup>, Raul R. IUGA<sup>2</sup>, Octavian-Gabriel O. POP<sup>3</sup>

<sup>1</sup>Faculty of Building Services Engineering, Technical University of Cluj-Napoca  
Strada Memorandumului 28, Cluj-Napoca, Romania  
e-mail: [nascatudor@gmail.com](mailto:nascatudor@gmail.com)

<sup>2</sup>Faculty of Building Services Engineering, Technical University of Cluj-Napoca  
Strada Memorandumului 28, Cluj-Napoca, Romania  
e-mail: [rauliuga12@gmail.com](mailto:rauliuga12@gmail.com)

<sup>3</sup>Faculty of Building Services Engineering, Technical University of Cluj-Napoca  
Strada Memorandumului 28, Cluj-Napoca, Romania  
e-mail: [octavian.pop@termo.utcluj.ro](mailto:octavian.pop@termo.utcluj.ro)

DOI: 10.37789/rjce.2025.16.4.8

*Abstract* - This paper investigates the potential for improving the energy efficiency of electric boilers through the implementation of two innovative solutions. The first involves replacing the conventional electric resistance, typically immersed in water, with a mesh of carbon fiber conductors installed tangentially on the boiler shell, beneath the thermal insulation. This system operates similarly to a heating blanket, uniformly covering the boiler surface and providing a significantly larger contact area compared to traditional heating elements. Subsequently, phase change materials (PCMs) are integrated inside the boiler, with the role of storing thermal energy during the heating process and gradually releasing it during hot water consumption periods, thereby enhancing thermal performance. The study includes a detailed monitoring of the thermal behavior by installing temperature sensors at key points to analyze thermal stratification and energy efficiency. Comparative tests were conducted for three configurations: a standard boiler, a boiler with a carbon fiber conductor, and a boiler equipped with both the carbon fiber conductor and phase change materials.

*Index Terms* - Carbon Fiber Conductor, Electric Boiler, Phase Change Materials

## INTRODUCTION

Electric boilers have experienced a significant increase in usage across Europe, being increasingly adopted for domestic hot water production in the residential sector. According to available data from the literature, the energy consumption associated with domestic hot water preparation accounts for approximately 14.8% of the total household energy consumption on average. In this context, the identification and implementation of efficient technological solutions to reduce the energy consumption of electric boilers becomes a priority, considering their growing adoption.[1,2]

This trend is further reinforced by the widespread deployment of renewable energy generation systems, particularly photovoltaic panels, which promote a shift towards electricity consumption at the expense of fossil fuels. Consequently, there is a growing interest in the use of electric appliances in the residential sector and in the modernization of household equipment, including boilers, towards more sustainable solutions that are better integrated into emerging energy paradigms.[3]

Carbon fiber conductors (CFCs) are increasingly employed in heating applications due to their high electrical efficiency and remarkable mechanical properties. A notable example is their use in concrete pavements for de-icing, where carbon fiber wires are directly embedded into the road structure to prevent ice accumulation during the winter season. Furthermore, the durability and mechanical strength of carbon fiber wires allow their operation under extreme conditions without significant degradation or performance loss [4]. This technology has also been extended to other heating applications, such as underfloor heating, radiant panels, and textiles (e.g., heated clothing, carpets, benches, covers, etc.), where their flexibility and uniform heat distribution make them an efficient and versatile alternative to conventional solutions [5,6].

In the case of electric boilers, the heating elements already exhibit high efficiency, and their thermal insulation has reached an advanced level of performance. Therefore, one of the most feasible directions for enhancing the energy efficiency of these devices is the optimization of thermal energy storage capacity.

In this context, an increasing number of studies focus on improving thermal energy storage capabilities. Phase Change Materials (PCMs) have attracted growing research interest due to their ability to store substantial amounts of thermal energy: *“The storage of PCM thermal energy is more beneficial than sensible energy storage because of its high density of storage energy per unit volume/mass.”* [7]

Numerous studies have investigated the integration of Phase Change Materials (PCMs) into boilers, providing relevant solutions depending on the specific challenges addressed. For instance, in applications involving hot water tanks used for swimming pool heating, the use of PCMs enabled a reduction of the nominal tank volume by up to 25%, while energy consumption and CO emissions were decreased by 5% to 11.97% [8]. Another relevant example is the application of PCMs in solar- heated boilers, where the total amount of heat stored in a boiler equipped with phase change materials is 2.59 to 3.45 times higher compared to a conventional boiler [9].

## EXPERIMENTAL PROJECT DESCRIPTION

To evaluate the influence of these technologies, an experimental setup was developed to enable comparative testing. For this purpose, two identical electric boilers, each with a volume of 80 liters, were used. One of the boilers was kept in its original configuration and served as the control, while the second was modified according to the details presented in the following sections.

A dedicated electric meter was used to monitor the electricity consumption. The volume of water introduced into the boilers, as well as the flow rate recorded during the simulation of hot water usage, were measured using a water meter. Temperatures at different points in the system were determined using temperature sensors connected to an Arduino board, with values recorded at 2- second intervals.

The sensors used to measure water temperature were installed in 15 mm diameter copper pipes, while those intended for monitoring the temperature within the Phase Change Material (PCM) were immersion sensors, placed directly within the PCM mass. Considering the impossibility of installing temperature sensors inside the control boiler, comparisons between it and the modified variants were carried out using a single temperature sensor, positioned in the sheath of the electric resistance immersed in water.

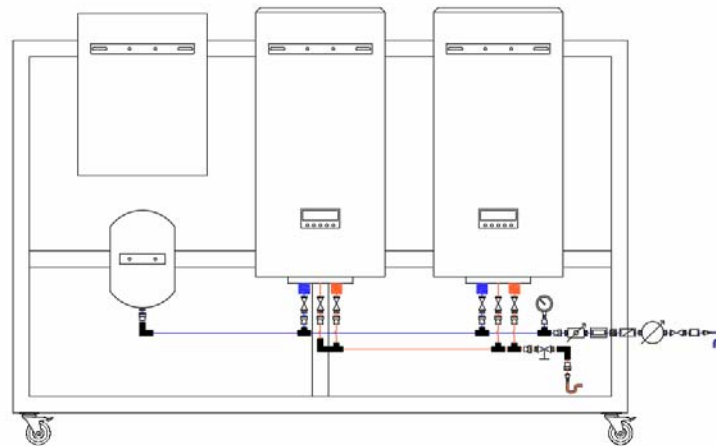


*Figure 1 Experimental Setup Layout*

Considering the need to install the carbon fiber conductor (CFC) on the boiler shell, the original polyurethane foam casing and insulation were removed. After mounting the CFC, the boiler was insulated with glass wool, protected externally by a metal sheet casing. To facilitate interior access for modifications or additional testing, the boiler was cut, and a DN400 flange was installed, allowing repeated opening. Additionally, four threaded fittings were welded onto the top cover to accommodate the connection of temperature sensor cables.



*Figure 2 CFC Mounted on the Exterior*

The Phase Change Material used was sodium thiosulfate pentahydrate ( $\text{Na}_2\text{S}_2\text{O}_5 \cdot 5\text{H}_2\text{O}$ ). To introduce the material into the boiler, 54 copper tubes, each with a diameter of  $28 \times 1 \text{ mm}$  and a length of 410 mm, were installed. These tubes were arranged in four concentric circles, containing 5, 11, 17, and 21 tubes, respectively. Temperature sensors were installed in one central tube and in one tube of the outermost circle. The PCM was poured in liquid form into each tube in an amount of approximately 330–340 g, resulting in a total of about 18 kg of PCM material.



*Figure 3 PCM Tube Assembly*

The temperature sensors are represented in Figure 4 as green squares. The tubes containing PCM are shown in red, two of which also include temperature sensors. The black tubes (left and middle) correspond to those housing the temperature sensors for water.

Improving the energy efficiency of electric domestic water heaters through alternative heating and thermal energy storage solutions

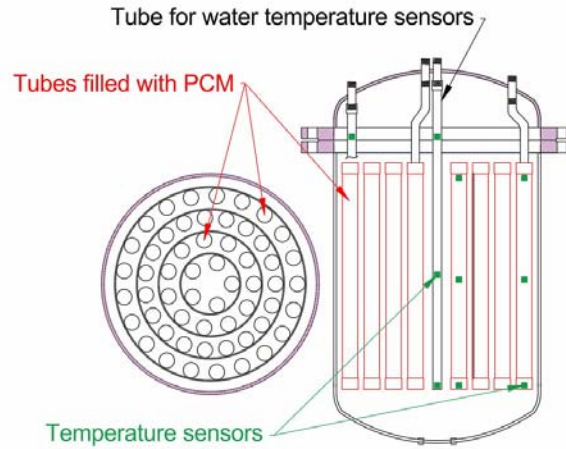


*Figure 4 Boiler Diagram Equipped with PCM*

The completed experimental stand is shown in Figure 5, while Figure 6 illustrates the electrical panel used for controlling the start and stop of the heating elements, as well as for measuring the electricity consumption.



*Figure 5 Experimental Test Stand*



*Figure 6 Control and Measurement Electrical Panel*

## DATA PRESENTATION AND DISCUSSION

In the first stage, the temperature evolution during the water heating process was analyzed, from an initial temperature of approximately 22 °C up to 60 °C inside the boiler. The heated water volumes differ slightly among the three analyzed cases and will be specified individually for each scenario. Subsequently, all obtained results are normalized to a common unit of measurement to allow comparison of the efficiency of the three configurations.

The efficiency of a heating system is defined as the ratio of required energy to total energy consumption. The efficiency for the three variants is calculated using (1).

$$\eta = \frac{Q_{\text{req}}}{Q_{\text{cons}}} * 100 \quad (1)$$

where  $\eta$  = Efficiency [%];  $Q_{\text{req}}$  = Energy required to heat the water [kJ];  $Q_{\text{cons}}$  = Energy consumption [kJ]

The required energy represents the amount of energy needed to raise the water temperature from the initial value to the final value. It can be determined using (2).

$$Q_{\text{req}} = m * c * \Delta T \quad (2)$$

where  $m$  = Mass [kg];  $c$  = Specific heat capacity [kJ/(kg·K)];  $\Delta T$  = Temperature difference between the final and initial values [°C, K]

In the case of the reference boiler, 81 kg of water were heated from an initial temperature of 23 °C to 60 °C. The total electricity consumption recorded was 3.62 kWh. Knowing the specific heat capacity of water,  $c = 4,18$  kJ/kg·K, the energy required to heat the water ( $Q_{\text{req}}$ ) is calculated using (2), and the boiler efficiency is determined based on (1).

In the case of the boiler modified with a carbon fiber conductor (CFC), 81 kg of water were heated from an initial temperature of 22 °C to 60 °C. The total electricity consumption was 3,68 kWh. As in the first case, the required energy ( $Q_{\text{req}}$ ) and the system efficiency are determined.

In the case of the boiler modified with a carbon fiber conductor (CFC) and Phase Change Material (PCM), determining the required energy is more complex due to the phase change process of the PCM. The total required energy consists of three contributions: the energy needed to heat the water, the energy accumulated by the copper (considering approximately 16 kg within the system), and the energy associated with the PCM. For the latter, the required energy is divided into three stages: heating the material in the solid phase up to the melting point, the energy absorbed during melting, and the additional heating in the liquid phase.

In this system, there are 65 kg of water, 16 kg of copper, and 18 kg of Phase Change Material (PCM). The specific heat capacity of copper is known and has a value of  $c = 0,385$  kJ/kg·K. For sodium thiosulfate pentahydrate, according to a study [10], the specific heat capacity in the solid phase is  $c_{\text{solid}} = 1,46$  kJ/kg·K and in the liquid

phase cliquid = 2,38 kJ/kg·K. The analyzed temperatures remain unchanged compared to the other cases, from 22 °C to 60 °C. The total energy consumption of this system was 3.76 kWh. By applying (2), the required energy is determined for each component: water, copper, PCM in the solid phase, and PCM in the liquid phase.

According to laboratory analyses performed on the Phase Change Material (PCM), the data required to determine the energy during the melting stage are presented in Figure 7. These data indicate that the melting process begins at a temperature of 50.46 °C and ends at 52.19 °C. The same analysis also determined the latent heat, with a value of 181.75 kJ/kg. To calculate the required energy associated with the melting of the material, this value is multiplied by the total mass of PCM, namely 18 kg.

Differential Scanning Calorimetry (DSC) was used to determine the thermal properties of the PCM. A DSC 822 instrument (Mettler Toledo, Columbus, OH, USA) was employed for sample characterization. The dynamic method was applied, with an air flow rate of 25 ml/min and a scanning temperature range of 8–50 °C. The measurements were carried out at the Faculty of Pharmacy, “Iuliu Hațieganu” University of Medicine and Pharmacy, Cluj-Napoca.

Table 1

Summary of Required Energy Values for Heating in Case 3

Energy Required by type	Value
Qreq water	7167.36 [kJ]
Qreq copper	233,12 [kJ]
Qreq solid PCM	748,42 [kJ]
Qreq Liquid PCM	333,94 [kJ]
Qreq melting PCM	3271,5 [kJ]
Qreq total	3,27 [kWh]



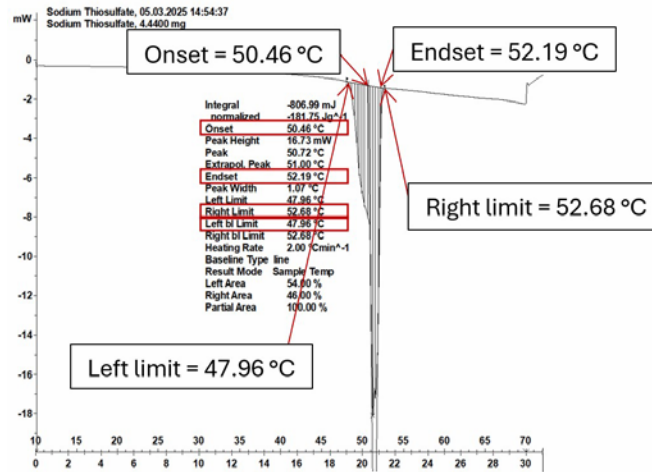


Figure 7 Melting of Sodium Thiosulfate Pentahydrate

Table 2

Summary of Heating Values

Parameter	Control Boiler	CFC Boiler	CFC/Cu/PCM Boiler
Mass [kg]	81	81	65 / 16 / 18
Temperature [°C]	23-60	22-60	23-60
Qreq [kWh]	3,48	3,57	3,62
Qcons [kwh]	3,62	3,68	3,76
Efficiency [%]	96,13	97,11	96,5

As the results indicate, the boiler modified with CFC shows an efficiency 0.98% higher than the control boiler, performing at a practically similar level. In the case of the boiler with both CFC and PCM, the efficiency is lower than that of the CFC-only boiler, due to the higher amount of stored energy. Nevertheless, its efficiency remains higher than that of the control boiler.

Figure 8 illustrates the temperature evolution over time for each of the three analyzed configurations. It can be observed that in all three cases, the heating process is linear and constant over time. The reference boiler heats up faster due to its higher electric resistance. Its heating element has a power of 1500 W, while the carbon conductor has a power of 1250 W.

## Improving the energy efficiency of electric domestic water heaters through alternative heating and thermal energy storage solutions

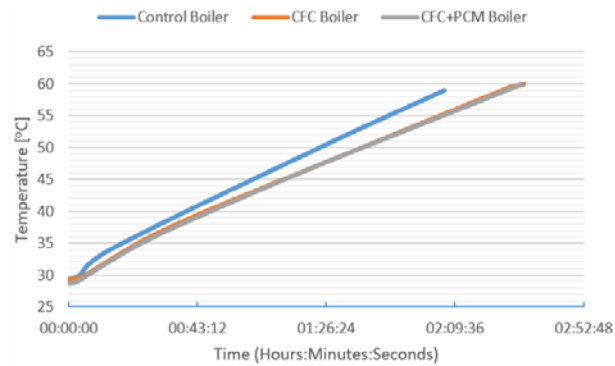


Figure 8 Temperature Variation Graph

To analyze the temperature behavior of the boilers under water consumption conditions, the inlet and outlet valves were opened, and the flow rate was adjusted to approximately 5.25 liters per minute. Simultaneously with the initiation of the water flow, the electric heating elements were activated in each case to ensure water heating during operation. The water flow was stopped when the outlet temperature reached approximately 35°C.

As observed in Figure 9, the reference boiler delivers hot water for the shortest period among the three configurations. The boiler with CFC is able to provide hot water for a longer duration within the high-temperature range, but the temperature drops more abruptly than in the reference boiler. This behavior is due to the position of the heating element. The carbon conductor boiler is able to deliver a greater amount of hot water.

Examining the temperature curve of the boiler with CFC and PCM, it is evident that an even larger quantity of hot water is supplied. This is due to the additional energy stored in the PCM, which is transferred to the water as it cools. In other words, the entire area between the grey CFC+PCM curve and the blue reference boiler curve represents the extra energy delivered to the water.

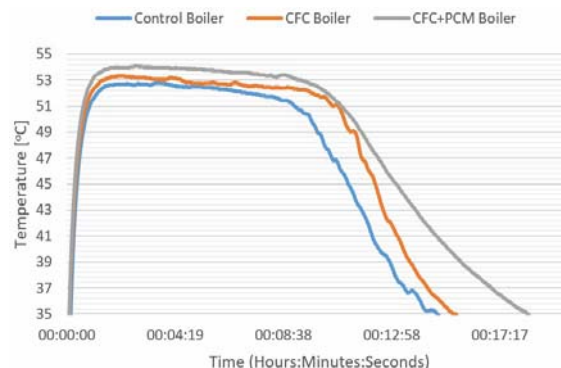


Figure 9 Temperature Variation under Water Consumption

Another, more intuitive interpretation is to consider a shower requiring a

minimum temperature of 45 °C. With the reference boiler, a shower could last approximately 11 minutes. Using the CFC boiler, the shower could last 12 minutes, and with the CFC+PCM boiler, 13 minutes, effectively providing an additional 2 minutes of hot water.

## CONCLUSIONS

The carbon fiber conductor provides a small increase in energy efficiency. However, even if its performance were considered equivalent to that of a conventional electric resistance immersed in water, the carbon fiber conductor offers numerous advantages. CFC is significantly more flexible, has a much larger contact surface ensuring more uniform heat transfer, is mechanically more durable, its electrical properties are less affected by temperature, eliminates corrosion issues, can be easily adapted into various shapes to accommodate different constructions, and has a lower carbon footprint associated with its production. Therefore, the carbon fiber conductor not only provides a modest energy efficiency gain but also offers a wide range of constructive benefits.

Phase Change Materials (PCMs) contribute to increasing energy efficiency. We observed that they help deliver a greater amount of hot water due to their ability to store more energy than water. However, I believe even greater benefits could be obtained from these materials compared to those presented in this study.

Before simulating water consumption, the boiler was left idle for 10 minutes at a temperature of 60 °C. From several separate tests on the PCM, we observed that it takes a longer time for the entire PCM mass to melt, especially in the center of the tube. It is likely that in the conducted simulation, the PCM melted in the outer part, but the heat did not reach the interior sufficiently to melt all the material. This would suggest that this configuration could potentially deliver even more hot water than the previous measurements, although with a higher energy consumption for heating.

It would be interesting to study how these configurations behave not only during heating from 22 °C to 60 °C followed by a simulated water draw-off, but also when maintaining the boiler at 60 °C for an extended period, as it is typically used, in order to assess the efficiency of maintaining water temperature, and then simulate water consumption.

Furthermore, it would be interesting to study the behavior of the carbon fiber conductor if it were placed inside the boiler, immersed in water. Another option could be to combine the exterior-mounted configuration with an additional conductor immersed in water.

## ACKNOWLEDGEMENTS

This work was funded through the project “*Bright Ideas for Real Solutions*”, under the Department for Relations with the Socio-Economic Environment of the Technical University of Cluj-Napoca, internal grant contract no. 20441/17.06.2024.

The authors would like to thank Mrs. S.L. Pharm. Dr. Lucia Tefas for her assistance in performing the DSC measurements.

The authors would also like to thank ThermalTechnology for the material support provided regarding the carbon fiber conductor.

## REFERENCES

- [1] Sarabia-Escriba, E. J., Soto-Francés, V. M., Pinazo-Ojer, J. M., & Acha, S. (2023). Economic and environmental analysis of domestic hot water systems for single-family homes. *Energy and Buildings*, 286, 112925. <https://doi.org/10.1016/J.ENBUILD.2023.112925>
- [2] Fuentes, E., Arce, L., & Salom, J. (2018). A review of domestic hot water consumption profiles for application in systems and buildings energy performance analysis. *Renewable and Sustainable Energy reviews*, 81, 1530–1547. <https://doi.org/10.1016/J.RSER.2017.05.229>
- [3] Yildiz, B., Bilbao, J. I., Roberts, M., Heslop, S., Dore, J., Bruce, A., MacGill, I., Egan, R. J., & Sproul, A. B. (2021). Analysis of electricity consumption and thermal storage of domestic electric water heating systems to utilize excess PV generation. *Energy*, 235, 121325. <https://doi.org/10.1016/J.ENERGY.2021.121325>
- [4] Zhao, H., Wu, Z., Wang, S., Zheng, J., & Che, G. (2011). Concrete pavement deicing with carbon fiber heating wires. *Cold Regions Science and Technology*, 65(3), 413–420. <https://doi.org/10.1016/J.COLDREGIONS.2010.10.010>
- [5] Huanhong Yang (2017) Research on application of carbon fiber heating material in clothing IOP Conf. Ser.: Earth Environ. Sci. 81 012042; <https://doi.org/10.1088/1755-1315/81/1/012042>
- [6] Pei, Y., Luo, Z., Xiao, H., Chen, Z., Zhou, X., & Yang, Z. (2022). A simple carbon fiber heating wire design method for preventing ice accretion on stay cables. *Case Studies in Thermal Engineering*, 34, 101996. <https://doi.org/10.1016/J.CSITE.2022.101996>
- [7] Sharif, M. K. A., Al-Abidi, A. A., Mat, S., Sopian, K., Ruslan, M. H., Sulaiman, M. Y., & Rosli, M. A. M. (2015). Review of the application of phase change material for heating and domestic hot water systems. *Renewable and Sustainable Energy Reviews*, 42, 557–568. <https://doi.org/10.1016/J.RSER.2014.09.034>
- [8] Pop, O. G., & Balan, M. C. (2021). A numerical analysis on the performance of DHW storage tanks with immersed PCM cylinders. *Applied Thermal Engineering*, 197, 117386. <https://doi.org/10.1016/J.APPLTHERMALENG.2021.117386>
- [9] Kousksou, T., Bruel, P., Cherreau, G., Leoussoff, V., & el Rhafiki, T. (2011). PCM storage for solar DHW: From an unfulfilled promise to a real benefit. *Solar Energy*, 85(9), 2033–2040. <https://doi.org/10.1016/J.SOLENER.2011.05.012>
- [10] Ekmekyapar, A. (2005). Enhancement of solar thermal energy storage performance using sodium thiosulfate pentahydrate of a conventional solar water-heating system. *Energy and Buildings*.

# Development of a Digital Twin for a thermal manikin used in the evaluation of indoor environmental quality

Dezvoltarea unui geamăn digital pentru un manechin termic utilizat în evaluarea calității mediului interior

Diana LEMIAN, Ilinca NASTASE

Technical University of Civil Engineering of Bucharest  
122-124 Bvd Lacul Tei, Bucharest, Sector 2, Romania

Email: [lemian.diana@gmail.com](mailto:lemian.diana@gmail.com), [ilincanastase@utcb.ro](mailto:ilincanastase@utcb.ro)

DOI: 10.37789/rjce.2025.16.4.9

*Abstract*-This paper presents an innovative digital twin solution for thermal manikins used to evaluate indoor environmental quality in buildings. While digital twin technology is gaining traction across industrial sectors, its adoption in building sector remains limited due to the industry's slow integration of innovative technologies. The research addresses the need for more accessible tools to analyze thermal comfort, which is often treated superficially in building design phases despite its fundamental importance for occupant well-being and energy efficiency. Traditional approaches rely on costly physical testing or simplified models that fail to capture complex human-building thermal interactions, leading to suboptimal designs and post-occupancy comfort issues. The proposed solution consists of a MATLAB application that provides an intuitive interface for monitoring thermal comfort parameters and real-time visualization of thermophysiological models applied to thermal manikins. A key innovation is the bidirectional data integration with ANSYS Fluent solver, enabling real-time simulations using data extracted from physical thermal manikin and vice versa. This work contributes to understanding and implementing digital twin concepts in thermal comfort evaluation, offering an innovative technological platform that balances occupant comfort with energy efficiency while providing a foundation for future research in this evolving field.

*Index Terms*-Energy efficiency, Indoor environmental quality, Manikin Digital Twin, Thermal comfort.

## I. INTRODUCTION

In 2023, the construction sector was responsible for nearly 34% of total carbon dioxide (CO<sub>2</sub>) emissions and 32% of total energy demand, suggesting that solutions are needed to improve these numbers in order to achieve our 2050 climate targets [1]. Approximately one-third of a building's energy consumption is due to heating, ventilation and air conditioning (HVAC) systems, therefore, one impactful way to reduce a building's CO<sub>2</sub> emissions and associated energy consumption is to improve the energy

consumption of the HVAC system by adopting efficient operating and design methods, while ensuring indoor thermal comfort and a satisfactory level of indoor air quality [2].

Indoor environmental quality (IEQ) refers to thermal comfort, indoor air quality (IAQ), visual comfort, lighting quality and acoustics and they have an impact on occupant health and productivity [3]. While only thermal comfort and IAQ have been extensively studied, standards like EN 16798-1 and ASHRAE guidelines, alongside net zero energy building (NZEB) initiatives, aim to minimize environmental impact while prioritizing occupant wellbeing [4]. Building energy dynamics are directly influenced by occupants' thermal comfort needs, especially in non-automated HVAC systems where users control thermostats and windows. Unmet thermal preferences lead to occupant discomfort and complaints, making it essential to balance energy efficiency with thermal comfort satisfaction. In addition to the thermal environment, we must also address IAQ, which is not as widely discussed as thermal comfort due to its low direct impact on occupants and the fact that thermal comfort is better understood in terms of parameters of interest and their ranges that define comfort conditions [5]. Regarding methods of improving the energy efficiency of buildings from a thermal perspective, modifications are made to the building envelope, which could result in lower ventilation rates to maintain thermal comfort, but this could lead to higher concentrations of pollutants in the indoor environment, causing discomfort and even health problems for occupants [6].

To evaluate the indoor thermal comfort of a building, it is necessary to measure physical parameters such as temperature and air velocity, which are used to evaluate the thermal sensation of the occupants which represents the heat exchange between the occupant and the environment, as well as the thermoregulatory mechanisms implemented by the body to maintain a stable internal temperature [7]. The evaluation of indoor thermal comfort is provided by thermal comfort models who fall into two categories: thermal equilibrium models (developed from climate chamber experiments) and adaptation models (based on field study data) [2]. Fanger's 1970 model remains foundational, calculating PMV (Predictive Mean Vote) and PPD (Percentage of People Dissatisfied) from air temperature, radiant temperature, air velocity, and relative humidity [8]. Unlike these measurable thermal parameters, IAQ evaluation presents significant complexity due to the ambiguous nature of air contaminants. Pollutants vary widely in type, concentration, source, and health impact, making comprehensive assessment challenging. Experts in the field recognize that new indices should consider the latest findings in human thermal physiology and biophysics in order to evaluate the IEQ [9].

A recent growing demand for robust computer models predicting human thermophysiological responses spans military, automotive, aerospace, meteorology, clinical research, textiles, and medical engineering sectors, addressing performance, tolerance limits, and thermal comfort [10]. Since heat transfer, temperature regulation, and occupant comfort are crucial for buildings and IEQ analyses, thermoregulation models now incorporate skin temperature variations, regulatory responses, clothing properties, and environmental conditions including humidity, temperature, and air contaminants [9].

With the evolution of research, the building sector has begun to adopt emergent technologies such as machine learning or artificial intelligence and in consequence it has opened up new avenues of research in this field. Although new methods of assessing IEQ have emerged over time, one method that has always stood out and yielded results as

close as possible to actual or experimental results has been the use of a thermal manikin. Initially used only to assess thermal comfort, recent studies show their complexity and ability to represent not only heat transfer and thermoregulation in the human body, but also respiration and perspiration, in order to represent reality more accurately [11].

Thermal manikins have evolved over 80 years, adapting to new technologies through increased controlled surfaces, improved skin-mimicking materials, and advanced automation systems to create the most "human-like" models possible [12]. Their recent popularity in IEQ analysis, textiles, automotive, and aerospace industries stems from being more cost-effective and practical than human subjects [13].

An analysis of the history of thermal manikin reveals three main categories [14]: **traditional thermal manikins** (measure environmental impacts on the human body, including thermal radiation and surface heat transfer), **thermoregulatory thermal manikins** (use physiological thermal regulation models to simulate complex human responses like shivering, vasomotor control, and sweating in response to temperature changes), **digital thermal manikins** (represent virtual copies of physical manikins based on numerical simulations such as computational fluid dynamics (CFD)).

The category of digital thermal manikins has sparked exponential growth in research in this field due to the simplicity and efficiency they bring to the study of heat transfer and physiological responses in different environmental conditions and for a better understanding these phenomena the manikins are often coupled with CFD and thermoregulations models. Control equations model thermoregulation by managing blood flow, metabolic rates, and perspiration to maintain homeostasis [15]. When coupled with CFD models, these equations enable detailed analysis of heat transfer and physiological responses at local body levels, allowing experiments under extreme conditions unsafe for human subjects [16].

With the transition to Industry 5.0, the symbiotic relationship between humans and emerging technologies such as deep learning techniques, brain-computer interfaces, multisensory and multimedia reality, or geospatial Digital Twin (DT) via building information modeling (BIM) and real-time building operation with the Internet of Things (IoT) is becoming increasingly crucial [17], [18]. A DT comprises a virtual model faithfully replicating its physical counterpart, connected through real-time data transfer [19]. Unlike static digital models or predetermined co-simulation scenarios, DTs maintain continuous bidirectional data exchange with physical systems, enabling real-time adaptation and predictive capabilities that evolve based on actual sensor feedback. In this paper, the thermal manikin represents the physical model, CFD simulation the virtual model, and sensor-acquired data the real-time link.

Unlike Human Digital Models or Computer-Simulated Persons found in literature, DTs are distinguished by real-time data exchange [17]. These digital thermal manikin models aim to develop customized HVAC control algorithms for improved building energy efficiency [20].

Regarding DT integration prospects in construction and energy efficiency, a thermal manikin DT for evaluating thermal comfort and indoor air quality can deliver precise, realistic results. By faithfully simulating real-world phenomena and continuously exchanging data, it enables real-time comparison between model and actual conditions while facilitating emerging technology integration for continuous digital model improvement. This dynamic enhancement involves parameter adjustments to

better reflect reality. Such DTs also enable development of personalized HVAC systems, self-adaptive algorithms that respond to environmental changes, and intuitive interfaces that simplify data control and streamline experimental analysis processes.

## II. METHODS

### A. Thermal manikin

The thermal manikin used in this study is one the simplified prototypes developed at UTCB described in [21]. It represents an average adult male, and it can control its surface temperature using PID controller with an Arduino microcontroller. The surface of the manikin can only be heated, and the surface is heated by means of nickel-plated wires placed on the surface of a polyurethane medical manikin. The manikin comprises 6 individual segments that can be independently heated, with each segment equipped with its own temperature sensor. A layer of Kapton foil was used to electrically insulate the nickel wires, and guides were used to eliminate any air pockets that might form. A layer of Kapton was added on top to electrically insulate the aluminum layer that will be added later used to better distribute the heat on the manikin surface. A schematic representation of the manikin's physical composition is presented in Fig. 1.

### B. CFD model

The geometry of the manikin used for the CFD simulation comes from the open-source geometry platform GrabCAD. The geometry was chosen to be as close as possible to that of the existing thermal manikin. This geometry was selected to ensure a balance between complexity and simplicity: detailed enough to capture the relevant aspects of the human anatomy in numerical simulations but simplified enough not to significantly affect computation time. Details about the geometry can be seen in Fig. 2.

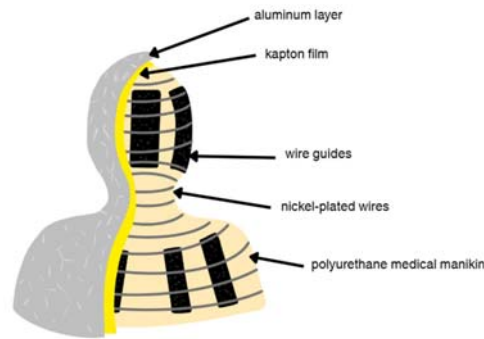


Figure 1. Physical composition of the thermal manikin

Within the CFD simulation the geometry of the virtual manikin is positioned as seated in a  $3 \times 3 \times 2.5$  m room to simulate the microclimate around it. We considered the geometry to be a simple parallelepiped in order to simplify subsequent numerical calculations. The chair was also omitted for the same reasons, to avoid detailed geometries that could interfere with the numerical calculation and because it does not show the object of the work. Fig. 3 shows the location of the mannequin in the center of the room; this geometry will be used for the following calculations.



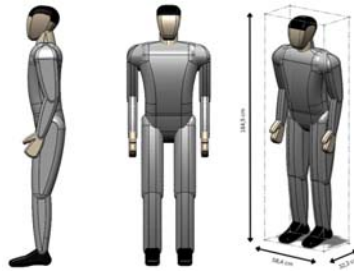


Figure 2. 3D geometry of the virtual manikin and boundary dimensions in standing position

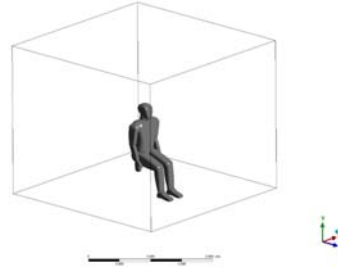


Figure 3. The geometry of the microclimate studied and the seated position of the thermal mannequin

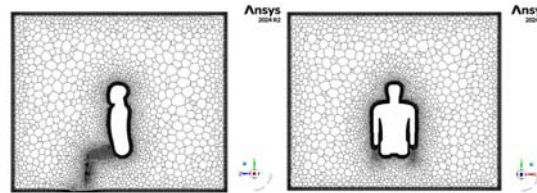


Figure 4. Grid used for CFD calculation using ANSYS Fluent

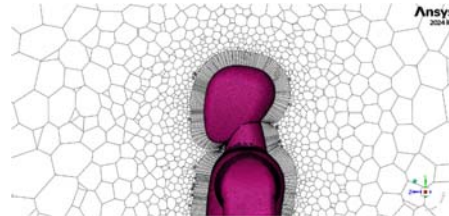


Figure 5. Inflation of the grid around the mannequin

The CFD numerical simulations were performed using the ANSYS Fluent 2024 R2 program, running on a system equipped with an AMD Ryzen processor, 32 cores, and Windows 11 operating system. Sixteen cores were used in the solver calculation, without double precision enabled. The solver used is a pressure-type, steady-state solver with gravity enabled active energy transfer and an SST k-omega turbulence model. The material considered for the numerical simulation domain is air. The calculation scheme used is a coupled type, for faster convergence and better numerical stability.

The numerical grid for the selected geometry was constructed in light of previous findings that identify the region above the head as critical for heat-transfer and microclimate analysis. Because a convective (buoyancy-driven) plume forms close to the body in this area, leading to higher velocities and turbulence, we applied local mesh refinement there. We therefore created the numerical grid shown in Fig. 4, which comprises 2 million elements and 4.8 million nodes, after transforming the elements into polyhedrons in order to obtain a more accurate calculation. Similarly, Fig. 5 shows the

inflation of the elements around the manikin in order to better capture the results in this area, which is important from the point of view of air velocities.

### C. *Thermophysiological model*

The surface temperature of the manikin can be controlled in two ways: using fixed temperature setpoints which allow for a constant surface temperature, and using Gagge's thermophysiological model to achieve a surface temperature adapted to changes in the environment.

The best-known model is Gagge's 'Pierce two-node model', used to study thermal comfort in uniform environments. It accounts for core and skin temperature variations, weighted by proportion. For moderate activity in constant environments, it describes thermoregulation (sweating, blood flow, shivering) based on thermal signals from core, skin and body [22]. The model applies to sedentary people in normal clothing and ventilation.

Gagge's model is suited to uniform, active and moderate environmental conditions for the individual, which corresponds to our experimental case [23]. The thermophysiological model is of the type with one segment and two nodes representing the core and skin. The code for Gagge's thermophysiological model has been taken from Fortran and converted to MATLAB. The model was created for a man weighing 81.7 kg, measuring 1.77 m height and with a DuBois body surface area of 2 m<sup>2</sup>. The mass of the core is estimated at 78.3 kg and the mass of the skin at 3.4 kg.

### D. *Digital Twin*

For the Digital Twin approach, we created a user interface using MATLAB's App Designer for the thermal manikin DT. The interface created is used for operating and visualizing data for the thermal manikin. This interface is needed for the DT because it represents the connection between the physical model and the digital model. In Fig. 6, we have highlighted the data flow between the user, the digital copy and the physical copy to show that the DT created fulfils the necessary conditions to be called a 'digital twin', thus the presence of a two-way data flow between the digital model and the physical model.

Fig. 7 shows the interface created for the thermal mannequin. It has five main blocks, each with different functionalities described in detail below.

**Input data block** - Located top left, allows manual entry of air temperature, radiant temperature, air velocity, and humidity (real-time sensors may be added later). It also enables exploration of metabolic rate, activity level, and clothing insulation to assess thermal comfort variations.

**Temperature display block** - Central intuitive display showing the thermal manikin with color-coded temperatures for each of 6 individually controlled segments, viewable in real-time Celsius readings.

**Temperature control block** - Bottom left block offering two temperature control methods via selectable tabs. Each tab has an activation button with current mode indication. Segment colors match the central manikin display for easy monitoring.

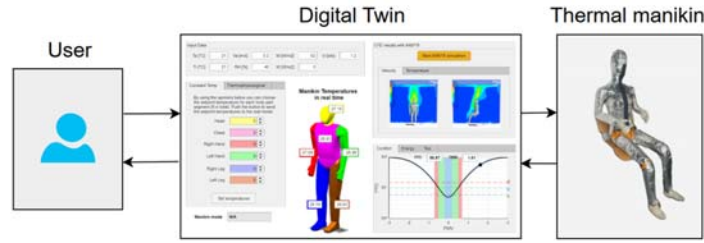


Figure 6. Data flow between user, Digital Twin and thermal manikin

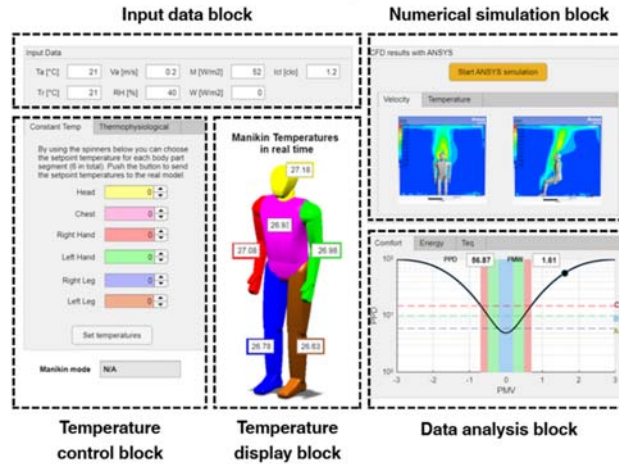


Figure 7. The user interface created in MATLAB AppDesigner for the thermal mannequin and its functional blocks

In Fig. 8\_-it can be seen the experimental setup representing the thermal manikin, Digital Twin accessed from a computer and the user.

**Numerical simulation block** - Top right block with button to initialize CFD calculations in ANSYS Fluent. Uses weak MATLAB-ANSYS coupling to extract manikin surface temperatures and generate velocity/temperature profiles in sagittal and coronal planes.

**Data analysis block** - Bottom right module organizing numerical model data into user-friendly displays. Shows thermal comfort via PMV/PPD indicators, energy consumption, equivalent temperature, and seasonal comfort representations.

### III. RESULTS AND DISCUSSIONS

#### A. Model validation

To validate the thermophysiological model, we compared the results obtained by our model with those obtained by Gagge [37]. In order to compare them, we entered the input data used in the article [37] and we calculated the exposure for one hour for the temperature range 10-40°C and for different relative humidity values. The mean error obtained was 8.6%. The errors are due to the method used by Gagge to extract the values, as he used a program that extracts data from figures, and we estimate that the poor quality of the graphs due to their age may have introduced certain errors.

To validate the numerical model, we decided to compare the results with those obtained by Danca et al. [21], in which the same thermal plume created by the manikin

was used and validated. The validation was performed by acquiring data using temperature sensors and 2D PIV velocity measurements.

For the validation in terms of velocity field, we introduced the same boundary conditions, and we extracted the velocity and temperature values above the head of the thermal manikin where the thermal plume is formed. Fig. 9 shows a comparison of the velocity results in the sagittal plane for the experimental results and the numerical CFD results obtained by them with the model used for DT in this article. We can conclude that the values are similar and that the model is validated in terms of velocities. We can observe that the same maximum values of approximately 0.25 m/s are obtained and that the velocity airflow is similar.

We also compared the results obtained by Danca et al. [21] for the temperature profiles above the manikin, where temperature variations are most pronounced. In Fig. 10, we can see the comparison between the temperature profiles obtained from the numerical model of Danca et al. and the results of the numerical model of the DT manikin. We can conclude that the model is validated in terms of the temperatures obtained, as the values are similar. Differences exist due to the shape of the head, which is different in the two models.

Due to high element counts and long simulation times in DT applications, we chose a model with fewer elements and iterations, accepting some calculation errors for faster processing within technical limitations. Validation used 3,500 iterations. In Fig. 11, velocity comparisons across 500, 2,000, and 3,500 iterations showed minimal differences between 2,000 and 3,500 iterations, but 500 iterations introduced  $\sim 0.2$  m/s velocity differences. This accuracy compromise achieves lower simulation times while maintaining overall consistency rather than high precision.



Figure 8. Experimental setup of the thermal manikin Digital Twin used by a person

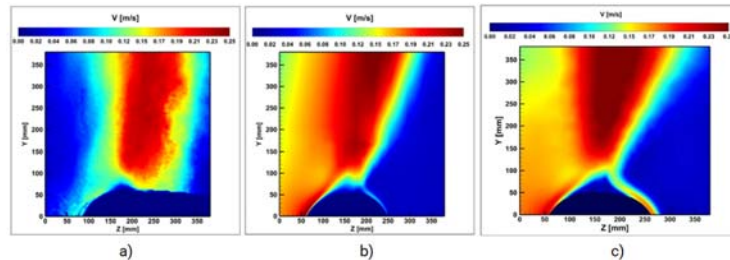


Figure 9. Comparison of velocities values in the sagittal plane for results obtained by Danca et al. [26] a) using PIV measurements, b) numerical CFD results and c) CFD results from manikin Digital Twin

In Fig. 12, temperature profile comparisons showed even smaller differences, a maximum of  $0.2^{\circ}\text{C}$  between 500 and 2,000 iterations. The goal remains capturing realistic temperature variations without prioritizing accuracy over computation time.

We also reduced computing time by decreasing grid elements. Our simplified grid (Fig. 13) removed element inflation around the mannequin (Fig. 14), resulting in 181,245 elements and 1,029,691 nodes while maintaining adequate sophistication.

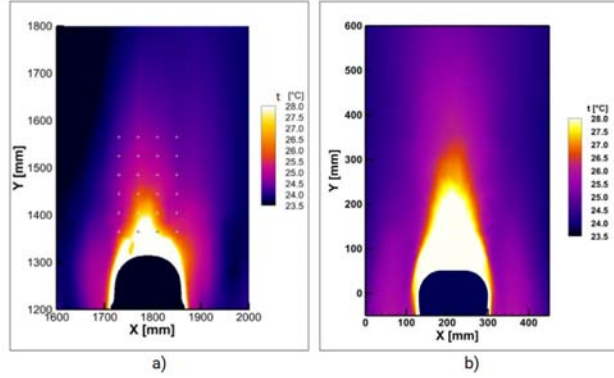


Figure 10. Comparison of temperature profiles for a) CFD results obtained by Danca et al. [26] and b) CFD results obtained from the manikin Digital Twin

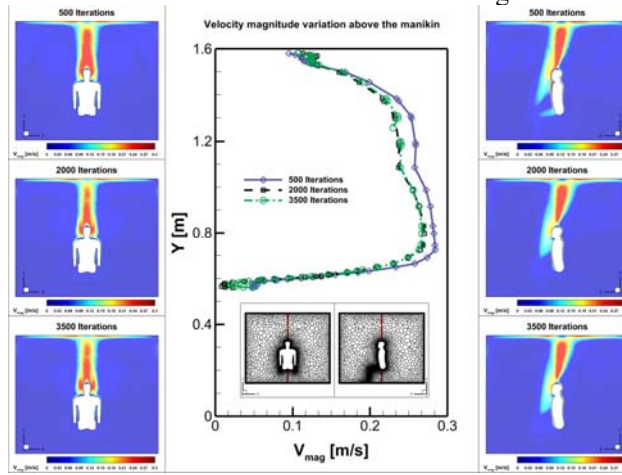


Figure 11. Comparison of velocity profiles obtained by CFD numerical simulation for different numbers of iterations

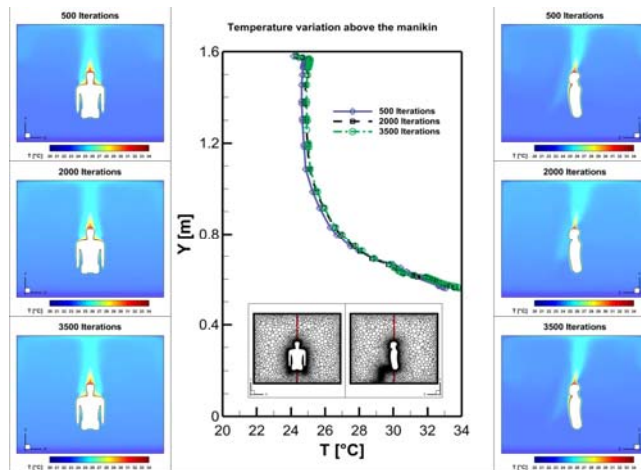


Figure 12. Comparison of temperature profile results obtained by CFD numerical simulation for different numbers of iterations



### B. Data assimilation and integration

The DT created for the thermal mannequin using the MATLAB App Designer application is capable of reading, processing, and sending various values. There is a constant exchange of data between the different components of the DT, some in real time and others entered manually. The data to be entered manually includes air temperature, radiant temperature, air velocity, and relative humidity. In the future, this data may be extracted automatically using various sensors.

Adjusting manikin surface temperatures is a key DT application with two available methods within temperature control block. The first method is simple and intuitive, using user-entered data to impose specific temperatures, useful for obtaining desired conditions or scenarios. The second method employs Gagge's thermophysiological model, which automatically estimates skin surface temperature based on environmental conditions and human thermal response. This approach enables real-time monitoring of the thermal manikin's thermophysiological reactions correlated with ambient parameter changes.

To calculate the PMV and PPD comfort parameters, certain data must be provided by the user, as the sensors required to acquire this data were not available at the time the DT was developed. To facilitate the process, this data can be added by the user, which also allows different scenarios to be explored and visualized, as seen in Fig. 15 that shows the interface displaying PMV and PPD parameters along with comfort classes A, B, and C. It is also possible, using the application created, to view the thermal mannequin's energy consumption in real time. Fig. 16 shows a graph of the evolution of consumption during DT operation. Energy consumption is calculated from the PWM values and the power installed in the nickel wires.

Another parameter that users can monitor is the equivalent temperature ( $T_{eq}$ ) specific to the thermal manikin to assess thermal comfort. The DT can display the comfort level according to the season, summer or winter, as shown in Fig. 17. The temperature and power are calculated using a moving average over a predefined period.

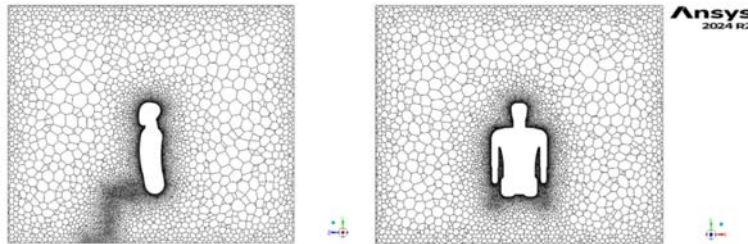


Figure 13. Simplified numerical grid used for the thermal manikin Digital Twin

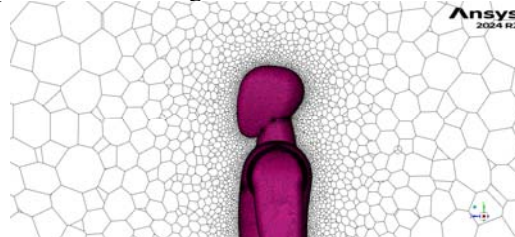


Figure 14. Simplified numerical grid around the manikin for the manikin Digital Twin

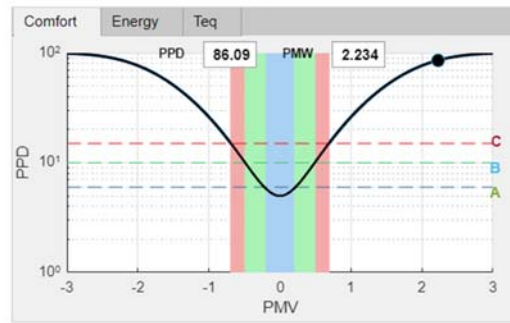


Figure 15. The DT visual interface for displaying PMV and PPD parameters

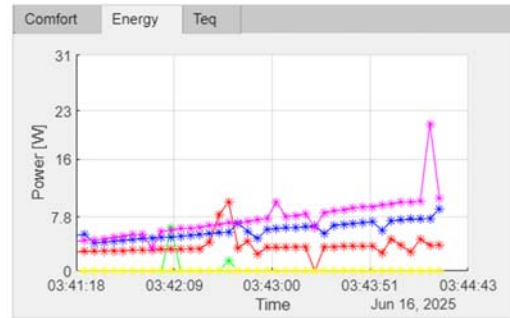


Figure 16. The DT visual interface displaying the power consumed by the thermal manikin

All of the data we have discussed can be extracted and saved in Excel files for post-processing or storage. The application is versatile and can be adapted to the user's needs. It is also possible to add different sensors or actuators to improve the DT's operation or give it new applications.

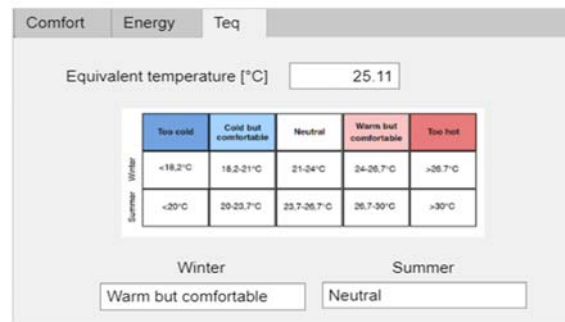


Figure 17. The DT visual interface displaying the equivalent temperature of the thermal manikin

#### IV. CONCLUSIONS

This work successfully created a Digital Twin for a thermal manikin used in built indoor environment quality analysis. The main achievement was developing a MATLAB application that communicates in real-time with the thermal manikin, featuring an interactive interface for analyzing thermal comfort parameters, real-time CFD simulations of indoor environments, and temperature control using both user-defined values and Gagge's thermophysiological model. The CFD model was validated against literature data and optimized to balance accuracy with computational efficiency for real-

time applications. Key contributions include the simplified CFD model, dual temperature control methods, and the visual interface integrating all functionalities.

While technological limitations affected simulation complexity and coupling processes, this work establishes a foundation for intelligent indoor climate control systems and opens perspectives for applications in smart buildings, vehicles, and medical environments through integration of artificial intelligence and more sophisticated physiological models.

This work represents a promising contribution to the field that will be further developed and improved in future research endeavors. The digital twin framework established here provides a solid state-of-the-art foundation and serves as an excellent starting point for future research directions. The integration of real-time thermal manikin control with CFD simulations and thermophysiological modeling demonstrates significant potential for advancing indoor environmental quality assessment. As computational capabilities continue to evolve and new sensing technologies emerge, this foundational work will enable more sophisticated implementations, paving the way for next-generation intelligent building systems and occupant-centered environmental control strategies.

#### ACKNOWLEDGEMENT

This work was supported by the grant of CCCDI - UEFISCDI, project number 60PHE din 01/04/2024 2024-2026.

#### REFERENCES

- [1] U. N. Environment, “Global Status Report for Buildings and Construction 2024/2025 | UNEP - UN Environment Programme.” Accessed: Apr. 30, 2025. [Online]. Available: <https://www.unep.org/resources/report/global-status-report-buildings-and-construction-20242025>
- [2] L. Yang, H. Yan, and J. C. Lam, “Thermal comfort and building energy consumption implications – A review,” *Applied Energy*, vol. 115, pp. 164–173, Feb. 2014.
- [3] G. A. Ganesh, S. L. Sinha, T. N. Verma, and S. K. Dewangan, “Investigation of indoor environment quality and factors affecting human comfort: A critical review,” *Building and Environment*, vol. 204, p. 108146, Oct. 2021.
- [4] T. Al Mindeel, E. Spentzou, and M. Eftekhari, “Energy, thermal comfort, and indoor air quality: Multi-objective optimization review,” *Renewable and Sustainable Energy Reviews*, vol. 202, p. 114682, Sept. 2024.
- [5] A. K. Persily and S. J. Emmerich, “Indoor air quality in sustainable, energy efficient buildings,” *HVAC&R Research*, vol. 18, no. 1–2, pp. 4–20, Feb. 2012.
- [6] M. Derbez, G. Wyart, E. Le Ponner, O. Ramalho, J. Ribéron, and C. Mandin, “Indoor air quality in energy-efficient dwellings: Levels and sources of pollutants,” *Indoor Air*, vol. 28, no. 2, pp. 318–338, Mar. 2018.
- [7] S. Tanabe, E. A. Arens, F. Bauman, H. Zhang, and T. Madsen, “Evaluating Thermal Environments by Using a Thermal Manikin with Controlled Skin Surface Temperature”.
- [8] Y. A. Horr, “Occupant productivity and office indoor environment quality: A review of the literature”.
- [9] D. Fiala, G. Havenith, P. Bröde, B. Kampmann, and G. Jendritzky, “UTCI-Fiala multi-node model of human heat transfer and temperature regulation,” *Int J Biometeorol*, vol. 56, no. 3, pp. 429–441, May 2012.
- [10] D. Fiala and G. Havenith, “Modelling Human Heat Transfer and Temperature Regulation,” in *The Mechanobiology and Mechanophysiology of Military-Related Injuries*, vol. 19, A. Gefen and Y.



- Epstein, Eds., in *Studies in Mechanobiology, Tissue Engineering and Biomaterials*, vol. 19., Cham: Springer International Publishing, 2015, pp. 265–302.
- [11] I. Holmer, “Thermal manikin history and applications,” *Eur J Appl Physiol*, vol. 92, no. 6, pp. 614–618, Sept. 2004.
- [12] C. Croitoru, I. Năstase, and F. Bode, *Calitatea ambientală în mediul interior construit*. Editura Conspres, 2021.
- [13] I. Simova, R. A. Angelova, D. Markov, R. Velichkova, and P. Stankov, “Thermal Manikins – General Features and Applications,” in *2021 6th International Symposium on Environment-Friendly Energies and Applications (EFEA)*, Sofia, Bulgaria: IEEE, Mar. 2021, pp. 1–5
- [14] Z. Lei, “Review of application of thermal manikin in evaluation on thermal and moisture comfort of clothing,” *Journal of Engineered Fibers and Fabrics*, vol. 14, p. 1558925019841548, Jan. 2019.
- [15] T. Miller, D. Nelson, G. Bue, and L. Kuznetz, “Dynamic Simulation of Human Thermoregulation and Heat Transfer for Spaceflight Applications,” in *41st International Conference on Environmental Systems*, Portland, Oregon: American Institute of Aeronautics and Astronautics, July 2011.
- [16] T. Gulati, R. Hatwar, G. Unnikrishnan, J. E. Rubio, and J. Reifman, “A 3-D virtual human model for simulating heat and cold stress,” *Journal of Applied Physiology*, vol. 133, no. 2, pp. 288–310, Aug. 2022.
- [17] Q. He *et al.*, “From Digital Human Modeling to Human Digital Twin: Framework and Perspectives in Human Factors,” *Chin. J. Mech. Eng.*, vol. 37, no. 1, p. 9, Feb. 2024.
- [18] M. H. Elnabawi and N. Hamza, “Review on Gaps and Challenges in Prediction Outdoor Thermal Comfort Indices: Leveraging Industry 4.0 and ‘Knowledge Translation,’” *Buildings*, vol. 14, no. 4, p. 879, Mar. 2024.
- [19] D. Lemian and F. Bode, “Digital twins in the building sector: Implementation and key features,” *E3S Web Conf.*, vol. 608, p. 05004, 2025.
- [20] V. A. Arowoia, R. C. Moehler, and Y. Fang, “Digital twin technology for thermal comfort and energy efficiency in buildings: A state-of-the-art and future directions,” *Energy and Built Environment*, vol. 5, no. 5, pp. 641–656, Oct. 2024.
- [21] P. Danca, C. I. Coșoiu, I. Nastase, F. Bode, and M. R. Georgescu, “Personalized Ventilation as a Possible Strategy for Reducing Airborne Infectious Disease Transmission on Commercial Aircraft,” *Applied Sciences*, vol. 12, no. 4, p. 2088, Feb. 2022.
- [22] C. Croitoru, I. Nastase, F. Bode, A. Meslem, and A. Dogeanu, “Thermal comfort models for indoor spaces and vehicles—Current capabilities and future perspectives,” *Renewable and Sustainable Energy Reviews*, vol. 44, pp. 304–318, Apr. 2015.
- [23] K. Katić, R. Li, and W. Zeiler, “Thermophysiological models and their applications: A review,” *Building and Environment*, vol. 106, pp. 286–300, Sept. 2016

# Efficiency Enhancement of Photovoltaic Panels through Passive Heat Pipe Technology

Creșterea eficienței panourilor fotovoltaice prin utilizarea tehnologiei pasive cu țevi termice

Sebastian BREZAN, Suraj-Laurențiu-Gabriel DIACONU

Universitatea Tehnică „Gheorghe Asachi” Iași  
Bdul Prof. Dimitrie Mangeron nr.67, Iași, România

E-mail: [robert-stefan.vizitiu@academic.tuiasi.ro](mailto:robert-stefan.vizitiu@academic.tuiasi.ro)

DOI: 10.37789/rjce.2025.16.4.10

*Abstract-* Photovoltaic (PV) technology is a key renewable energy source; however, its performance is significantly hindered by overheating, which reduces efficiency and output. This study investigates passive cooling solutions for PV panels, with a focus on heat pipe integration. The research builds upon previous simulation-based work by extending experiments to real outdoor operating conditions, enabling a more accurate assessment of thermal and electrical behavior. Two types of heat pipes—narrow copper water-based pipes and flat aluminum acetone-based pipes—were integrated into aluminum transfer plates and tested against a conventional PV panel. Measurements were conducted over multiple days under comparable irradiance and ambient conditions, with performance indicators including panel surface temperature and electrical output. Results demonstrate that while the conventional PV panel reached average temperatures of 46.31 °C and produced 38.65 W, the narrow heat pipe-cooled module reduced the temperature to 44.28 °C and delivered 43.32 W. The flat heat pipe-cooled module achieved the best performance, lowering the temperature to 41.20 °C and increasing power output to 55.45 W. These findings confirm that passive heat pipe cooling is a practical and efficient method to mitigate PV panel overheating, significantly improving energy output and long-term system reliability.

*Index Terms* - Energy efficiency, Heat pipes, Passive cooling, Photovoltaic Panels

## A. Introduction

Photovoltaic conversion is currently considered as the most promising renewable energy technology for electricity generation, as a clean and sustainable energy source. It is not harmful to the environment; photovoltaic (PV) panels have a long lifetime and no associated CO<sub>2</sub> emissions and low loss in transmission of electricity due associated to onsite production [1], [2].

Overheating of PV panels is a major obstacle to their operation, since just a temperature rise of 1 °C can lead to a reduction in power output by 0.65–0.85 % [3]. This

issue is intensified during the summer season, when the PV temperatures can reach 40–70 °C, resulting in a significant 7.5–22.5 % decline in conversion efficiency [4]. There are a lot of passive cooling PV methods that along the time were proved or simply considered theoretical. To discuss about the new ways to cool a PV panel there are some references done in the past few years.

It is important to mention that there are two types of passive cooling systems for PV solar panels: direct and indirect. Direct cooling involves a heat sink that is directly attached to the PV panel. Indirect cooling, however, utilizes an intermediate medium, like heat pipes, to transfer heat from the panel to a remote heat sink or in the air.[5]

In 2021 A.M. Elbreki et al., experimentally analyzed the cooling of a PV module using fins and a planar reflector at the geographical location of the National University of Malaysia. Two different heat sink configurations including longitudinal and lapping fins were chosen as the passive cooling system. Economic analysis has also been done to find out the shortest payback period of each cooling system compared with the reference module. In the latter study, under an average solar irradiance of 1000 W/m<sup>2</sup> and ambient temperature of 33 °C, passive cooling with lapping fins was used, which resulted in a mean PV module temperature, electrical efficiency, and power output of 24.6 °C, 10.68%, and 37.1 W, respectively, as the best performance. [6].

Another article written in 2023 by S.N. Razali et. al. presents another way of passive cooling a PV panel using multidirectional tapered fin heat sinks to improve the efficiency by utilizing aluminum alloy material as heatsinks. After readings and measuring the results S.N. Razali et. al. obtains some considerable changes in PV panel by lower temperature by 12 °C and increases the efficiency by 1.53% difference compared with a normal PV panel measured in the same conditions. In conclusion the integration of multidirectional tapered fin heat sinks proves to be a promising solution for managing PV module temperatures, enhancing electrical efficiency, and optimizing the performance of solar modules in tropical climates. [7]

To get along with the studies about our main topic about passive PV panel cooling using heat pipes, there are some things already know about this process and well presented below.

In 2024 Yahya Sheikh et. al. designed and performance assessed a solar PV panel integrated with heat pipes and bio-based phase change material. This study presents a hybrid way of cooling a PV panel (passive and active). The choice of utilizing heat pipes, rather than directly attaching phase change material PCM based heat sink to the PV panel is because of low thermal conductivity of PCMs. The aluminum flat sheet, which is attached to condenser sections of heat pipes, further enhances the system by providing increased contact surface area, facilitating efficient convection heat transfer to the surrounding air. The study had some impressive results, there were 4 cases and the most efficient one reduced the temperature of PV panel by 37 °C under a radiative heat flux of 1000W/m<sup>2</sup> . But even so the study demonstrates an efficiency enhancement of up to 17.3% beating the other ways of PCM and heat pipes cooling techniques studied. In conclusion with this hybrid technique of colling a PV, Yahya Sheikh et. al succeeded in giving us proper and usefull information. [5]

## Passive cooling methods for photovoltaic panels

### PCM - Based Cooling

Different from the heat pipe cooling methods, the PCM-based cooling methods for PV panels introduced in this section refer to cooling methods which utilize solid–liquid phase change [8]. The typical PV/PCM integrated system mainly comprises a PV panel and a PCM container made of high-thermal-conduction metal [9].

### Pure PCM - Based Cooling

For typical simulation studies on PV panel cooling based on pure PCMs, Kant et al. [10] studied the effects of convection inside melted PCMs, wind speed, and tilt angle of the PV panel on the cooling performance of a PV system (see Figure 1) with PCM cooling through simulations. The PCM was assumed to be RT35. The simulation results indicated that when both the convection and conduction heat transfers in the PCM were considered, the PV panel temperature could be reduced by 6.0 °C.

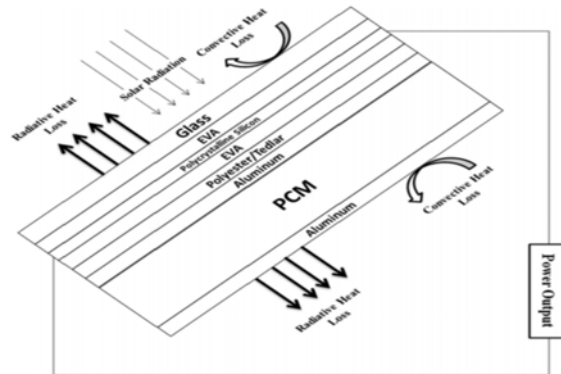


Figure 1. Diagram of a PV system using PCM cooling studied by Kant et al. [10]

For typical experimental studies, Ranawa and Nalwa [11] evaluated the cooling performance of PV panels using different multi-layer PCM cooling schemes through the experimental method. Figure 2 presents the diagrams and experimental device for PV panels with multi-layer PCM cooling. OM37 and OM42 were used as the PCMs.

The results revealed that compared with the PV panel with only single-layer OM42, the temperature reductions of the panels using OM37/OM37/OM42 and OM37/OM42/OM42 were 3.0 °C and 1.9 °C, respectively.

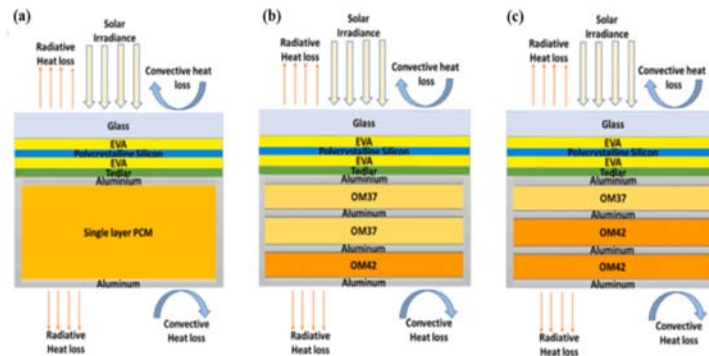


Figure 2. Diagrams of PV panels with multi-layer PCM cooling studied by Ranawa and Nalwa: (a) OM42, (b) OM37/OM37/OM42, and (c) OM37/OM42/OM42 [11].

### Spectral Beam Splitting - Based Cooling

An important characteristic of PV cells is that they have spectral response curves [12]. This means that only a certain part of the full solar spectrum can be utilized by PV panels to generate electricity, and the rest absorbed by PV panels can only become waste heat and makes the panel temperature increase, thereby reducing photo-electric efficiency [13].

Though traditional PV/T systems can solve this problem to a certain extent, the temperature of the outlet working fluid is limited by the PV panel temperature [14]. Solar PV/T systems using beam splitting technology can not only reduce the PV panel temperature but also eliminate the limitation of PV panel temperature on working fluid temperature.

The operating principle of solid beam splitter-based PV/T systems is shown in Figure 3. Regarding studies on beam splitting PV/T systems with solid beam splitters, Liang et al. [15] conducted experiments on a solar beam splitting PV/T system using a  $\text{SiO}_2/\text{TiO}_2$  film beam splitter. They found that the use of  $\text{SiO}_2/\text{TiO}_2$  film reduced the PV panel temperature by  $3.0^\circ\text{C}$ .

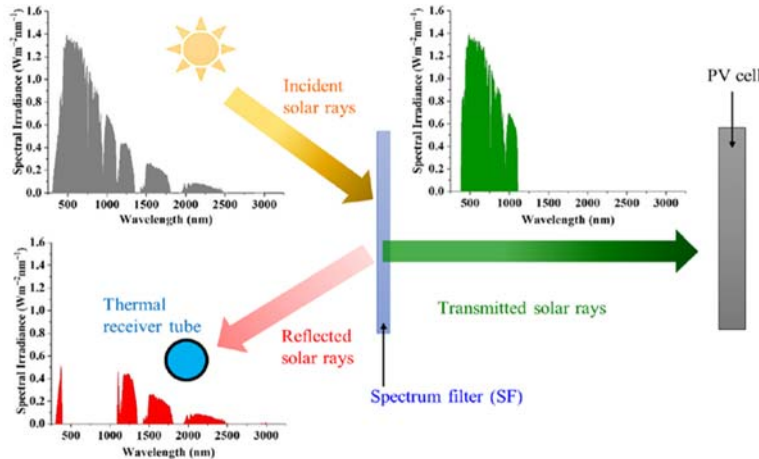


Figure. 3. Operating principle of solid beam splitter-based PV/T systems.

### Heat Pipe Cooling

Heat pipe is an effective passive heat transfer element which utilizes phase change in a medium inside a fully enclosed vacuum pipe for heat transfer. It mainly consists of three parts, namely, evaporation, insulation, and condensation sections [16]. The heat transfer inside a heat pipe primarily depends on the gas-liquid phase change in the working fluid and does not require a large temperature difference between the heat source and the heat sink. It can have high temperature uniformity, high thermal conductivity, and variable heat flux without additional energy consumption [17]. Additionally, heat pipes also have advantages of low cost, high reliability, long service life, and diverse structure and can be freely designed according to the heat dissipation requirements and structural characteristics of different PV systems. Concentrated solar photovoltaic (CPV) systems with heat pipe cooling can not only obtain effective cooling effects for PV panels but also collect some heat for thermal utilization. When heat pipes

for PV systems are designed, water, ethanol, ammonia, toluene, pentane, and other materials can be selected as the working fluid.

### Air Cooling

The natural circulation air cooling method belongs to the passive cooling technology. It takes heat away from PV panels through natural circulation flow on the front or back of the PV panels, reducing the PV panel temperature. An effective method for the natural circulation air cooling of PV panels is to add heat sinks on the back of the PV panels to further enhance the cooling effect [18]. The heat sink is normally a thermal conductor (e.g., fin) which can absorb heat from PV panels and dissipate it to the surrounding environment [19]. Appropriately increasing the heat transfer area of fins or adjusting the fin layout can enhance the PV panel cooling effects [20]. Bayrak et al. [21] analyzed the influences of fin parameters on the temperature and electrical power of PV panels under the natural convection condition through experiments. The experimental devices in the study are presented in Figure 4. They found that the PV panel using fins with  $7.0 \text{ cm} \times 20.0 \text{ cm}$  dimensions had the best cooling performance, with the output power being 9.4 W higher than that of the PV panel with no fins. Another similar experimental study was conducted by Selimefendigil et al. [22], who cooled PV panels by porous fins. The results indicated that the use of porous fins brought an increase of 7.26 W in output power.

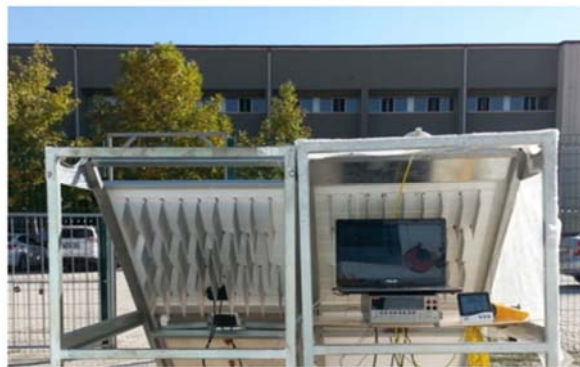


Figure 4. Experimental devices of fin-based natural circulation air cooling method for PV panels [21].

This research focuses on the passive cooling of photovoltaic (PV) panels through the use of flat and narrow heat pipes, a technique aimed at enhancing both the electrical efficiency and the overall reliability of PV systems. The experimental stand employed in this study was initially designed and constructed by Dr. Eng. Marius Branoaea within the framework of his doctoral dissertation entitled “Numerical and Experimental Research for Improving the Energy Efficiency of Solar Systems with Simultaneous Production of Electricity and Heat”. In that work, the PV modules were tested under controlled conditions using a solar simulator, and the results demonstrated promising improvements in performance.

While simulator-based experiments provide valuable insight under repeatable and well-defined irradiation and thermal conditions, they cannot fully reproduce the variability and complexity of outdoor environments. For this reason, the present article extends the scope of investigation by testing the heat pipe-cooled PV panels under real operating conditions. The objective is to evaluate their thermal and electrical behavior

under real outdoor operating conditions and to assess the potential of passive heat pipe cooling as a practical solution for improving the long-term efficiency of PV installations.

### B. Methods

The PV (photovoltaic) panels will be fixed to a metal frame made of square steel profiles with cross-section of 300mm x 30 mm. The frame has height 1740 mm and a width of 1.0 mm. From the base of the frame to the level of the wheels, the vertical bars have a length of 240 mm, resulting in a total height of 1980 mm. Further details are shown in Figure 5.

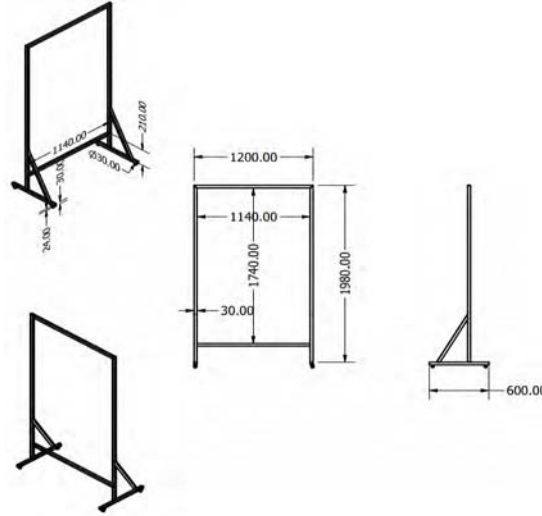


Figure 5. Metal frame of the PV panel

For ease of transportation, each frame is equipped with four wheels with a diameter of 30 mm. To improve the thermal efficiency of PV(photovoltaic) panels it was considered the use of heat pipes technology because these devices have high thermal properties and few disadvantages. For this purpose, two types of heat pipes were selected, both presenting favorable characteristics in terms of constructive parameters as well as heat transfer efficiency.

The heat pipes used for extracting heat from the surface of the photovoltaic panel are of two types: wide heat pipes with a rectangular cross-section, and narrow heat pipes with an oval cross-section and flat sides. The narrow heat pipes are manufactured by Advanced Thermal Solutions Inc., are made of copper, and use distilled water as the working fluid.

The heat pipe model ATS-HP-F8L300S21W is made of copper and uses distilled water as the working fluid. It has a width of 10.65 mm, a thickness of 4 mm, and a length of 300 mm  $\pm$  2.0%, operating within a temperature range of 30–120 °C. Its thermal performance varies with effective length, with a maximum heat transfer capacity ( $Q_{max}$ ) of 25.7 W at 180 mm and a recommended  $Q_{max}$  of 20.6 W at 225 mm. The power of the heat pipe fluctuates depending on the distance between the evaporator and the condenser, with the relationship between distance and power expressed in equations (1) and (2).

$$Q_{max} = \frac{Q_t}{L_{eff}} \times 1000 \quad (1)$$



$$L_{eff} = L - \frac{L_e + L_c}{2} \quad (2)$$

$Q_t$  = amount of thermal energy transferred per unit [W/m]

$Q_{max}$  = maximum power of heat pipe [W]

$L_{eff}$  = effective operating length [mm]

$L$  – length of the heat pipe [mm]

$L_e$  = evaporator length [mm]

$L_c$  = condensator length [mm]

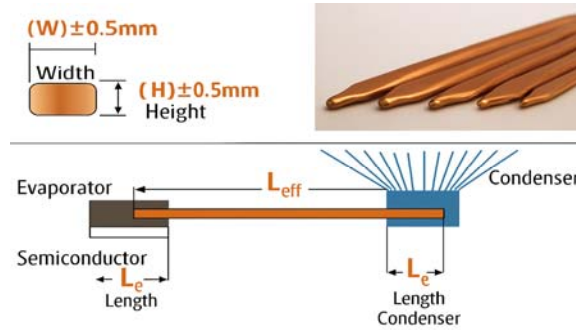


Figure 6. Constructive details of narrow heat pipes

The flat heat pipes are manufactured by AMEC THERMASOL, made of aluminum, and use acetone as the working fluid. These heat pipes were considered because, due to their constructive design, they have a larger contact surface with the photovoltaic panel.

The ATS-HP-F8L300S21W heat pipe is made from Aluminum 1070 and uses acetone as the working fluid. It has dimensions of  $50 \pm 0.5$  mm width,  $2.5 \pm 0.5$  mm thickness, and  $250 \pm 0.5$  mm length, with a working temperature range from  $-40$  °C to  $100$  °C. It supports heat transfer rates between 75 and 300 W, operates at angles between  $0^\circ$  and  $90^\circ$ , and has a thermal resistance of less than  $0.2$  °C/W.

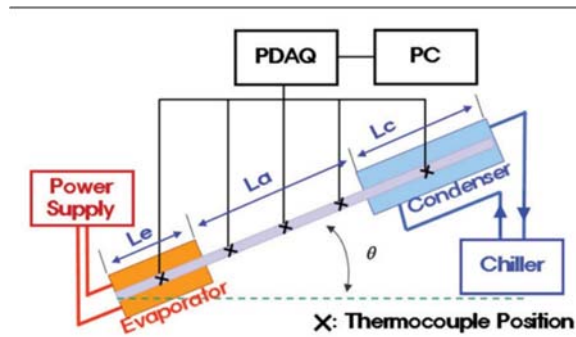


Figure 7. Constructive details of flat heat pipes

To improve the heat transfer from the photovoltaic panel to the heat pipes and to secure the pipes in place, two metal plates for enhancing thermal transfer were designed. Depending on the type of heat pipe used, the plate was constructed in two variants: one for wide pipes and the other for narrow pipes. The width and height of the plates match the dimensions of the panel, while their thickness is 10 mm.



The thermal transfer plates are made of aluminum because aluminum is a metal with a thermal conductivity of  $237 \text{ W/(m}\cdot\text{K)}$  for pure aluminum or approximately  $160 \text{ W/(m}\cdot\text{K)}$  for most alloys.

*Design of a PV panel cooled with narrow heat pipes:*

In this version of the photovoltaic panel cooling system, the dimensions of the photovoltaic panel and the narrow heat pipes were taken into account to design the thermal transfer plate in which the heat pipes will be integrated.

The thermal transfer plate is made from an aluminum sheet measuring 1620 mm in height, 960 mm in width, and 10 mm in thickness. At the upper part of the plate, a rectangle measuring  $150 \text{ mm} \times 130 \text{ mm}$  was cut out at a distance of 415 mm from the sides, corresponding to the location of the photovoltaic panel junction box.

On the surface of the plate, 63 ( $7 \times 9$ ) heat pipes are evenly spaced, with a vertical distance of 55 mm and a horizontal distance of 106 mm between them. Based on the heat pipe dimensions from the manufacturer's datasheet and by verifying the correspondence between technical data and reality, the narrow heat pipe was modeled with a  $45^\circ$  inclination and an evaporator length of 70 mm to maximize its efficiency.

For the placement of a heat pipe on the plate, it was necessary to design two rectangular-section holes. The first hole measures 70 mm in height, 14 mm in width, and 6 mm in depth, serving to hold the pipe in position, while the second hole measures 35 mm in height, 14 mm in width, and 10 mm in depth, allowing the heat pipe to pass through the plate.

*Design of a PV panel cooled with flat heat pipes:*

In the case of flat heat pipes, similarly to the plate for narrow heat pipes, the design started from an aluminum plate measuring 1620 mm in height, 960 mm in width, and 10 mm in thickness, with a rectangle of  $150 \text{ mm} \times 130 \text{ mm}$  cut out at the upper part. On the surface of the plate, 40 ( $5 \times 8$ ) heat pipes are arranged, with a vertical spacing of 80 mm and a horizontal spacing of 108 mm. Similar to the narrow heat pipes, a wide heat pipe bent at  $45^\circ$  was designed, with an evaporator length of 50 mm.

Considering the dimensions of the heat pipes, the mounting hole on the plate measures 60 mm in height, 52 mm in width, and 4 mm in depth, while the plate penetration is made through a section measuring 40 mm in height and 52 mm in width.

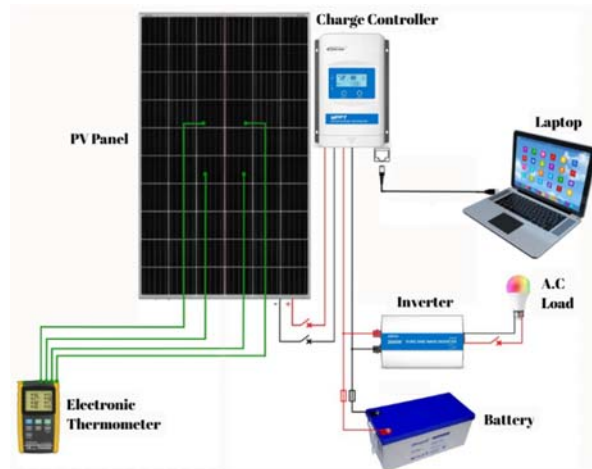


Figure 8. Operating principle of the experimental setup

In Figure 8 we have the operating principle of the experimental setup:

The EPSolar – EPEver XTRA2210N MPPT controller measure the parameters of the PV panel, directs the electrical energy to the inverter and to the storage battery. The device connects to a computer and transmits information about the PV panel parameters.

The off-grid pure sine wave inverter convert electrical energy from DC (direct current) into AC (alternating current).

The Lutron Electronic thermometer, model BTM-4208SD measures the temperatures of the photovoltaic panel at four distinct points using K-type thermocouples for surface temperature measurement.

### C. Data presentation

In this subsection, we present the results obtained from the experiments. The experiments were carried out over six separate days, with two days assigned to each type of PV (photovoltaic) panel: the conventional panel, the panel with narrow heat pipes, and the one with flat heat pipes. To ensure the reliability of the findings, we compared only the time intervals during which the testing conditions were most similar.

The measurements transmitted by the controller were recorded every minute, obtaining clearer results regarding the power output, the same approach was applied to the PV panel temperature.

The analysis was conducted over the time interval between 9:00 and 10:00 a.m., during which the measured parameters-such as solar irradiance and ambient temperature-exhibited comparable values.

The general results obtained from the measurements are presented in Table I.

Table I

Techninal specification of wide heat pipes

<i>Parameters</i>	<i>Conventional PV panel</i>	<i>PV panel cooled with narrow heat pipes</i>	<i>PV panel cooled with flat heat pipes</i>
Solar irradiance	794 W/m <sup>2</sup>	835 W/m <sup>2</sup>	848 W/m <sup>2</sup>
The ambient temperature measured	18.33°C	21.00°C	19.67°C
PV panel temperature	46.31°C	44.28°C	41.20°C
Power measured (W)	38.65 W	43.32 W	55.45 W

It should also be emphasized that the efficiency of a photovoltaic module is generally influenced by its operating temperature, since the output power decreases as the module temperature increases. In this regard, Figure 9 illustrates the average temperature variation (resulted from the 4 temperature sensors which were installed on the PV panel) of the tested modules as a function of their configuration (cooled or uncooled).

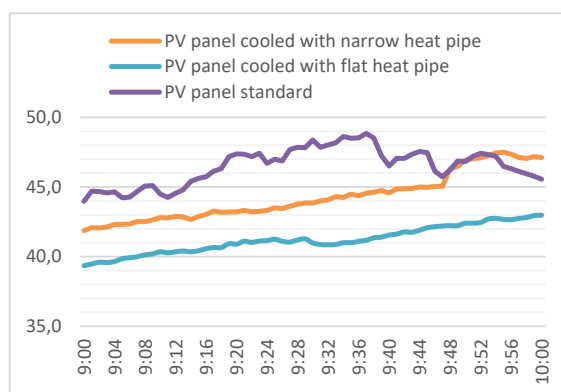


Figure 9. Average temperature variation of the PV panel

The temperature of the PV panels is between 39.5 °C and 48.85 °C. The highest value is for the standard PV panel, and the lowest one is for the PV panel cooled with flat heat pipes.

The initial power values corresponded to the average power measured during the 9:00–10:00 a.m. interval. For a more detailed analysis and to observe the fluctuations of the PV panel, Figure 10 presents the power measured every minute.

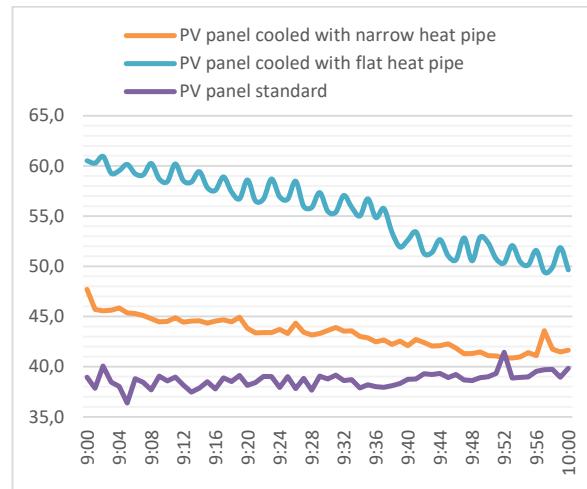


Figure 10. Average power variation of the PV panel

The power of the PV panels is between 36.38 W and 60.94 W. The highest value is for the PV panel cooled with flat heat pipes, and the lowest one is for the conventional PV panel.

#### D. Conclusions

This work shows that passive heat-pipe cooling can keep PV modules cooler and raise power in real outdoor use. In side-by-side morning tests, both cooled panels ran at lower temperatures than the standard panel, and the flat heat-pipe design performed best. These results support a simple idea: if we move heat away from the back of the cells more effectively, we recover electrical output without adding fans, pumps, or extra controls.

Over the 09:00–10:00 window, the reference panel averaged 46.31 °C and 38.65 W, the narrow copper/water design reached 44.28 °C and 43.32 W, and the flat aluminum/acetone design reached 41.20 °C and 55.45 W. Even after accounting for small differences in sun (using power-per-irradiance), specific power improved by ~6–7% for the narrow pipes and ~34% for the flat pipes versus the reference, which points to real thermal gains rather than irradiance alone.

The flat heat-pipe layout proved to be the better solution, because it is likely has better contact with the module rear and lower interface resistance, which spreads heat more evenly and reduces hot spots.

Although the results confirm that passive cooling solutions are effective, the study has some limitations. The analysis focused only on a one-hour testing window on selected days, which does not reflect the full daily or seasonal performance of the panels. In addition, the influence of wind speed was not considered. Future research should extend testing over full days and across different seasons, while also accounting for wind effects and other environmental variables, in order to provide a more complete picture of the long-term benefits and practical applications of passive heat-pipe cooling in PV systems.

## REFERENCES

- [1] Hudişteanu, Sebastian Valeriu, et al. "Enhancement of PV panel power production by passive cooling using heat sinks with perforated fins." *Applied Sciences* 11.23 (2021): 11323.
- [2] Ebhota, W. S., and P. Y. Tabakov. "Influence of photovoltaic cell technologies and elevated temperature on photovoltaic system performance." *Ain Shams Engineering Journal* 14.7 (2023): 101984.
- [3] Abdulmunem, Abdulmunem R., et al. "Numerical and experimental analysis of the tilt angle's effects on the characteristics of the melting process of PCM-based as PV cell's backside heat sink." *Renewable Energy* 173 (2021): 520-530.
- [4] Huang, Pingrui, et al. "Numerical investigation of a dual-PCM heat sink using low melting point alloy and paraffin." *Applied Thermal Engineering* 189 (2021): 116702.
- [5] Sheikh, Yahya, et al. "Design and performance assessment of a solar photovoltaic panel integrated with heat pipes and bio-based phase change material: A hybrid passive cooling strategy." *Journal of Energy Storage* 100 (2024): 113706.
- [6] Elbreki, A. M., et al. "Experimental and economic analysis of passive cooling PV module using fins and planar reflector." *Case Studies in Thermal Engineering* 23 (2021): 100801.
- [7] Razali, Siti Nuraisyah, et al. "Performance enhancement of photovoltaic modules with passive cooling multidirectional tapered fin heat sinks (MTFHS)." *Case Studies in Thermal Engineering* 50 (2023): 103400.
- [8] Hachem, F.; Abdulhay, B.; Ramadan, M.; Hage, H.E.; Rab, M.G.E.; Khaled, M. Improving the performance of photovoltaic cells using pure and combined phase change materials: Experiments and transient energy balance. *Renew. Energy* 2017, 107, 567–575.
- [9] Hossain, M.S.; Pandey, A.K.; Selvaraj, J.; Rahim, N.A.; Islam, M.M.; Tyagi, V.V. Two side serpentine flow based photovoltaic thermal-phase change materials (PVT-PCM) system: Energy, exergy and economic analysis. *Renew. Energy* 2019, 136, 1320–1336.
- [10] Kant, K.; Shukla, A.; Sharma, A.; Biwale, P.H. Heat transfer studies of photovoltaic panel coupled with phase change material. *Sol. Energy* 2016, 140, 151–161.
- [11] Ranawade, V.; Nalwa, K.S. Multilayered PCMs-based cooling solution for photovoltaic modules: Modelling and experimental study. *Renew. Energy* 2023, 216, 119136.
- [12] Wang, G.; Wang, B.; Yuan, X.; Lin, J.; Chen, Z. Novel design and analysis of a solar PVT system using LFR concentrator and nano-fluids optical filter. *Case Stud. Therm. Eng.* 2021, 27, 101328.
- [13] Wang, G.; Yao, Y.; Lin, J.; Chen, Z.; Hu, P. Design and thermodynamic analysis of a novel solar CPV and thermal combined system utilizing spectral beam splitter. *Renew. Energy* 2020, 155, 1091–1102.
- [14] Wang, G.; Zhang, Z.; Chen, Z. Design and performance evaluation of a novel CPV-T system using nano-fluid spectrum filter and with high solar concentrating uniformity. *Energy* 2023, 267, 126616.
- [15] Liang, H.; Han, H.; Wang, F.; Cheng, Z.; Lin, B.; Pan, Y.; Tan, J. Experimental investigation on spectral splitting of photovoltaic/ thermal hybrid system with two-axis sun tracking based on SiO<sub>2</sub>/TiO<sub>2</sub> interference thin film. *Energy Convers. Manag.* 2019, 188, 230–240.
- [16] Zhang, H.; Zhuang, J. Research, development and industrial application of heat pipe technology in China. *Appl. Therm. Eng.* 2023, 23, 1067–1083.
- [17] Jouhara, H.; Chauhan, A.; Nannou, T.; Almahmoud, S.; Delpech, B.; Wrobel, L.C. Heat pipe based systems-Advances and applications. *Energy* 2017, 128, 729–754.
- [18] Amr, A.A.; Hassan, A.A.M.; Abdel-Salam, M.; El-Sayed, A.M. Enhancement of photovoltaic system performance via passive cooling: Theory versus experiment. *Renew. Energy* 2019, 140, 88–133.
- [19] Johnston, E.; Szabo, P.S.B.; Bennett, N.S. Cooling silicon photovoltaic cells using finned heat sinks and the effect of inclination angle. *Therm. Sci. Eng. Prog.* 2021, 23, 100902.

- [20] Mankani, K.; Chaudhry, H.N.; Calautit, J.K. Optimization of an air-cooled heat sink for cooling of a solar photovoltaic panel: A computational study. *Energy Build.* 2022, 270, 112274.
- [21] Bayrak, F.; Oztop, H.F.; Selimefendigil, F. Effects of different fin parameters on temperature and efficiency for cooling of photovoltaic panels under natural convection. *Sol. Energy* 2019, 188, 484–494.
- [22] Selimefendigil, F.; Bayrak, F.; Oztop, H.F. Experimental analysis and dynamic modeling of a photovoltaic module with porous fins. *Renew. Energy* 2018, 125, 193–205.
- [23] Kong, M.; Joo, H.; Kwak, H. Experimental identification of effects of using dual airflow path on the performance of roof-type BAPV system. *Energy Build.* 2020, 226, 110403.
- [24] Hernandez-Perez, J.G.; Carrillo, J.G.; Bassam, A.; Flota-Banuelos, M.; Patino-Lopez, L.D. A new passive PV heatsink design to reduce efficiency losses: A computational and experimental evaluation. *Renew. Energy* 2020, 147, 1209–1220.

# Mioritic Loop: A Smart and Sustainable Closed-Loop Farm Based on Renewable Resources

Mioritic Loop: O fermă inteligentă și durabilă, cu circuit închis, bazată pe resurse regenerabile

Diana Patricia ȚUCU<sup>1</sup>

<sup>1</sup> Building Services Engineering, Faculty of Constructions, Polytechnic University of Timisoara, Victoriei Square No. 2, 300006 Timișoara, jud. Timiș, Romania,

E-mail: [diana.tucu@student.upt.ro](mailto:diana.tucu@student.upt.ro)

DOI: 10.37789/rjce.2025.16.4.11

*Abstract* - The study presents a closed-loop sustainable farm concept that combines photovoltaic energy generation, livestock farming, greenhouse horticulture, and grain agriculture in a year-round, autonomous production model. The system was designed to minimize external inputs and environmental impact while maximizing the efficiency of internal resources. The farm model illustrates how agriculture could transition to a more efficient and self-sustaining system, aligned with the European Union's vision of a greener, climate-resilient future. Furthermore, the model will generate constant capital inflows, promoting a stable and predictable economic environment.

*Index Terms* - circular economy, closed-loop system, renewable energy, sustainable agriculture.

## Introduction

The paper focuses on the concept of a smart and sustainable farm - *Mioritic Loop* - (ML) organized as a closed-loop ecosystem, which means it will provide all of its resources on its own (food, water, and energy) and process waste internally. It will combine efficient resource management, sustainable farming methods and renewable energy sources into an independent and reliable model. In order to balance energy production and consumption with agricultural output, the system will be built to run year-round with minimal external inputs. The topic is part of a larger framework for the agricultural transition to sustainability, in line with European directives on climate neutrality [1], such as the 2023/2413 European Directive (the revised Renewable Energy Directive) and the Fit for 55 legislative packages. The motivation comes from the need to reduce dependence on external resources (fossil fuels, chemical fertilizers) and vulnerability to climate change, by creating an autonomous, efficient, and

environmentally friendly model. The main objectives are: integrating renewable energy (floating photovoltaic panels), ensuring efficient resource management, valorising waste, and developing a sustainable agricultural cycle that guarantees year-round production, economic resilience, and a positive social impact.

## II. METHODS

The proposed model is based on the design of a closed-loop agricultural system that integrates a variety of components: floating photovoltaic panels on the irrigation lake, fixed-point irrigation systems, cereal cultivation, livestock farming, biogas production, and greenhouse horticulture. Each subsystem was examined in terms of its inputs, outputs, and interactions with the farm ecosystem. This methodology includes:

- assessment of renewable energy production potential by simulating solar energy generation using PVGIS;
- assessment of irrigation demand and energy consumption;
- integration of animal waste conversion into bioenergy; (planned for future work)
- design of a greenhouse powered by renewable heat sources (planned for future work).

This systematic approach ensures the autonomous functioning of the farm's production cycle and minimizes external inputs.

The methodological flow of the present study is illustrated in Figure 1, outlining the sequence of steps used to design, implement, and evaluate the Mioritic Loop farm concept.

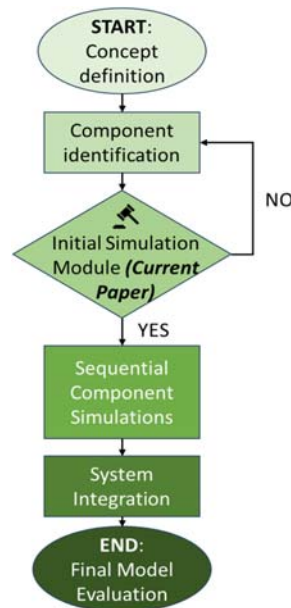


Figure 1. Methodological Flow of the present study

The present paper serves as a feasibility study, analysing just the efficiency of the floating photovoltaic panels (the first module of the farm) in order to decide if the analysis of the sequential components is worth continuing or if the initial component identification should be revised.



### A. Site description

The idea came from a farm located in the west of Romania, near Voiteg, Timiș county. The farm has about 500 hectares of agricultural land which is currently irrigated from an artificial irrigation lake, created by the farm owner. Although the system is performing well, it is vulnerable to increasing energy costs and most importantly, climate change, such as the risk of its reservoir drying up due to prolonged drought. Thus, the transition to an autonomous farm model would not only ensure year-round productivity but also reduce the reliance on external energy and water sources. Moreover, it would improve the farm's resistance to environmental challenges, increase resource efficiency and align with global trends in sustainable agriculture, while ensuring long-term economic and environmental friendliness.

### B. The proposed farm design and structure



Figure 2. Proposed farm concept. 1-floating photovoltaic panels installed on the irrigation lake, 2-fixed point irrigation system, 3-crop harvesting, 4-livestock farming, 5-biogas plant, 6-greenhouse horticulture

The closed-loop farm concept incorporates various eco-friendly systems to create an autonomous and profitable agricultural environment. Floating photovoltaic panels will be installed on the irrigation lake, harnessing solar energy to power the farm's operations. To increase the system's energy and financial efficiency, the photovoltaic panels will work in combination with the field irrigation systems to produce clean and cheap electricity to power the systems. The harvested crops will bring financial gains to the business and will also serve as food for the livestock. Furthermore, the waste of the animals is then collected and converted into biogas, which will be used for two key purposes: to generate renewable energy and to provide heat for a greenhouse, where vegetables will be grown. Moreover, the waste from the livestock will also serve as natural fertilizer for the crops, thus closing the loop.

Figure 2 presents an overview of the proposed farm concept, illustrating the main components and their purposes, as well as the outputs, that generate additional income.

## III. DATA PRESENTATION AND DISCUSSION

### A. Renewable energy potential of the model

Using floating photovoltaic panels (FPV), it is possible to harness solar energy in a slightly more efficient way, since the water surface generates a cooling effect, therefore

reducing the operating temperature of the panel. Another benefit of this system is the reduction of the water evaporation rate, contributing to the conservation of a natural resource [2]. The notable size of the irrigation lake, circa 566 meters in length, 100 meters in width and an average depth of 8 meters, makes it a good candidate for harvesting solar energy. Additionally, the lake introduces the possibility of fish farming, which would not only increase biodiversity within the closed-loop system but could also transform the farm into a recreational area for tourists and fishing enthusiasts, providing an additional source of income and increasing the farm's social and entrepreneurial value.

Considering a 2,15 m<sup>2</sup> solar radiation absorption area, the irrigation lake could accommodate over 26.000 photovoltaic panels. This equates to an installed power of almost 12 MW, considering a nominal power per panel of 445 W. Using PVGIS to simulate the annual production of the FPV field, a maximum of about 15 GWh of energy could be obtained per year [3].

For the considered farmland of approximately 500 hectares, 14 fixed point irrigation systems have been considered, with the following technical particularities:

- Arm length: 300 meters [4];
- Irrigation rate: 36 ha in 12,6 hours [4];
- Water flow: 850 m<sup>3</sup>/h;
- Energy consumption: 46 kW/h.

The irrigation system has been proposed as such due to the limited amount of sun light, so that the system's operation can be powered by the energy generated from the photovoltaic panels. Approximate calculations have shown that for one irrigation event, 8,15 MWh of energy is needed. The results from the solar energy production simulation state that circa 64 MWh of energy can be produced by the FPV on an average day in July, as shown in Figure 3. The big overproduction rate of energy will be assessed, and the number of installed panels will be adjusted in accordance with the cost-benefit analysis.

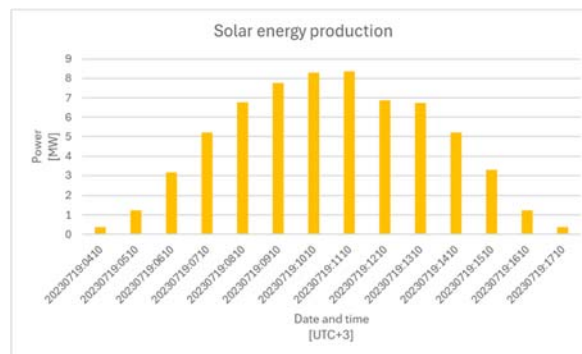


Figure 3. Solar energy production of the FPV field on an average day in July

By having the possibility to irrigate in a sustainable and economically feasible way, it is possible to increase the overall crop and biomass yield of the agricultural land [5]. This allows the farmer to value the secondary product of the harvest, the straw, as biofuel in two ways: directly combusting it to generate heat, and to use fermenting or anaerobic digestion to turn it into biogas or bioethanol [6]. A second crop, such as ryegrass, maize silage or sorghum, can be grown on the same parcel of land after the primary cereal crops have been harvested. These quickly growing species are ideal for

post-harvest times and can be used livestock feed as well as biomass inputs for biogas production, increasing land productivity while supporting the circular economy of the farm [7,8].

The biofuels obtained from the harvesting process can be used as an energy source for keeping a greenhouse functioning during the winter, allowing the farmer to maintain production in the cold season and to also obtain a head start on the seasonal vegetable merchandising.

Table 1 presents the main components of the proposed closed-loop, sustainable farm system, highlighting the necessary inputs for establishing each component, the final outputs generated, and how they function within the farm ecosystem. Additionally, the table also highlights the ways in which these components support local employment opportunities by creating varied workspaces that are open to people with any level of educational background. In the end, the system's outputs support the farm's long-term sustainability and financial viability.

Table I

Functional Overview of the proposed Closed-loop Sustainable Farm

Component	Input	Purpose	Output / Incoming Funds
Floating Photovoltaic Panels	-Solar energy	Converts solar energy into electricity for powering the fixed-point irrigation systems	-Renewable electricity for farm operations -Surplus energy delivered into the national grid -Water evaporation reduction
Irrigation Lake	-Rainwater -Ground-water	Acts as a water reservoir and as a base for the photovoltaic panels	-Water source for irrigation and livestock -Fish farm -Recreational area for tourists and fish enthusiasts
Cereal Cultivation (Primary and Secondary Crop)	-Irrigation water -Sunlight -Seeds -Soil -Organic fertilizer from animal waste	Production of food, animal feed (realized all year round due to the secondary harvest), bioenergy after processing and economical gain	-Cereal grains, serving as animal feed and incoming funds -Straw bales valued as biofuel
Livestock Farming	-Cereal feed -Water -Shelter	Raising animals for dairy and meat production, fed from the farm's own production	-Dairy and meat -Waste used as fertilizer for crops or converted into biogas for greenhouse heating
Biogas Plant or Biomass thermal power plant	-Livestock waste -Straw bales	Anaerobic digestion of waste materials and energy valorisation by direct combustion of bales	-Biogas for heating the greenhouse, animal shelters and farmer's house or for the animal feed manufacturing unit
Greenhouse (Vegetables)	-Heat from the Biogas Plant or biomass	Controlled-environment agriculture with year-round vegetable production	-Organic vegetables that generate financial income

Component	Input	Purpose	Output / Incoming Funds
	thermal power plant -Water -Light		
Social Component	-Local population	Providing well-paid jobs year-round to the local population to reduce depopulation	A motivated and economically developed local community based on sustainable principles

### B. Cost-Benefit Analysis

The first stage of the cost - benefit analysis focuses on evaluating the current farm scenario, where the farmer depends on the electricity provider for irrigation. Setting a baseline for the farm's operating costs and identifying the main economic challenges, particularly the high electricity costs related to irrigations, are the goals of this first step. By first analysing this scenario, we can better understand the current inefficiencies and evaluate how the use of photovoltaic panels could have a visible and quantifiable effect on reducing the energy costs. This initial analysis aims to establish the foundation of the future evaluation consisting in the more complex full closed-loop system, providing valuable information regarding the energy needs of the farm.

Thus, for the present paper, two scenarios have been taken into consideration. The first one, with no investment, presented in table 2, shows the approximate price that the farmer must pay for the irrigation of the fields. The price includes the water pumping costs and the system operation costs. In the second scenario, illustrated in table 3, a floating photovoltaic system was proposed, with a total of 1034 panels, resulting an installed power of 460 kW. The monthly energy production was considered, so that the system would be capable to produce sufficient energy to cover the pumping and irrigation system energy demands.

Table II

Scenario I: No investment

Component	Quantity [MWh]	Cost/ MWh [€]	Total Cost [€]
Annual electricity cost for irrigation	244.5	200	48 900

Table III

Scenario II: Floating Photovoltaic Panels

Component	Quantity [MWh]	Unit	Cost/ Unit [€]	Total Cost [€]
Floating Photovoltaic Panel (P=445 W)	1034	Pcs.	150	155 100
Simple Invertor (P=115 kW)	4	Pcs.	5000	20 000
Installation cost	1	Est.	35 020	35 020

By considering the initial cost of investment, energy production, and the possibility of selling the excess energy to the grid (a conservative 0,1 euros/kWh were considered, as shown in table 4), the payback period will amount to about 3 to 4 years, depending on economic and environmental factors.

Table IV

Energy Production Simulation			
Component	Quantity [MWh]	Cost/ MWh [€]	Total Income [€]
Simulated annual energy production with FPV	577.4	0	0
Annual electricity cost for irrigation covered by the FPV field	244.5	0	0
Estimated annual energy surplus sale	332.9	100	33 290

Taking into consideration the technical and economic aspects of the proposed farm model, the size of the floating photovoltaic panel system ought to be correlated with the real farming energy demands (irrigation, powering facilities, equipment, lighting, etc.). Therefore, the installed power in Scenario 2 can be augmented if the farm owner has equipment with high energy consumption.

### CONCLUSIONS

The paper aims to show that the closed-loop farming model embodies a holistic and systems-based approach to a sustainable agriculture. By integrating various components, such as crop cultivation, irrigations systems, livestock farming and biofuel management into a self-sustaining cycle, closed-loop systems significantly reduce external inputs and environmental externalities. The model not only enhances efficient resource management but also promotes long-term agricultural resilience. Moreover, the implementation of such systems can generate positive social impacts by creating employment opportunities within nearby communities, fostering local economic development and strengthening rural livelihoods.

Next step of the research will focus on continuing the simulation by including the livestock farm, crop production, greenhouse, and the biogas plant to create a more complete and realistic model of the system. Moreover, future research could focus on improving the current developed closed-loop system by combining more precise resource management technologies, such as automatic irrigation, compost monitoring, and renewable energy integration, in order to improve both environmental and economic performance. Expanding the model to other Romanian regions might help in determining its adaptability to varied soils, climates, and local people, as well as investigating ways to improve local employment and educational opportunities. Long-term studies on the farm's productivity, waste reduction, and financial sustainability would also provide useful insights for expanding the Mioritic Loop concept and promoting it as a model for sustainable agriculture in Romania.

### REFERENCES

- [1] Directive (EU) 2023/2413 of the European Parliament and of the Council, October 18<sup>th</sup>, 2023.
- [2] Nisar H., Janjua A. K., Hafeez H., “Thermal and electrical performance of solar floating PV system compared to on-ground PV system-an experimental investigation”, *Solar Energy*, vol. 241, July 15<sup>th</sup>, 2022.

- [3] \*\*\*, Photovoltaic Geographical Information System (PVGIS), Available online: [https://joint-research-centre.ec.europa.eu/photovoltaic-geographical-information-system-pvgis\\_en](https://joint-research-centre.ec.europa.eu/photovoltaic-geographical-information-system-pvgis_en), Accessed on April 14<sup>th</sup>, 2025.
- [4] \*\*\*, Instalație de irigație tip pivot fix de 300 m, Available online: <https://etufarm.ro/produs/instalatie-de-irigat-tip-pivot-fix-de-300m/>, Accessed on April 14<sup>th</sup>, 2025.
- [5] Moghbel F., Fazel F., Aguilar J., “Long-term investigation of the irrigation intervals and supplementary irrigation strategies effects on winter wheat in the U.S. Central High Plains based on a combination of crop modeling and field studies”, *Agricultural Water Management*, vol. 304, November 1<sup>st</sup>, 2024.
- [6] Buchspies, B., Kaltschmitt, M., & Junginger, M., “Straw utilization for biofuel production: A consequential assessment of greenhouse gas emissions from bioethanol and biomethane provision with a focus on the time dependency of emissions”, *GCB Bioenergy*, vol. 12, October 2020.
- [7] Baldinger, L., Zollitsch, W., & Knaus, W. F., “Maize silage and Italian ryegrass silage as high-energy forages in organic dairy cow diets: Differences in feed intake, milk yield and quality, and nitrogen efficiency”, *Renewable Agriculture and Food Systems*, vol. 29(4), pp. 378–387, 2014.
- [8] Wannasek, L., Ortner, M., Kaul, H.-P., Amon, B., & Amon, T., “Double-cropping systems based on rye, maize and sorghum: Impact of variety and harvesting time on biomass and biogas yield.”, *European Journal of Agronomy*, vol. 110, 125934, October 2019.

## Testul de răspuns termic pentru utilizarea eficientă a aplicațiilor geotermale în România

Thermal Response Test for the Efficient Use of Geothermal Applications in Romania

Virgil FLORESCU<sup>1</sup>, Bahadır KIVANC<sup>2</sup>, Tiberiu CATALINA<sup>3</sup>

<sup>1</sup> Technical University of Civil Engineering of Bucharest  
122-124 Bvd Lacul Tei, Bucharest, Sector 2, Romania  
E-mail: [virgil.florescu@utcb.ro](mailto:virgil.florescu@utcb.ro)

<sup>2</sup> Societatea Română Geoexchange,  
str. Fabricilor nr. 2F, Oradea, Romania  
E-mail: [bahadir.kivanc@phd.utcb.ro](mailto:bahadir.kivanc@phd.utcb.ro)

<sup>3</sup> Technical University of Civil Engineering of Bucharest  
122-124 Bvd Lacul Tei, Bucharest, Sector 2, Romania

<sup>3</sup> Societatea Română Geoexchange,  
str. Fabricilor nr. 2F, Oradea, Romania  
E-mail: [tiberiu.catalina@gmail.com](mailto:tiberiu.catalina@gmail.com)

DOI: 10.37789/rjce.2025.16.4.12

*Abstract.* The Thermal Response Test – abbreviated as TRT – is a standardized procedure for geothermal heat pump systems with closed-loop heat exchangers. The test enables the determination of key physical properties of the ground – thermal conductivity and borehole thermal resistance – which are essential for the correct sizing of the ground heat exchanger system, ensuring it meets the requirements of the building's HVAC system. Additionally, the TRT provides valuable information regarding the technical and financial effort required for the drilling operation.

*Keywords:* Thermal Response Test, TRT, geothermal heat pumps, ground heat exchangers

### 1 Principle of the method

The thermal response test is performed for closed-loop heat exchangers. In most cases, the thermal response test is carried out by injecting or extracting a constant heat flux per unit length into the ground. Electric resistances (connected according to the borehole depth) are typically used to generate heat, as this method allows for easier monitoring of operating parameters. In some cases, a gas boiler can also be used. The

thermal response of the ground is determined by measuring the temperature difference  $\Delta T$  between the supply and return lines of the circuit. The average temperature of the fluid is:

$$T_b = (T_{wi} + T_{wo}) / 2 \quad (1)$$

The equation that describes the evolution of the average temperature  $T_b$  as a function of the thermal load after the heat generator is started is usually derived from the line source model and has the form:

$$T_b - T_0 = \frac{q}{4\pi\lambda} E \left( \frac{r_b^2 S_{VC}}{4\lambda t} \right) + qR_b \quad (2)$$

For large time values ( $t > 5-10$  hours), the equation can be simplified to a logarithmic function, which is commonly used in the analysis of Thermal Response Test (TRT) data. The simplified form is:

$$T_b - T_0 = \frac{q}{4\pi\lambda} \left[ \ln \left( \frac{4\lambda t}{S_{VC} r_b^2} \right) - 0.5772 \right] + qR_b \quad (3)$$

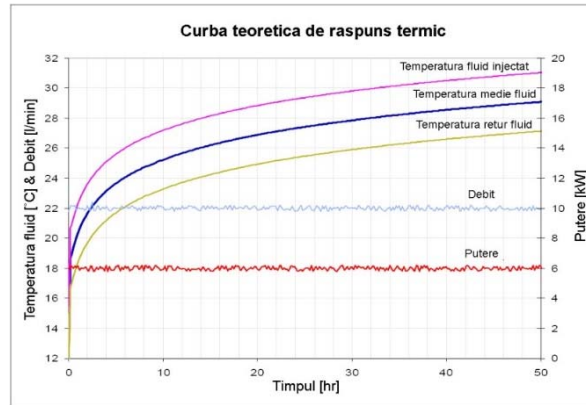


Figure 1-1. Parameters Monitored During the Thermal Response Test (TRT) [1]

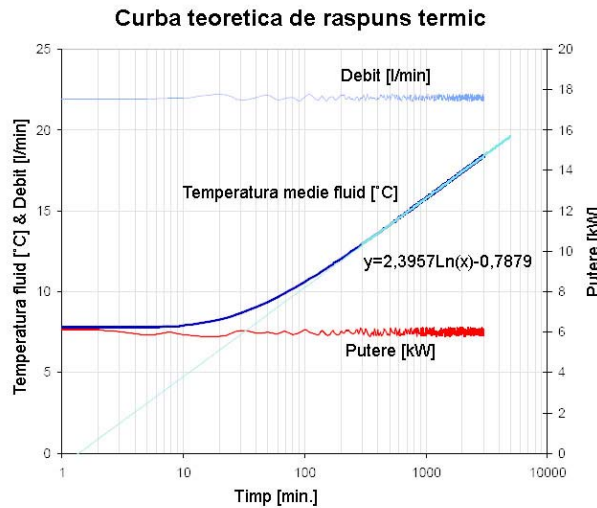


Figure 1-2. Theoretical Thermal Response Curve [1]



The linear interpolation equation describing the variation of temperature as a function of the natural logarithm of time is:

$$y = A \ln(t) + B \quad (4)$$

It can be observed that determining the coefficient A (the slope of the line) is sufficient to determine the thermal conductivity of the analyzed ground.

$$A = q / 4 \pi \lambda \quad (5)$$

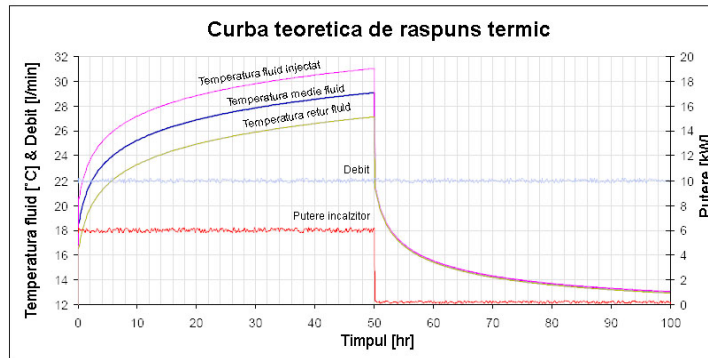


Figure 1-3. Theoretical thermal response curve after stopping the heating [1]

The thermal response test provides the results:

- Thermal conductivity of the ground  $\lambda$
- Thermal resistance of the borehole  $R_b$
- Additionally, it provides the contractor with information regarding the level of effort required for the execution and outfitting of the borehole

In accordance with the guidelines related to TRT published by GSHPA (Ground Source Heat Pump Association) [2], ASHRAE (American Society of Heating, Refrigerating and Air-Conditioning Engineers), and IEA (International Energy Agency), the Thermal Response Test must comply with the following conditions:

- Test duration over 36 hours (according to GSHPA), but preferably over 50 hours (according to IEA);
- Constant heat flux injected at a level of 50–80 W/m of borehole;
- Constant heat flux extracted at a level of 20–50 W/m of borehole;
- The fluid flow inside the heat exchanger pipes must occur under turbulent flow conditions;
- The test should be conducted at least 5 days after the completion of the drilling;
- The testing equipment should be placed as close as possible to the borehole, and the connections to its pipes must be thermally insulated to limit heat losses to a value below 2%;
- If the test needs to be repeated, it should be done after an interval of 10 to 14 days following the completion of the first test.

Forajul experimental realizat are adâncimea de 50 m, diametrul de 160 mm, și este dotat cu un schimbător de căldură cu pământul de tip double-U, conducta având diametrul de 32 mm.

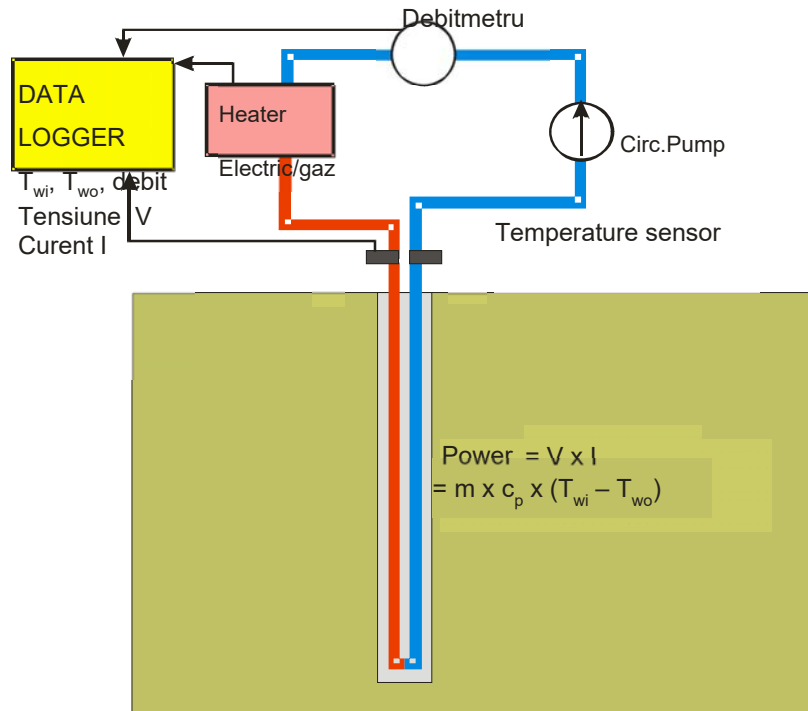


Figure 1-4. The principle of the Thermal Response Test [1]

## 2 Experimental equipment

The determinations were carried out using the mobile geothermal laboratory – consisting of the following equipment:

- GeoCube – Portable unit for measuring thermal conductivity (TC), thermal response (TRT) for different soil types, as well as for determining the BTR factor (Borehole Thermal Resistance)
- 3x16 mm<sup>2</sup> cable for the electrical supply of the resistors in the GeoCube unit from an electrical panel located very close to the experiment;
- Specialized software – TC/TRT Software and Ground Loop Design Software.





Figure 2-1. GeoCube Equipment

### 3 Drilling Equipment Used in the GEO4CIVHIC Project

To enable the installation of vertical heat exchangers in the built environment, the objectives of the drilling equipment were as follows:

- Capable of installing U-type, double U-type, and W-type heat exchangers
- Capable of accessing and operating in confined and small spaces in cities and villages
- Designed to have a minimal environmental footprint in terms of emissions and noise generated by the equipment
- Provides safe and less tiring conditions for rod operation (loading and unloading), as well as a user-friendly system for operating and handling the equipment

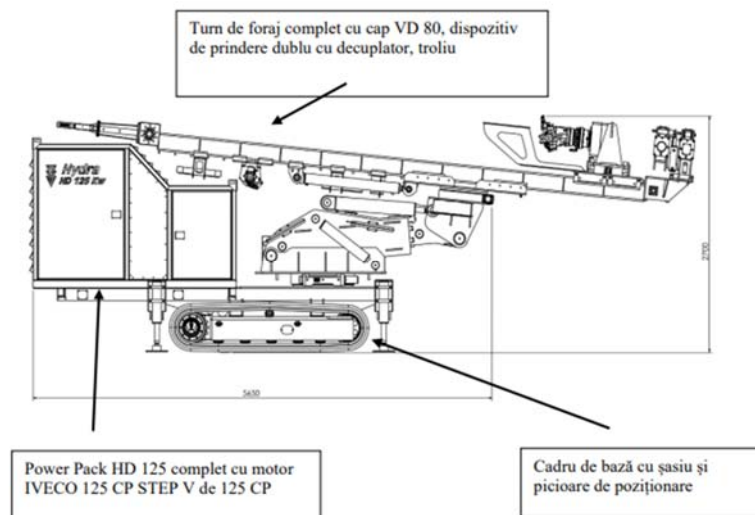


Figure 3-1. The main systems of the drilling machine are:

The main systems of the drilling machine are:

- **Drilling system** – includes the spindle, drill rods, drill bit, and rotation mechanism for the actual digging.
- **Feed and retract system** – allows the up and down movement of the drill rods and bit, controlling the drilling depth.

- **Hydraulic or pneumatic system** – provides the energy needed to operate the spindle, feed systems, and other components.
- **Cooling and lubrication system** – ensures cooling and lubrication of the drill bit and rods, usually by circulating drilling fluid (water or special solutions).
- **Cuttings removal system** – helps efficiently remove the excavated material (cuttings) from the borehole.
- **Control and monitoring system** – control panel, instruments for measuring depth, pressure, rotation, and other essential parameters.
- **Stabilization and positioning system** – ensures the stability of the drilling machine during operation, e.g., supports and anchors.

The equipment shown in Figure 3-1 is capable of drilling both vertically and horizontally at angles between 15° and 30° for the installation of coaxial probes, allowing the total length to increase substantially. Additionally, the mast can rotate 90° to the left or right. This feature enables the equipment to drill up to 3 meters to the left or right from the center of the machine. The drilling diameter used was 160 mm (Figure 3-2).



*Figure 3-2 Drilling head 160 mm*

With the new drilling method, during drilling in soils containing clay and sand, a bentonite-water mixture was used simultaneously as a composite material to stabilize the borehole walls (Figure 3-3).



Figure 3-3. Bentonite and water mixture for borehole wall stabilization

In the below link, you can see all the steps carried out for the drilling and obtaining data about the thermal response test (TRT) performed at Romexpo.

[https://photos.google.com/share/AF1QipMgogCQOxrtWRME6q1OTayzJCe\\_qI9\\_ckC4uvkZ\\_jPhBJCcTOeP8nblC4SSI7BWbg?pli=1&key=bFBDWDVftGE5Z04tSWpYTVRTZFh3NWIKTlo1bjln](https://photos.google.com/share/AF1QipMgogCQOxrtWRME6q1OTayzJCe_qI9_ckC4uvkZ_jPhBJCcTOeP8nblC4SSI7BWbg?pli=1&key=bFBDWDVftGE5Z04tSWpYTVRTZFh3NWIKTlo1bjln)

#### 4 In situ determination results

Following the processing of the experimental data, the following results were obtained:

- Thermal conductivity 1.71 [W/m\*K]
- Thermal diffusivity 0.073 [m<sup>2</sup>/zi]
- Average heat flux 49.2 [W/m]
- Borehole thermal resistance 0.19 [m\*K/W]
- Average flow rate 0.61 [l/s]
- Test duration 12 [h]
- Calculation interval 1.5 – 13.5 [ore]
- Unperturbed ground temperature 12.9 [°C]

Thermal Conductivity Report

- 12/1/2019

Project Name: Testare put 50 m RomExpo		
Project Address: Dd. Marasti nr. 65-67		
City: Bucuresti	State: Romania	Zip:
Prepared By: Ing. Bahadir Kivanc		
Email: bahadir.kivanc@phd.utcb.ro	Phone: +40720 003 074	
Drill Date 11/19/2019		
TC Test Date(s) 11/25/2019	>>	11/29/2019
Client Name: UTCB		
Address Line 1: Bd. Lacul Tei nr. 122-124		
Address Line 2:		
City: Romania	Phone:	
State:	Fax:	
Zip:	Email:	

## Testul de răspuns termic pentru utilizarea eficientă a aplicațiilor geotermale în România

Calculation Results		
Thermal Conductivity (W/(m*K)) :	1.71	
Thermal Diffusivity (est.) (m <sup>2</sup> /day) :	0.073	
Average Heat Flux (W/m) :	49.2	
BH Thermal Resist (BTR) (m*K/W) :	0.19	
Average Flow Rate (L/s) :	0.61	
Test Duration (hr) :	12	
Calculation Interval :	1.5 - 13.5	Hours
Borehole Input Parameters		
Undisturbed Ground Temperature (°C) :	12.9	(Auto-Estimated)
Depth (m) :	50	
Borehole Diameter (mm) :	160.0	
Pipe Size:	1 1/4 in. (32 mm)	
Grout Thermal Conductivity (W/(m*K)) :	2.10	
Drilling Method :	Standard	
Drilling Time (hr) :	10.0	
Diffusivity Input Parameters		
Soil/Rock Specific Heat - Dry (kJ/(K*kg)) :	0.837	
Soil/Rock Density - Dry (kg/m <sup>3</sup> ) :	1601.8	
Moisture (0-100) (%) :	15.0	
Flow Rate Input Parameters		
ITC Unit Model Name	GeoCube Standard	

Figure 4-1. Geocube final results

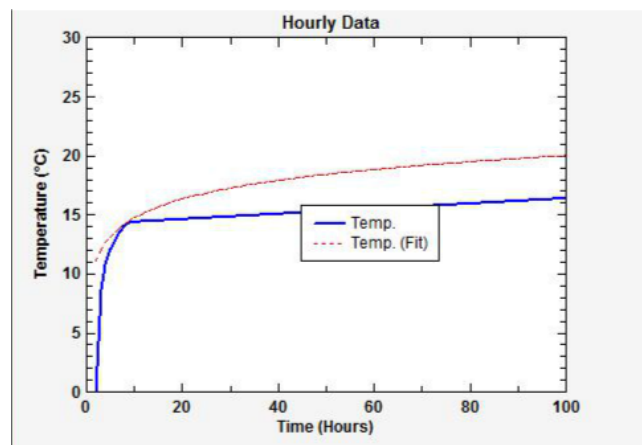
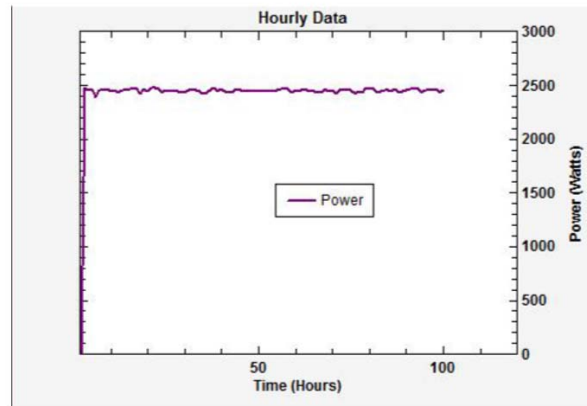
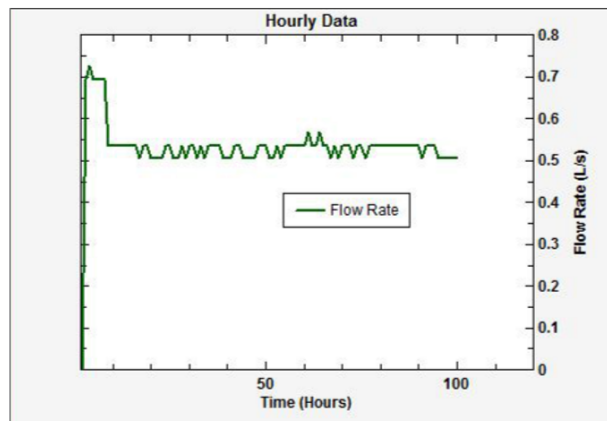


Figure 4-2. Variation of temperature in the borehole during the TRT (Thermal Response Test)



Average Power 2457.8 Watts

Figure 4-3. Variation of the injected power in the borehole during the TRT (Thermal Response Test)



Average Flow Rate 0.61

Figure 4-4. Variation of the flow rate during the Thermal Response Test (TRT)

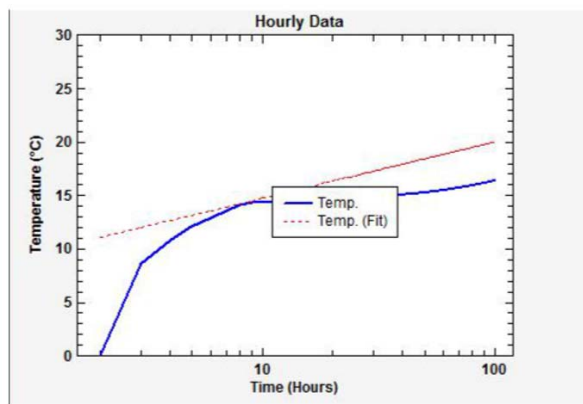


Figure 4-5. Variation of temperature as a function of the natural logarithm of time during the Thermal Response Test (TRT)

## 5 Conclusions

The in situ measured value of the thermal conductivity – 1.71 [W/m·K] – represents an average value over the depth of the 50-meter lithological column (up to which the test borehole was drilled). According to [5], this lithological column is composed of the following layers:

- Layer of topsoil
- Layer of Bucharest clays
- Layer of Colentina sands and gravels
- Layer of intermediate clays
- Layer of intermediate sands

If the sizing calculation of the ground heat exchanger were to be performed based solely on the thermal conductivity values extracted from Table 1, the degree of uncertainty in the results would be extremely high, as the range of thermal conductivity values is very wide, spanning from 0.4 [W/mK] (*for dry sand*) to 2.4 [W/mK] (for saturated clay and sand). The calculation error for the total required length of the ground heat exchanger is approximately  $\pm 10\%$ , an error which may lead to the following consequences:

- **Undersizing of the ground heat exchanger** – if the thermal conductivity of the ground is assumed to be greater than 1.71 [W/m·K] – leading to immediate effects such as the failure to meet the technical and comfort parameters of the HVAC system based on geothermal heat pumps, or, conversely...

- **Oversizing of the ground heat exchanger** – if the thermal conductivity of the ground is assumed to be less than 1.71 [W/m·K] – resulting in immediate effects such as increased costs for its installation by tens, or even hundreds of thousands of euros, depending on the installed capacity of the HVAC system based on geothermal heat pumps.

**Tabel 1.**  
**Thermal conductivity and specific heat capacity according to VDI 4640 [4]**

	Type of rock	Thermal conductivity [W/m.K]		Specific heat capacity [kWh/m <sup>3</sup> .K]	Density [10 <sup>3</sup> g/m <sup>3</sup> ]
		Range	Recommended value		
Unconsolidated	Dry clay/silt	0,4÷1,0	0,5	0,42÷0,44	1,8÷2,0
	Saturated clay/silt	1,1÷3,1	1,8	0,55÷0,78	2,0÷2,2
	Dry sand	0,3÷0,9	0,4	0,36÷0,44	1,8÷2,2
	Wet sand	1,0÷1,9	1,4	0,28÷0,61	1,9÷2,2



	Type of rock	Thermal conductivity [W/m.K]		Specific heat capacity [kWh/m <sup>3</sup> .K]	Density [10 <sup>3</sup> g/m <sup>3</sup> ]
		Range	Recommended value		
	Saturated sand	2,0÷3,0	2,4	0,61÷0,78	1,9÷2,3
	Gravel/cobble, dry	0,4÷0,9	0,4	0,36÷0,44	18÷2,2
	Gravel/cobble, saturated	1,6÷2,5	1,8	0,61÷0,72	1,9÷2,3
	Fill/clay (fat clay)	1,1÷2,9	2,4	0,42÷0,69	1,8÷2,3
	Peat/weak lignite (woody brown coal)	0,2÷0,7	0,4	0,14÷1,06	0,5÷1,1
Sedimentary rocks	Clay/silty (fine sandstone)	1,1÷3,4	2,2	0,58÷0,67	2,4÷2,6
	Sandstone	1,9÷4,6	2,8	0,50÷0,72	2,2÷2,7
	Conglomerate/breccia	1,3÷5,1	2,3	0,50÷0,72	2,2÷2,7
	Marna	1,8÷2,9	2,3	0,61÷0,64	2,3÷2,6
	Limestone	2,0÷3,9	2,7	0,58÷0,67	2,4÷2,7
	Dolomite	3,0÷5,0	3,5	0,58÷0,67	2,4÷2,7
	Dolomitic rocks (anhydrite)	1,5÷7,7	4,1	0,55	2,8÷3,0
	Dolomitic rocks (gypsum)	1,3÷2,8	1,6	0,55	2,2÷2,4

Thermal Response Test (TRT) is therefore recommended for geothermal heat pump systems with a total thermal power greater than 50 kW, allowing the acquisition of real technical information directly from the project implementation site. Performing the TRT can save significant financial resources—both by avoiding unnecessary additional drilling and by meeting the heating and cooling demands of the consumer with high energy efficiency.

The in-situ results obtained through the TRT must be used with great caution, as practical implementations need to correspond to the physico-mathematical model used for interpreting the experimental results from the TRT. Since the experimentally determined thermal conductivity represents an average value over the entire borehole length, this value can be applied for similar depths of ground heat exchangers. Also, the borehole thermal resistance value cannot be extrapolated to energy piles, because the boundary geometric conditions differ due to the different length-to-diameter ratio, and the applicable physico-mathematical model is that of an infinite cylindrical source-

unlike ground heat exchangers where the physico-mathematical model used is that of an infinite line source.

## 6 Standard Finite Line Source Model (FLS) (H.S. Carslaw, J.C. Jaeger, 1959)

Traditionally, heat transfer in the porous soil medium without groundwater flow is described by the heat conduction equation as follows (H.S. Carslaw, J.C. Jaeger, 1959):

$$\rho c \frac{\delta T}{\delta t} - \nabla * (\lambda \nabla T) = 0 \quad (6.1)$$

where:

- $\rho$  is the density of the soil [kg/m<sup>3</sup>],
- $c$  is the specific heat capacity of the soil [J/kg·K],
- $T$  is the temperature [°C or K],
- $t$  is time [s],
- $k$  is the thermal conductivity of the soil [W/m·K],
- $Q$  is the internal heat source term [W/m<sup>3</sup>].

$$\rho c = n\rho_w c_w + (1 - n)\rho_s c_s \quad (6.2)$$

$\lambda$  – Thermal conductivity [W/m·K]

$\rho c$  – Volumetric heat capacity of the porous medium

$\rho_s c_s$  – Weighted average of the solids in the aquifer medium

$\rho_w c_w$  – Weighted average of the water in the aquifer medium

The solution of the partial differential equation for heat transfer from a source in a porous medium with an initial uniform temperature  $T_0$  is given by the relation:

$$\Delta T(x, y, z, t) = \frac{Q}{4\pi\lambda r} \operatorname{erfc} \left[ \frac{r}{\sqrt{4at}} \right] \quad (6.3)$$

The temperature difference in the borehole,  $\Delta T = T_0 - T$ , where  $T_0$  is the initial uniform temperature and  $T$  is the local temperature, is related to the heat  $Q$  extracted or injected from the borehole. The thermal diffusivity is defined as  $(a = \frac{\lambda}{\rho c})$ , where  $\lambda$  is the thermal conductivity and  $\rho c$  is the volumetric heat capacity of the porous medium. The distance  $r = \sqrt{x^2 + y^2 + (z - z')^2}$  to the heat source, located along the  $z$ -axis at coordinates  $(0, 0, z')$

The Finite Line Source (FLS) model can be expressed as follows (H.Y. Zeng, N.R. Diao, Z.H. Fang, 2002): (D. Marcotte, P. Pasquier, F. Sheriff, M. Bernier, 2010), (L. Lamarche, B. Beauchamp, 2007). [6], [7]

$$\Delta T_{FLS}(x, y, z, t) = \frac{q_L}{4\pi\lambda} \left[ \int_0^H \frac{1}{r} \operatorname{erfc} \frac{1}{\sqrt{4at}} dz' - \int_{-H}^0 \frac{1}{r} \operatorname{erfc} \frac{r}{\sqrt{4at}} dz' \right] \quad (6.4)$$

## 7 Bibliography

1. GEOTRAINET – Manual for designers (GEOTRAINET – "Geo–Education for a sustainable heating and cooling market" - IEE /07/581 / SI2.499061), [www.geotrainet.eu](http://www.geotrainet.eu))
2. Closed loop vertical borehole design, installation & materials standards – Issue 1.0 (Sept. 2011)
3. Ground Loop Design Software Manual
4. VDI 4640 - Part 1 – Calculation of the seasonal coefficient of performance of heat pumps – Electric heat pumps for space heating and domestic hot water
5. I.A. Ciocaniu, D.A. Teofilescu, L. Batali, R. Gavriluc, C. Arion - Metode utilizate în execuția lucrărilor de teren pentru investigarea complexă a terenului de fundare (Conferința Națională de Geotehnica și Fundații 2021)
6. L. Lamarche, B. Beauchamp. A new contribution to the finite line-source model for geothermal boreholes. Energy Build. 2007, pg. 188-198.
7. D. Marcotte, P. Pasquier, F. Sheriff, M. Bernier. The importance of axial effects for borehole design of geothermal heat-pump systems, Renew. Energ. s.l. : Renew. Energ., 2010, pg. 763-770
8. H.Y. Zeng, N.R. Diao, Z.H. Fang A finite line-source model for boreholes in geothermal heat exchangers.. 2002, Heat Transfer Asian Res., Vol. 7, pg. 558-567